
Università degli Studi di Napoli Federico II
Facoltà di Ingegneria



Susanna Tortorelli

ON THE FLEXURAL PERFORMANCE
OF STEEL BEAMS

*Tesi di Dottorato
XXIII ciclo*

*Il Coordinatore
Prof. Ing. Federico M. MAZZOLANI*

Dottorato di Ricerca in Ingegneria delle Costruzioni

On the front cover: "Lunch atop a Skyscraper" (New York Construction Workers Lunching on a Crossbeam of the Rockefeller Center), Charles C. Ebbets, 1932.

Susanna Tortorelli

ON THE FLEXURAL PERFORMANCE OF STEEL BEAMS

Copyright © 2010 Università degli Studi di Napoli Federico II - P.le Tecchio 80, 80136 Napoli, Italy -
web: www.unina.it

Proprietà letteraria, tutti i diritti riservati. La struttura ed il contenuto del presente volume non possono essere riprodotti, neppure parzialmente, salvo espressa autorizzazione. Non ne è altresì consentita la memorizzazione su qualsiasi supporto (magnetico, magnetico-ottico, ottico, cartaceo, etc.).

Benché l'autore abbia curato con la massima attenzione la preparazione del presente volume, Egli declina ogni responsabilità per possibili errori ed omissioni, nonché per eventuali danni dall'uso delle informazione ivi contenute.

Finito di stampare il 01/12/2011

Engineering is the art of modelling materials we do not wholly understand,
into shapes we cannot precisely analyse,
so as to withstand forces we cannot properly assess,
in such a way that the public has no reason to suspect the extent of our ignorance.

- *Dr AR Dykes*
British Institution of Structural Engineers, 1976

TABLE OF CONTENTS

Table of Contents.....	i
List of Figures.....	v
List of Tables.....	xiii
Abstract.....	xv
Acknowledgements.....	xvii
About the Author.....	xix
1 INTRODUCTION.....	1
1.1 Motivation and Scope of the Study.....	1
1.2 Outline of the Work.....	2
2 SEISMIC-RESISTANT STEEL STRUCTURES.....	5
2.1 Design of Seismic-Resistant Steel Structures.....	5
2.1.1 The issue of buildings in seismic areas.....	5
2.1.2 Design philosophy and multi-level design criteria.....	6
2.1.3 Design approaches and strategies.....	8
2.1.4 Seismic behaviour of steel structures.....	10
2.2 Concentric Braced Frame Structures.....	12
2.2.1 Concept and design criteria.....	12
2.2.2 Innovative solutions.....	13
2.2.3 Design criteria according to EC8.....	15
2.3 Eccentric Braced Frame Structures.....	19
2.3.1 Concept and design criteria.....	19
2.3.2 Design criteria according to EC8.....	20
2.4 Moment Resisting Frame Structures.....	25
2.4.1 Concept and design criteria.....	25
2.4.2 Innovative solutions.....	26
2.4.3 Design criteria according to EC8.....	28
2.5 Worked Examples and Comparisons.....	32
2.5.1 Structural design according to EC8: the case study.....	32
2.5.2 Seismic analysis.....	36
2.5.3 Results and comparative analysis.....	45
3 FLEXURAL CAPACITY OF STEEL BEAMS.....	49
3.1 Ductility of Steel Structures.....	49
3.2 Rotation Capacity of Steel Beams.....	52

3.2.1	Definitions	52
3.2.2	Predictive methods	53
3.2.3	Rotation capacity in current codes	55
3.3	Overstrength of Steel Beams	56
3.3.1	Definitions	56
3.3.2	Predictive methods	57
3.3.3	Flexural overstrength in current codes	58
3.4	Seismic Classification Criteria of Steel Beams	62
3.4.1	Eurocode 8 classification criterion	63
3.4.2	OPCM 3274 classification criterion	65
3.4.3	Italian code NTC '08 classification criterion	67
4	EXPERIMENTAL ACTIVITY	69
4.1	Planning of the Experimental Campaign	69
4.2	Description of the Testing System	75
4.2.1	Test set-up scheme	75
4.2.2	Measuring devices	77
4.2.3	Loading protocols	79
4.3	Results	81
4.3.1	Tensile coupon tests on materials	81
4.3.2	Bending tests on beams	86
4.4	Concluding Remarks	105
5	CALIBRATION OF THE NUMERICAL MODELS	109
5.1	Finite Element Method	109
5.1.1	FEA in engineering applications	110
5.1.2	FEA with Abaqus 6.10 software	111
5.2	Modeling of Tested Beams	114
5.2.1	Definition of the materials	114
5.2.2	Element type and mesh: sensitivity study	116
5.2.3	Loads and boundary conditions	120
5.3	Comparison of Results	122
5.4	Concluding Remarks	140
6	MONOTONIC BEHAVIOUR OF STEEL BEAMS	141
6.1	Parametrical Analysis: Planning	141
6.2	Numerical Modeling	146
6.3	Parametric Analysis: Results	149
6.3.1	Double T profiles	149
6.3.2	Hollow profiles	157
6.4	New Empirical Formulation for “R” and “s”	165
6.5	Concluding Remarks	169

7	CYCLIC BEHAVIOUR OF STEEL BEAMS	171
7.1	Parametrical Analysis: Planning	171
7.2	Numerical Modeling	172
7.3	Parametric Analysis: Results	176
7.3.1	IPE profiles	176
7.3.2	HEA profiles	180
7.3.3	HEB profiles	185
7.4	Concluding Remarks.....	190
8	CONCLUSIONS	193
	REFERENCES	195

LIST OF FIGURES

Figure 2.1 Performance objectives, SEAOC Vision, 1995.	7
Figure 2.2 Taipei Tower 101, C.Y.Lee & Partners, Taiwan , 2004.	9
Figure 2.3 Isolated building: Government Building in Nagoya.....	10
Figure 2.4 CBF with active tension diagonal (EC8).....	12
Figure 2.5 CBF with V and K bracings (EC8).....	12
Figure 2.6 Innovative solutions for CBFs: pin and U connections.	13
Figure 2.7 Behaviour of compressed brace for CBF and BRB.	14
Figure 2.8 Buckling Restrained Brace: all steel solution.	14
Figure 2.9 Reduced Section Solution for CBFs.	15
Figure 2.10 Example of application of the expression 2.1.....	16
Figure 2.11 Configurations of frames with eccentric braces.....	19
Figure 2.12 Geometrical parameters for I sections.	21
Figure 2.13 Equal moments and unequal moments at link ends.	22
Figure 2.14 Moment resisting frame structures.	25
Figure 2.15 Dog-bone in moment resisting frame structures.....	26
Figure 2.16 Metal shear panels.	27
Figure 2.17 Stiffened and unstiffened shear panels with openings.....	27
Figure 2.18 Beam deflection for the calculation of θ_p	31
Figure 2.19 Architectural plan of the typical floor.	33
Figure 2.20 Structural plan of the typical floor and plan location of braces in CBFs and EBF.	34
Figure 2.21 Vertical configuration and cross sections of CBFs.	35
Figure 2.22 Vertical configuration and cross sections of EBFs.	35
Figure 2.23 Cross sections of MRFs.....	35
Figure 2.24 Modal shapes of CBFs in X and Y direction.	37
Figure 2.25 Inelastic Modal Pushover curves compared with Elastic Spectra for different a_g in ADRS format for CBFs.	37
Figure 2.26 Inter-storey drifts for X-CBFs.....	38
Figure 2.27 Inter-storey drifts for inverted-V CBFs.	38
Figure 2.28 Ductility demand for braces in X direction.	38
Figure 2.29 Ductility demand for braces in Y direction.	39
Figure 2.30 Modal shapes of EBFs in X and Y direction.	39
Figure 2.31 Inelastic Modal Pushover curves compared with Elastic Spectra for different a_g in ADRS format for EBFs.....	40

Figure 2.32 Inter-storey drifts for EBFs in X direction.	40
Figure 2.33 Inter-storey drifts for EBFs in Y direction.....	41
Figure 2.34 Ductility demand for braces in X direction.....	41
Figure 2.35 Ductility demand for braces in Y direction.	42
Figure 2.36 Modal shapes of MRFs in X and Y direction.	43
Figure 2.37 Inelastic Modal Pushover curves compared with Elastic Spectra for different a_g in ADRS format for MRFs.....	43
Figure 2.38 Inter-storey drifts for MRFs in X direction.....	43
Figure 2.39 Inter-storey drifts for MRFs in Y direction.....	44
Figure 2.40 Ductility demand for beams in X direction.....	44
Figure 2.41 Ductility demand for beams in Y direction.....	44
Figure 2.42 Incidence of steel weight on the total seismic weight (a); incidence of the seismic-resistant weights on the total steel weight (b)..	45
Figure 2.43 Comparison of the pushover curves of the three structures in X and Y direction.	46
Figure 2.44 Comparison of the roof drift normalized to building height at different a_g	46
Figure 3.1 Ductility types (Gioncu & Mazzolani, 2002).....	50
Figure 3.2 Moment-curvature and moment-rotation curves.	52
Figure 3.3 Different approaches to the definition of s	57
Figure 3.4 Member ductility classification criterion (Galambos & Lay, 1965).....	62
Figure 3.5 Frame ductility classification criterion (Ivanyi 1992).....	63
Figure 3.6 EC3 classification of cross sections.	64
Figure 3.7 OPCM 3274 classification of members.....	66
Figure 4.1 Length parameter for each test set-up scheme.	71
Figure 4.2 Variability range for the parameter λ_p	71
Figure 4.3 Variability range for the parameter λ_w	71
Figure 4.4 Variability range for the ratio L/h	72
Figure 4.5 Variability range for the ratio b/h	72
Figure 4.6 Variability range for the ratio b/L	72
Figure 4.7 Geometrical parameters for I and hollow profiles.	73
Figure 4.8 Reacting steel frame and specimen with lateral-torsional restrain.....	75
Figure 4.9 Adopted test set-up scheme.....	76
Figure 4.10 Basement connection and deformed end on the other side.....	77
Figure 4.11 Connection of the specimen to the hydraulic actuator.....	77
Figure 4.12 Central unit and pc for the hydraulic actuator.	78
Figure 4.13 Layout of measuring devices and pc for data acquisition.....	78

Figure 4.14	Layout of front and back measuring devices (LVDTs).	79
Figure 4.15	Displacement history for monotonic tests.	79
Figure 4.16	Displacement history for cyclic tests.	80
Figure 4.17	Universal testing machine and coupon specimens.	81
Figure 4.18	Stress-strain diagrams for HEA 160 web and flange.	82
Figure 4.19	Stress-strain diagrams for HEB 240 web and flange.	82
Figure 4.20	Stress-strain diagrams for IPE 300 web and flange.	82
Figure 4.21	Stress-strain diagrams for RHS 150x100x5.	83
Figure 4.22	Stress-strain diagrams for RHS 160x80x4.	83
Figure 4.23	Stress-strain diagrams for RHS 250x100x10.	83
Figure 4.24	Stress-strain diagrams for SHS 160x160x6.3.	84
Figure 4.25	Stress-strain diagrams for SHS 200x200x10.	84
Figure 4.26	Stress-strain diagrams for SHS 250x250x8.	84
Figure 4.27	Geometric properties of specimen HEA 160.	87
Figure 4.28	Failure mechanism for monotonic and cyclic loading.	88
Figure 4.29	Flexural performance of specimen HEA 160.	88
Figure 4.30	Geometric properties of specimen HEB 240.	89
Figure 4.31	Failure mechanism for monotonic and cyclic loading.	90
Figure 4.32	Flexural performance of specimen HEB 240.	90
Figure 4.33	Geometric properties of specimen IPE 300.	91
Figure 4.34	Failure mechanism for monotonic and cyclic loading.	92
Figure 4.35	Flexural performance of specimen IPE 300.	92
Figure 4.36	Geometric properties of specimen RHS 150x100x5.	93
Figure 4.37	Failure mechanism for monotonic and cyclic loading.	94
Figure 4.38	Flexural performance of specimen RHS 150x100x5.	94
Figure 4.39	Geometric properties of specimen RHS 160x80x4.	95
Figure 4.40	Failure mechanism for monotonic and cyclic loading.	96
Figure 4.41	Flexural performance of specimen RHS 160x80x4.	96
Figure 4.42	Geometric properties of specimen RHS 250x100x10.	97
Figure 4.43	Failure mechanism for monotonic and cyclic loading.	98
Figure 4.44	Flexural performance of specimen RHS 250x100x10.	98
Figure 4.45	Geometric properties of specimen SHS 160x160x6.3.	99
Figure 4.46	Failure mechanism for monotonic and cyclic loading.	100
Figure 4.47	Flexural performance of specimen SHS 160x160x6.3.	100
Figure 4.48	Geometric properties of specimen SHS 200x200x10.	101
Figure 4.49	Failure mechanism for monotonic and cyclic loading.	102
Figure 4.50	Flexural performance of specimen SHS 200x200x10.	102
Figure 4.51	Geometric properties of specimen SHS 250x250x8.	103
Figure 4.52	Failure mechanism for monotonic and cyclic loading.	104

Figure 4.53 Flexural performance of specimen SHS 250x250x8.	104
Figure 4.54 Dissipated energies for double T profiles.	107
Figure 4.55 Dissipated energies for rectangular hollow profiles.	107
Figure 4.56 Dissipated energies for square hollow profiles.	107
Figure 5.1 Example of finite element model and analysis results.	110
Figure 5.2 Finite Element Method Software ABAQUS 6.10.	111
Figure 5.3 Finite Element families (Abaqus User's Manual).	112
Figure 5.4 Stress-strain diagram resulting from experimental tests.	116
Figure 5.5 Average engineering and true stress - true strain diagrams.	116
Figure 5.6 Examples of solid and shell modeling.	117
Figure 5.7 Element type vs computational costs.	118
Figure 5.8 Element type vs simulation accuracy.	119
Figure 5.9 Different levels of mesh refinements (double T profiles).	119
Figure 5.10 Different levels of mesh refinements (hollow profiles).	120
Figure 5.11 Displacement history for monotonic simulation.	121
Figure 5.12 Displacement history for cyclic simulations.	121
Figure 5.13 Failure mechanism for monotonic loading HEA 160.	122
Figure 5.14 Experimental vs numerical monotonic curve HEA 160.	122
Figure 5.15 Failure mechanism for cyclic loading HEA 160.	123
Figure 5.16 Experimental vs numerical cyclic curve HEA 160.	123
Figure 5.17 Failure mechanism for monotonic loading HEB 240.	124
Figure 5.18 Experimental vs numerical monotonic curve HEB 240.	124
Figure 5.19 Failure mechanism for cyclic loading HEB 240.	125
Figure 5.20 Experimental vs numerical cyclic curve HEB 240.	125
Figure 5.21 Failure mechanism for monotonic loading IPE 300.	126
Figure 5.22 Experimental vs numerical monotonic curve IPE 300.	126
Figure 5.23 Failure mechanism for cyclic loading IPE 300.	127
Figure 5.24 Experimental vs numerical cyclic curve IPE 300.	127
Figure 5.25 Failure mechanism for monotonic loading 150x100x5.	128
Figure 5.26 Experimental vs numerical monotonic curve 150x100x5.	128
Figure 5.27 Failure mechanism for cyclic loading 150x100x5.	129
Figure 5.28 Experimental vs numerical cyclic curve 150x100x5.	129
Figure 5.29 Failure mechanism for monotonic loading 160x80x4.	130
Figure 5.30 Experimental vs numerical monotonic curve 160x80x4.	130
Figure 5.31 Failure mechanism for cyclic loading 160x80x4.	131
Figure 5.32 Experimental vs numerical cyclic curve 160x80x4.	131
Figure 5.33 Failure mechanism for monotonic loading 250x100x10.	132
Figure 5.34 Experimental vs numerical monotonic curve 250x100x10.	132

Figure 5.35 Failure mechanism for cyclic loading 250x100x10.....	133
Figure 5.36 Experimental vs numerical cyclic curve 250x100x10.....	133
Figure 5.37 Failure mechanism for monotonic loading 160x160x6.3. ..	134
Figure 5.38 Experimental vs numerical monotonic curve 160x160x6.3.	134
Figure 5.39 Failure mechanism for cyclic loading 160x160x6.3.....	135
Figure 5.40 Experimental vs numerical cyclic curve 160x160x6.3.....	135
Figure 5.41 Failure mechanism for monotonic loading 200x200x10. ...	136
Figure 5.42 Experimental vs numerical monotonic curve 200x200x10.	136
Figure 5.43 Failure mechanism for cyclic loading 200x200x10.....	137
Figure 5.44 Experimental vs numerical cyclic curve 200x200x10.....	137
Figure 5.45 Failure mechanism for monotonic loading 250x250x8.	138
Figure 5.46 Experimental vs numerical monotonic curve 250x250x8. .	138
Figure 5.47 Failure mechanism for cyclic loading 250x250x8.	139
Figure 5.48 Experimental vs numerical cyclic curve 250x250x8.....	139
Figure 6.1 Commercial profile list for IPE sections.....	142
Figure 6.2 Commercial profile list for HE sections.	142
Figure 6.3 Commercial profile list for RHS sections.	143
Figure 6.4 Commercial profile list for SHS sections.....	143
Figure 6.5 Integration of the existing database for IPE-HE profiles. ...	144
Figure 6.6 Integration of the existing database for IPE-HE profiles. ...	144
Figure 6.7 Integration of the existing database for RHS-SHS profiles. .	144
Figure 6.8 Integration of the existing database for RHS-SHS profiles. .	145
Figure 6.9 Different levels of mesh refinements (double T profile).....	146
Figure 6.10 Different levels of mesh refinements (hollow profile).....	146
Figure 6.11 Displacement and boundary conditions (double T profile).	147
Figure 6.12 Displacement and boundary conditions (hollow profile)...	147
Figure 6.13 Stress-strain diagram resulting from experimental tests.	148
Figure 6.14 Monotonic response of IPE 270 and IPE 300.	149
Figure 6.15 Monotonic response of IPE 330 and IPE 360.	149
Figure 6.16 Monotonic response of IPE 400 and IPE 450.	149
Figure 6.17 Monotonic response of IPE 500 and IPE 550.	150
Figure 6.18 Monotonic response of IPE 600.....	150
Figure 6.19 Comparison of monotonic response of all IPE profiles. ..	150
Figure 6.20 Monotonic response of HEA 240 and HEA 260.	151
Figure 6.21 Monotonic response of HEA 280 and HEA 300.	151
Figure 6.22 Monotonic response of HEA 320 and HEA 340.	151

Figure 6.23 Monotonic response of HEA 360 and HEA 400.	152
Figure 6.24 Monotonic response of HEA 450 and HEA 500.	152
Figure 6.25 Monotonic response of HEA 550 and HEA 600.	152
Figure 6.26 Comparison of monotonic response of all HEA profiles.	153
Figure 6.27 Monotonic response of HEB 240 and HEB 260.	154
Figure 6.28 Monotonic response of HEB 280 and HEB 300.	154
Figure 6.29 Monotonic response of HEB 320 and HEB 340.	154
Figure 6.30 Monotonic response of HEB 360 and HEB 400.	155
Figure 6.31 Monotonic response of HEB 450 and HEB 500.	155
Figure 6.32 Monotonic response of HEB 550 and HEB 600.	155
Figure 6.33 Comparison of monotonic response of all HEB profiles.	156
Figure 6.34 Monotonic response of 200x100x5 and 200x100x8.	157
Figure 6.35 Monotonic response of 200x100x10 and 200x120x8.	157
Figure 6.36 Monotonic response of 200x120x10 and 200x150x8.	157
Figure 6.37 Monotonic response of 200x150x10 and 250x100x8.	158
Figure 6.38 Monotonic response of 250x150x10 and 300x100x8.	158
Figure 6.39 Monotonic response of 300x100x10 and 300x150x8.	158
Figure 6.40 Monotonic response of 300x150x9 and 300x200x9.	159
Figure 6.41 Monotonic response of 350x150x6 and 350x250x6.	159
Figure 6.42 Monotonic response of 400x200x6 and 400x200x8.	159
Figure 6.43 Monotonic response of 400x200x9 and 400x250x8.	160
Figure 6.44 Monotonic response of 400x250x9.	160
Figure 6.45 Comparison of monotonic response of all RHS profiles.	160
Figure 6.46 Monotonic response of 150x150x6 and 150x150x10.	161
Figure 6.47 Monotonic response of 160x160x5 and 160x160x6.	161
Figure 6.48 Monotonic response of 160x160x10 and 175x175x5.	161
Figure 6.49 Monotonic response of 175x175x8 and 175x175x10.	162
Figure 6.50 Monotonic response of 180x180x8 and 180x180x10.	162
Figure 6.51 Monotonic response of 200x200x6 and 200x200x8.	162
Figure 6.52 Monotonic response of 220x220x6 and 220x220x8.	163
Figure 6.53 Monotonic response of 220x220x10 and 250x250x8.	163
Figure 6.54 Monotonic response of 250x250x9 and 260x260x8.	163
Figure 6.55 Monotonic response of 300x300x8 and 300x300x9.	164
Figure 6.56 Monotonic response of 325x325x9.	164
Figure 6.57 Comparison of monotonic response of all SHS profiles.	164
Figure 6.58 Experimental - numerical data vs theoretical R (double T profiles).	167
Figure 6.59 Experimental - numerical data vs theoretical R (hollow profiles).	168

Figure 6.60 Experimental - numerical data vs theoretical s (double T profiles).....	168
Figure 6.61 Experimental - numerical data vs theoretical s (hollow profiles).....	168
Figure 7.1 Different levels of mesh refinements (double T profile).....	173
Figure 7.2 Displacement and boundary conditions (double T profile).	173
Figure 7.3 Displacement history for cyclic simulations.	174
Figure 7.4 Stress-strain diagram resulting from experimental tests.....	175
Figure 7.5 Cyclic response of IPE 270 and monotonic comparison....	176
Figure 7.6 Cyclic response of IPE 300 and monotonic comparison....	176
Figure 7.7 Cyclic response of IPE 330 and monotonic comparison....	176
Figure 7.8 Cyclic response of IPE 360 and monotonic comparison....	177
Figure 7.9 Cyclic response of IPE 400 and monotonic comparison....	177
Figure 7.10 Cyclic response of IPE 450 and monotonic comparison..	177
Figure 7.11 Cyclic response of IPE 500 and monotonic comparison..	178
Figure 7.12 Cyclic response of IPE 550 and monotonic comparison..	178
Figure 7.13 Cyclic response of IPE 600 and monotonic comparison..	178
Figure 7.14 Comparison of cyclic envelope response of all IPE profiles.	179
Figure 7.15 Cyclic response of HEA240 and monotonic comparison.	180
Figure 7.16 Cyclic response of HEA260 and monotonic comparison.	180
Figure 7.17 Cyclic response of HEA280 and monotonic comparison.	180
Figure 7.18 Cyclic response of HEA300 and monotonic comparison.	181
Figure 7.19 Cyclic response of HEA320 and monotonic comparison.	181
Figure 7.20 Cyclic response of HEA340 and monotonic comparison.	181
Figure 7.21 Cyclic response of HEA360 and monotonic comparison.	182
Figure 7.22 Cyclic response of HEA400 and monotonic comparison.	182
Figure 7.23 Cyclic response of HEA450 and monotonic comparison.	182
Figure 7.24 Cyclic response of HEA500 and monotonic comparison.	183
Figure 7.25 Cyclic response of HEA550 and monotonic comparison.	183
Figure 7.26 Cyclic response of HEA600 and monotonic comparison.	183
Figure 7.27 Comparison of cyclic envelope response of all HEA profiles.	184
Figure 7.28 Cyclic response of HEB240 and monotonic comparison.	185
Figure 7.29 Cyclic response of HEB260 and monotonic comparison.	185
Figure 7.30 Cyclic response of HEB280 and monotonic comparison.	185
Figure 7.31 Cyclic response of HEB300 and monotonic comparison.	186
Figure 7.32 Cyclic response of HEB320 and monotonic comparison.	186
Figure 7.33 Cyclic response of HEB340 and monotonic comparison.	186

Figure 7.34 Cyclic response of HEB360 and monotonic comparison.187
Figure 7.35 Cyclic response of HEB400 and monotonic comparison.187
Figure 7.36 Cyclic response of HEB450 and monotonic comparison.187
Figure 7.37 Cyclic response of HEB500 and monotonic comparison.188
Figure 7.38 Cyclic response of HEB550 and monotonic comparison.188
Figure 7.39 Cyclic response of HEB600 and monotonic comparison.188
Figure 7.40 Comparison of cyclic envelope response of all HEB profiles.189

LIST OF TABLES

Table 3.1 Values of γ_{0V} for different steel type (OPCM 3274).....	60
Table 3.2 EC8 cross-section requirements for dissipative elements.....	64
Table 3.3 Stress-strain characteristics of common European steel	65
Table 3.4 Classification of members in terms of ductility.....	66
Table 4.1 Tests available in technical literature for IPE-HE profiles.....	70
Table 4.2 Tests available in technical literature for RHS-SHS profiles...	70
Table 4.3 Programmed experimental tests.	73
Table 4.4 Tested profiles with slenderness ratios.	74
Table 4.5 Material properties of tested beams for double T profiles.	85
Table 4.6 Material properties of tested beams for hollow profiles.	85
Table 4.7 Flexural performance of tested beams.....	105
Table 4.8 Classification of tested beams according to existing codes. ..	106
Table 4.9 Dissipated energies.	106
Table 5.1 Material properties of tested beams for double T profiles. ...	115
Table 5.2 Material properties of tested beams for hollow profiles.	115
Table 5.3 Element type vs computational costs.	118
Table 6.1 Database of sections for the parametric analysis.	145
Table 6.2 Stress-strain characteristics of common European steel	165
Table 6.3 C_i coefficients in the new expression of “s” factor.....	166
Table 6.4 C_i coefficients in the new expression of “R” factor.....	167
Table 7.1 Database of sections for the parametric analysis.	172
Table 7.2 Comparison between monotonic and cyclic results (HEA). .	190
Table 7.3 Comparison between monotonic and cyclic results (HEB). .	191
Table 7.4 Comparison between monotonic and cyclic results (IPE). ...	191

ABSTRACT

In this thesis the results of different kinds of investigation about both monotonic and cyclic behaviour of steel beams are presented.

With the aim to quantify the rotation capacity and flexural overstrength of steel beams an experimental activity was performed in the Civil Engineering Laboratory at the University of Salerno in the framework of ReLUIS project.

At the light of the experimental results, and with the aim to continue the study on the behaviour of steel beams avoiding additional expensive experimental campaigns, finite element models has been used to perform numerical simulations (in Abaqus 6.10) of the experimental tests actually carried out. The numerical results have been compared with the experimental ones to demonstrate the validity of the assumptions made in the modelling phase, with positive response.

Then, a wide parametrical analysis, carried out by means of finite element simulations, has been performed, on the basis of the previous calibration of the numerical models. In this way, the obtained results goes to enlarge the existing database of results, to be able, in the end, to propose a new empirical formulation for the parameters “R” and “s” in case of monotonic loads.

The proposed equations are obtained from a multiple linear regression of experimental and numerical data on monotonic tests, from literature and from the work carried out for this thesis. It was observed that interaction between web and compression flange slenderness could limit the rotation capacity of flexural members. This interaction can lead to reduced inelastic deformation capacity, measured as rotation capacity, when either the web or the compression flange slenderness is too large.

So, steel beam classification can be considered outdated, due to the fact that the rotation capacity “R” and the flexural overstrength “s” can be properly calculated by means of the tools provided by this work.

The correct value of the flexural overstrength “s”, as calculated with the new proposed formulation, can be properly used for the application of the capacity design criteria.

An analogous parametric analysis has been performed for cyclic loading pattern, demonstrating that the experimental and numerical results indicated that the loading condition has a significant influence on rotation capacity. In particular, it decreased when the loading is cyclic, and cyclic rotation capacity “R” can be estimated as about 30% of monotonic “R”. So, for seismic application, it is auspicious the use of the cyclic rotation capacity “R”, and not the monotonic one.

These critical considerations on the differences between the monotonic and the cyclic behaviours that were made, in future can be used to go beyond the final scope of this thesis. In particular it can be used to start a study to establish a connection between seismic demand and seismic capacity of steel beams. In particular, for seismic design it will be necessary to correlate cyclic “R” and behaviour factor “q” for steel structures.

ACKNOWLEDGEMENTS

Only in the printed version.

ABOUT THE AUTHOR

Susanna Tortorelli was born in Naples on November 18th, 1982.

She graduated cum laude in Architecture at the University of Naples “Federico II” in July 2007, with a thesis developed in the field of Structural Engineering, with the title: “Seismic-resistant structural typologies for the design of steel buildings”.

Since November 2007 she is a PhD student in Structural Engineering at the University of Naples “Federico II” (XXIII cycle). In these years she has been involved in studies and research activities in the “Department of Constructions and Mathematical Methods in Architecture” at the University of Naples “Federico II”. In particular her research activity was focussed on the design principles of steel structures in seismic areas and on the flexural behaviour of steel beams for seismic applications.

She was also involved in national (ReLUIS-DPC) and international research projects (COST C26).

1 INTRODUCTION

1.1 MOTIVATION AND SCOPE OF THE STUDY

Initially, the motivation for the beginning of this research work was the ReLUIIS-DPC 2005-2008 Research Project (ReLUIIS: Rete di Laboratori Universitari di Ingegneria Sismica: Seismic Engineering University Laboratories Network; DPC: Dipartimento di Protezione Civile: Emergency Management Association).

When my doctorate course was at the beginning in 2007, this research project was started yet. Dr. Ing. Manuela Brescia was already working on the topic of rotational capacity of steel members, and the experimental campaign, in collaboration with the University of Salerno at the Civil Engineering Laboratory, based on the financial support of the ReLUIIS Project, has been starting.

In particular the activity was framed in the ReLUIIS Project, Task 5: “Development of innovative approaches to design steel and composite steel-concrete structures” (coordinators: Proff. F. M. Mazzolani and R. Zandonini) and Subtask 2: “Rotation Capacity and classification criteria for steel members” (coordinator: Prof. R. Landolfo). The experimental activity was planned with the aim to provide tools to quantify and predict the flexural capacity of steel members, but at the end of the Project, not all experimental tests have been carried out, and so not all the possible considerations and elaborations could be made.

So, at the same time of the completion of the experimental campaign, the numerical activity started, in terms of attempt of modelling first, and parametrical analysis then.

During the work, the importance of the influence of loading pattern, and in particular of cyclic loading, was recognized, and so it was fixed as final scope of this work, that is to obtain a large database of cyclic simulations, to make significant considerations on the difference between the monotonic and the cyclic behaviour of steel beams. But, by now, for time reasons, this is not a completely reached goal, because the cyclic simulations are more expensive in terms of computational costs

than monotonic ones. In particular, starting from this work and its achieved results, it can be interesting to study the possible connections between seismic demand and seismic capacity of steel beams, joining the cyclic rotational capacity “R” with the behavioural factors “q”.

By now, this is a goal that goes beyond the final scope of this thesis, but it can be continued the work that started in 2008 in the framework of COST Action C26 (Urban Habitat Constructions under Catastrophic Events), on the investigation of connections between seismic capacity and seismic demand under catastrophic events (Landolfo et al, 2008).

In this work, starting from the consideration that in steel MRFs, designed according to the capacity design criteria, the overall ductile behaviour is ruled by the rotation capacity of steel beams, some MRF structures have been analysed in order to evaluate the rotation demand under catastrophic seismic events.

This kind of work can not be continued in terms of comparison between rotation capacity and seismic demand, for lack of significative amount of data, but now, after the numerical parametrical analyses, and with the aim to complete it with other cyclic loading patterns and other kind of sections to be analyzed, the long-term goal to complete this work can be finally achieved.

In the same framework of COST C26, another work has been instead completed, with the same topic of the seismic capacity of steel structures. But in this case the field was extended to various typologies, and the final scope was not so ambitious (to compare capacity and demand), so a final comparison between the capacities of steel structures designed according to EC8 principles under catastrophic seismic events, was made (Tortorelli et al. 2010). Some results are reported in Chapter 2.

1.2 OUTLINE OF THE WORK

This thesis work is organized in eight chapters. In the present **Chapter 1**, the Introduction, the motivation at the base of the study and the final aim that this research want to reach are briefly explained.

Then the following two chapters are about the state of the art, one more general, and one more specific. In particular **Chapter 2** presents an overview on the question of seismic design and in particular on the seismic design of steel structures. Starting far away from the question of

buildings in seismic areas, and considering steel structures as a reliable and versatile solution, the attention is focussed on the traditional steel structure typologies, with a little mention to innovative solutions and a wide deepening on EC8 design and detailing rules, also through some worked design examples.

Chapter 3 is also about the state of the art, but dealing with the more specific topic of the flexural capacity of steel beams. Starting from the concepts of global and local ductility, and the consideration that in steel MRFs, the overall ductile behaviour is assured by the rotation capacity of steel beams, definitions and methods for the prediction of both rotation capacity and flexural overstrength of steel beams are provided. In the end, the interpretation of these concepts by current codes is analyzed.

Chapter 4 presents details on the experimental activity performed in the Civil Engineering Laboratory at the University of Salerno in the framework of ReLUIIS project. In particular, it has been exposed the planning of the experimental campaign and the reasons of choices made about the test set-up scheme, the tested profiles and the loading history paths. Moreover, the main results of the experimental tests are given.

And the following **Chapter 5** is dedicated to the description of the finite element models, calibrated on the basis of the experimental tests data, that has been used to perform numerical simulations (in Abaqus 6.10) of the experimental tests actually carried out. The numerical results have been compared with the experimental ones to demonstrate the validity of the assumptions made in the modelling phase.

The work presented in this chapter is preparatory to the one presented in the subsequent chapters. In particular **Chapter 6** presents the results of a wide parametrical analysis, carried out by means of finite element simulations, on the basis of the previous calibration of the numerical models, avoiding additional expensive experimental campaigns.

The varied parameters are those investigated by technical literature yet, so the obtained results goes to enlarge the existing database of results, to be able, in the end, to propose a new empirical formulation for the parameters “R” and “s” in case of monotonic loads.

Moreover, **Chapter 7** has quite the same structure of the previous chapter, but in this case it focuses on the behaviour of steel beams under cyclic actions. An analogous parametric analysis has been performed, but this time it was not extracted another analytical formulation. Instead, critical considerations on the differences between the monotonic and the cyclic behaviours were made, and in future they can be used to go

beyond the final scope of this thesis. In particular it can be used to start a study to establish a connection between seismic demand and seismic capacity of steel beams, and so steel framed structures in general.

In the end, **Chapter 8** is a brief recapitulation of the achieved results and considerations on the innovative contents of the thesis.

2 SEISMIC-RESISTANT STEEL STRUCTURES

This chapter presents an overview on the question of seismic design and in particular on the seismic design of steel structures. Starting far away from the question of buildings in seismic areas, and considering steel structures as a reliable and versatile solution, the attention is focussed on the traditional steel structure typologies, with a little mention to innovative solutions and a wide deepening on EC8 design and detailing rules, also through some worked design examples.

2.1 DESIGN OF SEISMIC-RESISTANT STEEL STRUCTURES

2.1.1 The issue of buildings in seismic areas

Earthquakes are natural phenomena, which cause ground shaking, that are considered the most dangerous in terms of large-scale destruction to life and property.

According to the theory of plate tectonics, the entire surface of the earth can be considered subdivided into several plates, constantly moving. These plates brush against each other or collide at their boundaries giving rise to earthquakes. So, regions close to the plate boundary are highly seismic. But the study of why and where earthquakes occur comes under geology.

Instead the study of the characteristics of the earthquake ground motion and its effects on structures are the subjects of earthquake and structural engineering. In particular, the effect of earthquakes on structures and the design of structures to withstand earthquakes with no or minimum damage is the subject of earthquake resistant structural design.

An important thing to remember is that the time, the place and the intensity (amplitude, duration, and frequency) of an earthquake cannot be predicted by any scientific means or otherwise. Moreover, deaths and injuries caused by earthquakes are variable according to a lot of factors,

and the most important is the safety of structures. In fact, most of human losses are not due to the destructive force of the earthquake, but to the failure of constructions. This happens because buildings usually designed to resist static vertical loads, due to a seismic event, have to resist to a different stress pattern: horizontal dynamic forces, transmitted by the ground-foundations interface.

Therefore, a conscious and accurate design is important. This can be made by applying preliminary assessments and analyses that implies special attention to the morphology of the structure, the choice of the materials, the elements, joints, and in particular an adequate seismic-resistant system.

2.1.2 Design philosophy and multi-level design criteria

Severe earthquakes have a low probability of occurrence during the service life of a structure. If a structure has to resist such earthquakes elastically, it would require a lateral load resisting system that results too expensive. But also if the structure loses its functional requirements due to minor seismic waves, so needing lots of repairs, the design is not well done. So the better strategy is to ensure elastic behaviour under a moderate earthquake which has a return period equal to the life of the structure and prevent collapse under the extreme probable earthquake.

However, structures are designed to prevent collapse and loss of life under the most severe earthquake.

Under a moderate earthquake, the properties of structures which contribute to their elastic resistance, are its yield strength and elastic stiffness. Instead, during a severe earthquake, the structure to be able to have inelastic deformations, has to rely on its ductility and hysteretic energy dissipation capacity to avoid collapse and to undergo large plastic deformations without significant loss of strength.

Conventional methods of seismic design, as said before, have the objectives to provide for life safety and damage control. The design criteria are defined by limits on stresses and member forces calculated from prescribed levels of applied lateral shear force. But in the last years structural engineers have initiated the development of a concept of seismic design called Performance Based Seismic Design (PBSD). This design approach is a more general design philosophy in which the design criteria are expressed in terms of achieving stated performance objectives when the structure is subjected to stated levels of seismic hazard.

The idea of designing the structure based on performance objective is not new. A limit state is a form of performance objective. But to reduce the high costs associated with loss of use and repair of heavily damaged structures, more than two different levels of performance objectives need to be considered. Therefore, performance based-design can be considered a powerful new approach that includes traditional methods of seismic design with significant upgrades.

The most appropriate definition of PBSB is that performance-based design refers to the methodology in which structural design criteria are expressed in terms of achieving a set of performance objectives. This is based on the idea that performance objectives can be related to the level of damage to the structure (Fig. 2.1).

Moreover Performance-Based Earthquake Engineering (PBEE) is a more encompassing concept that includes design, evaluation and construction engineering.

The general methodology for performance-based design may include various approaches. In one approach, traditional force-based analysis is conducted and, after the design is completed, the deformation and damage may be estimated and checked against established displacement limits. Other approaches may start by establishing the displacement or drift associated with a certain performance, proportion the structure and then conduct the response analysis.

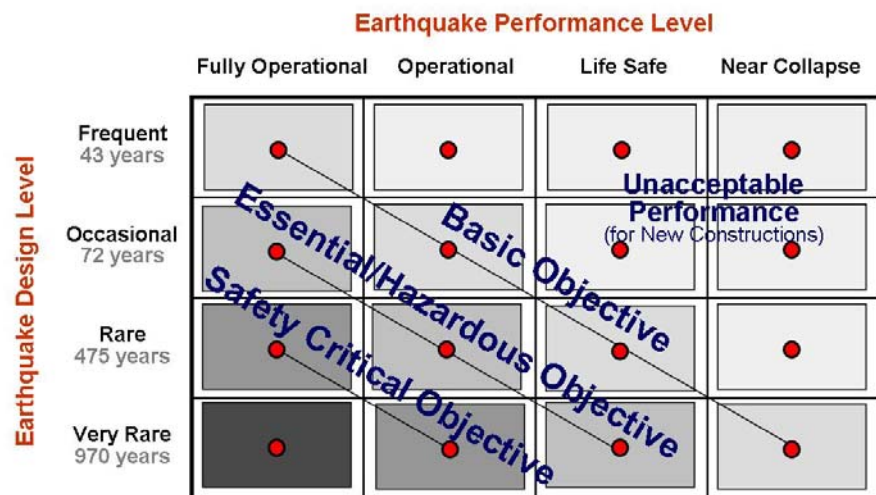


Figure 2.1 Performance objectives, SEAOC Vision, 1995.

Three documents are credited with laying the foundation for performance-based design concepts: SEAOC Vision 2000; ATC 40; and FEMA 273 and 274. The documents attempted to develop procedures that can be used as seismic provisions in building codes (Ghobarah, 2001).

2.1.3 Design approaches and strategies

The current approach to seismic design is based on the resistance required by the earthquake to an elastic system with a single degree of freedom (SDOF) equivalent in terms of strength and damping to the real structure, that is an inelastic system with multiple degrees of freedom.

The required resistance is calculated by means of the elastic response spectrum, evaluated considering a seismic event with a return period congruent with the service life of the structure.

The knowledge of structural behaviours is so fundamental in seismic design of structures because there are several possibilities in the choice of design strategies. Depending on their way to absorb/dissipate the energy input, structural behaviours can be divided into: dissipative and non-dissipative.

Non-dissipative structures, also called iper-resistant, are designed in order to remain in elastic field without any damage, also in case of destructive earthquake. This design approach is used in case of strategic buildings, or in case of construction systems with very low and not reliable dissipative properties. In this case the resistance is the only parameter to be verified, no ductility (local or global) requirements are needed.

Dissipative structures are designed with the aim to dissipate the seismic energy input. The energy input control can be active or passive.

The active energy input control strategies act on the peculiarities of the system in order to change the structural response artificially. The structural system is able to adapt itself to the acceleration caused by the earthquake, by means of devices that participate to the dynamic process. An example are the active mass damper structures (Fig.2.2).

The passive energy input control strategies can be also divided into isolated systems and dissipative systems.

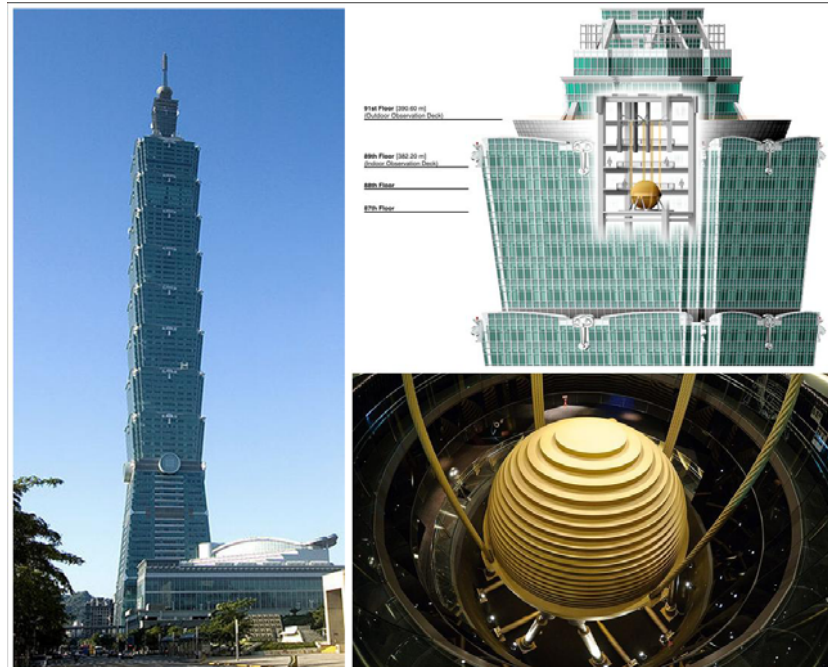


Figure 2.2 Taipei Tower 101, C.Y.Lee & Partners, Taiwan, 2004.

For the Base Isolation system, the design strategy is to modify the vibration period of the structure, by means of special devices between the foundations and the structure itself. These devices, called seismic isolators, exhibit a large horizontal deformation capacity and a large vertical stiffness, in order to carry the vertical loads from the structure to the foundations. The vibration period of the structure is enlarged, so that the part of the elastic response spectrum with high accelerations is avoided. The practical result is a de-coupling of the structure and soil motions and vibrations (Fig. 2.3).

The inter-storey drift for this system is negligible, so that damages in structural and non-structural elements are avoided.

The devices used in this typology can be: rubber bearings (elastomeric isolators), rolling isolators or sliding isolators.

In dissipative systems the seismic energy input is dissipated through inelastic deformation of specific elements. Differently from active control and base isolation, in this case the energy balance is respected, and the dissipated energy is incremented.

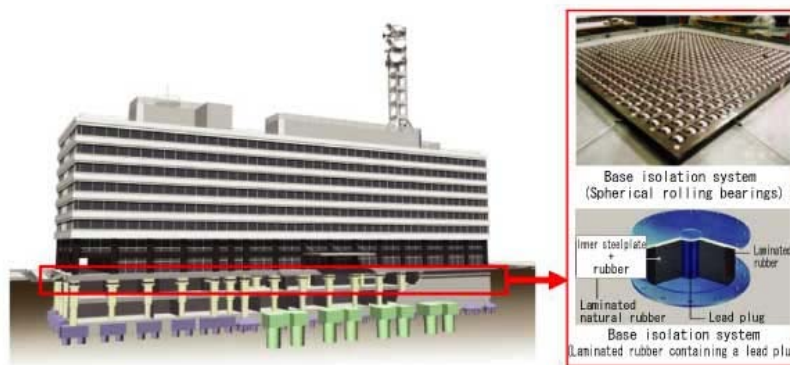


Figure 2.3 Isolated building: Government Building in Nagoya.

Every structure has a their own capacity of dissipating energy, but this can be incremented inserting special devices in the structure or making the plasticization happen in specific parts of the structure.

Seismic design of a structure with dissipative behaviour is based on the Capacity Design philosophy. The preliminary and proper identification of the dissipative zones is a key point. The design has to guarantee the ductility of the dissipative zones or elements and the overstrength of the rest of the structure. In this way it's possible to activate the desired collapse mechanism.

2.1.4 Seismic behaviour of steel structures

Steel structures are extensively used in high seismic risk regions, because of their excellent performances in terms of strength and ductility.

The fulfilment of the design requirements is possible thanks to the mechanical behaviour of materials, structural elements and non structural elements, but also to the wide range of possibilities, in choosing an adequate structural seismic-resistant typology (among traditional and innovative ones).

Structural steel is a ductile material, equally strong in compression and tension, so it is ideally suited for earthquake resistant structures. The common grades of mild steel have adequate ductility and perform well under cyclic reversal of stresses. Moreover, steel is a material produced with high quality control, which aids in Capacity Design.

The sequence of formation of plastic hinges is important in capacity design and so it is necessary to be able to predict the actual yield stress accurately. If the actual strength of members is larger than their design strength, plastic hinges may develop in other members first. In order to avoid this kind of situation, some codes introduce a factor, which is the ratio of the expected yield strength to the specified minimum yield strength for various grades of steel. This factor is also used to ensure that members or connections that must withstand the development of plastic hinges in other members have sufficient strength.

Different criteria have been adopted in order to define the structural collapse under seismic loading. The most used is based on the required maximum plastic deformation: the collapse condition is attained when the required local ductility is greater than available one.

The desired collapse mechanism in case of seismic action is always an overall collapse mechanism. The technique of ensuring a preferred collapse mechanism by suitably adjusting the capacities of the members is called Capacity Design. In practice, it is ensured that the members and joints of the structure have adequate ductility and energy dissipation capacities and the structure as a whole will fail in a preferred collapse mechanism. The type of collapse mechanism in case of steel structures is strictly connected to the particular structural typology adopted.

Traditionally, three families of structural systems have been used for multi-storey buildings in seismic regions: the concentrically braced frames, the moment-resisting frames, and the eccentrically braced frames, which provide a suitable compromise between the properties of the previous two systems.

Steel buildings shall be assigned to one of the structural typologies mentioned before according to the behaviour of their primary resisting structure under seismic actions:

- Moment resisting frames, are those in which the horizontal forces are mainly resisted by members acting in an essentially flexural manner.
- Frames with concentric bracings, are those in which the horizontal forces are mainly resisted by members subjected to axial forces.
- Frames with eccentric bracings, are those in which the horizontal forces are mainly resisted by axially loaded members, but where the eccentricity of the layout is such that energy can be dissipated in seismic links by means of either cyclic bending or cyclic shear.

2.2 CONCENTRIC BRACED FRAME STRUCTURES

2.2.1 Concept and design criteria

Concentric Braced Frame Structures (CBFs) are those in which the horizontal forces are mainly resisted by members subjected to axial forces, so the dissipative zones should be mainly located in the tensile diagonals.

The bracings may belong to one of the following categories:

- active tension diagonal bracings, in which the horizontal forces can be resisted by the tension diagonals only, neglecting the compression diagonals (Fig. 2.4);
- V bracings, in which the horizontal forces can be resisted by taking into account both tension and compression diagonals. The intersection point of these diagonals lies on a horizontal member which shall be continuous (Fig. 2.5);
- K bracings, in which the intersection of the diagonals lies on a column may not be used in seismic zones (Fig. 2.5).

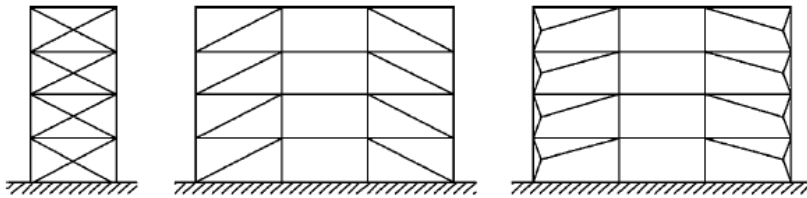


Figure 2.4 CBF with active tension diagonal (EC8).

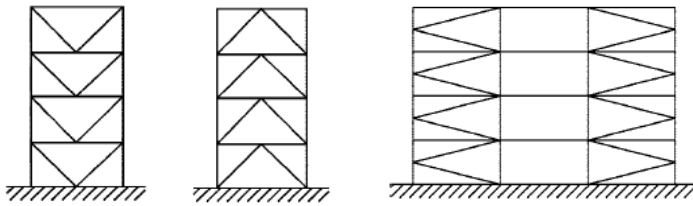


Figure 2.5 CBF with V and K bracings (EC8).

The overall mechanism is activated by the diagonal members that plasticize, granted that the yielding of diagonals in tension happens before than the instability failure of compressed ones.

The inelastic cyclic performance of concentric bracings is rather unsatisfactory due to the repeated buckling of diagonal bars. This produces a progressive reduction of the area of the hysteresis loops, which corresponds to a significant decreasing in the capability of the structure to absorb and dissipate energy. Different behaviours are performed according to the type of bracings. On the other hand, the diagonal members give an elevated stiffness to the structure.

2.2.2 Innovative solutions

In the last years, structural engineering moved towards the study of innovative solutions, to improve the performances of traditional steel typologies in the field of seismic design and retrofitting. In general, these solutions are based on the weakening of the end sections of some elements, to induce the plasticization in specific parts of the structure, or on the insertion of special devices, with the evident advantage of simple substitution of damaged parts after the earthquake.

For CBFs, the solution that consists in the insertion of special devices is that of replacing traditional joints with special dissipative joints. They are semi-rigid joints, and can be divided into pin-connections and U-connections. These kinds of joints are designed with a lower resistance with respect to the one corresponding to the diagonal member instability, to avoid the brace yielding.

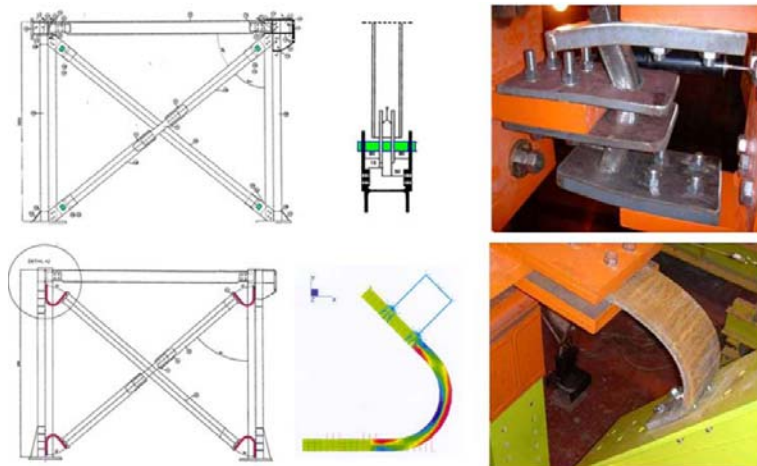


Figure 2.6 Innovative solutions for CBFs: pin and U connections.

Another innovative solution for CBFs are Buckling Restrained Braces (BRB) that are special devices for the dissipation of seismic energy, that differently from conventional concentric bracings, don't exhibit the progressive reduction of resistance in case of cyclic loads, due to the buckling of compressed diagonals.

This new type of braces is composed of two parts: the internal core, designed to the dissipated seismic energy through local buckling, and an external tube, designed to restrain the lateral displacements and so to permit the axial deformation of the internal core. The practical result is the decoupling of the resistance to the axial load from the buckling resistance. In this way, the cyclic response of the BRB results to be more stable than the same response corresponding to a conventional concentric bracing (Fig. 2.7).

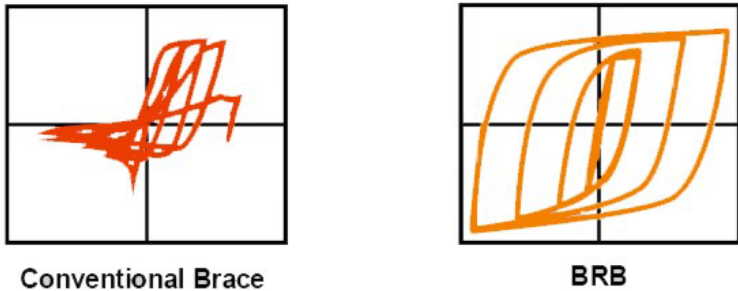


Figure 2.7 Behaviour of compressed brace for CBF and BRB.

There are different kinds of BRB, but the current practice is oriented on two principal models: the unbonded and the all steel solutions (Fig. 2.8).



Figure 2.8 Buckling Restrained Brace: all steel solution.

The first consists in a steel tube, filled with concrete, and a layer of elastomeric material between the concrete and the internal core. The second solution is all made of steel, with the internal core directly in contact with the external tube. In this case the substitution after the damage is simpler.

A further advantage of the BRB solution is that the devices can be simply hid in the external walls, so it can be used successfully also for retrofitting of existing buildings.

Another innovative solution for CBFs is the strategy of weakening of the end sections of diagonal members, obtained making holes in these parts.



Figure 2.9 Reduced Section Solution for CBFs.

The Reduced Section Solution (RSS) (Fig. 2.9) is an innovative solution created to solve a problem of CBF structures, due to seismic codes, that prescribe slenderness limits that cause over-dimensioning of diagonal members. This can cause not-global collapse mechanisms.

So, reducing, by means of holes, the end sections of diagonal members, the global ductility of the structure is increased, inducing the plastic deformations to happen in these zones.

2.2.3 Design criteria according to EC8

Eurocode 8 (UNI EN 1998-1) is the current seismic code for Europe, and in chapter 6 there are the specific rules for steel buildings. In particular, design and detailing rules for frames with concentric bracings are listed below.

Design criteria:

- Concentric braced frames shall be designed so that yielding of the diagonals in tension will take place before failure of the connections and before yielding or buckling of the beams or columns.
- The diagonal elements of bracings shall be placed in such a way that the structure exhibits similar load deflection characteristics at each storey in opposite senses of the same braced direction under load reversals.
- To this end, the following rule should be met at every storey:

$$\frac{|A^+ - A^-|}{A^+ + A^-} \leq 0,05 \quad (2.1)$$

where A^+ and A^- are the areas of the horizontal projections of the cross-sections of the tension diagonals, when the horizontal seismic actions have a positive or negative direction respectively (Fig.2.10).

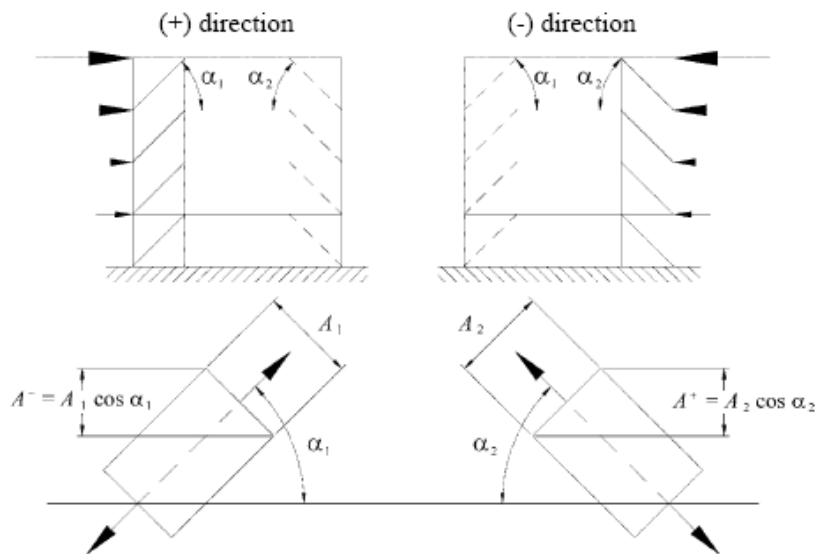


Figure 2.10 Example of application of the expression 2.1.

Analysis:

- Under gravity load conditions, only beams and columns shall be considered to resist such loads, without taking into account the bracing members.

- The diagonals shall be taken into account as follows in an elastic analysis of the structure for the seismic action:
 - in frames with diagonal bracings, only the tension diagonals shall be taken into account;
 - in frames with V bracings, both the tension and compression diagonals shall be taken into account.
- Taking into account of both tension and compression diagonals in the analysis of any type of concentric bracing is allowed provided that all of the following conditions are satisfied:
 - a non-linear static (pushover) global analysis or non-linear time history analysis is used;
 - both pre-buckling and post-buckling situations are taken into account in the modelling of the behaviour of diagonals and;
 - background information justifying the model used to represent the behaviour of diagonals is provided.

Diagonal members:

- In frames with X diagonal bracings, the non-dimensional slenderness $\bar{\lambda}$ as defined in EN 1993-1-1:2004 should be limited to: $1,3 < \bar{\lambda} \leq 2,0$.
The 1,3 limit is defined to avoid overloading columns in the prebuckling stage (when both compression and tension diagonals are active) beyond the action effects obtained from an analysis at the ultimate stage where only the tension diagonal is taken as active.
- In frames with diagonal bracings in which the diagonals are not positioned as X diagonal bracings, the non-dimensional slenderness $\bar{\lambda}$ should be less than or equal to 2,0.
- In frames with V bracings, the non-dimensional slenderness $\bar{\lambda}$ should be less than or equal to 2,0.
- In structures of up to two storeys, no limitation applies to $\bar{\lambda}$.
- The yield resistance $N_{pl,Rd}$ of the cross cross-section of the diagonals should be such that $N_{pl,Rd} \leq N_{Ed}$.
- In frames with V bracings, the compression diagonals should be designed for the compression resistance in accordance with EN 1993.
- The connections of the diagonals to any member should satisfy the following expression:

$$R_d \geq 1,1\gamma_{0V}R_{fy} \quad (2.2)$$

where R_d and R_{fj} are respectively the resistance of the connection and the plastic resistance of the connected dissipative member, and γ_{0V} is the overstrength factor.

- In order to satisfy a homogeneous dissipative behaviour of the diagonals, it should be checked that the maximum overstrength defined as $\Omega_i = N_{pl,Rd,i} / N_{Ed,i}$ does not differ from the minimum value Ω by more than 25%.

- Dissipative semi-rigid and/or partial strength connections are permitted, provided that all of the following conditions are satisfied:

- the connections have an elongation capacity consistent with global deformations;
- the effect of connections deformation on global drift is taken into account using nonlinear static (pushover) global analysis or nonlinear time history analysis.

Beams and columns:

- Beams and columns with axial forces should meet the following minimum resistance requirement:

$$N_{pl,Rd}(M_{Ed}) \geq N_{Ed,G} + 1,1\gamma_{0V}\Omega N_{Ed,E} \quad (2.3)$$

where:

$N_{pl,Rd}(M_{Ed})$ is the design buckling resistance of the beam or the column in accordance with EN 1993, taking into account the interaction of the buckling resistance with the bending moment M_{Ed} , defined as its design value in the seismic design situation;

$N_{Ed,G}$ is the axial force in the beam or in the column due to the non-seismic actions included in the combination of actions for the seismic design situation;

$N_{Ed,E}$ is the axial force in the beam or in the column due to the design seismic action;

γ_{0V} is the overstrength factor;

Ω is the minimum value of Ω_i defined before over all the diagonals of the braced frame system;

- In frames with V bracings, the beams should be designed to resist:

- all non-seismic actions without considering the intermediate support given by the diagonals;

- the unbalanced vertical seismic action effect applied to the beam by the braces after buckling of the compression diagonal. This action effect is calculated using $N_{pl,Rd}$ for the brace in tension and for the brace in compression $\gamma_{pb} N_{pl,Rd}$.

Where γ_{pb} is used for the estimation of the post buckling resistance of diagonals in compression. The recommended value is 0,3.

- In frames with diagonal bracings in which the tension and compression diagonals are not intersecting, the design should take into account the tensile and compression forces which develop in the columns adjacent to the diagonals in compression and correspond to compression forces in these diagonals equal to their design buckling resistance.

2.3 ECCENTRIC BRACED FRAME STRUCTURES

2.3.1 Concept and design criteria

Eccentric Braced Frame Structures (EBFs) are those in which the horizontal forces are mainly resisted by axially loaded members, but where the eccentricity of the layout is such that energy can be dissipated in seismic links by means of either cyclic bending or cyclic shear.

This typology ensures high stiffness and good capabilities of ductility and dissipation of energy.

It can be used a lot of possible configurations that are able to ensure that all links will be active (Fig. 2.11).

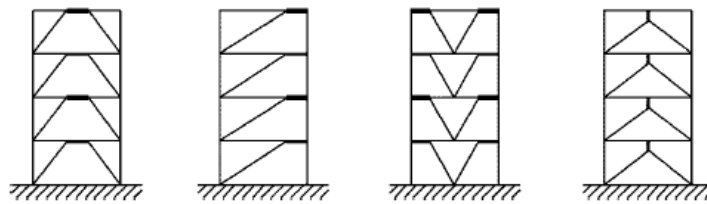


Figure 2.11 Configurations of frames with eccentric braces.

The active link must be designed in order to obtain that its bending and shear limit strength precedes the attainment of the tension and compression limit strength of other elements.

The length of the active link is responsible of the collapse mechanism which dissipates energy. Short links dissipate energy mainly by inelastic shear deformation in the web and so are called shear links; long links dissipate energy mainly by inelastic normal strain in the flanges and so are called moment links.

A careful design of seismic links can lead good hysteresis loops with large stiffness and energy absorption. EBF structures exhibit good strength and stiffness in elastic range, so avoiding non-structural damage, and are also able to provide enough ductility to dissipate large amounts of energy in the inelastic range.

2.3.2 Design criteria according to EC8

Design and detailing rules for frames with eccentric bracings according to Eurocode 8 (UNI EN 1998-1) are listed below.

Design criteria:

- Frames with eccentric bracings shall be designed so that specific elements or parts of elements called seismic links are able to dissipate energy by the formation of plastic bending and/or plastic shear mechanisms.
- The structural system shall be designed so that a homogeneous dissipative behaviour of the whole set of seismic links is realised.
- The rules given hereafter are intended to ensure that yielding, including strain hardening effects in the plastic hinges or shear panels, will take place in the links prior to any yielding or failure elsewhere.
- Seismic links may be horizontal or vertical components.

Seismic links:

- The web of a link should be of single thickness without doubler plate reinforcement and without a hole or penetration.
- Seismic links are classified into 3 categories according to the type of plastic mechanism developed:
 - short links, which dissipate energy by yielding essentially in shear;
 - long links, which dissipate energy by yielding essentially in bending;
 - intermediate links, in which the plastic mechanism involves bending and shear.

- For I sections, the following parameters are used to define the design resistances and limits of categories:

$$M_{p,link} = f_y b t_f (h - t_f) \quad (2.4)$$

$$V_{p,link} = (f_y / \sqrt{3}) t_w (h - t_f) \quad (2.5)$$

where the geometrical parameters are those showed in Figure 2.12.

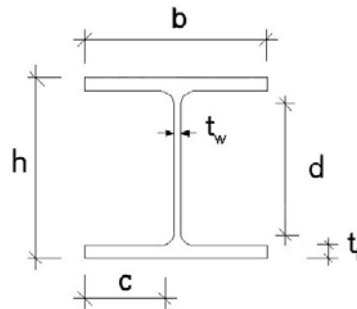


Figure 2.12 Geometrical parameters for I sections.

- If $N_{Ed}/N_{pl,Rd} \leq 0,15$ the design resistance of the link should satisfy both of the following relationships at both ends of the link:

$$V_{Ed} \leq V_{p,link} \quad (2.6)$$

$$M_{Ed} \leq M_{p,link} \quad (2.7)$$

- If $N_{Ed}/N_{pl,Rd} > 0,15$ expressions (2.6) and (2.7) should be satisfied with the following reduced values $V_{p,link,r}$ and $M_{p,link,r}$:

$$V_{p,link,r} = V_{p,link} \left[1 - (N_{Ed} / N_{pl,Rd})^2 \right]^{0,5} \quad (2.8)$$

$$M_{p,link,r} = M_{p,link} \left[1 - (N_{Ed} / N_{pl,Rd}) \right] \quad (2.9)$$

- If $N_{Ed}/N_{pl,Rd} > 0,15$ the link length e should not exceed:

$$e \leq 1,6 M_{p,link} / V_{p,link} \quad \text{when } R < 0,3 \quad (2.10)$$

$$e \leq (1,15 - 0,5R) 1,6 M_{p,link} / V_{p,link} \quad \text{when } R \geq 0,3 \quad (2.11)$$

$$\text{where } R = N_{Ed} t_w (h - 2t_f) / (V_{Ed} A) \quad (2.12)$$

- To achieve a global dissipative behaviour of the structure, it should be checked that the individual values of the ratios $\Omega_i = 1,5 V_{pl,Rd,i} / V_{Ed,i}$ for

short link and $\Omega_i = 1,5 M_{pl,Rd,i} / M_{Ed,i}$ for long links, do not exceed the minimum value Ω by more than 25% .

- In designs where equal moments would form simultaneously at both ends of the link (Fig. 2.13.a), links may be classified according to the length e . For I sections, the categories are:

- short links $e < e_s = 1,6 M_{p,link} / V_{p,link}$ (2.13)

- long links $e < e_L = 3,0 M_{p,link} / V_{p,link}$ (2.14)

- intermediate links $e_s < e < e_L$ (2.15)

- In designs where only one plastic hinge would form at one end of the link (Fig. 2.13.b), the value of the length e defines the categories of the links. For I sections the categories are:

- short links $e < e_s = 0,8(1 + \alpha) M_{p,link} / V_{p,link}$ (2.16)

- long links $e < e_L = 1,5(1 + \alpha) M_{p,link} / V_{p,link}$ (2.17)

- intermediate links $e_s < e < e_L$ (2.18)

where α is the ratio of the smaller bending moments $M_{Ed,A}$ at one end of the link in the seismic design situation, to the greater bending moments $M_{Ed,B}$ at the end where the plastic hinge would form, both moments being taken as absolute values.

- The link rotation angle θ_p (Fig. 2.13) between the link and the element outside of the link should be consistent with global deformations. It should not exceed the following values:

- short links $\theta_p \leq \theta_{pR} = 0,08$ radians (2.19)

- long links $\theta_p \leq \theta_{pR} = 0,02$ radians (2.20)

- intermediate links $\theta_p \leq \theta_{pR} =$ the value determined by linear interpolation between the above values (2.21)

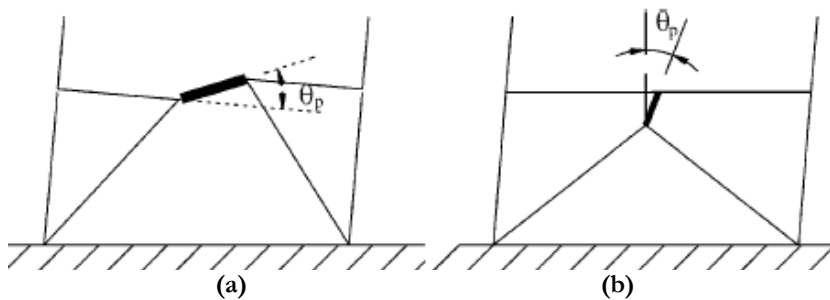


Figure 2.13 Equal moments and unequal moments at link ends.

- Full-depth web stiffeners should be provided on both sides of the link web at the diagonal brace ends of the link. These stiffeners should have a combined width of not less than $(b_f - 2t_w)$ and a thickness not less than $0,75 t_w$ nor 10 mm, whichever is larger.
- Links should be provided with intermediate web stiffeners as follows:
 - short links should be provided with intermediate web stiffeners spaced at intervals not exceeding $(30 t_w - b/5)$ for a link rotation angle θ_p of 0,08 radians or $(52 t_w - b/5)$ for link rotation angles θ_p of 0,02 radians or less. Linear interpolation should be used for values of θ_p between 0,08 and 0,02 radians;
 - long links should be provided with one intermediate web stiffener placed at a distance of 1,5 times b from each end of the link where a plastic hinge would form;
 - intermediate links should be provided with intermediate web stiffeners meeting the requirements above;
 - intermediate web stiffeners are not required in links of length e greater than $5 M_p/V_p$;
 - intermediate web stiffeners should be full depth. For links that are less than 600 mm in depth b , stiffeners are required on only one side of the link web. The thickness of one-sided stiffeners should be not less than t_w or 10 mm, whichever is larger, and the width should be not less than $(b/2) - t_w$. For links that are 600 mm in depth or greater, similar intermediate stiffeners should be provided on both sides of the web.
- Fillet welds connecting a link stiffener to the link web should have a design strength adequate to resist a force of $\gamma_{0V} f_y A_{st}$, where A_{st} is the area of the stiffener. The design strength of fillet welds fastening the stiffener to the flanges should be adequate to resist a force of $\gamma_{0V} A_{st} f_y / 4$.
- Lateral supports should be provided at both the top and bottom link flanges at the ends of the link. End lateral supports of links should have a design axial resistance sufficient to provide lateral support for forces of 6% of the expected nominal axial strength of the link flange computed as $f_y b t_f$.
- In beams where a seismic link is present, the shear buckling resistance of the web panels outside of the link should be checked to conform to EN 1993-1-5:2004, Section 5.

Members not containing seismic links:

- The members not containing seismic links, like the columns and diagonal members, if horizontal links in beams are used, and also the beam members, if vertical links are used, should be verified in compression considering the most unfavourable combination of the axial force and bending moments:

$$N_{Rd}(M_{Ed}, V_{Ed}) \geq N_{Ed,G} + 1,1\gamma_{0V}\Omega N_{Ed,E} \quad (2.22)$$

where $N_{Rd}(M_{Ed}, V_{Ed})$ is the axial design resistance of the column or diagonal member in accordance with EN 1993, taking into account the interaction with the bending moment and the shear taken at their design value in the seismic situation; $N_{Ed,G}$ is the compression force in the column or diagonal member due to the non-seismic actions included in the combination of actions for the seismic design situation; $N_{Ed,E}$ is the compression force in the column or diagonal member due to the design seismic action.

Connections of the seismic links:

- If the structure is designed to dissipate energy in the seismic links, the connections of the links or of the element containing the links should be designed for action effects E_d computed as follows:

$$E_d \geq E_{d,G} + 1,1\gamma_{0V}\Omega_r E_{d,E} \quad (2.23)$$

where $E_{d,G}$ is the action effect in the connection due to the non-seismic actions included in the combination of actions for the seismic design situation; $E_{d,E}$ is the action effect in the connection due to the design seismic action.

- In the case of semi-rigid and/or partial strength connections, the energy dissipation may be assumed to originate from the connections only. This is allowable, provided that all of the following conditions are satisfied:

- the connections have rotation capacity sufficient for the corresponding deformation demands;
- members framing into the connections are demonstrated to be stable at the ULS;
- the effect of connection deformations on global drift is taken into account.

- When partial strength connections are used for the seismic links, the capacity design of the other elements in the structure should be derived from the plastic capacity of the links connections.

2.4 MOMENT RESISTING FRAME STRUCTURES

2.4.1 Concept and design criteria

Moment resisting frame Structures (MRFs) are composed by beams and columns, with rigid or semi-rigid connections, in which the horizontal forces are mainly resisted by members acting in an essentially flexural manner (Fig.2.14). The dissipative zones should be mainly located in plastic hinges in the beams or the beam-column joints so that energy is dissipated by means of cyclic bending. The dissipative zones may also be located in columns: at the base of the frame, at the top of the columns in the upper storey of multi-storey buildings or at the top and bottom of columns in single storey buildings in which N_{Ed} in columns conform to the inequality $N_{Ed} / N_{pl,Rd} < 0,3$.

The distribution of the plastic hinges along the structure has to result in a global collapse mechanism, avoiding local failures.

This system is widely used for low-rise buildings. For medium and high-rise buildings framed structures exhibit too large elastic deformations under low lateral actions, which can produce damage to non-structural elements.

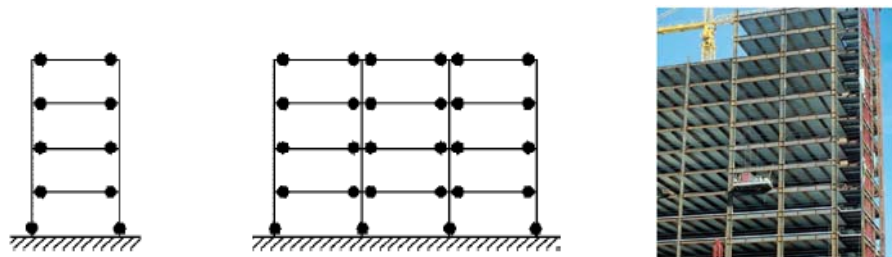


Figure 2.14 Moment resisting frame structures.

On the other hand, the lateral stiffness is low, so the dimensions of members are influenced by the control of lateral displacements, and so

the resulting structure exhibit a huge overstrength and so is overdimensioned with respect to the fulfilment of requirements for ULS. This typology is generally preferred for its architectural versatility, because it permits the maximum flexibility in the use of space, because of the lack of diagonal members.

2.4.2 Innovative solutions

In the last years, structural engineering moved towards the study of innovative solutions, to improve the performances of traditional steel typologies in the field of seismic design and retrofitting. In general, these solutions are based on the weakening of the end sections of some elements, to induce the plasticization in specific parts of the structure, or on the insertion of special devices, with the evident advantage of simple substitution of damaged parts after the earthquake.

For MRFs, a simple and typical solution is the dog-bone, that consists in the weakening of the end section of the beams, where is expected to be the plastic hinge, to encourage the plasticization in the zone with the section reduction, avoiding damage in the rest of the beam, in the column, and in the beam to column joint.

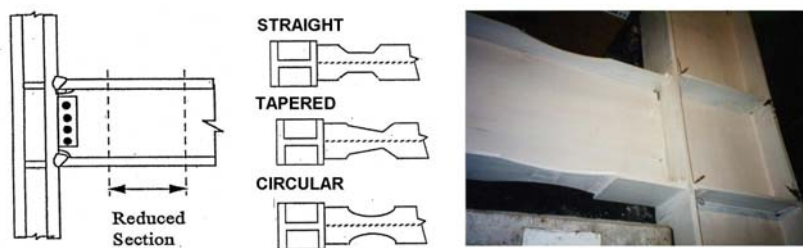


Figure 2.15 Dog-bone in moment resisting frame structures.

Another innovation for MRFs, that consists in the insertion of special devices is the use of the metal shear panels.

These are composed by metallic (steel or aluminium) sheets, inserted in a beam and column frame, with or without stiffening (Fig.2.16). These devices give a good lateral resistance to the structure. Initially used as covering panels, with no structural scope, it was noticed their important influence on the global behaviour of the structure, measuring lateral displacements minor than those expected.



Figure 2.16 Metal shear panels.

Metal shear panels are typical energy dissipation systems, based on the principle of the metal yielding, that are activated by the inter-storey drift, when the structure is subjected to horizontal forces. They are bi-dimensional elements, and so have low transversal resistance and stiffness, but high axial resistance and stiffness.

In metal shear panels, the energy dissipation is basically due to shear mechanism: pure shear or tension field, in which shear buckling in elastic field appears for the panel slenderness, and the lateral load is carried by the tension diagonal that develops in the panel along the direction parallel to the tension field. A pure shear mechanism would be better, because it will produce an inelastic cyclic behaviour and a stable and uniform distribution of the buckling of the panel, able to dissipate energy for the whole structure, protecting it from structural damaging.

The other advantages of this innovation are the low construction costs, the low installation time, and the possibility to make openings, that is important from the architectural point of view (Fig. 2.17).

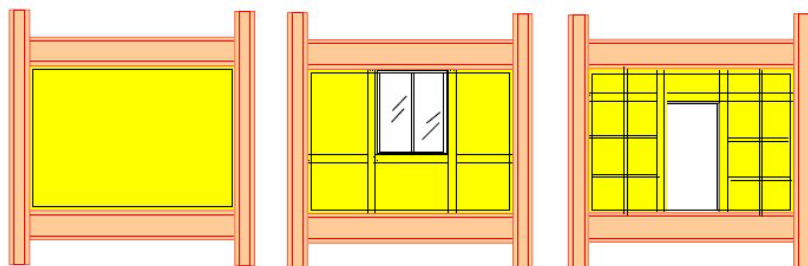


Figure 2.17 Stiffened and unstiffened shear panels with openings.

2.4.3 Design criteria according to EC8

Design and detailing rules for moment resisting frames according to Eurocode 8 (UNI EN 1998-1) are listed below.

Design criteria:

- Moment resisting frames shall be designed so that plastic hinges form in the beams or in the connections of the beams to the columns, but not in the columns. This requirement is waived at the base of the frame, at the top level of multi-storey buildings and for single storey buildings.
- Depending on the location of the dissipative zones:
 - if dissipative zones are located in the structural members, the non-dissipative parts and the connections of the dissipative parts to the rest of the structure shall have sufficient overstrength to allow the development of cyclic yielding in the dissipative parts.
 - if dissipative zones are located in the connections, the connected members shall have sufficient overstrength to allow the development of cyclic yielding in the connections.
- The required hinge formation pattern should be achieved by conforming to the following rules:
 - capacity design provisions shall be satisfied in order to obtain the hierarchy of resistance of the various structural components necessary for ensuring the intended configuration of plastic hinges and for avoiding brittle failure modes.
 - in multi-storey buildings formation of a soft storey plastic mechanism shall be prevented, as such a mechanism might entail excessive local ductility demands in the columns of the soft storey.
 - to satisfy these requirements in moment resisting frame buildings, the following condition should be satisfied at all joints of primary or secondary seismic beams with primary seismic columns:

$$\sum M_{Rc} \geq 1,3 \sum M_{Rb} \quad (2.24)$$

where $\sum M_{Rc}$ is the sum of the design values of the moments of resistance of the columns framing the joint. The minimum value of column moments of resistance within the range of column axial forces produced by the seismic design situation should be used in expression; and $\sum M_{Rb}$ is the sum of the design values of the moments of resistance of the beams framing the joint. When partial strength

connections are used, the moments of resistance of these connections are taken into account in the calculation of ΣM_{Rb} .

Beams:

- Beams should be verified as having sufficient resistance against lateral and lateral torsional buckling in accordance with EN 1993, assuming the formation of a plastic hinge at one end of the beam. The beam end that should be considered is the most stressed end in the seismic design situation.

- For plastic hinges in the beams it should be verified that the full plastic moment of resistance and rotation capacity are not decreased by compression and shear forces. To this end, for sections belonging to cross-sectional classes 1 and 2, the following expressions should be verified at the location where the formation of hinges is expected:

$$M_{Ed} \leq M_{pl,Rd} \quad (2.25)$$

$$N_{Ed} \leq 0,15N_{pl,Rd} \quad (2.26)$$

$$V_{Ed} \leq 0,5V_{pl,Rd} \quad (2.27)$$

where $V_{Ed} = V_{Ed,G} + V_{Ed,M}$, $V_{Ed,G}$ is the design value of the shear force due to the non-seismic actions, and $V_{Ed,M}$ is the design value of the shear force due to the application of the plastic moments with opposite signs at the end sections of the beam.

Columns:

- The columns shall be verified in compression considering the most unfavourable combination of the axial force and bending moments. In the checks, N_{Ed} , M_{Ed} , V_{Ed} should be computed as:

$$N_{Ed} = N_{Ed,G} + 1,1\gamma_{0V}\Omega N_{Ed,E} \quad (2.28)$$

$$M_{Ed} = M_{Ed,G} + 1,1\gamma_{0V}\Omega M_{Ed,E} \quad (2.29)$$

$$V_{Ed} = V_{Ed,G} + 1,1\gamma_{0V}\Omega V_{Ed,E} \quad (2.30)$$

- In columns where plastic hinges form the verification should take into account that in these plastic hinges the acting moment is equal to $M_{pl,Rd}$.

- The resistance verification of the columns should be made in accordance with EN 1993-1-1:2004, Section 6.

- The shear resistance of framed web panels of beam/column connections should satisfy the following expression:

$$V_{wp,Ed} \leq V_{wp,Rd} \quad (2.31)$$

where $V_{wp,Ed}$ is the design shear force in the web panel due to the action effects, taking into account the plastic resistance of the adjacent dissipative zones in beams or connections; and $V_{wp,Rd}$ is the shear resistance of the web panel. It is not required to take into account the effect of the stresses of the axial force and bending moment on the plastic resistance in shear.

- The shear buckling resistance of the web panels should also be checked to ensure that it conforms to EN 1993-1-5:2004, Section 5:

$$V_{wp,Ed} \leq V_{wb,Rd} \quad (2.32)$$

where $V_{wb,Rd}$ is the shear buckling resistance of the web panel.

Beam to column connections:

- If the structure is designed to dissipate energy in the beams, the connections of the beams to the columns should be designed for the required degree of overstrength taking into account the moment of resistance and the shear force:

$$R_d \geq 1,1\gamma_{0V}R_{fy} \quad (2.32)$$

where R_d is the resistance of the connection and R_{fy} is the plastic resistance of the connected members, based on the design yield stress of the material.

- Dissipative semi-rigid and/or partial strength connections are permitted, provided that all of the following requirements are verified:

- the connections have a rotation capacity consistent with the global deformations;
- members framing into the connections are demonstrated to be stable at the ultimate limit state (ULS);
- c) the effect of connection deformation on global drift is taken into account using nonlinear static (pushover) global analysis or nonlinear time history analysis.

- The connection design should be such that the rotation capacity of the plastic hinge region θ_p is not less than 35 mrad for structures of ductility class DCH and 25 mrad for structures of ductility class DCM with $q > 2$. The rotation θ_p is defined as (Fig. 2.18):

$$\theta_p = \delta / 0,5L \quad (2.33)$$

where δ is the beam deflection at midspan and L is the beam span.

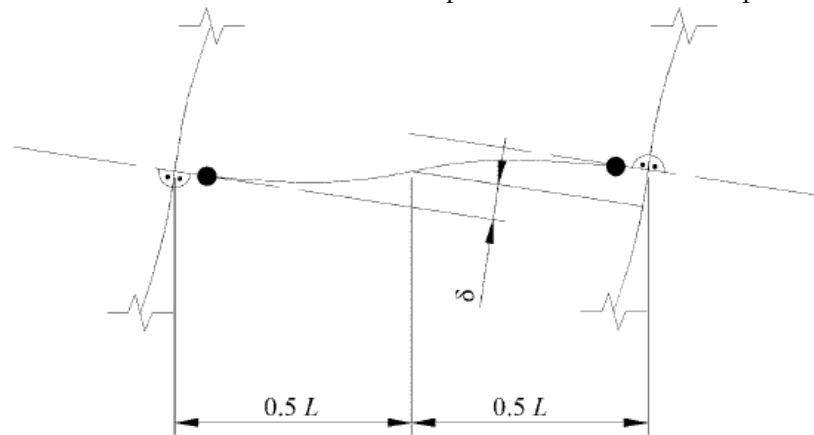


Figure 2.18 Beam deflection for the calculation of θ_p .

- The rotation capacity of the plastic hinge region θ_p should be ensured under cyclic loading without degradation of strength and stiffness greater than 20%. This requirement is valid independently of the intended location of the dissipative zones.
- The column elastic deformation should not be included in the evaluation of θ_p .
- When partial strength connections are used, the column capacity design should be derived from the plastic capacity of the connections.

2.5 WORKED EXAMPLES AND COMPARISONS

The philosophy of Performance-based design (PBD) aims all the modern seismic codes. As it is well known, EN 1998:1-1 implements a performance-based structural engineering framework, providing two performance objectives: life safety and damage limitation of a buildings at two corresponding levels of earthquake motions. EN 1998:1-1 does not provide any further design and verification criteria against strong ground motion corresponding to the collapse prevention limit state. This implies that frames designed according to EN 1998:1-1 have to exhibit some extra-capacity in order to face such unexpected catastrophic events. With the aim to evaluate this residual capacity, different steel structural typologies (CBFs, EBFs, MRFs), designed according to Eurocode 8 principles, exposed in the above paragraphs, have been analyzed by means of non linear multimodal pushover analyses (Chopra 2004). The drifts and the local ductility demand have been monitored in order to evaluate both the seismic performance and the erection costs for the different examined structural typologies.

2.5.1 Structural design according to EC8: the case study

In order to compare the seismic performance the erection and the erection costs, a six-storey residential building has been used as a case study. The seismic-resistant system has been alternatively designed for the same initial input data. In such a way it has been possible to directly compare the relevant outcomes.

The case study is a six storey residential building with a rectangular plan, 31.00 m x 24.00 m (Fig. 2.19).

The storey height is equal to 3.50 m with exception of the first floor, which is 4.00 m high.

A uniform mass distribution on the floor has been assumed. The floor mass assigned to each frame are obtained by the applied design loads that are $G_k=4.20\text{kN/m}^2$ and $Q_k= 2\text{kN/m}^2$.

The elastic design spectrum is taken from EC8: type 1, ground type C, PGA on bedrock = 0.25g.

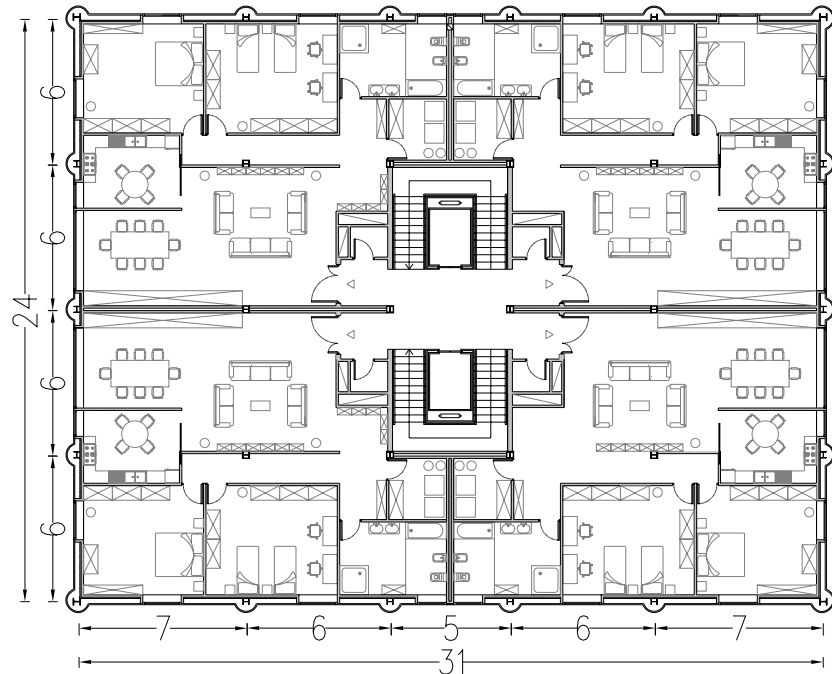


Figure 2.19 Architectural plan of the typical floor.

Under these assumptions the seismic-resistant systems have been alternatively designed as follows:

- For the CBFs solution two different bracing typologies were adopted: X bracings in X direction and inverted V bracings in Y direction. There are four braced frames in each main plan direction and two braced field in each frame, with a total amount of eight braced fields in each direction. S275 steel grade was used for both beams and columns and S235 steel grade for diagonal bracings, which are made of circular hollow cold formed sections.

- For the EBFs solution the short link typology was adopted for both directions. There are two braced frames for each direction and one braced field for each frame, with the total amount of four braced fields in the whole structure. S275 steel grade was used for beams columns and diagonal bracings.

- For MRFs it was adopted the spatial frame configuration. S275 steel grade was used for beams and S355 steel grade for columns. The latter are made of two double-T shaped sections placed orthogonally (by

cutting one of them into two parts and then welding on the web of the other one).

Figure 2.20 shows the schematic view of the structural layout of the typical floor and the location in plan of bracings for CBFs and EBFs and Figures 2.21 to 2.23 show the vertical configuration of the three seismic resistant systems in the two main plan directions and the relevant cross-section labelling.

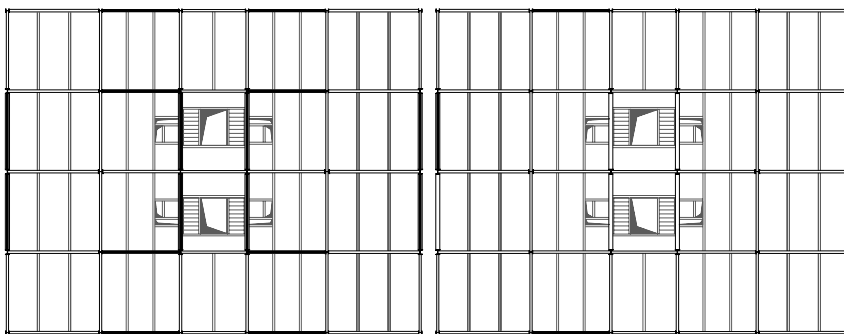


Figure 2.20 Structural plan of the typical floor and plan location of braces in CBFs and EBF.

The numerical models of steel CBFs, EBFs and MRFs have been developed adopting the software SAP2000 v.11. For all the examined cases, planar models with lumped masses and mono-dimensional elements having lumped plasticity have been used, moreover $P-\Delta$ effects have been taken into account.

In detail, for CBFs axial plastic hinges in braces and columns have been positioned at their middle length. The linear branches in the post-buckling response have been obtained on the basis of an equal energy approximation of the brace axial force-deformation relationship given by Georgescu (1996).

For EBFs the non-linear behaviour of shear links has been simulated using the shear force vs. shear displacement relationship proposed by Ricles & Popov (1994).

For MRFs the non-linear behaviour of beams and columns has been simulated by perfectly plastic non-linear hinges.

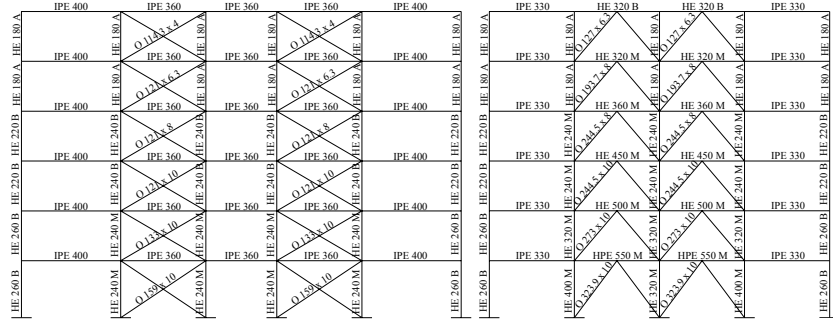


Figure 2.21 Vertical configuration and cross sections of CBFs.

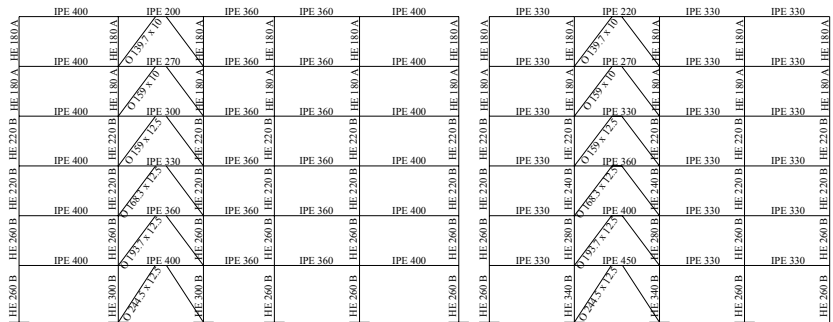


Figure 2.22 Vertical configuration and cross sections of EBFs.

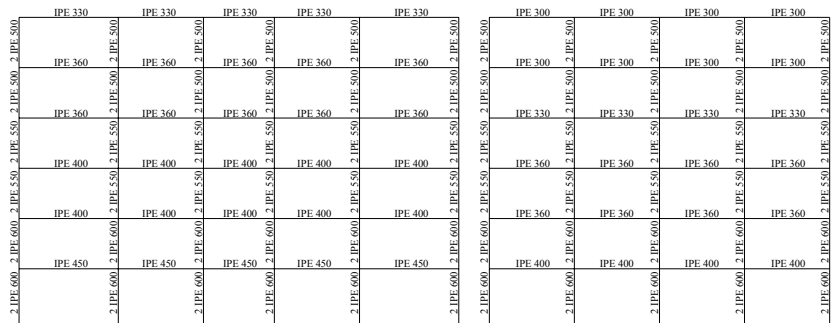


Figure 2.23 Cross sections of MRFs.

2.5.2 Seismic analysis

For the preliminary assessment of the actual capacity and seismic demand, a set of nonlinear static analyses of all the structural models have been performed. Taking into account the regularity of structures, among the pushover procedures suggested by literature, the modal pushover analysis (MPA) procedures proposed by Chopra (2004) was selected. This method combines the improved estimation of demands (allowing to take into account the contribution of higher modes) with the conceptual simplicity and computational attractiveness of nonlinear static pushover procedures.

Therefore, the seismic assessment is performed comparing in Acceleration Displacement Response Spectrum (ADRS) format, the demand, that is represented by the response spectrum, to the structural capacity, that is represented by the modal pushover curves. The modal pushover is performed drawing up to the target displacement demand relevant to each mode. The inelastic displacement demand is computed using available $R-\mu-T$ relationships for each mode and then peak displacement demands associated to the first two modes are combined according to SRSS rule.

Concentric Braced Frame structures:

Figure 2.24 illustrates the fundamental modal shapes of the X-CBFs (placed in the X-direction of the building) and inverted-V CBFs (placed in the Y-direction of the building).

Figure 2.25 shows the two inelastic modal pushover curves normalized in the ADRS format, both for X and Y directions, compared with the elastic demand ADRS spectra, obtained scaling from 0.1 to 2.5 the design PGA (a_g).

In Figures 2.26, 2.27 the SRSS combination of the peak displacement demands in terms of inter-storey drift ratios associated to the first two modes are shown.

Figures 2.28, 2.29 show the ductility demands at the peak displacement response of compression braces normalized as respect to their displacement capacity estimated according to the Tremblay (2002).

Both damage parameters are calculated for different scaled values of PGA to show the different behaviour of the structure at different performance levels.

At the design PGA ($1a_g$), both structures are characterized by a first-mode dominated response with buckling in compression of braces and, only for inverted-V CBFs, non relevant plastic flexural engagement of beams. Increasing the seismic demand up to $2.5 a_g$ the damage concentration of the buckled braces was clearly evident at some storey. For X CBFs, braces in tension are moderately engaged in plastic range, while in case of inverted-V CBFs they are still in elastic field.

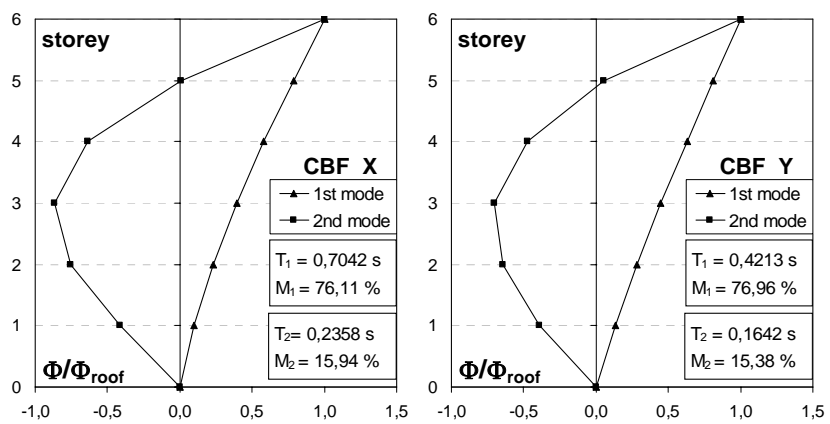


Figure 2.24 Modal shapes of CBFs in X and Y direction.

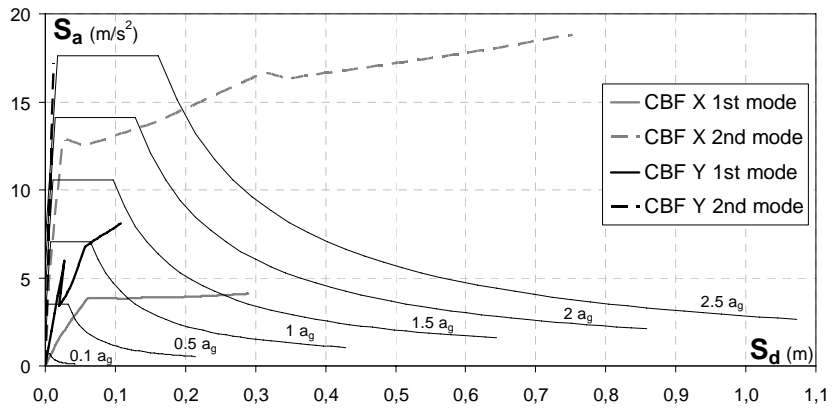


Figure 2.25 Inelastic Modal Pushover curves compared with Elastic Spectra for different a_g in ADRS format for CBFs.

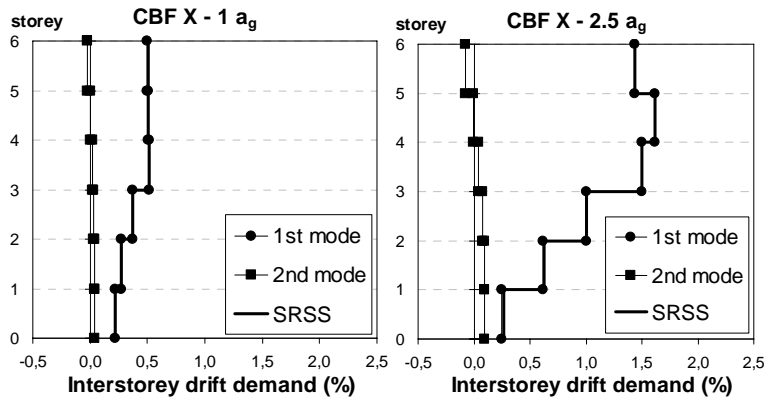


Figure 2.26 Inter-storey drifts for X-CBFs.

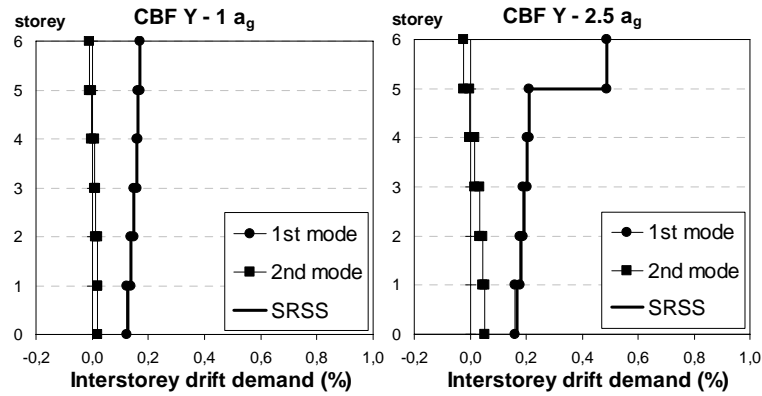


Figure 2.27 Inter-storey drifts for inverted-V CBFs.

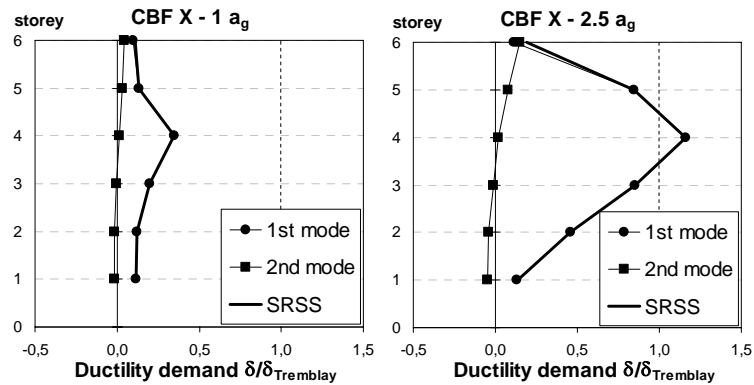


Figure 2.28 Ductility demand for braces in X direction.

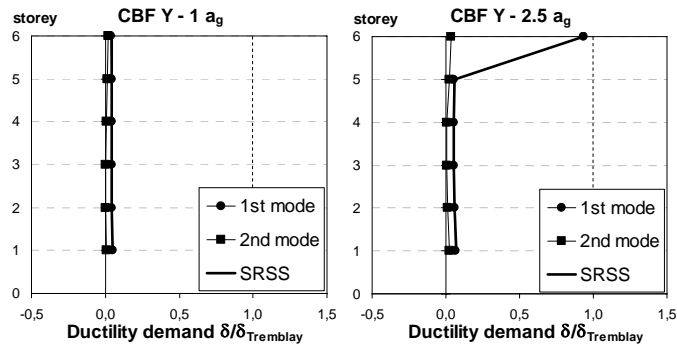


Figure 2.29 Ductility demand for braces in Y direction.

Eccentric Braced Frame structure:

Figure 2.30 illustrates the fundamental modal shapes of the EBFs. Figure 2.31 shows the two inelastic modal pushover curves normalized in the ADRS format, both for X and Y directions, compared with the elastic demand ADRS spectra, obtained scaling from 0.1 to 2.5 the design PGA (a_g).

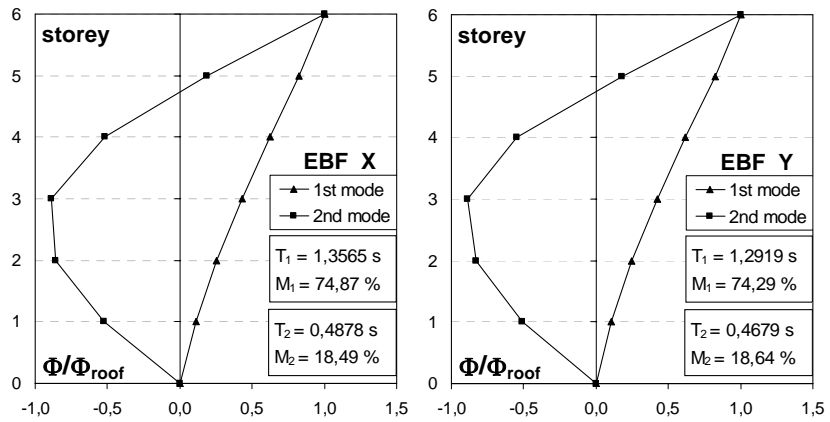


Figure 2.30 Modal shapes of EBFs in X and Y direction.

The SRSS combination of peak displacement demands in terms of inter-storey drift ratios associated to the first two modes are shown in Figures 2.32, 2.33.

The ductility demands at the peak displacement response of shear links normalized as respect to their rotation capacity equal to 0.08 rad are shown in Figures 2.34, 2.35.

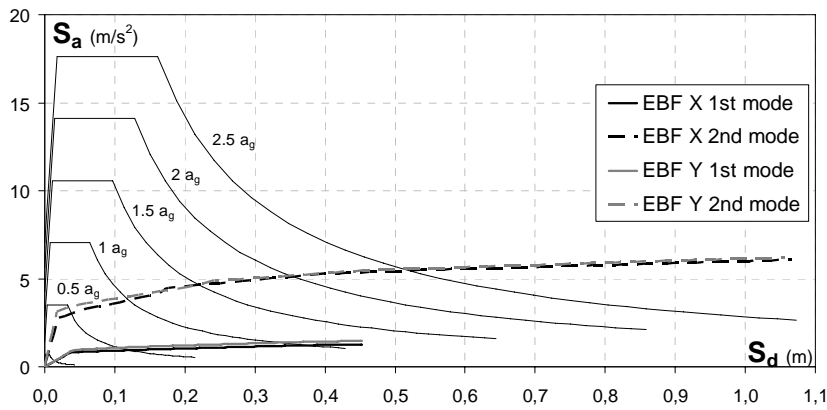


Figure 2.31 Inelastic Modal Pushover curves compared with Elastic Spectra for different a_g in ADRS format for EBFs.

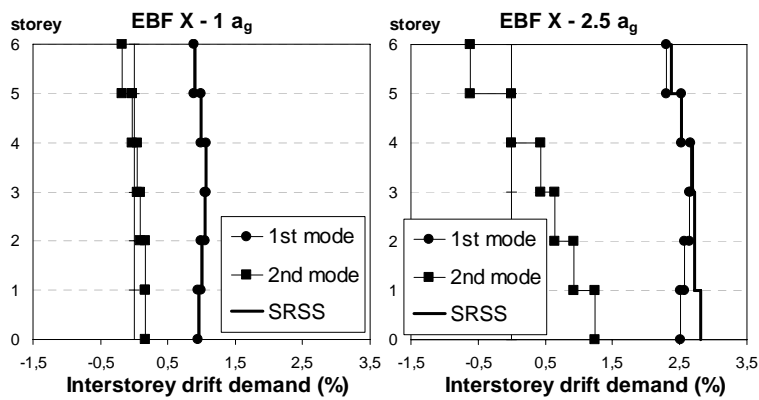


Figure 2.32 Inter-storey drifts for EBFs in X direction.

Both damage parameters are calculated for different values of a_g to show the different behaviour of the structure at different performance levels. For brevity sake, in this paper are shown the ductility demand at $1a_g$ (corresponding to the design acceleration) and $2.5a_g$ (corresponding to the maximum expected seismic event).

The structure is characterized by a first-mode dominated response developing an overall mechanism, with plastic engagement of shear links well distributed along the height of the building. However, differently from the previous case the effect of the second mode is not negligible. Indeed, as shown in Figures 2.34, 2.35, the second modes modify the displacement distribution along the height of the building.

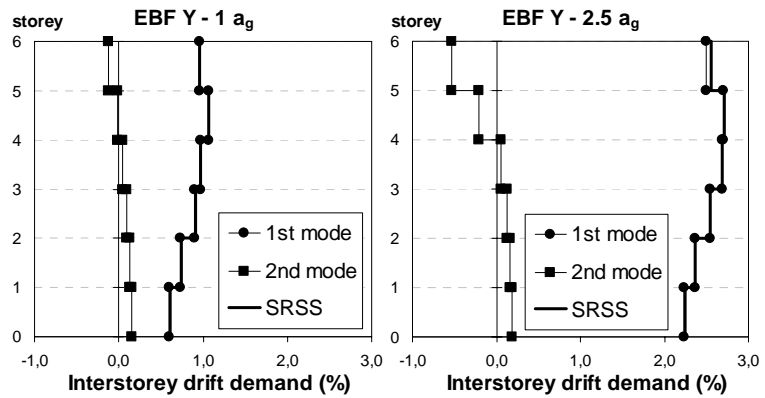


Figure 2.33 Inter-storey drifts for EBFs in Y direction.

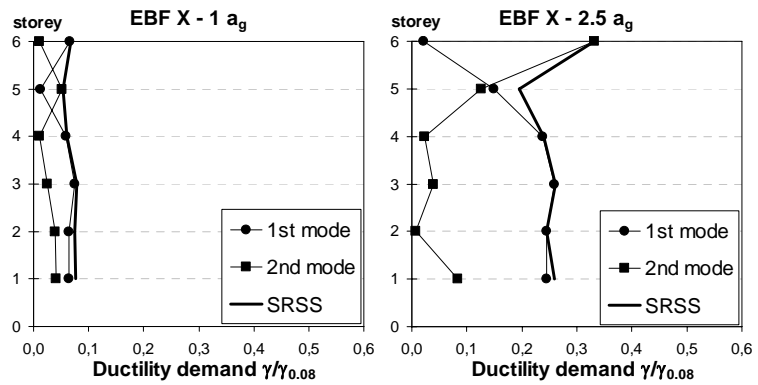


Figure 2.34 Ductility demand for braces in X direction.

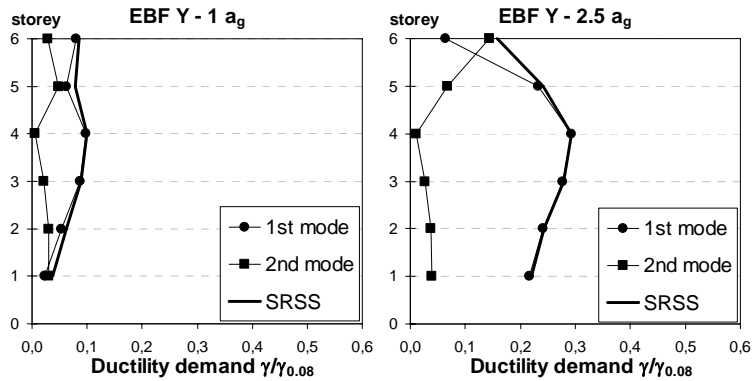


Figure 2.35 Ductility demand for braces in Y direction.

Moment Resisting Frame structure:

Figure 2.36 illustrates the fundamental modal shapes of the MRFs. Figure 2.37 shows the two inelastic modal pushover curves normalized in the ADRS format, both for X and Y directions, compared with the elastic demand ADRS spectra, obtained scaling from 0.1 to 2.5 the design PGA (a_g).

The structure is characterized by a first-mode dominated response with all beams at each storey involved in the plastic mechanism.

Figures 2.38, 2.39 show the SRSS combination of the peak displacement demands in terms of inter-storey drift ratios associated to the first two modes.

Figures 2.40, 2.41 show the ductility demand in terms of beam rotation, normalized as respect to their rotation capacity estimated by means of the relationship proposed by Mazzolani & Piluso (1996).

Both damage parameters are calculated for different values of a_g to show the different behaviour of the structure at different performance levels.

As it can be observed the ductility demand at the design PGA. (a_g) is far from the ultimate deformation capacity of the beams, while it is theoretically exceeded at $2.5a_g$.

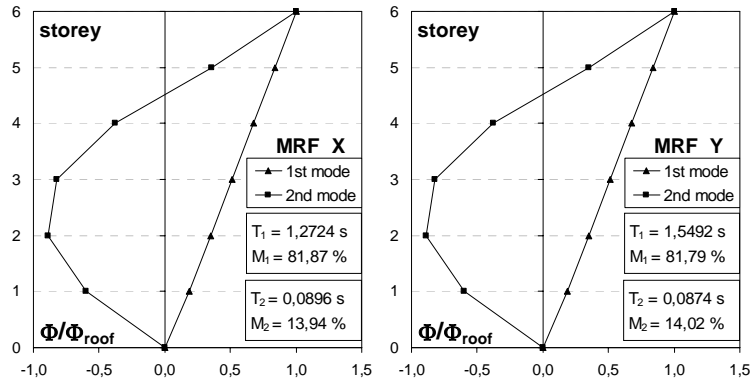


Figure 2.36 Modal shapes of MRFs in X and Y direction.

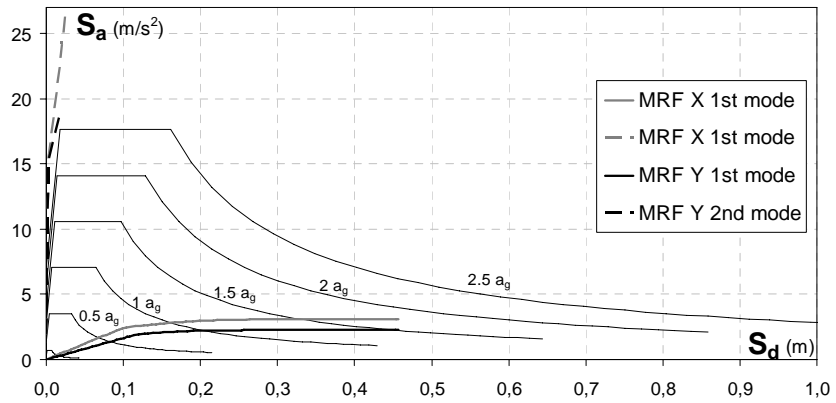


Figure 2.37 Inelastic Modal Pushover curves compared with Elastic Spectra for different a_g in ADRS format for MRFs.

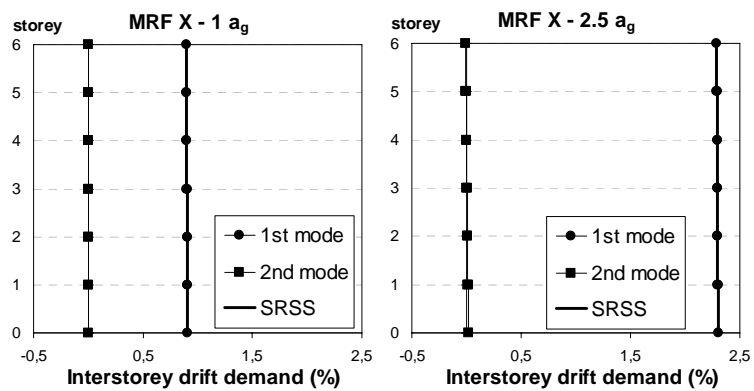


Figure 2.38 Inter-storey drifts for MRFs in X direction.

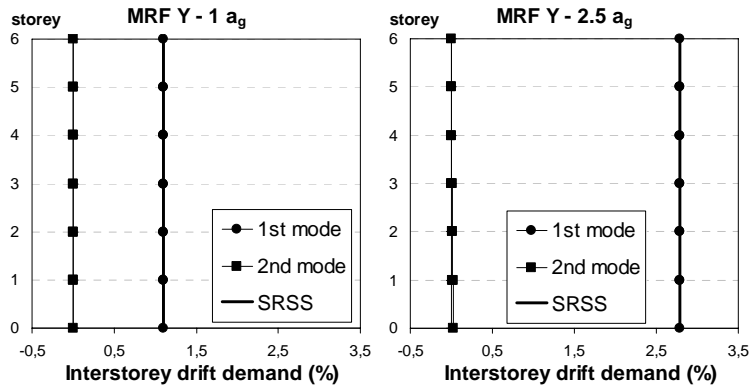


Figure 2.39 Inter-storey drifts for MRFs in Y direction.

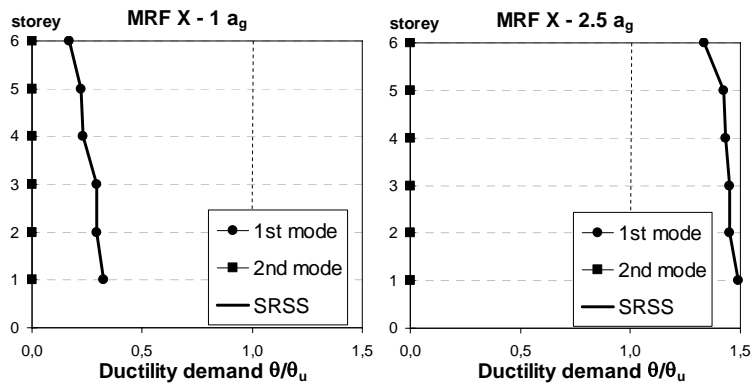


Figure 2.40 Ductility demand for beams in X direction.

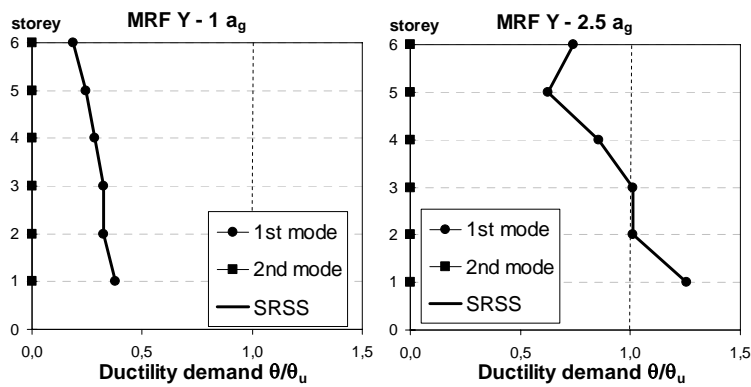


Figure 2.41 Ductility demand for beams in Y direction.

2.5.3 Results and comparative analysis

Weight incidence:

The three structural solutions significantly differ in terms of self weight. In particular, EBF is the less expensive in terms of steel weight as respect to the total seismic weight, with a percentage of steel weight equal to 8.9%. While 12,5% and 11,2% are estimated for CBFs and MRFs, respectively.

This difference is more evident comparing the weight incidence of the seismic resistant structure on the total structural members' weight. In this case EBFs incidence is of 3,9% , while 34,8% for CBFs and 26,1% for MRFs (Fig. 2.42).

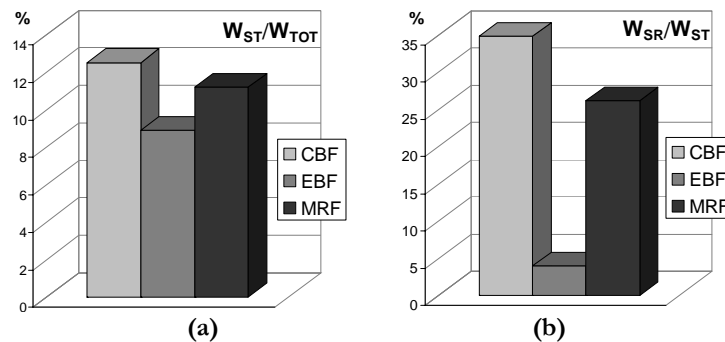


Figure 2.42 Incidence of steel weight on the total seismic weight (a); incidence of the seismic-resistant weights on the total steel weight (b).

Seismic performance:

Comparing the pushover capacity curves of all examined structural typologies (Fig. 2.43) it is possible to recognize that both EBFs and MRFs exhibit large displacement ductility as respect to CBFs. Indeed, displacement capacity of the latter structures is impaired by the ductility capacity of the braces in compression. In addition, the maximum base shear forces of CBFs are larger than those exhibited by EBFs and MRFs. This implies higher forces transmitted to foundations in the former case, which correspond to higher costs of construction.

On the contrary, EBFs and MRFs exhibit larger inter-storey drift demands and larger plastic engagement along the structure than those required to CBFs. This can be observed in Figure 2.44, where the roof displacement demand of the six structural models at different values of seismic input (obtained scaling the design peak ground acceleration from

0.1 to 2.5) is plotted. Indeed, the ductility demand does not increase linearly with a_g , and the EBFs and MRFs exhibit the larger displacement demands than CBFs.

As a consequence, in EBFs and MRFs the final damage should result harder, thus resulting in higher repairing costs and burdensome rehabilitation works (especially for MRFs which exhibit the larger plastic engagement of beams and inter-storey drift demand).

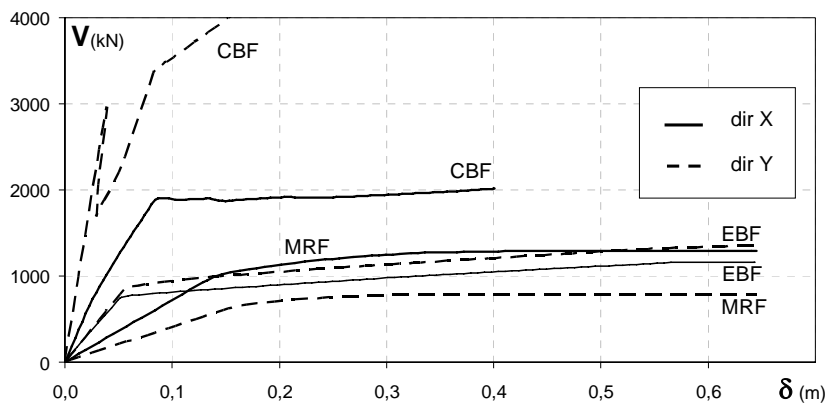


Figure 2.43 Comparison of the pushover curves of the three structures in X and Y direction.

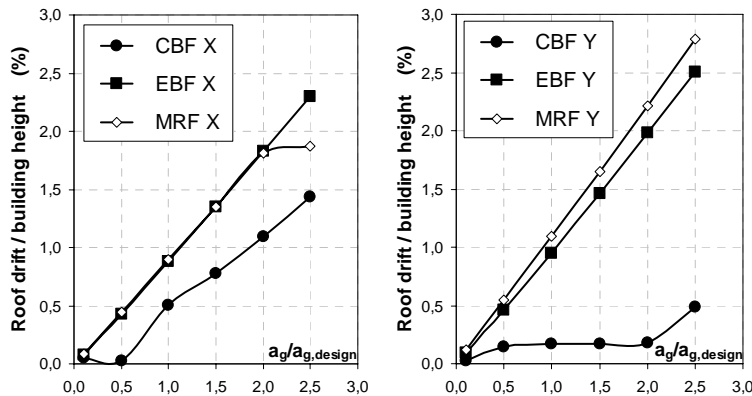


Figure 2.44 Comparison of the roof drift normalized to building height at different a_g .

The assessment of seismic capacity of EC8 compliant structures has been carried out under severe earthquake in order to quantify their extra-

resistance as respect to that strictly required by design earthquake. To this aim the same structure has been alternatively designed with Concentric Braced Frames (CBFs), Eccentric Braced Frames (EBFs) and Moment Resisting Frames (MRFs) according to EC8 and then analyzed. The numerical outcomes show that all the examined structures could exhibit a sufficient extra capacity as respect to the design demand. However, each structural typology showed a different seismic response. CBFs showed the lower drift demands and the lower level of damage, but the larger base shear forces which correspond higher forces transmitted to foundations than those exhibited by EBFs and MRFs. On the contrary, EBFs and MRFs exhibit larger inter-storey drift demands and larger plastic engagement along the structure than those required to CBFs. Thus a final damage state results with higher repairing costs. Therefore, a multi-criteria analysis must be performed to select the best structural typology, which depends on the peculiar design needs.

3 FLEXURAL CAPACITY OF STEEL BEAMS

The present chapter is about the state of the art on the flexural capacity of steel beams. Starting from the general concepts of global and local ductility, and the consideration that in steel MRFs, the overall ductile behaviour is assured by the rotation capacity of steel beams, definitions and methods for the prediction of both rotation capacity and flexural overstrength of steel beams are provided. In the end, the interpretation of these concepts by current codes is analyzed.

3.1 DUCTILITY OF STEEL STRUCTURES

Before 1960s the concept of ductility was used only for characterizing the material behaviour, but nowadays the term “ductility” has been extended to a structural level. In particular, in seismic resistant design, ductility is used referring to the evaluation of the performance of the structure, while for plastic design the ductility is the ability of a structure to undergo deformations beyond first yielding, without significant reduction of ultimate strength (Gioncu & Mazzolani, 2002) .

The following ductility types are widely used in technical literature (Gioncu,1999):

- material ductility, or deformation ductility, which characterizes the material plastic deformations for different loading types;
- cross-section ductility, or curvature ductility, which refers to the plastic deformations of the cross-section, considering the interaction between the parts composing the cross-section itself;
- member ductility, or rotation capacity, when the properties of members are considered;
- structure ductility, or displacement ductility, which considers the overall behaviour of the structure. This kind of ductility allows to predict the ultimate capacity of a structure, which is the most important criteria for the design of structures under conventional loads;

- energy ductility, when the ductility is considered the quantity of seismic energy dissipated through plastic deformations. In this case the use of ductility concept gives the possibility to reduce the seismic design forces and allows to produce some controlled damage in the structure also in case of strong earthquakes.

DUCTILITY TYPE	SCHEME	DEFINITION
MATERIAL DUCTILITY (deformation ductility)		$\mu_\epsilon = \frac{\epsilon_u - \epsilon_y}{\epsilon_y}$
CROSS-SECTION DUCTILITY (curvature ductility)		$\mu_\chi = \frac{\chi_u - \chi_y}{\chi_y}$
MEMBER DUCTILITY (rotation ductility)		$\mu_\theta = \frac{\theta_u - \theta_y}{\theta_y}$
STRUCTURE DUCTILITY (displacement ductility, kinematic ductility)		$\mu_\delta = \frac{\delta_u - \delta_y}{\delta_y}$
ENERGY DUCTILITY (hysteretic ductility)		$\mu_E = \frac{E_p - E_y}{E_y}$

Figure 3.1 Ductility types (Gioncu & Mazzolani, 2002).

The correlation between these different concepts is simple to explain: the energy ductility is the cumulation of structure and member ductilities, the member ductility depends on cross-section and material ductilities (Gioncu & Mazzolani, 2002).

In seismic design, also the concept of “ductility limit” is very important, that is not necessary the largest possible energy dissipation, but the value

of ductility beyond which the behaviour of structure is expected to change significantly.

Two ductility limits can be defined (Gioncu, 1998):

- available ductility, resulting from the behaviour of structures and taking into account its conformation, material properties, cross-section type, gravitational loads, degradation in stiffness and strength due to plastic excursions, etc.
- required ductility, resulting from the earthquake actions, in which all factors influencing these actions are considered: magnitude, ground motion type, soil influence, natural period of structure vs ground motion period, number of important cycles, etc.

For seismic design, the common practice to dissipate the seismic input energy is through the inelastic behaviour of the structure. So a predefined level of structure ductility has to be assured, through plastic deformations, using appropriate constructional details and accepting some damage during severe earthquakes.

The plastic behaviour of a structure depends upon the amount of moment redistribution. The attainment of the predicted collapse load is related to the position of the plastic hinges, where sections reach the full plastic moment, and to the plastic rotation which other hinges can develop elsewhere. Hence, a good behaviour of a plastic hinge requires a certain amount of ductility, in addition to its strength requirements. The rotation capacity is the more rational measure of this ductility. The limitation to plastic rotation is usually given by flexural-torsional instability, local buckling or brittle failure of members, that is the reason for the division in cross-section behavioural classes. The classification used for plastic design is also very useful for seismic design, but some corrections must be introduced, due to the fact that in plastic design the loading system is monotonic, while in the seismic design is cyclic, and an accumulation of plastic deformation occurs (Gioncu & Mazzolani, 2002). In brief, to obtain a globally ductile behaviour of the structure, members must show a locally ductile behaviour. The rotation capacity is a measure of local ductility, so in the following paragraphs there is a state of the art review on the definitions of rotation capacity existing in technical literature, and of the methods for the prediction of its values. Moreover, the same excursus was made for the flexural overstrength, that is another important factor influencing the member behaviour.

3.2 ROTATION CAPACITY OF STEEL BEAMS

3.2.1 Definitions

The rotation capacity (R) is the measure of the flexural ductility of steel beams, being the ability of a cross-section to satisfy the rotation requirement. R may be defined by two commonly ways: one is evaluated from the moment–curvature relationship and the other is based on the moment–rotation behaviour. Both approaches define the rotation capacity as a non-dimensional parameter, whose meaning is described in the following figures, where the generalized moment–curvature and moment–rotation curves for a section capable of sustaining plastic deformation is plotted.

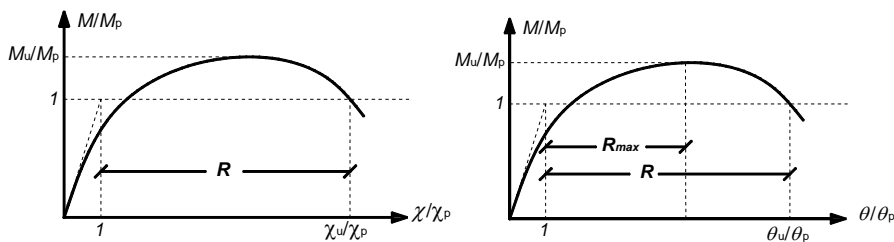


Figure 3.2 Moment-curvature and moment-rotation curves.

The moment–curvature based approach has been widely used in literature for the study of cold-formed steel sections in a four-point bending arrangement (Korol & Hudoba 1972, Hasan & Hancock 1989, Zhao & Hancock 1991, Wilkinson & Hancock 1998). According to this approach the parameter R is defined by the following equation:

$$R = \frac{\chi_u - \chi_p}{\chi_p} = \frac{\chi_u}{\chi_p} - 1 \quad (3.1)$$

where χ_p is evaluated as M_p/EI and χ_u is the limiting curvature at which the moment resistance drops back below M_p .

Similarly, the definition of R , based on the moment–rotation relationship has been commonly used in the literature, but on this base, two different approaches can be followed: to define the rotation capacity by

considering the stable part of the M- θ curve, being θ_p the rotation corresponding to the flexural yielding and θ_{\max} the plastic rotation corresponding to the maximum value of the moment M_{\max} . This approach has been followed by some authors such as Kemp (1985), Kato (1990) and others, and it can be described by the equation:

$$R_{\max} = \frac{\theta_{\max} - \theta_p}{\theta_p} = \frac{\theta_{\max}}{\theta_p} - 1 \quad (3.2)$$

The alternative approach is to define the rotation capacity by considering also the unstable branch of the M- θ curve, up to the value θ_u , the ultimate beam rotation, which corresponds to the plastic moment M_p in the lowering curve. This approach has been followed by some authors such as Luckey & Adams (1969), Kuhlman (1986), Spangemacher (1991) and others. Rotation capacity based on this kind of moment-rotation relationship is defined by the equation:

$$R = \frac{\theta_u - \theta_p}{\theta_p} = \frac{\theta_u}{\theta_p} - 1 \quad (3.3)$$

Thanks to its clearness, the moment-rotation approach is the most effective and useful for experimental purposes. This is the reason that induced most of the researches in using it. And in particular the second formulation, based on the ultimate rotation, seems to be the most accredited and spread.

3.2.2 Predictive methods

In general, R can be directly obtained from experimental tests, measuring and calculating the rotations θ_u and θ_p . However, several methods to evaluate the beam rotation capacity are proposed by different authors, which can be grouped in the following methods:

- **Theoretical methods:** the evaluation of the rotational capacity is based on the approximate theoretical evaluation of the relationship moment-curvature of the section and on the theoretical analysis of the instability phenomena (particularly the local instability of the compressed

flange). Indeed, both the effects derived from the geometric configuration of the section and the mechanical imperfections are neglected, although they affect the flexural curvature. Under this hypothesis, the theoretical investigation of the relationship moment - curvature can be addressed assuming an ideal section made of two concentrated masses. This approach has been adopted by Kato (1988, 1989, 1990) also in the analysis of the capacity of deformation of tubular square and circular sections. In any case, the equivalent section has the same area of the actual section, while its height is calculated imposing the equivalence of the two sections in terms of plastic moment. Moreover, Kato theory neglects the rotation due to the part of the member still in elastic field, thus assuming a rigid-perfectly plastic-hardening behaviour.

- **Semi-empirical methods:** differently from theoretical methods the local buckling phenomena are obtained experimentally. Indeed, in semi-empirical methods the moment-curvature relationship of the section depends on the experimental measurements of the critical stress, which corresponds to the local buckling of the flange in compression. Kato proposed a procedure (Kato 1988, 1989, 1990) to determine the rotation capacity. This theory is obtained assuming an ideal section made of two equivalent flanges characterized by a rigid-perfectly plastic-hardening material. The equivalency is maintained by equating the full plastic moment and axial strength for both actual and ideal sections. From the integration of member curvature simple equations of R are given for different level of axial force as function of two parameters, which are “ ρ ” and “ s ”. The former is the ratio between the axial force (N) and the axial strength (N_{pl}). The second is the normalized critical stress, given by the ratio between the critical stress (f_{cr}) and the yield stress (f_y). Kato proposed also a procedure (Kato 1988, 1989, 1990) to determine the parameter “ s ” as a function of flange and web slenderness.

- **Empirical methods:** based on statistic analyses of a large number of data obtained by experimental tests or on numerical simulations. Several empirical relationships for the evaluation of the rotation capacity of steel members have been proposed in the scientific literature. Kato & Akiyama (1980, 1981) have proposed a simplified moment-rotation relationship constituted by three linear branches for members subjected to a bi-triangular distribution of the bending moment. This equation has been obtained interpolating the experimental results performed by

Fukuchi (1969), Kato et al. (1973, 1976), Lukey & Adams (1969), Suzuki et al. (1974). Nakamura (1988) proposed a different equation for rotation capacity obtained by having processed the results of 121 tests carried out on beams having different lateral torsional-slenderness. The Spangemacher & Sedlacek (1992) proposed a method based on the results obtained from F.E.M. simulations. Particularly, they carried out a parametric numerical study, analyzing separately the influence of all parameter a time.

3.2.3 Rotation capacity in current codes

In modern steel design codes for plastic design, national reference values for rotation capacity have been established on the basis of available analytical, experimental and numerical studies. Design rules have then been developed with reference to this rotation capacity.

Indeed, after plastic design was introduced, Driscoll (1957, 1958) evaluated the rotation capacity required to achieve plastic collapse in a wide range of continuous beams and portals made of wide flange profiles, and concluded that the required R could be equal to 12 in the worst cases. Recently, this requirement has been relaxed because of the following influences:

- the flexibility of the connections, particularly bolted splices, increases the rotation in critical regions;
- tests on complete structures showed that the rate of strain weakening is less marked than in tests on statically determinate elements, where the energy absorbed in the testing equipment may be significant;
- improved resistance associated with strain hardening.

Kemp (1985) has first recommended lower limits for the rotation capacity ($R > 5$ and $R > 3$) to be used for different limit states in the South African Code for plastic design, whereas Yura et al. (1978) have already proposed $R > 3$ in the draft American LRFD Code. Nowadays, the North American standard has assumed a rotation capacity of 3 to be sufficient for most civil engineering structures as indicated in Yura et al. (1978) and AISC 2005 a,b. This rotation capacity of three is based on limiting the flange strain to four times the yield strain. The North American standard has then derived their limiting width-to-thickness ratios for compact sections on the basis of this value.

Similarly, in the background document to the European standard, Bild et al. (1989) and Sedlacek & Feldmann (1995) investigated and summarized

the rotation requirements for three-span continuous beams and single bay frames under point loads. They concluded that a rotation capacity equal to 3 is sufficient and corresponding limiting width-to-thickness ratios for Class 1 sections were developed.

Several studies were addressed also for cold-formed structural hollow sections. Korol & Hudoba (1972) recommended a rotation capacity equal to 4 for plastic design. To satisfy this requirement some design rules for limiting width-to-thickness ratios were then developed. This rotation capacity was further adopted by Hasan & Hancock (1989), Zhao & Hancock (1991) and Wilkinson & Hancock (1998). In Europe Stranghoner et al. (1994) performed parametric studies into the rotation requirements on square, rectangular and circular hollow sections on a three-span continuous beam subjected to a point load in the central span. The investigated factors included beam geometry, loading, cross-section, material and serviceability requirements. Results demonstrated a rotation capacity of 3 is sufficient.

3.3 OVERSTRENGTH OF STEEL BEAMS

3.3.1 Definitions

The flexural overstrength (s) is the measure of the maximum bending capacity of steel beams. According to Kemp (1985), Kato (1989) and Mazzolani & Piluso (1992). It could be intended as the ratio between the critical stress (f_{cr}) occurring at the local buckling and the yielding stress (f_y), but s may be defined also in terms of bending moments by the following equation:

$$s = \frac{M_u}{M_p} \quad (3.4)$$

where M_u is the peak bending moment and M_p is the plastic bending moment of the steel beam. This two approaches are described in the following figures.

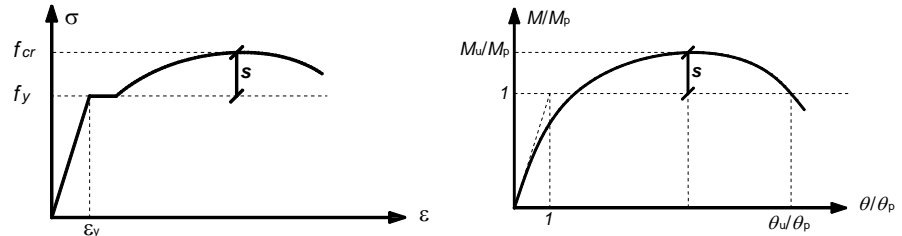


Figure 3.3 Different approaches to the definition of s .

3.3.2 Predictive methods

In general, s can be directly obtained from experimental tests, measuring and calculating the maximum bending moment M_u and the plastic moment M_p . However, several methods to evaluate the beam rotation capacity are proposed by different authors, which can be grouped in the following methods:

- **Theoretical methods:** the evaluation of the flexural overstrength is based on the theoretical evaluation of the critical strain occurring in the compressed flange when it buckled in plastic field. Kemp (1985) proposed a theoretical solution for an ideal I beam made of a perfectly plastic material, assuming that the critical strain could occur in the middle of the plastic zone. In addition the extension of plastic zone is considered to be equal to the semi-wave buckling length, as confirmed by the study of Lay & Galambos (1965).

- **Semi-empirical methods:** this approach provide the overstrength on the basis of experimental results, taking into account also mechanical parameters in addition to the geometrical slenderness. Indeed, the critical stress is influenced also by the relative restraint among the web and the flange and also by the stress distribution across the section depth. Besides, the theoretical analyses does not take into account the effects due to the stress gradient related to the variation of bending moment along the beam length. These effects have been early underlined by tests performed by Kuhlmann (1989), which showed that for I and H beams the buckling length of the flange is approximately 1.20 times larger the flange width (b_f). The influence of the stress gradient on the critical stress depends on the ratio b_f/L (being L the distance from the zero point to the maximum of the bending moment diagram).

Mazzolani & Piluso (1992) introduced this parameter. They provided a new formulation of s by processing the experimental results given by Kemp (1985), Kato (1988,1989) and Kuhlmann (1989) through a multiple regression.

- **Empirical methods:** Kato (1988, 1989, 1990) proposed empirical equations to predict the flexural overstrength based on the results of 68 tests carried out on “stub-columns” specimens having different steel grades and local (flange and web) slenderness. The normalized overstrength s was obtained by a multiple regression as function of the flange and web slenderness for each grade of steel

The analyzed procedures have to be integrated with the control of the conditions that determines the flexural-torsional instability.

3.3.3 Flexural overstrength in current codes

In modern steel design codes the value of flexural overstrength is provided only for seismic design, owing to the need to apply the hierarchy criterion.

According to AISC 341-05 the beam flexural overstrength is equal to $1.1R_y$, being 1.1 the factor to take into account the strain hardening and other possible overstrength, while R_y is ratio of the expected yield stress to the specified minimum yield stress (R_y varies in the range 1.1 to 1.5, depending on steel grade). The factor 1.1 has been obtained from the wide experimental research devoted to provide qualified moment-resisting connections during the SAC project (FEMA 350). Tests showed that this value is adequate to the overstrength that beams belonging to frames designed according to the code could experience.

The new Italian code NTC'08 and the EC8 proposed a similar equation. Indeed, the flexural overstrength is $1.1 \gamma_{ov}$, thus assuming the same factor 1.1 for the strain hardening, while the factor γ_{ov} takes into account the variability of yield stress of steel. EC8 does not provide a criterion for an appropriate evaluation of γ_{ov} , but suggests the use of $\gamma_{ov}=1.25$. This assumption leads to a local overstrength factor equal to $\gamma_{ov} \cdot 1.1=1.375$, which has an important role not only in the connection design but also in the application of capacity design at global level. Infact, in the case of moment resisting frame structures, the columns shall be verified under seismic actions considering the following combination:

$$S_{Ed} = S_{Ed,G} + I \cdot I \gamma_{ov} \Omega S_{Ed,E} \quad (3.5)$$

where:

$S_{Ed,G}$ represents the resistances (the compression force, the bending moment and shear force) in the column due to the non-seismic actions;

$S_{Ed,E}$ represents the resistances (the compression force, the bending moment and shear force) in the column due to the design seismic action;

γ_{ov} is the overstrength factor defined before;

Ω is the minimum value of the Ω_i of all the beams in which the dissipative zones are located, defined by the expression:

$$\Omega_i = \frac{M_{pl,Rd,i}}{M_{Ed,i}} \quad (3.6)$$

$M_{Ed,i}$ is the design value of the bending moment in beam i in the seismic design situation and $M_{pl,Rd,i}$ is the corresponding plastic moment.

It is worth noting that all current codes assumed a constant value of the hardening factor, that is not related with the class of the transversal cross section. Only the late Italian code OPCM 3274, nowadays no longer in use, overcome this limit. Indeed, in this code the flexural overstrength was provided using the s factor suggested by Mazzolani & Piluso (1992). In detail, for double T sections subjected to axial and/or flexural loads, considering usual steel types, the overstrength factor s can be calculated by means of the following analytical formulation:

$$s = \frac{1}{0.695 + 1.632 \cdot \lambda_f^2 + 0.062 \cdot \lambda_w^2 - 0.602 \cdot \frac{b_f}{L^*}} \leq \min \left\{ \frac{f_u}{f_y}; 1.25 \right\} \quad (3.7)$$

being:

b_f the flange width;

L^* the distance between the plastic hinge and the point of zero moment;

$$\lambda_f \text{ the flange slenderness } \lambda_f = \frac{b_f}{2 \cdot t_f} \sqrt{\frac{f_y}{E}} \quad (3.8)$$

$$\lambda_w \text{ the web slenderness } \lambda_w = \frac{d_{w,e}}{t_w} \sqrt{\frac{f_y}{E}} \quad (3.9)$$

in which $d_{w,e}$ is the parameter which takes into account the influence of the axial load because it represents the compressed part of the beam web.

$$d_{w,e} = \frac{1}{2} \left(1 + \frac{A}{A_w} \rho \right) d_w \quad (3.10)$$

In OPCM 3274 the application of capacity design to local level is given by the following equation:

$$M_{jRd} \geq s \gamma_{ov} M_{bRd} \quad (3.11)$$

where the γ_{ov} factor is not unique, but it is defined for every steel type as indicated in Table 3.1.

Table 3.1 Values of γ_{ov} for different steel type (OPCM 3274).

Steel grade	γ_{ov}
S235	1.2
S275	1.15
S355	1.1

Consequently, differently from the EC8, for which the necessary overstrength at the local level is constant and independent from the steel type and from of the transversal cross-section, the OPCM 3274 local overstrength depends on γ_{ov} and s factors. Particularly, in the most unfavourable situation, the necessary overstrength according to the OPCM 3274 reaches the value of about 50% ($\gamma_{ov}=1.2$; $s=s_{\max}=1.25$).

As far as the capacity design at global level (beam-column) is concerned, the OPCM 3274 requires its control only if the structural system is designed in high ductility. In this case the columns have to be verified considering the most unfavourable combination of the axial load and bending moments:

$$S_{c,Sd} = S_{c,Sd,G} + \alpha S_{c,Sd,E} \quad (3.12)$$

where:

$S_{c,Sd,G}$ represents the resistance (the compression force, the bending moment and shear force) in the column due to the non-seismic actions;

$S_{c,Sd,E}$ represents the resistance (the compression force, the bending moment and shear force) in the column due to the design seismic action;
 α is the minimum value of α_i of all beams connected to the examined column:

$$\alpha_i = \min \left\{ \frac{\gamma_{ov} S_i M_{b,pl,Rd,i} - M_{b,Sd,G,i}}{M_{b,Sd,E,i}}; q \right\} \quad (3.13)$$

where $M_{b,pl,Rd,i}$ is the plastic moment value for i beam, $M_{b,Sd,G,i}$ is the bending moment value due only to vertical actions, $M_{b,Sd,E,i}$ is the design bending moment value due to seismic actions.

A comparison between the EC8 and the OPCM 3274, regarding the application of the capacity design at global level, shows that, first of all, both codes require the amplification of the internal actions produced by the seismic input on the column, through a coefficient.

In the EC8, since the local overstrength is constant, the coefficient is $1.1\gamma_{ov}\Omega$; while in the OPCM 3274 it is also dependent on the variability of the local overstrength. In addition, in the case of the EC8, the coefficient Ω is calculated neglecting vertical loads contribution, which are, instead, taken into account in the α expression. Nevertheless, with reference to ordinary structures, this discordance does not involve a significant difference respect to OPCM 3274. Besides, small variations of these multipliers do not behave substantial differences in the choice of the adopted profiles, because of the great discontinuity of the available commercial sections.

3.4 SEISMIC CLASSIFICATION CRITERIA OF STEEL BEAMS

The seismic classification of steel members allows to know the provided cross-section ductility on the basis of geometric data, thus giving an idea of the potential ductility of the structure.

In the past, in addition to the cross-section classification, different criteria have been formulated to assess the ductility of structural systems. In particular, two approaches can be recognized, that are based on:

- member ductility, when the properties of members are considered;
- structural ductility, which consider the overall behaviour of the structure.

The former has been proposed by Galambos & Lay (1965) and illustrated in the following figure. According to this criterion, three ductility levels are identified:

- ductility class HD (high ductility) corresponds to a member for which the design, dimensioning and detailing provisions are such that they ensure the development of large plastic rotations;
- ductility class MD (medium ductility) corresponds to a member designed, dimensioned and detailed to assure moderate plastic rotations;
- ductility class LD (low ductility) corresponds to a member designed and dimensioned according to general code rules which assures low plastic rotations only.

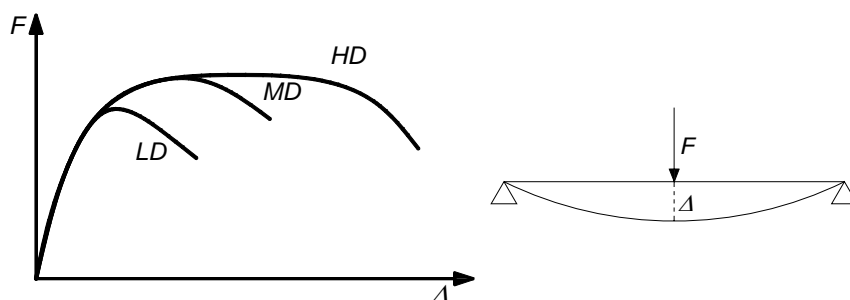


Figure 3.4 Member ductility classification criterion (Galambos & Lay, 1965).

The classification at the level of a frame has been proposed by Ivanyi (1992) and illustrated in the following figure. According to this criterion, four ductility level are identified:

- ductility class 1: full support corresponds to a frame for which the design, dimensioning and detailing provisions are such that they ensure the development of the plastic carrying capacity with large plastic rotations;
- ductility class 2: adequate support that ensures the development of the plastic carrying capacity without plastic rotations;
- ductility class 3: sufficient support, which ensures the development of the elastic carrying capacity;
- ductility class 4: poor lateral support under the elastic carrying capacity.

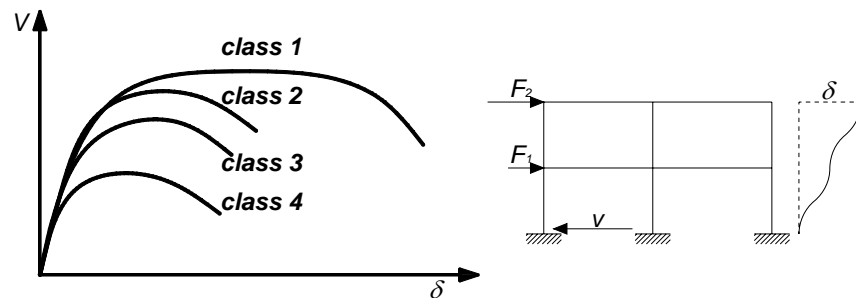


Figure 3.5 Frame ductility classification criterion (Ivanyi 1992).

3.4.1 Eurocode 8 classification criterion

The Eurocode 8 adopts the classification criterion proposed by the Eurocode 3, illustrated in the following figure, which subdivides the cross-sections into four classes:

- class 1 (plastic sections): sections belonging to class 1 are characterized by the capability to develop a plastic hinge with high rotation capacity;
- class 2 (compact sections): these sections are able to provide their maximum plastic flexural strength, but they have a limited rotation capacity, due to some local effects;
- class 3 (semi-compact sections): sections fall into this class when the bending moment capacity for the first yielding can be achieved without reaching the plastic moment;

- class 4 (slender sections): sections belonging to this class are not able to develop their total flexural resistance due to the premature occurrence of local buckling in the compressed parts.

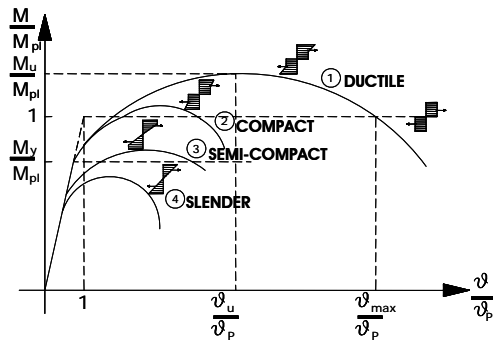


Figure 3.6 EC3 classification of cross sections.

Evidently, only the first two classes have sufficient ductility to assure the plastic redistribution of moments. This classification is limited to the cross-section level only, so it has many deficiencies.

The definition of the cross-section class is based on the local slenderness of flanges and web. The web and the flange are considered independent, neglecting their mutual interaction. Depending on the structural ductility class and on the behavioural factor q , the requirements regarding the cross-sectional classes of the dissipative elements are reported in the following table.

According to EC8, the cross-section class is the only parameter that influences the global ductility of the structure, but it does not influence the application of the capacity design neither at local nor at global level.

Table 3.2 EC8 cross-section requirements for dissipative elements.

Ductility class	Behaviour factor	Cross section class (dissipative zone)
DCM	$1.5 < q < 2$	Class 1,2 and 3
	$2 < q < 4$	Class 1 and 2
DCH	$q > 4$	Class 1

3.4.2 OPCM 3274 classification criterion

This code implemented the concept of member behavioural classes (Mazzolani & Piluso, 1993). It provided a classification criterion which subdivides members into three categories:

- Ductile: the local buckling of the compressed parts of the section develops in plastic range without significant reduction of the load carrying capacity, after the member exhibits large plastic hardening deformations ($s \geq 1.2$);
- Plastic: the local buckling of the compressed parts of the section develops in plastic range, allowing significant plastic rotations ($1 \leq s < 1.2$);
- Slender: the local buckling of the compressed parts of the section occurs in the elastic range ($s < 1$).

The classification criterion adopted by the late Italian code OPCM 3274 is based on the evaluation of the overstrength factor s , as defined by equation:

$$\frac{1}{s} = 0.546 + 1.632\lambda_f^2 + 0.062\lambda_w^2 - 0.602\frac{b_f}{L} + 0.001\frac{E}{E_h} + 0.007\frac{\varepsilon_h}{\varepsilon_y} \quad (3.14)$$

An alternative equation is obtained by the simplification of the terms E/E_h and $\varepsilon_h/\varepsilon_y$, assuming their average values with reference to the mechanical properties for the common steel grades:

$$\frac{1}{s} = 0.695 + 1.632\lambda_f^2 + 0.062\lambda_w^2 - 0.602\frac{b_f}{L} \quad (3.15)$$

Table 3.3 Stress-strain characteristics of common European steel .

Steel	f_y	f_u	E	E_h	E/E_h	ε_h	ε_y	$\varepsilon_h/\varepsilon_y$
	N/mm ²	N/mm ²	N/mm ²	N/mm ²	-	%	%	-
S 235	235	360	210000	5600	37.5	1.41	0.115	12.3
S 275	275	430	210000	4906	42.8	1.47	0.134	11.0
S 355	355	510	210000	4357	48.2	1.70	0.173	9.8

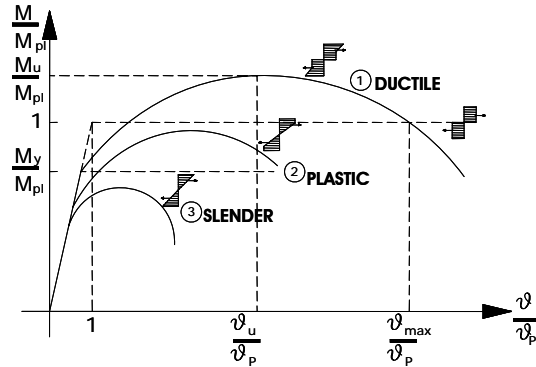


Figure 3.7 OPCM 3274 classification of members.

About the influence of the cross-section classification on the seismic design, it is important to underline, the explicit relationship between the value assumed by the s factor for the beams which contain plastic hinges and the behavioural factor. Indeed, the latter is expressed, for each steel structural type, such as moment resisting frames, concentric and eccentric braced frames, by the following relationship:

$$q = q_0 K_D K_R \quad (3.16)$$

In which:

q_0 is the reference value of the q -factor, as a function of both the structural typology and the ductility category of the structure;

K_D is a factor related to the local ductility resources of the dissipative zone by s factor;

K_R is the coefficient of structural regularity, which takes into account the elevation and the in-plane regularity characteristics of the building;

The limit values of the s parameter, which identify the ductility categories of members, are given in the following table, where the corresponding K_D values assumed for the determination of the design q factor are indicated too.

Table 3.4 Classification of members in terms of ductility.

Member categories	s	K_D
Ductile	$s \geq 1.2$	1
Plastic	$1 \leq s < 1.2$	0.75
Slender	$s < 1$	0.5

3.4.3 Italian code NTC '08 classification criterion

In the new Italian code NTC '08 the classification criterion for steel members is analogous to EC8 approach. Indeed, four classes are considered according to EC3 prescriptions, but providing limit values of rotation capacity R as explained in the following:

- class 1 : the section is able to develop a plastic hinge having the rotation capacity required for the structural analysis with the plastic method without strength reductions. These sections are characterized by rotational capacity of $R \geq 3$
- class 2 : the section is able to develop its plastic moment, but with limited rotation capacity. These sections are characterized by rotational capacity of $1.5 \leq R < 3$.
- class 3 : the stresses in the external compressed fibres of the section can reach the yielding stress, but local instability prevents the development of the plastic moment ($M_y < M_u < M_{pl}$)
- class 4 : to define the bending, shear or normal strength it is necessary to take into account the effects of the local instability in elastic range in the compressed parts of the section ($M_u < M_y$). In this case in the evaluation of the strength, the actual geometric section can be replaced of with an effective one.

From the conceptual point of view this classification criterion is consistent with the one adopted by the EC3, even there are some substantial differences:

- the performance level in terms of rotation capacity, that differentiates sections of first and second class, is made explicit.
- no one specific prescription is provided respect to the evaluation models of R , leaving such choice exclusively to the designer.

For the design in seismic zone, or rather for what concerns to the consequences of such classification in terms of global ductility and capacity design, no difference can be recognized between NTC '08 and Eurocode 8.

4 EXPERIMENTAL ACTIVITY

Experience serves not only to confirm theory, but differs from it without disturbing it, it leads to new truths which theory only has not been able to reach.

- D'Alembert

This chapter presents details on the experimental activity performed in the Civil Engineering Laboratory at the University of Salerno in the framework of ReLUIIS project. In particular, it has been exposed the planning of the experimental campaign and the reasons of choices made about the test set-up scheme, the tested profiles and the loading history paths. Moreover, the main results of the experimental tests are given.

4.1 PLANNING OF THE EXPERIMENTAL CAMPAIGN

In order to quantify and predict the flexural capacity of steel members an experimental activity was performed in collaboration with the University of Salerno at the Civil Engineering Laboratory.

This activity was based on the financial support of ReLUIIS-DPC 2005-2008 Project (ReLUIIS: Rete di Laboratori Universitari di Ingegneria Sismica: seismic engineering university laboratories network; DPC: Dipartimento di Protezione Civile: emergency management association).

In particular the activity was part of Task 5: “Development of innovative approaches to design steel and composite steel-concrete structures” (coordinators: Proff. F. M. Mazzolani and R. Zandonini) and Subtask 2: “Rotation Capacity and classification criteria for steel members” (coordinator: Prof. R. Landolfo).

In this framework, a full-scale laboratory testing programme was planned, taking into account the existing data available in scientific literature, dealing with experimental test also devoted to investigate rotation capacity and flexural overstrength of steel beams.

Available data of literature experimental tests was collected, analyzed and organized, to be able to subdivide them depending on the type of profile that was tested, the test set-up scheme that was used, and the loading history that was adopted.

In the tables below there is a summary of the collected data, with this kind of classification, for double T profiles and hollow profiles.

Table 4.1 Tests available in technical literature for IPE-HE profiles.

Author	year	n°of tests	Profile type	Test scheme	Loading History
Kulmann	1989	24	I welded	3PBT	MON
Spangemacher	1992	35	I hot rolled	3PBT	MON
Kemp	1985	12	I hot rolled	3PBT	MON
Kemp	1985	2	I welded	3PBT	MON
Boeraeve-Lognard	1993	5	I hot rolled	3PBT	MON
Lukey-Adams	1969	12	I hot rolled	3PBT	MON
Suzuki	1994	9	I welded	3PBT	MON
Ito-Karatani-Komuro	2002	12	I welded	3PBT	MON
Ito-Nazaka-Shirosaki-Yamasaki	2005	6	I welded	3PBT	MON
Nakashima-Nakamura-Wakabayashi	1963	14	I hot rolled	4PBT	MON

Table 4.2 Tests available in technical literature for RHS-SHS profiles.

Author	year	n°of tests	Profile type	Test scheme	Loading History
Wilkinson	1999	44	RHS cfs	4PBT	MON
Wilkinson	1999	2	RHS hot rolled	4PBT	MON
Dean-Wilkinson-Hancock	2001	7	RHS cfs	4PBT	MON

To be able to make a choice for the profiles to be tested, the collected data have been elaborated to calculate the main geometrical ratios that are commonly used for the classification of steel members and for the calculation of rotation capacity and flexural overstrength.

In this phase of the work it was important the previous organization of data, for example, with reference to the test set-up scheme, because this parameter influences the length to be considered (see figure below).

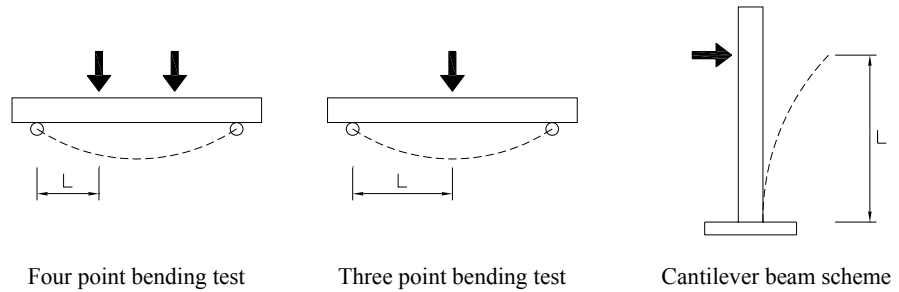


Figure 4.1 Length parameter for each test set-up scheme.

The experimental activity has been planned with the aim to integrate the data available in literature, in terms of slenderness and other geometrical ratios. In the following, there are some istograms showing the variability range of the principal useful geometrical ratios.

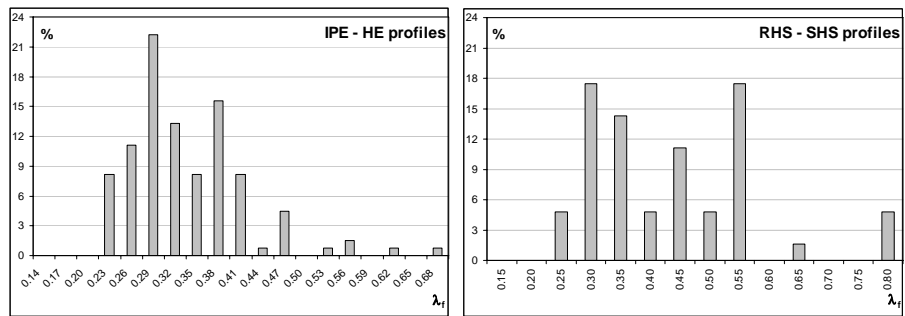


Figure 4.2 Variability range for the parameter λ_f .

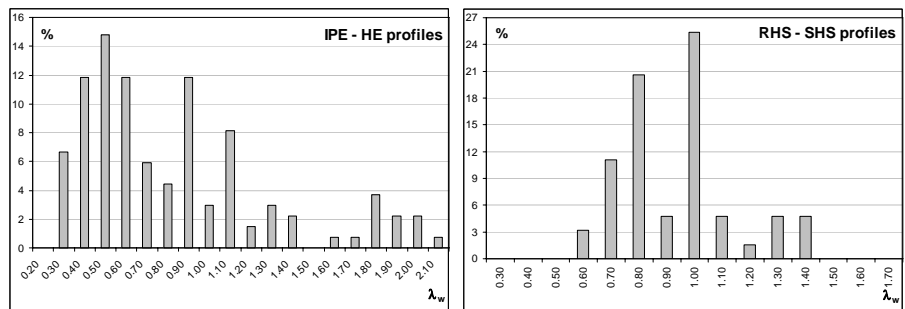


Figure 4.3 Variability range for the parameter λ_w .

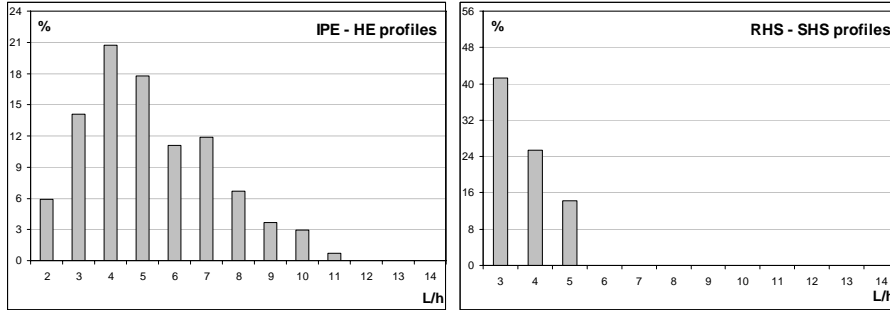


Figure 4.4 Variability range for the ratio L/h.

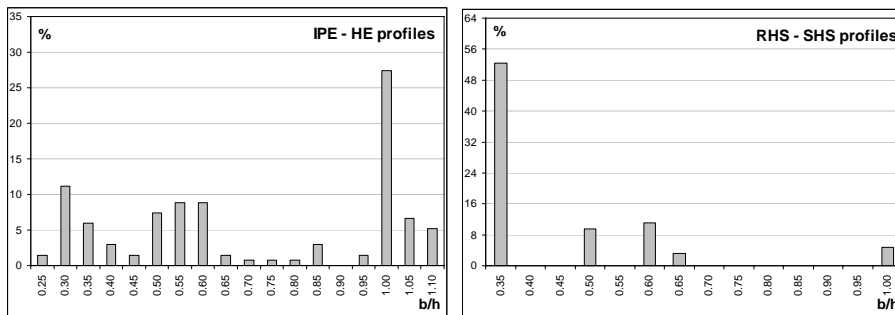


Figure 4.5 Variability range for the ratio b/h.

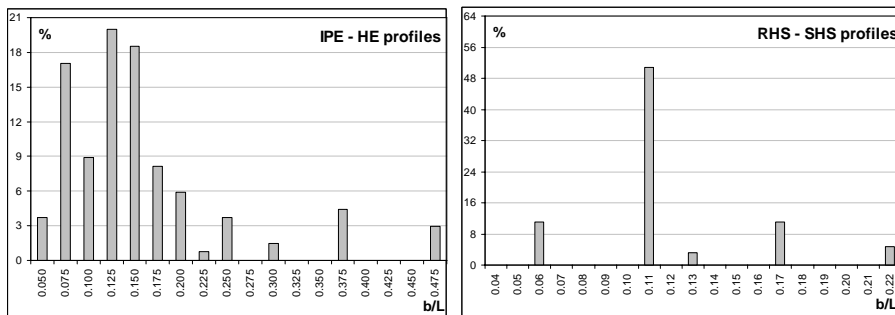


Figure 4.6 Variability range for the ratio b/L.

In figure 4.7 are showed the geometrical parameters for double T and hollow profiles to be referenced the previous ratios.

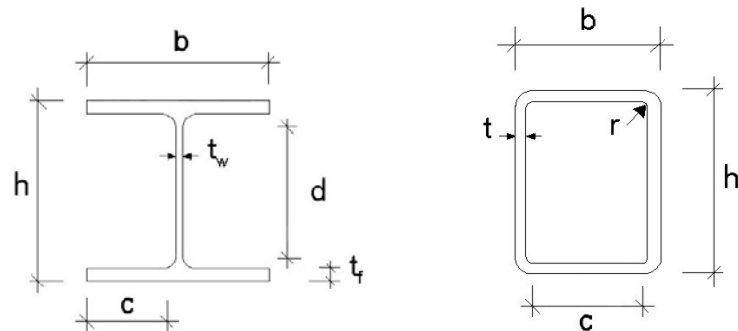


Figure 4.7 Geometrical parameters for I and hollow profiles.

As a result of this study, a set of sections to be tested has been proposed. The profiles and their geometrical and mechanical properties are listed in the table below. But, during the experimental campaign, for technical reasons, the actual tested profiles were only the ones highlighted in grey.

Table 4.3 Programmed experimental tests.

profiles	h	b	t_f	t_w	c	d	steel
IPE 240	240	120	9.8	6.2	60	220.4	S275
IPE 300	300	150	10.7	7.1	75	278.6	S275
HEB 240	240	240	17	10	120	206	S275
HEA 160	152	160	9	6	80	134	S275
HEA 240	230	240	12	7.5	120	206	S275
HEM 160	180	166	23	14	83	134	S275
150x100x5	150	100	5	5	100	140	S275
160x80x4	160	80	4	4	80	152	S275
200x100x8	200	100	8	8	100	184	S355
250x100x10	250	100	10	10	100	230	S275
300x100x12.5	300	100	12.5	12.5	100	275	S275
300x200x14.5	300	200	14.5	14.5	200	271	S275
150x150x5	150	150	5	5	150	140	S275
160x160x6.3	160	160	6.3	6.3	160	147,4	S355
200x200x10	200	200	10	10	200	180	S355
250x250x8	250	250	8	8	250	234	S355
250x250x5	250	250	5	5	250	240	S275
300x300x10	300	300	10	10	300	280	S275

To highlight the aim to integrate the data available in literature, the tested profiles are showed in the table below, with their slenderness and other geometrical ratios.

Table 4.4 Tested profiles with slenderness ratios.

profile	λ_f	c/t_f	λ_w	h/t_w	L/h	b/h	b/L
IPE 300	0.25	7.01	1.53	42.25	6.88	0.50	0.07
HEB 240	0.26	7.06	0.87	24.00	8.60	1.00	0.12
HEA 160	0.32	8.89	0.92	25.33	13.59	1.05	0.08
150x100x5	0.72	20.00	1.09	30.00	13.77	0.67	0.05
160x80x4	0.72	20.00	1.45	40.00	12.91	0.50	0.04
250x100x10	0.36	10.00	0.90	25.00	8.26	0.40	0.05
160x160x6.3	1.04	25.40	1.04	25.40	12.91	1.00	0.08
200x200x10	0.82	20.00	0.82	20.00	10.33	1.00	0.10
250x250x8	1.28	31.25	1.28	31.25	8.26	1.00	0.12

To recapitulate, the experimental activity was carried out on a wide range of cross section typologies (I sections, Square and Rectangular Hollow sections), and the influence of geometrical and mechanical parameters were analyzed. With the aim to obtain new information on the energy dissipation capacity of steel members, special attention has been paid to the parameters governing local buckling and, as a consequence, strength deterioration under cyclic actions.

The profiles to be tested have been selected to analyze geometrical parameters poorly investigated in the existing literature.

The test programme comprised a total of 9 monotonic and 9 cyclic in-plane bending tests.

In addition, standard coupon tests have been carried out to obtain the mechanical properties of the material by means of the corresponding stress-strain curve. For this reason, standard tensile coupon tests have been performed taking specimens both from flanges and webs.

4.2 DESCRIPTION OF THE TESTING SYSTEM

4.2.1 Test set-up scheme

As mentioned before, the experimental activity was carried out in collaboration with the University of Salerno. The Civil Engineering Laboratory of the University of Salerno has a large reinforced concrete slab of 1m thickness, to which is anchored a reacting wall, that is a steel frame, through the use of high resistance dywidag bars.

An hydraulic actuator (MTS 243), used to apply the displacement history during the experimental tests, is pin-mounted to the reaction wall and to the specimen by means of cylindrical clevis. This swivel joint is attached at the head of the actuator to permit free motion of beam in its flexural plane. The specimen to be tested has been bolted to the top flange of an horizontal steel base girder, directly connected to the r.c. slab.

During both the monotonic and cyclic tests, it has been necessary to employ an horizontal frame to avoid problems of flexural-torsional instability of the specimen, that was found in the pilot-test.



Figure 4.8 Reacting steel frame and specimen with lateral-torsional restraint.

The main scope of the experimental campaign is the study of the flexural behaviour of steel beams under monotonic and cyclic loads, for this reason the adopted scheme is the cantilever beam, which reproduces the behaviour of a beam in a frame subject to seismic actions.

In the following figure is illustrated the adopted test scheme, composed by the reacting vertical frame, the r.c. slab, the horizontal frame used as lateral-torsional restraint, the base girder and the tested specimen.

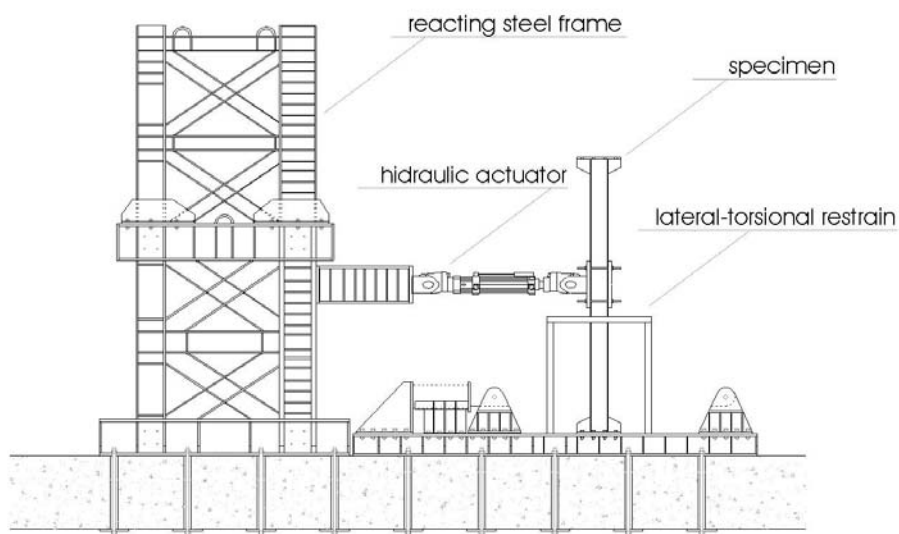


Figure 4.9 Adopted test set-up scheme.

In particular, each specimen has been arranged in such a way that one end could be tested monotonically and the other end cyclically. Indeed, setting the actuator in the middle of the specimen, during the test the outer part is un-deformed. Once the monotonic test on one end is concluded the beam can be dismantled, then turned and fixed to the basement, ready for the cyclic test. The net length of the experimental cantilever is equal to 1865 mm.

In the following figures the connections of the specimen to the testing system are shown.



Figure 4.10 Basement connection and deformed end on the other side.



Figure 4.11 Connection of the specimen to the hydraulic actuator.

4.2.2 Measuring devices

The hydraulic actuator (MTS 243) is connected to a central unit and so the a pc, that gives instructions on the displacents to be applied to the specimen. The maximum force that can be applied is of 250 kN.

A specific software (MTS station manager) is used to monitor the force-displacement data during the test.

In order to measure the deformation parameters a set of LVDT's (Linear Variable Displacement Transducers) have been positioned. In particular, one LVDT is used to monitor the displacement at the middle of the half-wave length of buckled flange, which is equal to $1.2b_f$ according to expressions by Haaijer (1957) and Lay (1965). Other two LVDT's are positioned at the end of the half-wave length of buckled flange. Two LVDT's are used to measure the web deformations. In addition, other two transducers are positioned to measure the relative deformation between the end beam and the basement.



Figure 4.12 Central unit and pc for the hydraulic actuator.

In order to measure reliably the beam rotation, a set of three inclinometers is used. In particular, one is positioned at the point where load is applied, the second at the middle of the experimental length of the beam (namely $\frac{1}{4}$ of the specimen length) and the third at the fixed end of the beam. All the measuring devices are connected to a central unit and a dedicated pc with a specific software (Strain Smart) for the acquisition of data during the tests.



Figure 4.13 Layout of measuring devices and pc for data acquisition.



Figure 4.14 Layout of front and back measuring devices (LVDTs).

Finally, standard coupon tests on materials are carried out by means of an universal testing machine, Schenck Hydropuls S56, with maximum load capacity of 630 kN and piston stroke of ± 125 mm equipped with an extensometer for strain measures.

4.2.3 Loading protocols

For monotonic tests, the displacement history is from 0 to 600mm, that is the complete hydraulic actuator stroke. The applied load rate is equal to 0.25mm/s. The following figure shows the applied displacement.

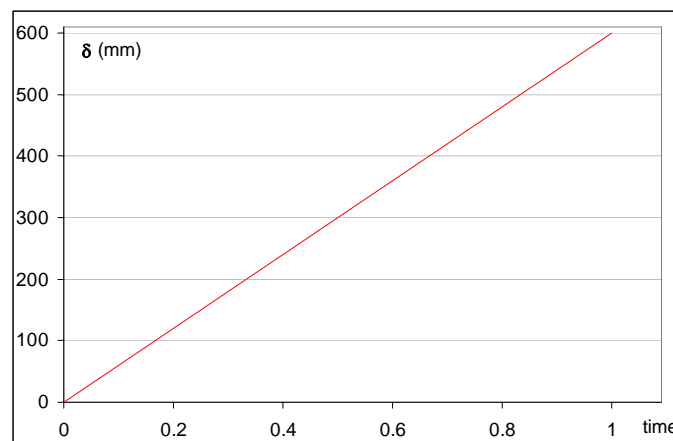


Figure 4.15 Displacement history for monotonic tests.

For cyclic tests, the AISC2005 loading protocol was used (Appendix S - Loading sequence for beam-to-column moment connections).

This procedure is characterized by the control of interstorey drift angle, imposed on the test specimen, as specified below (θ = chord rotation):

- 6 cycles with $\theta = 0.00375$ rad
- 6 cycles with $\theta = 0.005$ rad
- 6 cycles with $\theta = 0.0075$ rad
- 4 cycles with $\theta = 0.01$ rad
- 2 cycles with $\theta = 0.015$ rad
- 2 cycles with $\theta = 0.02$ rad
- 2 cycles with $\theta = 0.03$ rad
- 2 cycles with $\theta = 0.04$ rad

If failure does not occur, the test continues increasing the rotation amplitude of 0.01rad for 2 successive cycles up to collapse.

The following figure shows the applied displacement history for cyclic tests, displacements were obtained by rotations ($\delta = \theta L$).

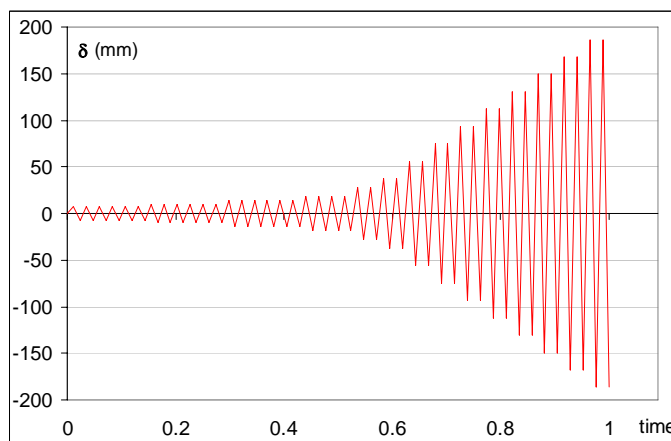


Figure 4.16 Displacement history for cyclic tests.

4.3 RESULTS

The experimental activity has been subdivided into two main parts:

- tensile coupon tests on materials, for the identification of mechanical properties, for each tested profiles;
- bending tests on beams, with monotonic and cyclic loading protocols, for the evaluation of the rotation capacity and flexural overstrength of the beams.

In the following paragraphs are exposed the main results of all the performed experimental tests.

4.3.1 Tensile coupon tests on materials

Tensile coupon tests on materials were performed to determine the engineering stress-strain response of the material, for each of the tested profiles, to be used in the analysis of the bending test results.

The used universal testing machine (Schenck Hydropuls S56) and some specimens, before and after the tests, are shown in the following figures.



Figure 4.17 Universal testing machine and coupon specimens.

In the following, the material test results are shown. There is a summarizing table for each tested profile, with stress-strain diagrams and results in terms of yielding and ultimate critical stresses.

Double T profiles:

HEA 160

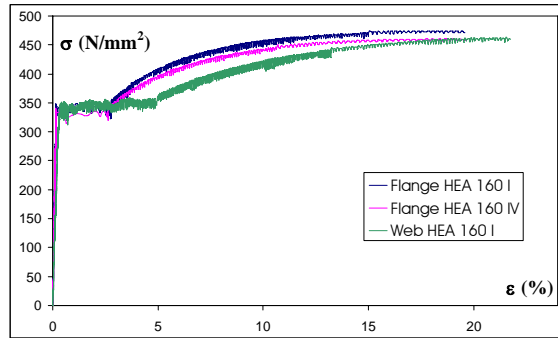
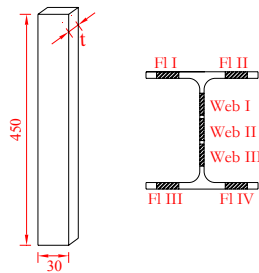


Figure 4.18 Stress-strain diagrams for HEA 160 web and flange.

HEB 240

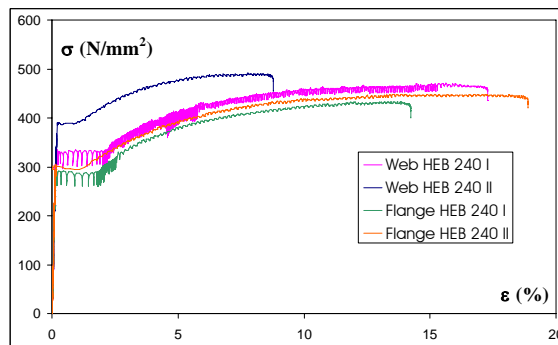
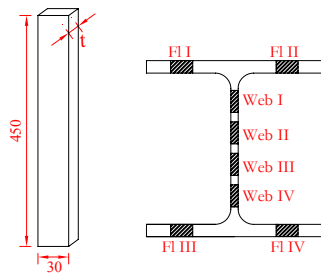


Figure 4.19 Stress-strain diagrams for HEB 240 web and flange.

IPE 300

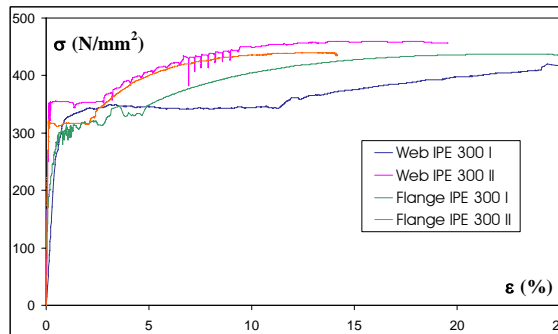
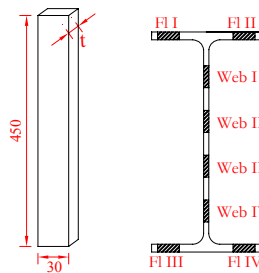


Figure 4.20 Stress-strain diagrams for IPE 300 web and flange.

Rectangular Hollow Section profiles:

RHS 150x100x5

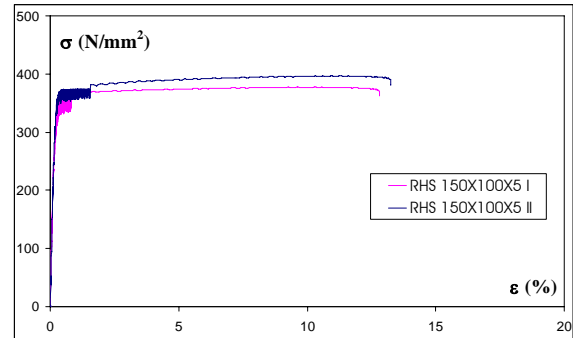
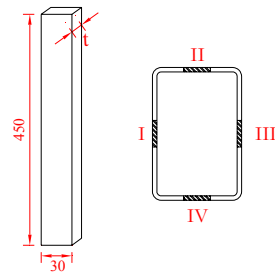


Figure 4.21 Stress-strain diagrams for RHS 150x100x5.

RHS 160x80x4

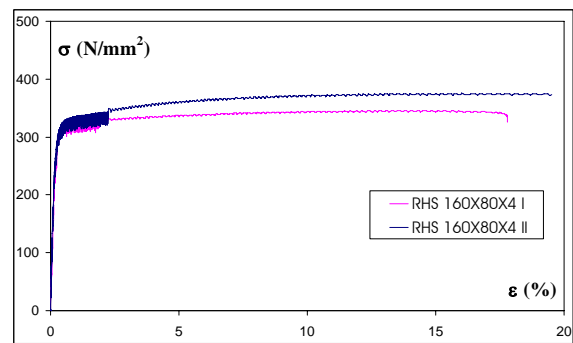
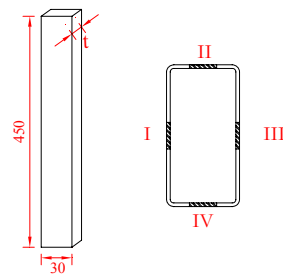


Figure 4.22 Stress-strain diagrams for RHS 160x80x4.

RHS 250x100x10

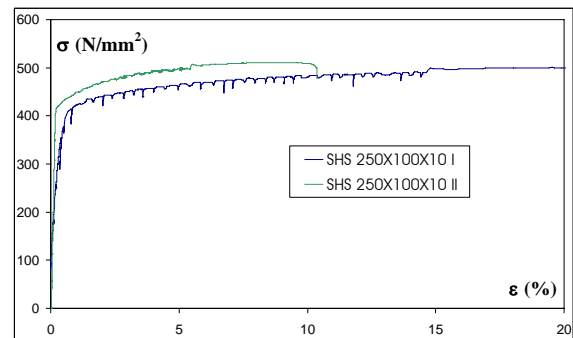
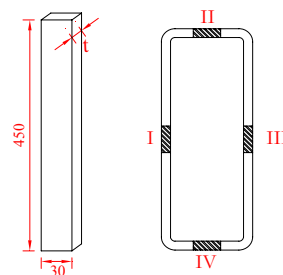


Figure 4.23 Stress-strain diagrams for RHS 250x100x10.

Square Hollow Section profiles:

SHS 160x160x6.3

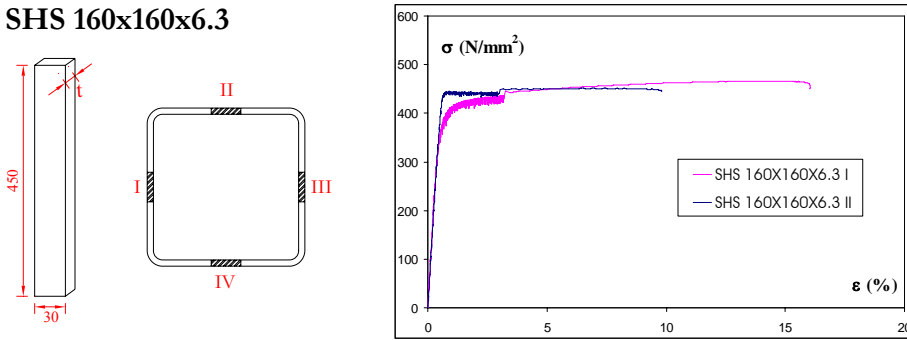


Figure 4.24 Stress-strain diagrams for SHS 160x160x6.3.

SHS 200x200x10

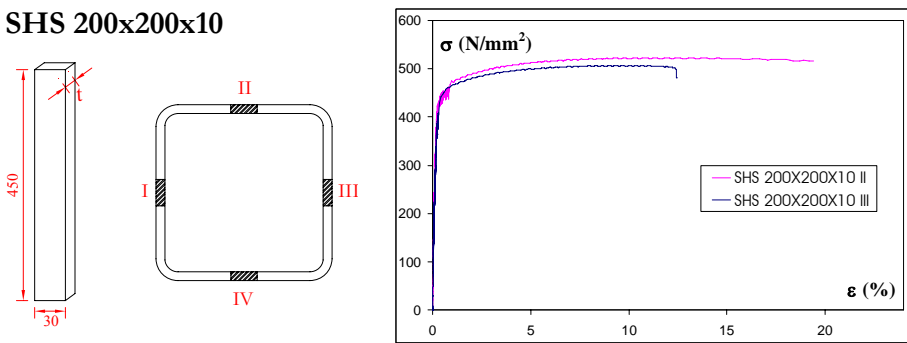


Figure 4.25 Stress-strain diagrams for SHS 200x200x10.

SHS 250x250x8

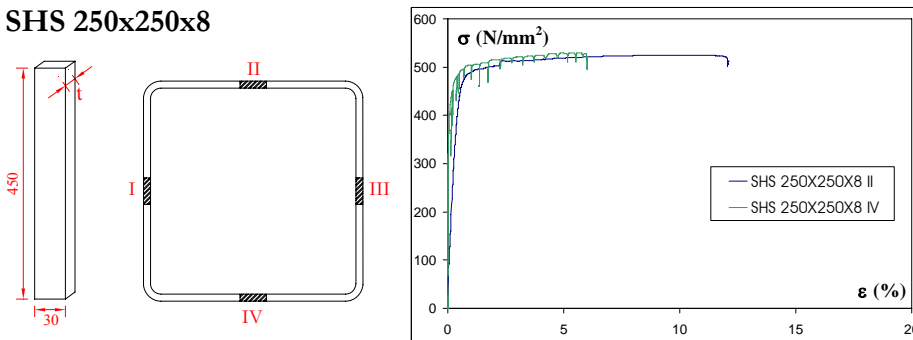


Figure 4.26 Stress-strain diagrams for SHS 250x250x8.

Table 4.5 Material properties of tested beams for double T profiles.

section	specimen		fy exp	ft texp
HEA 160	WEB	I	338	475
HEA 160	FLANGE	I	328	456
HEA 160	FLANGE	IV	346	463
HEB 240	WEB	I	318	351
HEB 240	WB	II	389	491
HEB 240	FLANGE	I	295	433
HEB 240	FLANGE	II	273	448
IPE 300	WEB	I	353	447
IPE 300	WEB	III	345	460
IPE 300	FLANGE	I	314	438
IPE 300	FLANGE	II	317	440

Table 4.6 Material properties of tested beams for hollow profiles.

section	specimen		fy exp	ft texp
RHS 150X100X5	I		342	377
RHS 150X100X5	II		365	397
RHS 160X80X4	I		315	346
RHS 160X80X4	II		333	376
RHS 250X100X10	I		415	500
RHS 250X100X10	II		420	511
SHS 160X160X6.3	I		420	466
SHS 160X160X6.3	II		444	451
SHS 200X200X10	II		450	522
SHS 200X200X10	III		455	506
SHS 250X250X8	II		482	525

4.3.2 Bending tests on beams

In this paragraph, the main results of bending tests on beams are illustrated. Both monotonic and cyclic test results are shown, and the obtained values of rotation capacity and flexural overstrength are summarized at the end.

In general, tests showed the importance of the loading history on the beam flexural response. All specimens under cyclic loading exhibited a lower rotation capacity than those under monotonic loading. But the flexural overstrength did not exhibit an analogous trend.

In case of double T profiles, the specimens under cyclic loading showed higher overstrength. This depended on the isotropic hardening and Bauschinger effect, which was not impaired by the local buckling phenomena, due to the cumulated plastic deformation.

In case of hollow profiles, the local buckling was dominant and the hardening effects had not significant influence.

In general, the specimens experienced different flexural performance depending on the type of failure mechanism:

- double T specimens showed a coupled mechanism made of a combination of in-plane and out-of plane buckling. The flange buckling occurred first and then the asymmetric-torsional buckling was triggered involving the web panel. It is very interesting to note that the height of the web plastic mechanism increased increasing flange width, and this increase is associated with a reduction of rotation capacity;
- hollow section specimens experienced the web local buckling, which produced a rapid decreasing of load with increased deflection. Each buckled web, due to the compatibility of rotation at the corner, caused the deformation of the flange. For these sections, the failure mechanisms were characterized by the so-called elephant foot shape, that is the bulging of the compressed plates at the base of the specimen. This particular failure shape was due to the concentration of deformation in the compressed plates.

Double T profiles:

HEA 160

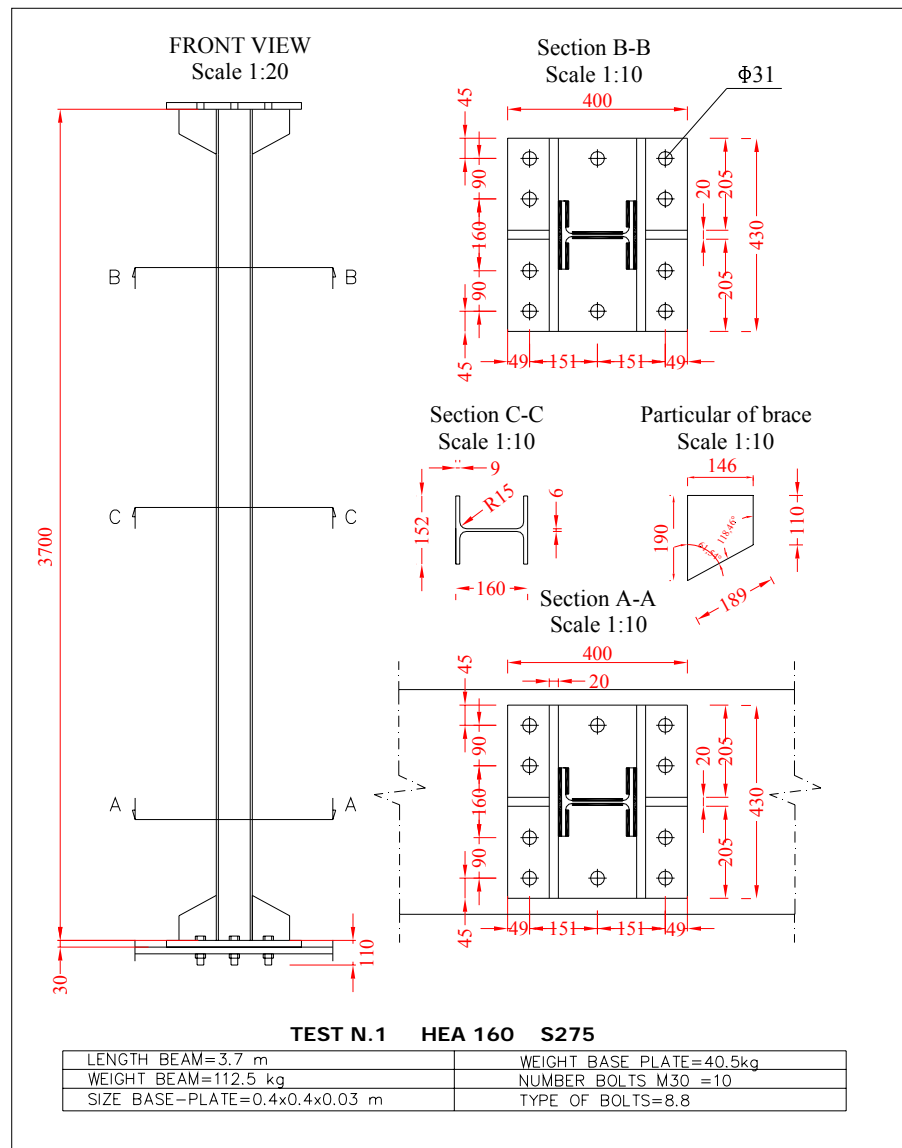


Figure 4.27 Geometric properties of specimen HEA 160.



Figure 4.28 Failure mechanism for monotonic and cyclic loading.

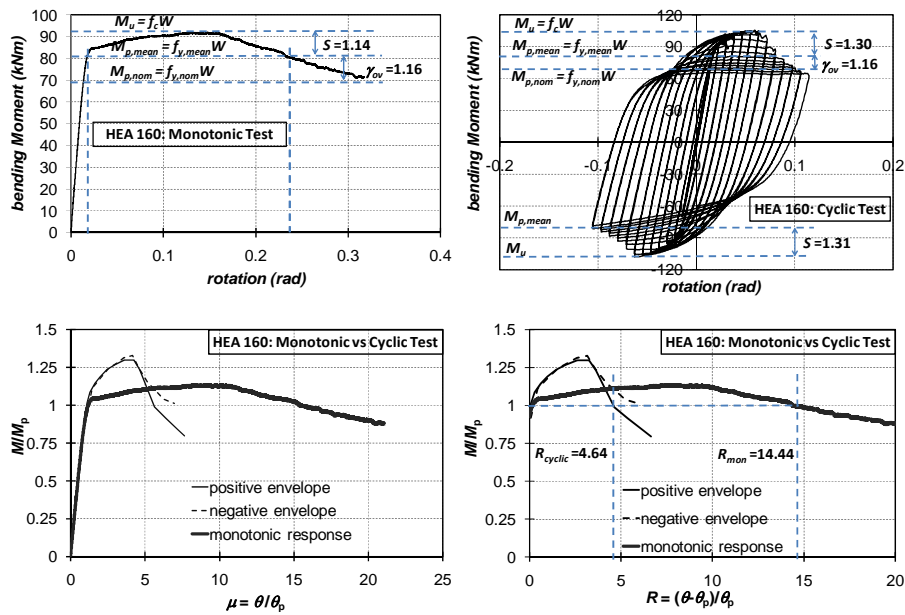


Figure 4.29 Flexural performance of specimen HEA 160.

HEB 240

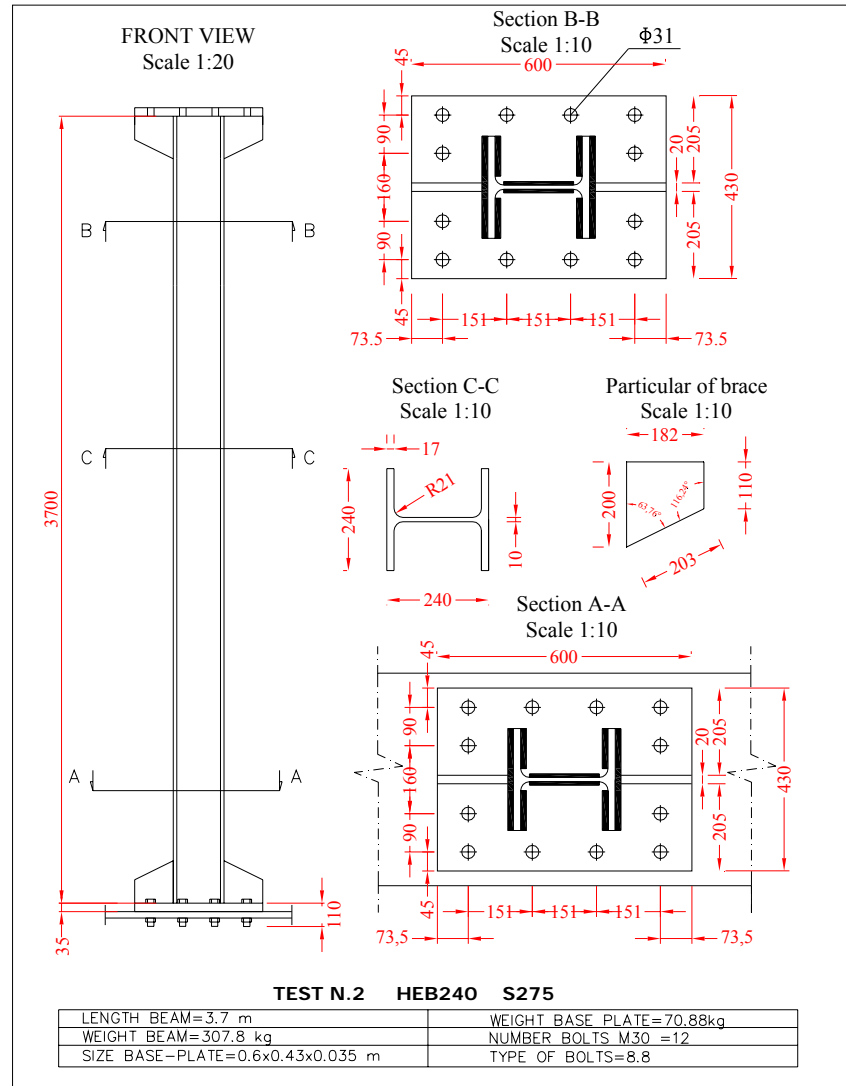


Figure 4.30 Geometric properties of specimen HEB 240.



Figure 4.31 Failure mechanism for monotonic and cyclic loading.

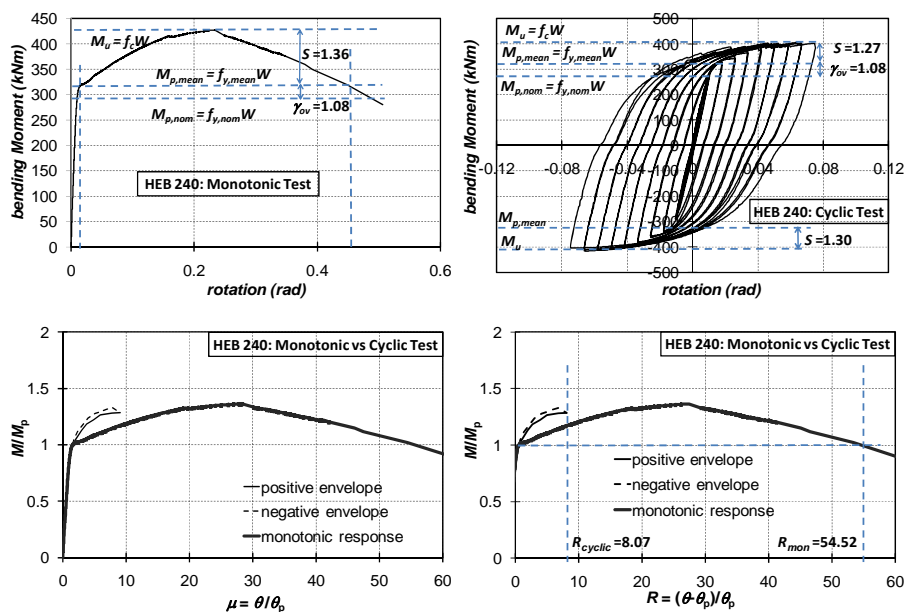


Figure 4.32 Flexural performance of specimen HEB 240.

IPE 300

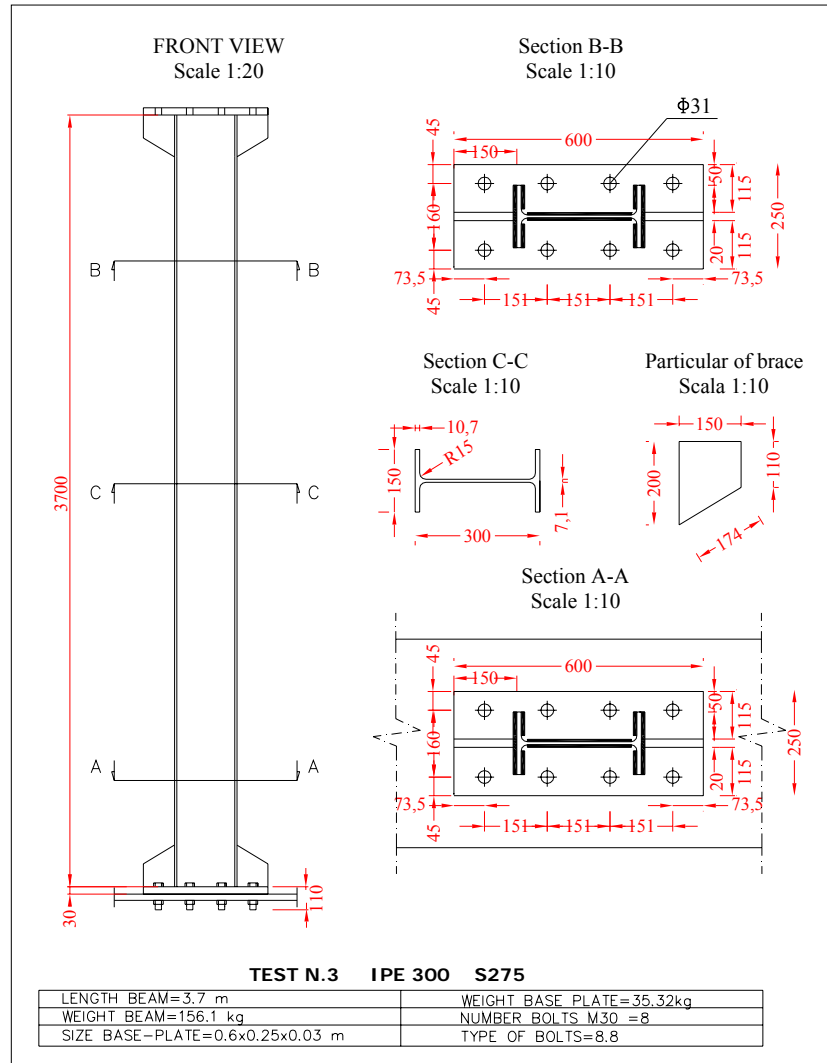


Figure 4.33 Geometric properties of specimen IPE 300.



Figure 4.34 Failure mechanism for monotonic and cyclic loading.

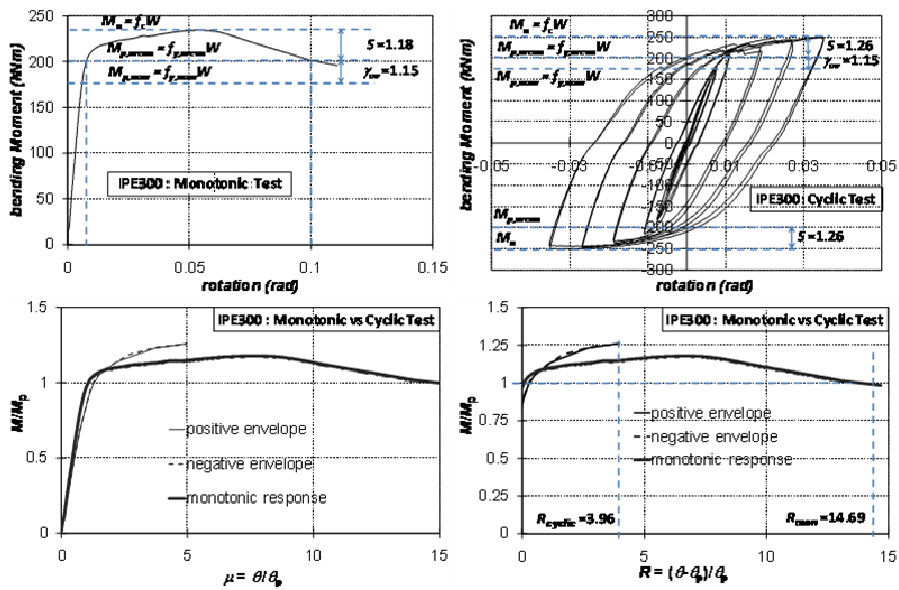


Figure 4.35 Flexural performance of specimen IPE 300.

Rectangular Hollow Section profiles:

RHS 150x100x5

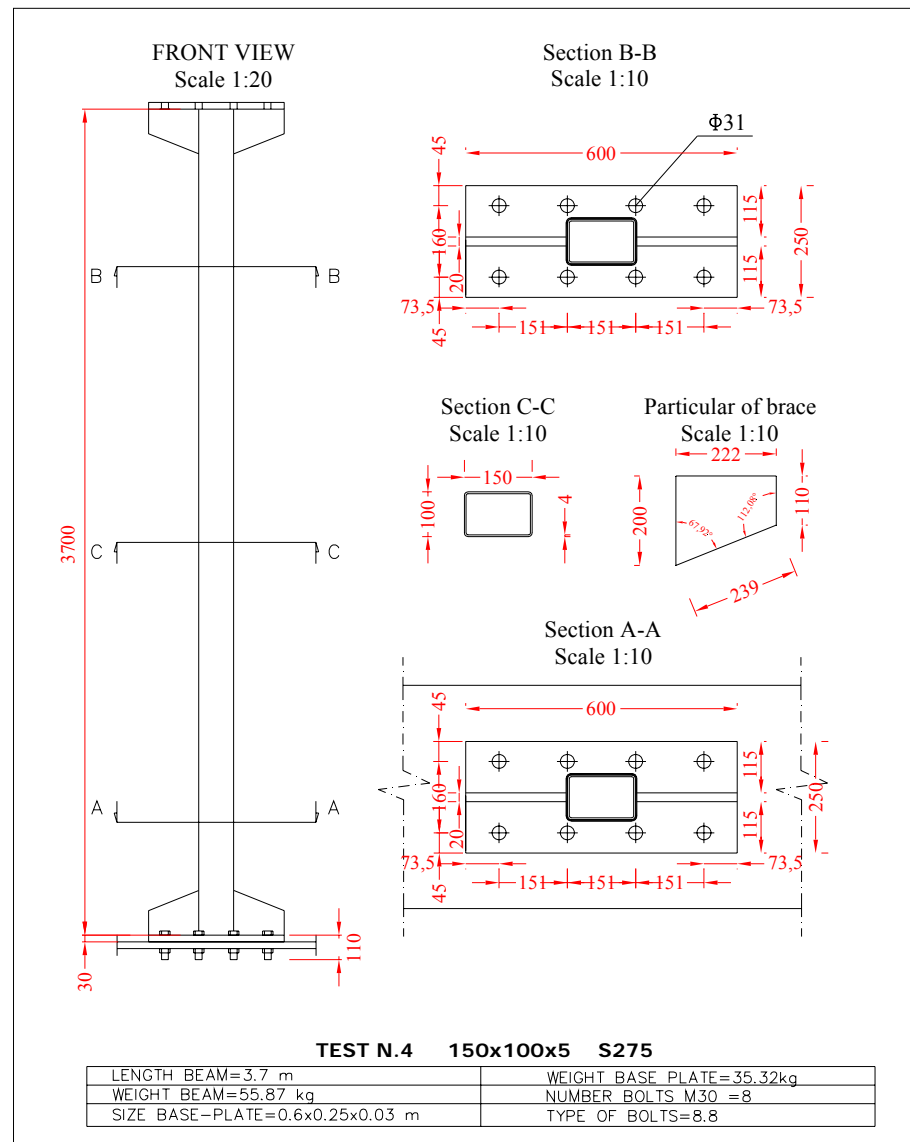


Figure 4.36 Geometric properties of specimen RHS 150x100x5.



Figure 4.37 Failure mechanism for monotonic and cyclic loading.

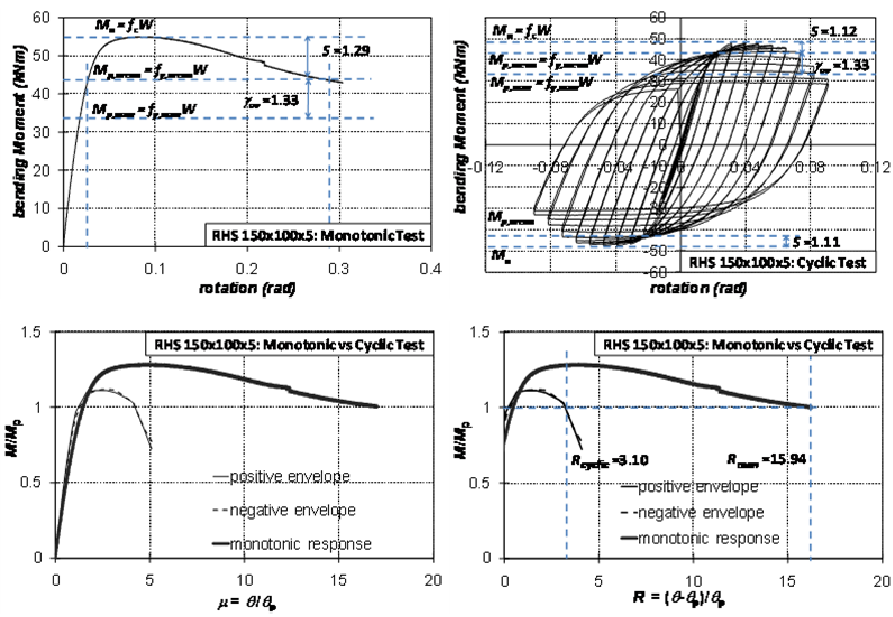


Figure 4.38 Flexural performance of specimen RHS 150x100x5.

RHS 160x80x4

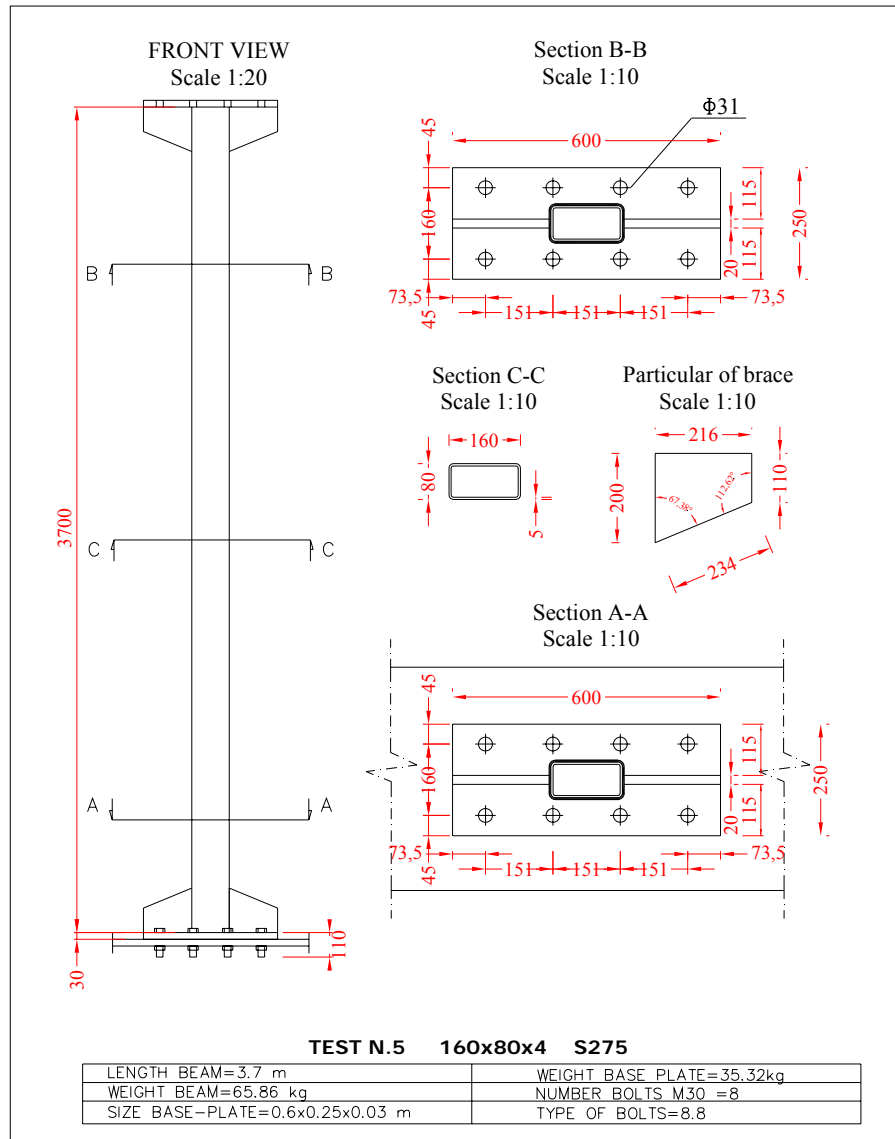


Figure 4.39 Geometric properties of specimen RHS 160x80x4.

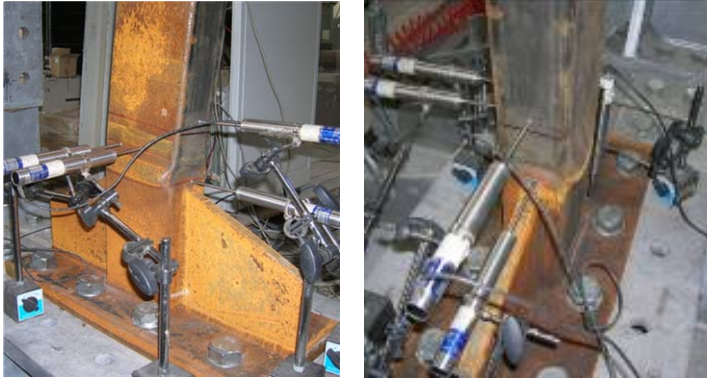


Figure 4.40 Failure mechanism for monotonic and cyclic loading.

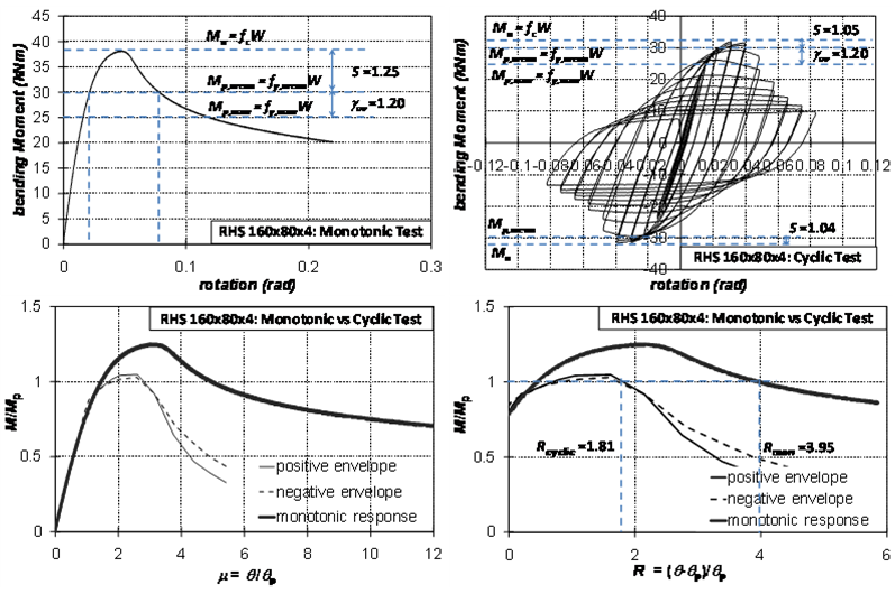


Figure 4.41 Flexural performance of specimen RHS 160x80x4.

RHS 250x100x10

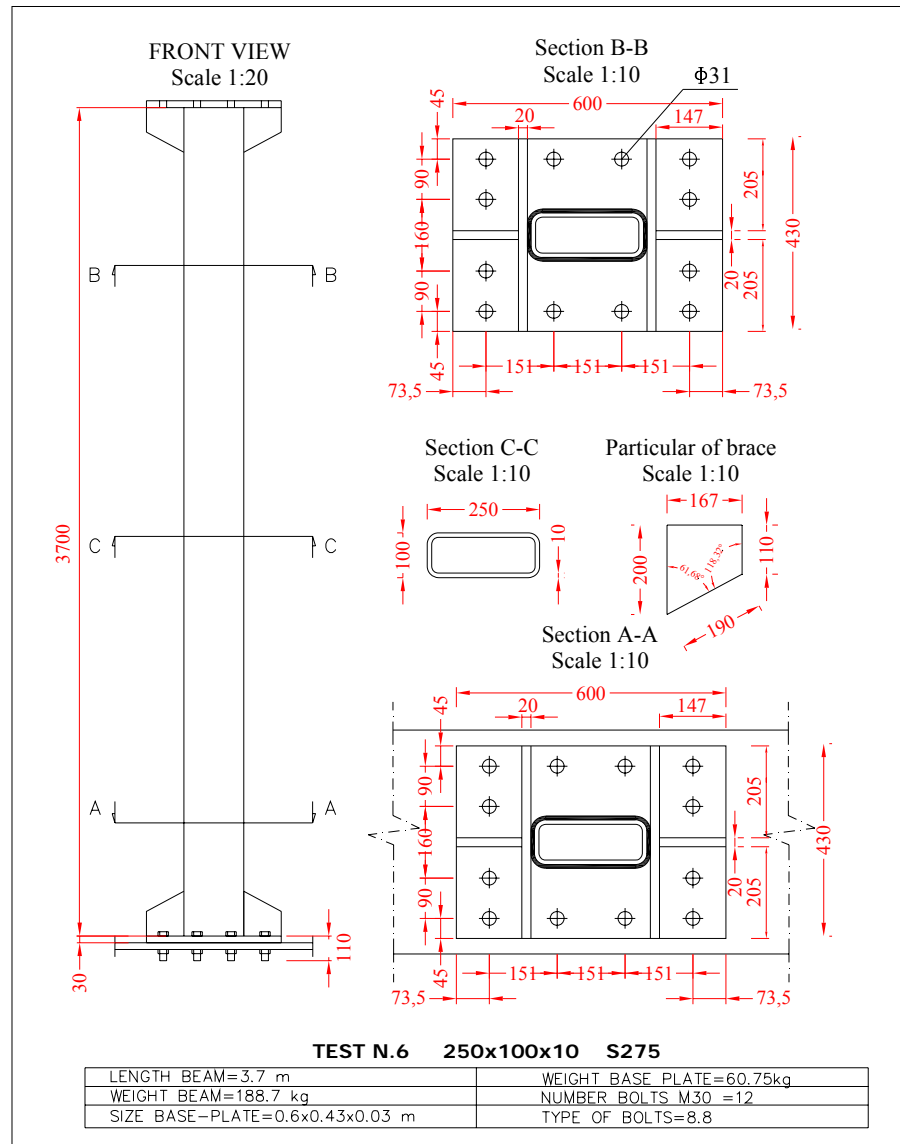


Figure 4.42 Geometric properties of specimen RHS 250x100x10.



Figure 4.43 Failure mechanism for monotonic and cyclic loading.

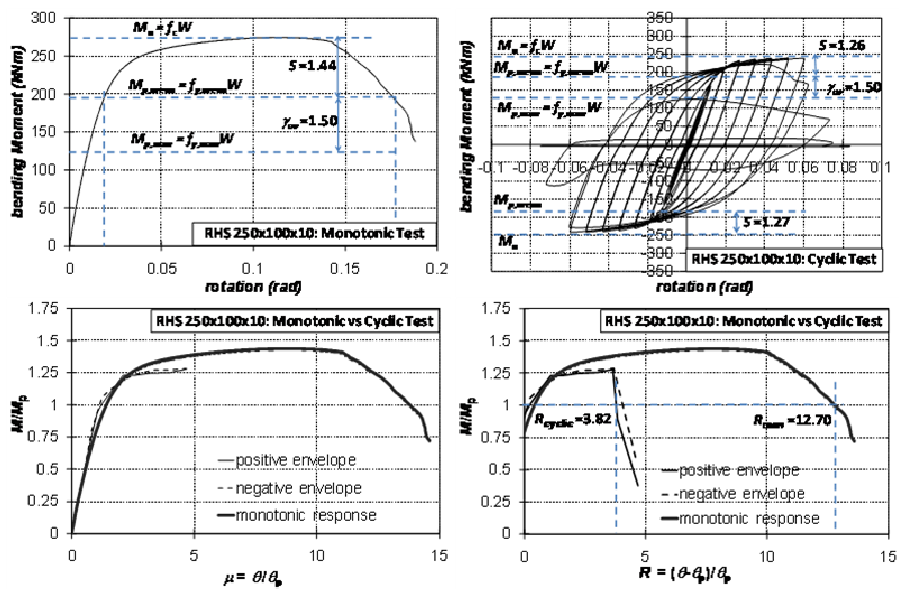


Figure 4.44 Flexural performance of specimen RHS 250x100x10.

Square Hollow Section profiles:

SHS 160x160x6.3

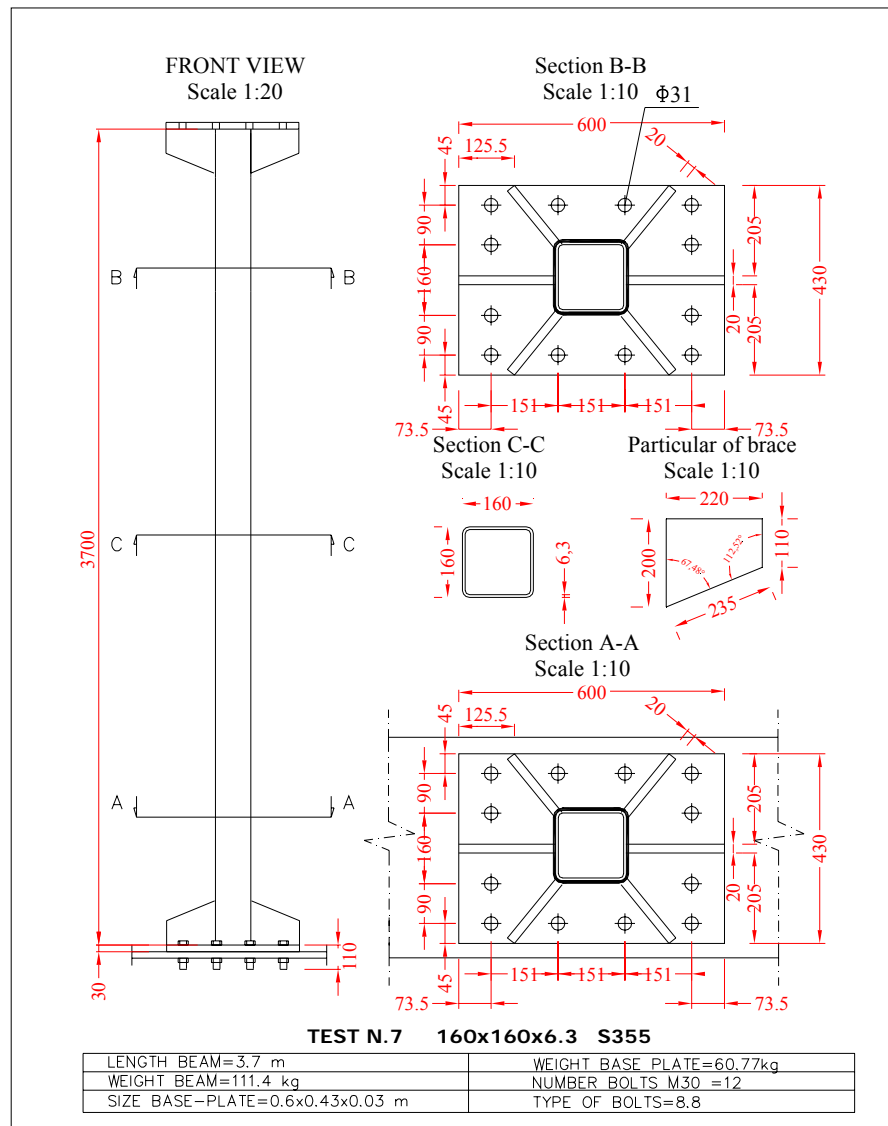


Figure 4.45 Geometric properties of specimen SHS 160x160x6.3.



Figure 4.46 Failure mechanism for monotonic and cyclic loading .

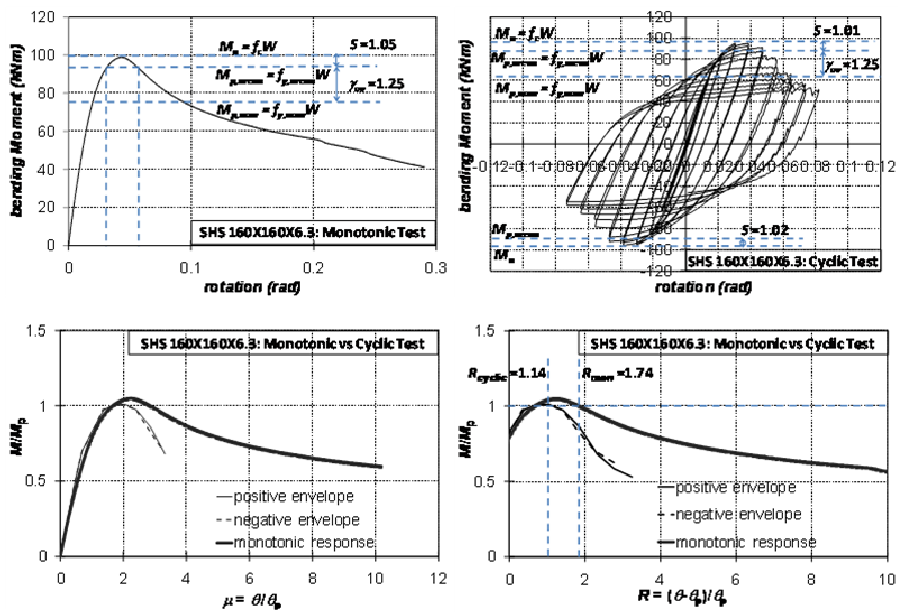


Figure 4.47 Flexural performance of specimen SHS 160x160x6.3.



Figure 4.49 Failure mechanism for monotonic and cyclic loading.

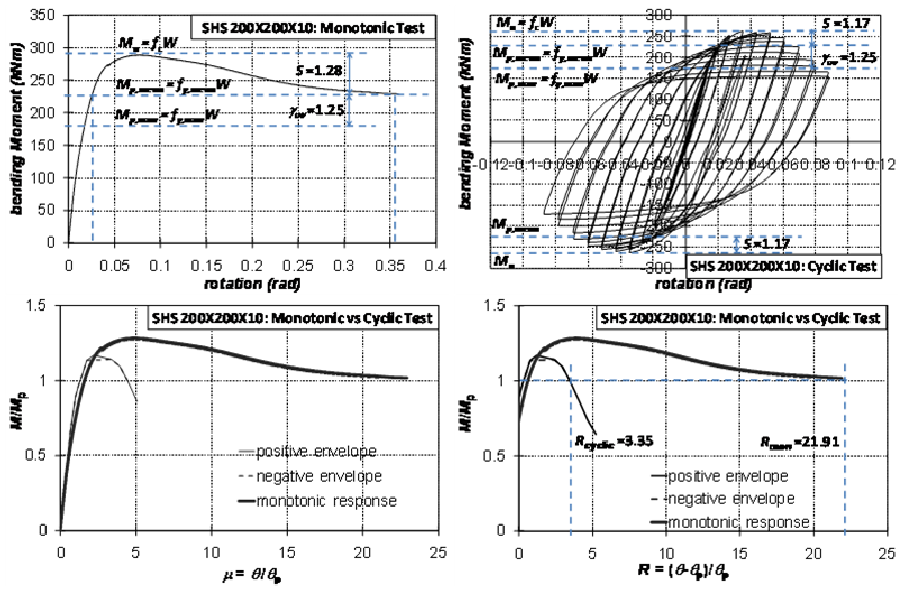


Figure 4.50 Flexural performance of specimen SHS 200x200x10.



Figure 4.52 Failure mechanism for monotonic and cyclic loading.

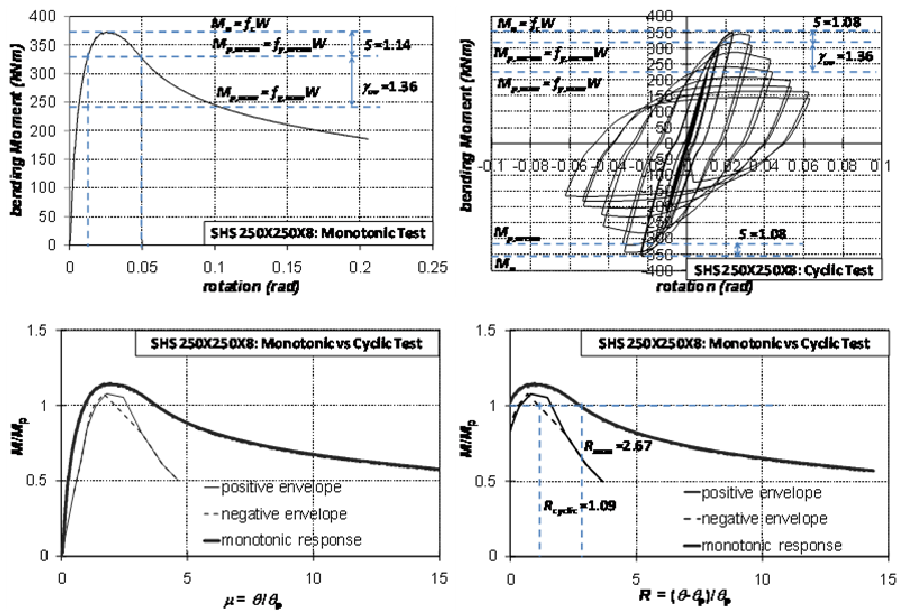


Figure 4.53 Flexural performance of specimen SHS 250x250x8.

4.4 CONCLUDING REMARKS

The exposed results for monotonic and cyclic tests in terms of rotation capacity and flexural overstrength need some considerations.

In general, tests showed the importance of the loading history on the beam flexural response. All specimens under cyclic loading exhibited a lower rotation capacity than those under monotonic loading (the average value is of $R_{cyc} = 30\% R_{mon}$). On the contrary, the flexural overstrength did not exhibit an analogous trend, as showed in the table below.

Table 4.7 Flexural performance of tested beams.

profile	R_{mon}	R_{cyc}	R_{cyc}/R_{mon}	S_{mon}	S_{cyc}	S_{cyc}/S_{mon}
HEA 160	14.44	4.64	0.32	1.14	1.31	1.15
HEB 240	54.52	8.07	0.15	1.36	1.3	0.96
IPE 300	14.69	3.96	0.27	1.18	1.26	1.07
150X100X5	15.94	3.1	0.19	1.29	1.12	0.87
160X80X4	3.95	1.81	0.46	1.25	1.05	0.84
250X100X10	12.7	3.82	0.30	1.44	1.27	0.88
160X160X6.3	1.74	1.14	0.66	1.05	1.02	0.97
200X200X10	21.91	3.35	0.15	1.28	1.17	0.91
250X250X8	2.67	1.09	0.41	1.14	1.08	0.95
average value (%)			32%	average value (%)		96%

The experimental performance of tested beams has been compared to those predicted by the examined codes (EC3/EC8, NTC '08 and OPCM 3274). As shown in the table below, it can be noticed that in case of hollow sections the codes provide different classification by different criteria. In particular, for wide flange profiles all codes are conservative. NTC'08 classification does not provide a reliable prediction of the rotation capacity of beam, underestimating it for wide flange but being unconservative for hollow profiles. Instead OPCM 3274 is conservative in terms of rotation capacity, but its criterion underestimates the flexural overstrength, especially for hollow sections.

Table 4.8 Classification of tested beams according to existing codes.

profile	Beam classification criterion		
	EC3-EC8	NTC08	OPCM3274
HEA160	2	2	2
HEB240	1	1	1
IPE300	1	1	1
RHS 150X100X5	2	2	2
RHS 160X80X4	2	2	2
RHS 250X100X10	2	2	1
SHS 160X160X6.3	2	2	3
SHS 200X200X10	2	2	2
SHS 250X250X8	2	2	3

Furthermore, to better evaluate the influence of cyclic loading on the rotation capacity and flexural overstrength, comparisons between energy dissipated by monotonic and cyclic tests have been performed. The dissipated energies by monotonic (E_{mon}) and cyclic (E_{cyc}) tests have been calculated as areas subtended by curves. Values and comparisons are showed in tables below.

Table 4.9 Dissipated energies.

profile	E_{cyc}	E_{mon}	E_{mon}/E_{cyc}
HEA 160	291049.02	25746.73	0.09
HEB 240	568804.55	131753.03	0.23
IPE 300	84271.89	20477.84	0.24
RHS 150X100X5	95849.80	16788.05	0.18
RHS 160X80X4	36021.11	5577.33	0.15
RHS 250X100X10	227387.75	43785.75	0.19
SHS 160X160X6.3	105263.14	20480.98	0.19
SHS 200X200X10	478273.48	80904.26	0.17
SHS 250X250X8	197456.35	51520.70	0.26
average value (%)			19%

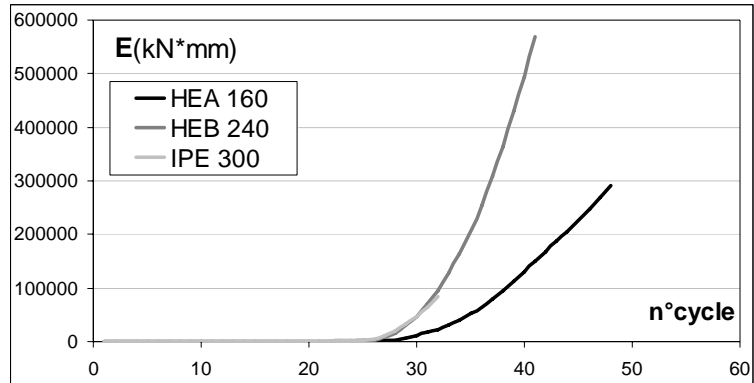


Figure 4.54 Dissipated energies for double T profiles.

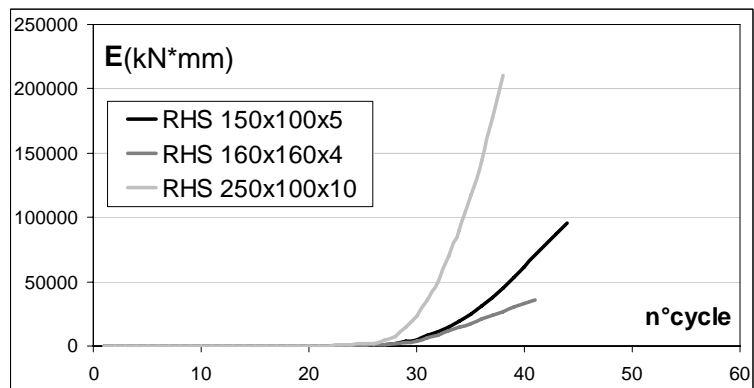


Figure 4.55 Dissipated energies for rectangular hollow profiles.

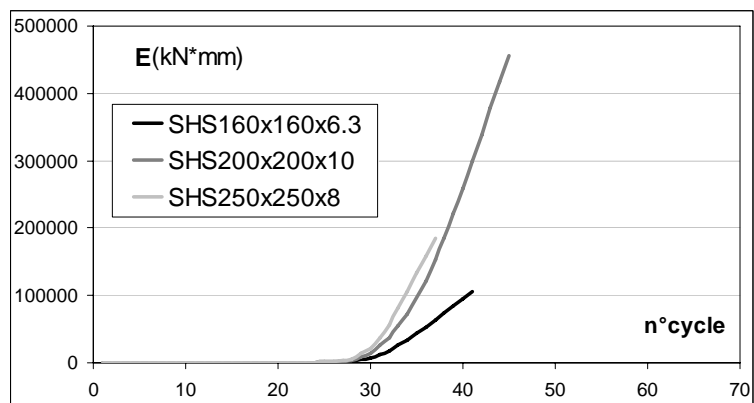


Figure 4.56 Dissipated energies for square hollow profiles.

5 CALIBRATION OF THE NUMERICAL MODELS

This chapter is dedicated to the description of the finite element models, calibrated on the basis of the experimental tests data, that has been used to perform numerical simulations (in Abaqus 6.10) of the experimental tests actually carried out. The numerical results have been compared with the experimental ones (Chapter 4) to demonstrate the validity of the assumptions made in the modelling phase.

The work presented in this chapter is preparatory to a parametrical analysis, presented in the next chapters, in which a lot of numerical analyses have been performed, with several varied parameters, without the necessity of additional expensive experimental campaigns, to reach the final scope of the thesis.

5.1 FINITE ELEMENT METHOD

The Finite Element Method (FEM) and its practical application, often known as Finite Element Analysis (FEA) is a numerical technique for finding approximate solutions of partial differential equations as well as integral equations.

FEM has been applied to a number of physical problems, where the governing differential equations are available. The method essentially consists of assuming the piecewise continuous function for the solution and obtaining the parameters of the functions in a manner that reduces the error in the solution. In solving partial differential equations, the primary challenge is to create an equation that approximates the equation to be studied, but is numerically stable, meaning that errors in the input and intermediate calculations do not accumulate and cause the resulting output to be meaningless. There are many ways of doing this, all with advantages and disadvantages. The finite element method is a good choice for solving partial differential equations over complicated

domains, when the domain changes, when the desired precision varies over the entire domain, or when the solution lacks smoothness.

5.1.1 FEA in engineering applications

A variety of specializations under the engineering discipline commonly uses integrated FEM in design and development of their products. FEM software provides a wide range of simulation options for controlling the complexity of both modeling and analysis of a system. Similarly, the desired level of accuracy required and associated computational time requirements can be managed simultaneously to address most engineering applications. FEM allows entire designs to be constructed, refined, and optimized before the design is manufactured.

This powerful design tool has significantly improved both the standard of engineering designs and the methodology of the design process in many industrial applications. The introduction of FEM has substantially decreased the time to take products from concept to the production line. In short, FEA are widely used in the product development cycles as a tool complementary to the experimental tests, since they usually reduce the overall cost of the products and the related development time.

In practice, FEA consists of a computer model of a product that is stressed and analyzed for specific results. In case of structural failure, FEA may be used to help determine the design modifications to meet the new condition.

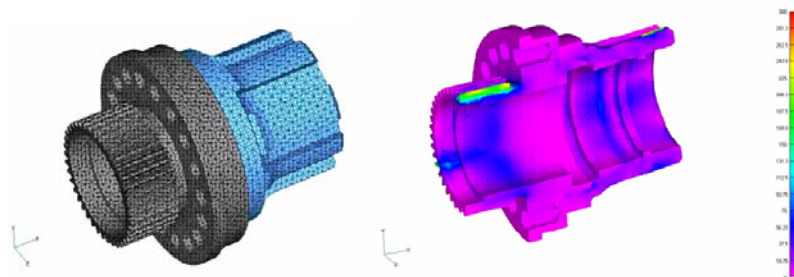


Figure 5.1 Example of finite element model and analysis results.

There are generally two types of analysis that are used in industry: 2-D modeling, and 3-D modeling. While 2-D modeling conserves simplicity and allows the analysis to be run on a relatively normal computer, it tends to yield less accurate results. 3-D modeling, however, produces

more accurate results while sacrificing the ability to run on all but the fastest computers effectively. Within each of these modeling schemes, the analysis can be made behave linearly or non-linearly. Linear systems are far less complex and generally do not take into account plastic deformation. Non-linear systems do account for plastic deformation, and many also are capable of testing a material all the way to fracture.

The division into elements may partly correspond to natural subdivisions of the structure. For example, an object may be divided into groups of elements corresponding to different material properties. Most or all of the model parameters have very direct relationships to the structure and material properties of the system. A finite-element model generally has relatively few free parameters whose values need to be adjusted to fit the data. This assumes, of course, that the parameters are known a priori from other measurements.

The elements may be 1-D, 2-D (triangular or quadrilateral), or 3-D (tetrahedral, hexahedral, etc.) and may be linear or higher-order.

The elements may model mechanics, acoustics, thermal fields, electromagnetic fields, etc., or coupled problems. In a mechanical problem, the elements may model membranes, beams, thin plates, thick plates, solids, fluids, etc.

5.1.2 FEA with Abaqus 6.10 software

The numerical analyses developed in this work have been carried out by means of the ABAQUS 6.10 multi-purpose software, that is based on the Finite Element Method.



Figure 5.2 Finite Element Method Software ABAQUS 6.10.

The FEA with ABAQUS software is subdivided into three main steps:

- the pre-processing phase, that is the one in which the finite element model of the real problem is created;
- the simulation phase, that is the one in which the software solves the numerical problem defined in the model;
- the post-processing phase, that is the one in which analysis results are obtained.

The essential components used to describe the physical problems in ABAQUS are: the discretized geometry, the element section properties, the material data, the loads and boundary conditions, the analysis type, and the output requests that are defined into the pre-processing phase.

Each finite element, in ABAQUS, is characterized by five features:

- the element FAMILY, that is essentially related to the used geometry type (beam, shell, solid, etc.);

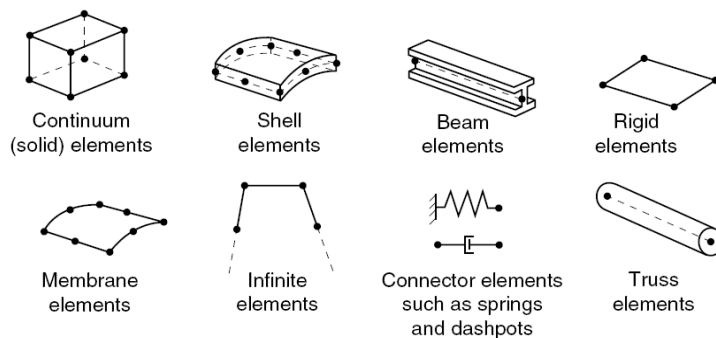


Figure 5.3 Finite Element families (Abaqus User's Manual).

- the DEGREES OF FREEDOM, that are the discrete parameters constituting the fundamental unknowns of the problem;
- the NUMBER OF NODES per element, that defines the order of interpolation used for defining the deformed shape of the element edges. A finite element with two nodes per edge (one at each corner of the element) uses a linear interpolation, at the end the deformed edges are still segments, and so such types of elements are usually called first-order or linear elements. Instead, elements with mid-side nodes use quadratic interpolation, the deformed edges fitting quadratic curves, and so they are usually called second-order or quadratic elements;

- the FORMULATION, that is referred to the mathematical theory used for defining the element behaviour. Lagrangian or Eulerian formulations may be used, the former being referred to problems in which the material associated to an element remains associated to that element during the whole analysis, and the latter being referred to problems in which the elements are fixed in space and the material flows through them;
- the INTEGRATION, that indicates the way different quantities are integrated over the volume of each element. Both full and reduced integration options are available, they being referred to the number of points required to integrate the polynomial terms in the stiffness matrix in an element.

Moreover, for the FEA in ABAQUS, it must be considered the non-linear problems. The analyses presented in this work are carried out by means of the ABAQUS implicit solver, which uses the Newton-Raphson method to obtain solutions for non-linear problems.

In general, in a non-linear analysis the solution cannot be calculated by solving a single system of equations, as would be done in a linear problem, and so the solution may be found by gradually and incrementally applying the specified loads, proceeding toward the final solution. Therefore, the simulation is subdivided into a number of load increments and the approximate equilibrium configuration at the end of each increment is found, by means of an iterative procedure. If the model is not in equilibrium at the end of the iteration, ABAQUS tries another iteration. At each iteration, the obtained solution should be closer to equilibrium, and sometimes the program may need many iterations to obtain a solution. For each iteration, ABAQUS forms the model's stiffness matrix and solves a system of equations. Consequently, in a computational costs perspective, each iteration is equivalent to a complete linear analysis. The latter consideration underlines the large computational expense of a non-linear analysis in ABAQUS.

The sum of all of the incremental responses is the approximate solution for the non-linear analysis. Thus, ABAQUS combines incremental and iterative procedures for solving non-linear problems. The user suggests the size of the first increment in each step of the simulation, and this can improve the control on the simulation convergence by the user, but the size of the load increments used for the solution of non-linear problems is automatically adjusted by ABAQUS (Esposto, 2008).

5.2 MODELING OF TESTED BEAMS

In the present paragraph, the assumptions at the base of the used numerical models are exposed. Both double T and hollow profiles were modelled, and both monotonic and cyclic tests have been simulated. The validity and reliability of the modelling technique was proved, to be authorized to extend it to appropriate and finalized parametric analyses. It is important to have a set of experimental data upon which to calibrate the finite element model. The multi-purpose software ABAQUS (Version 6.10), has been used to create the finite element models and to perform the finite element analyses.

5.2.1 Definition of the materials

The finite element software ABAQUS provides a wide range of material types, which allow to cover problems involving metals, plastics, rubbers, foams and so on. With particular regard to ductile materials, such as steel, plasticity can be reliably caught, also accounting for hardening phenomena, and so the non-linearity due to the material characteristics can be well included in the models (Esposto, 2008).

Usual engineering measures of strain and stress are the so called “nominal strain” (ϵ_{nom}) and “nominal stress” (σ_{nom}).

Nominal strain is defined as the ratio between the total elongation (Δl) of the specimen in tension and its initial length (l_0).

$$\epsilon_{nom} = \Delta l / l_0 \quad (5.1)$$

Nominal stress is defined as the ratio between the actual force (F) on the specimen and initial value of its cross-section area (A_0).

$$\sigma_{nom} = F / A_0 \quad (5.2)$$

In order to take adequately into consideration both the occurrence of finite deformations and the nearly incompressible nature of the plastic deformations in ductile metals, ABAQUS requires the material be defined in terms of “true strain” (ϵ_{true}) and “true stress” (σ_{true}).

True strain is conceptually obtained from nominal strain by considering the limit $\Delta l \rightarrow dl \rightarrow 0$.

True stress is obtained by imposing that the actual volume of the part undergoing plastic deformations is the same as the initial one: $A_0 l_0 = A l$.

On the basis of the above considerations, the relationships between the nominal and the true values of strain and stress are the following :

$$\sigma_{true} = \sigma_{nom} (1 + \varepsilon_{nom}) \quad (5.3)$$

$$\varepsilon_{true} = \ln(1 + \varepsilon_{nom}) \quad (5.4)$$

In addition, the plasticity model in ABAQUS requires the definition of the plastic true strain values (ε_{pl}), which is obtained by subtracting the true elastic strain from the total true strain:

$$\varepsilon_{pl} = \varepsilon_{true} - \frac{\sigma_{true}}{E} \quad (5.5)$$

In particular, for this study, the material properties were obtained from the experimental tests as exposed in Chapter 4, paragraph 4.3.1. For consultation simplicity, the tables that summarize the main test results are presented here again, but with their average values.

Table 5.1 Material properties of tested beams for double T profiles.

section	specimen	fy exp, av	ft texp, av
HEA 160	WEB	338	475
HEA 160	FLANGE	337	460
HEB 240	WEB	354	421
HEB 240	FLANGE	284	441
IPE 300	WEB	349	454
IPE 300	FLANGE	316	439

Table 5.2 Material properties of tested beams for hollow profiles.

section	fy exp, av	ft texp, av
RHS 150X100X5	354	387
RHS 160X80X4	324	361
RHS 250X100X10	418	506
SHS 160X160X6.3	432	459
SHS 200X200X10	453	514
SHS 250X250X8	482	525

For the final use of the material properties in the ABAQUS modeling, the experimental test results, their average values were transformed in “true stress” – “true strain” format, as explained before.

In the following figures there is an example of this procedure, but not all the results, because of their repetitiveness and uninterestingness.

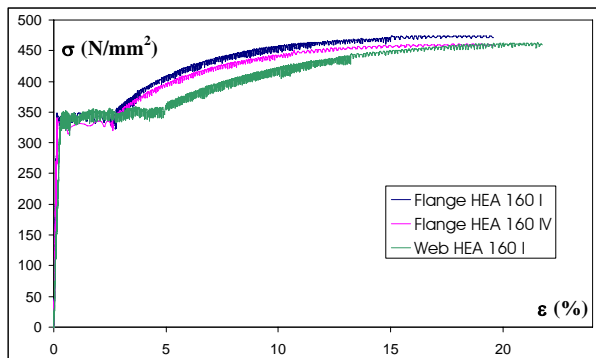


Figure 5.4 Stress-strain diagram resulting from experimental tests.

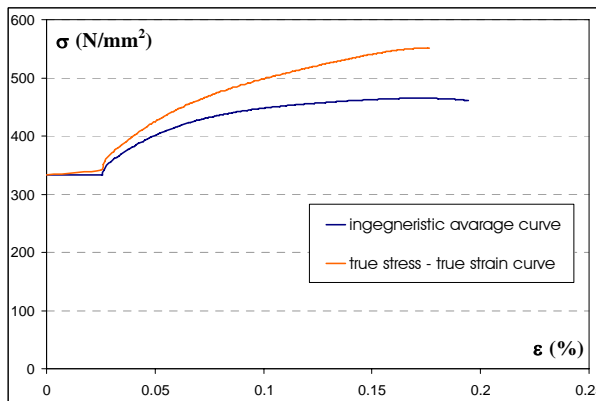


Figure 5.5 Average ingegneristic and true stress - true strain diagrams.

5.2.2 Element type and mesh: sensitivity study

For the choice of the more appropriate finite element type to use for the modeling, it has been performed a sensitivity analysis of this kind, devoted to find the combination of element type, geometric order and integration type, corresponding to the best compromise between the accuracy of the model and the computational costs.

The combinations element type - geometric order - integration that has been investigated are listed below:

- Shell - linear - reduced integration;
- Shell - linear - complete integration;
- Shell - quadratic - reduced integration.

For each of these combinations the thickness integration rule has been varied (Simpson, Gauss) as far as the thickness integration points:

- 3, 5, 7 for Simpson integration rule, the default value is 5;
- 3, 5, 7 for Gauss integration rule, the default value is 3.

There were also investigated solid element type, with the combinations element type - geometric order - integration as listed below:

- Solid - linear - reduced integration;
- Solid - linear - complete integration;
- Solid - quadratic - reduced integration;
- Solid - quadratic - complete integration.

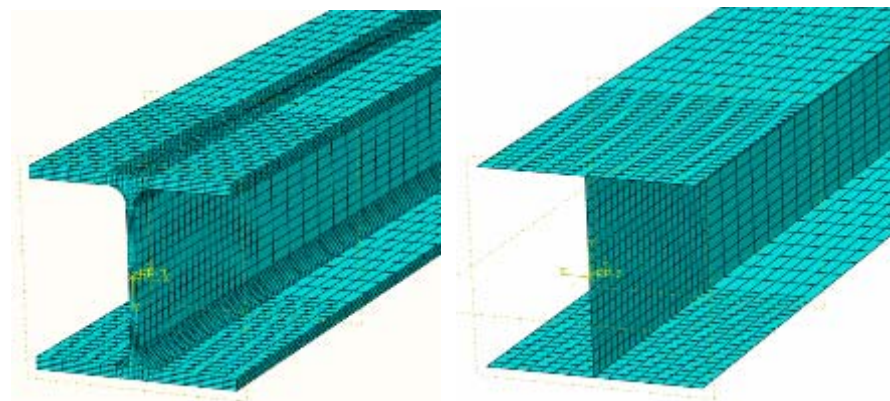


Figure 5.6 Examples of solid and shell modeling.

After this sensitivity study the 4-nodes shell element (S4) with 4 nodes per element, 6 degrees of freedom per node and a linear interpolation function was adopted for the modeling of all the beams corresponding to the experimentally tested ones. This kind of element matches the typical requirements of problems involving material plasticity, large size models and hot rolled section beams, reducing the high computational costs of solid elements.

Table 5.3 Element type vs computational costs.

Type	Order	Integration	Rule	Points	Time [sec]
SHELL	Linear	Reduced	Simpson	3	120
SHELL	Linear	Reduced	Simpson	5	108
SHELL	Linear	Reduced	Simpson	7	109
SHELL	Linear	Reduced	Gauss	3	149
SHELL	Linear	Reduced	Gauss	5	102
SHELL	Linear	Reduced	Gauss	7	160
SHELL	Linear	Complete	Simpson	3	180
SHELL	Linear	Complete	Simpson	5	147
SHELL	Linear	Complete	Simpson	7	137
SHELL	Linear	Complete	Gauss	3	146
SHELL	Linear	Complete	Gauss	5	163
SHELL	Linear	Complete	Gauss	7	165
SHELL	Quadratic	Reduced	Simpson	3	903
SHELL	Quadratic	Reduced	Simpson	5	2168
SHELL	Quadratic	Reduced	Simpson	7	2852
SHELL	Quadratic	Reduced	Gauss	3	915
SHELL	Quadratic	Reduced	Gauss	5	1990
SHELL	Quadratic	Reduced	Gauss	7	2779
SOLID	Linear	Reduced	-	-	1117
SOLID	Linear	Complete	-	-	1714
SOLID	Quadratic	Reduced	-	-	5305
SOLID	Quadratic	Complete	-	-	3512

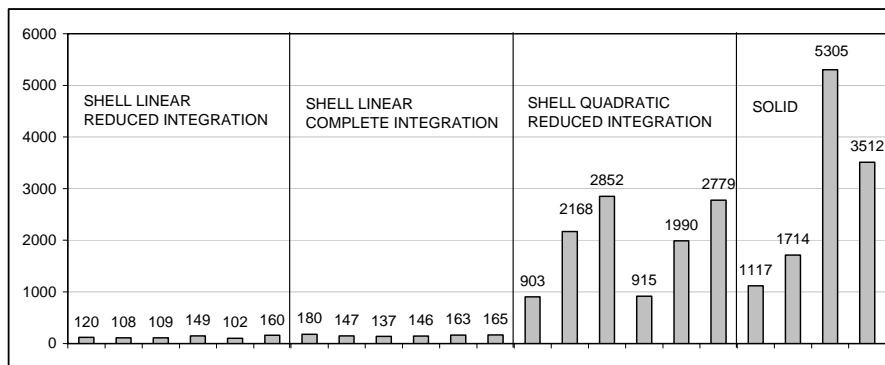


Figure 5.7 Element type vs computational costs.

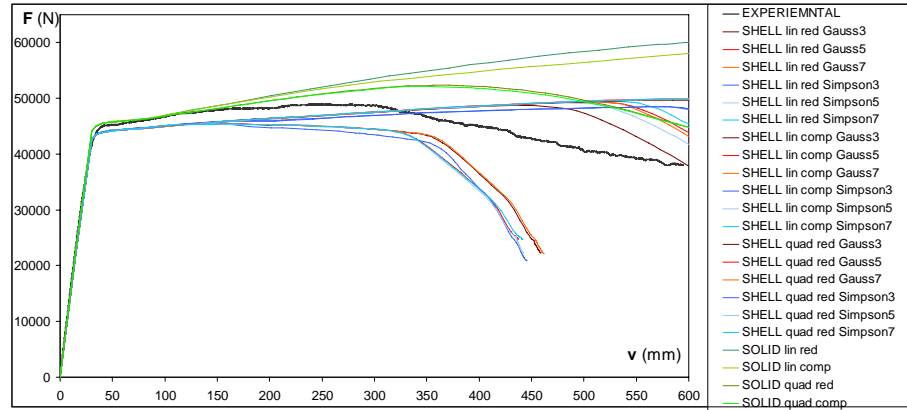


Figure 5.8 Element type vs simulation accuracy.

The geometry of the section of each shell model corresponds to the centerline dimensions of the tested beam, and the length of the whole model corresponds to the distance between the point in which is applied the load through the hydraulic actuator and the end of the stiffeners at the base of the beam bolted on the steel truss on the floor.

Moreover, a preliminary mesh refinement study was conducted to determine the level of refinement necessary to accomplish an accurate result pattern with the minimum computational effort.

The final decision was to use two different levels of mesh refinements: one for the plastic hinge zone (highly refined) and another for the remaining part of the beam (roughly refined), as shown in the following figure. The width of plastic hinge region, that is the one in which the main plastic deformations are expected, has been fixed case by case, calculating the length of the plastic hinge (L_m) by the equations available in scientific literature (Haaijer 1957 and Lay 1965).

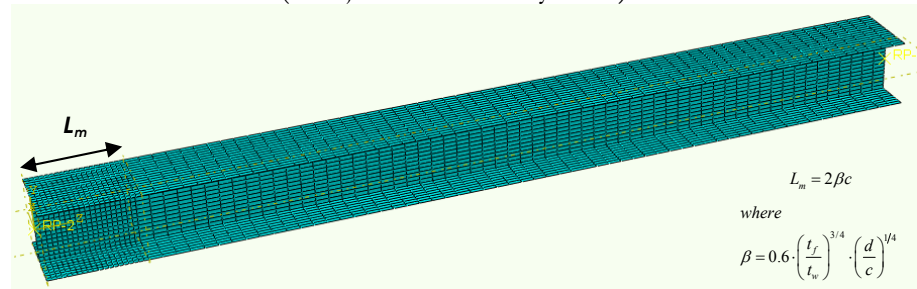


Figure 5.9 Different levels of mesh refinements (double T profiles).

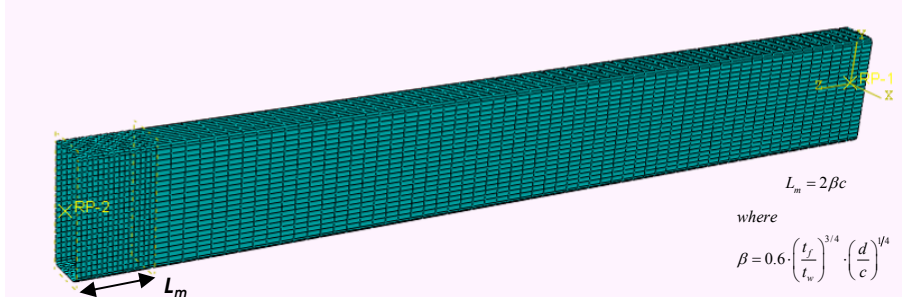


Figure 5.10 Different levels of mesh refinements (hollow profiles).

5.2.3 Loads and boundary conditions

To simulate the real boundary conditions in the numerical models, nodes belonging to the cross-sections at the ends of the beam were constrained to two reference points (RP-1 and RP-2).

RP-2 is the master node at the left end of the beam and was restrained against displacements and rotations in all directions.

RP-1 is the master node at the right end of the beam and was restrained against displacements in two directions and rotations in two directions, providing a restraint for the torsional degree of freedom and out-of plane displacements, and the beam deformation was imposed by applying displacements in the 2-direction (vertical).

The combination of these boundary conditions imposed a constant shear force in the element and a linear bending moment distribution (namely cantilever scheme).

The numerical analyses reproduce both the monotonic and cyclic experimental tests. In each model it has been created a static step, corresponding alternatively to the monotonic and the cyclic loading pattern, that was simulated by applying a displacement history.

In particular for the simulation of monotonic tests, the displacement history is from 0 to 600mm, that is the complete hydraulic actuator stroke. While for the simulation of cyclic tests, the AISC2005 loading protocol was used.

The sequence suggested by the code is reported below in terms of chord rotation (θ), then displacements were obtained by rotations ($\delta = \theta L$):

- 6 cycles with $\theta = 0.00375$ rad
- 6 cycles with $\theta = 0.005$ rad
- 6 cycles with $\theta = 0.0075$ rad

- 4 cycles with $\theta = 0.01$ rad
- 2 cycles with $\theta = 0.015$ rad
- 2 cycles with $\theta = 0.02$ rad
- 2 cycles with $\theta = 0.03$ rad
- 2 cycles with $\theta = 0.04$ rad

If failure does not occur, the test continues increasing the rotation amplitude of 0.01rad for 2 successive cycles up to collapse.

The following figures show the applied displacement histories for monotonic and cyclic simulations.

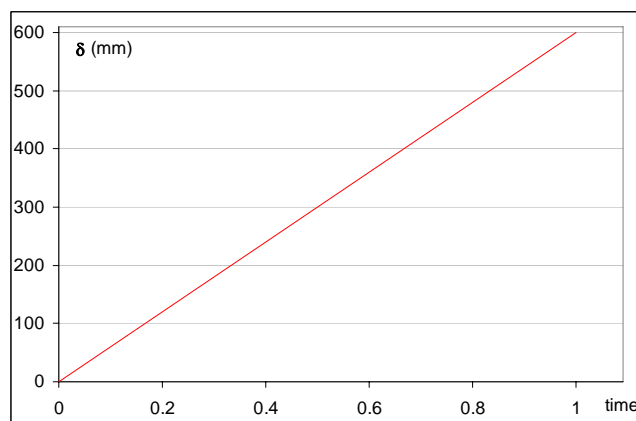


Figure 5.11 Displacement history for monotonic simulation.

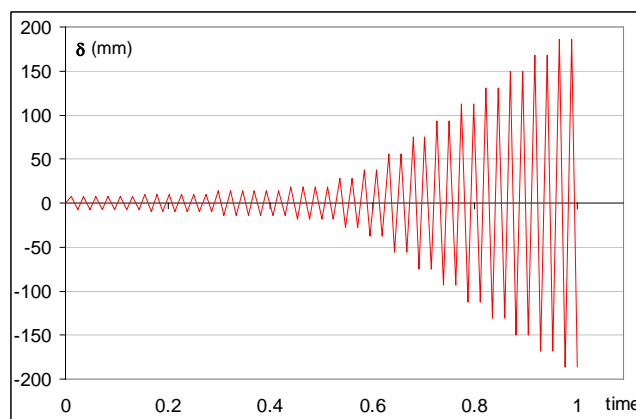


Figure 5.12 Displacement history for cyclic simulations.

5.3 COMPARISON OF RESULTS

Double T profiles:

HEA 160 monotonic

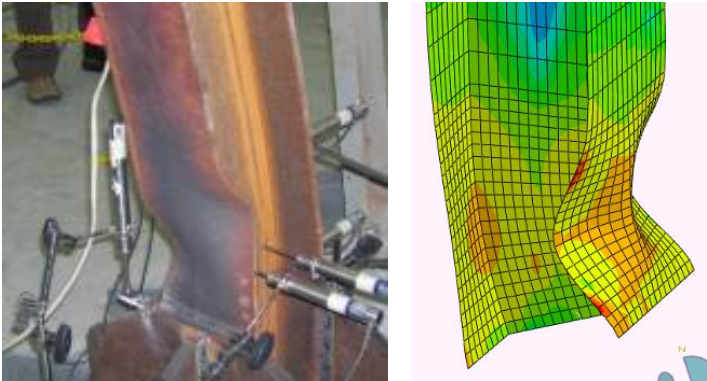


Figure 5.13 Failure mechanism for monotonic loading HEA 160.

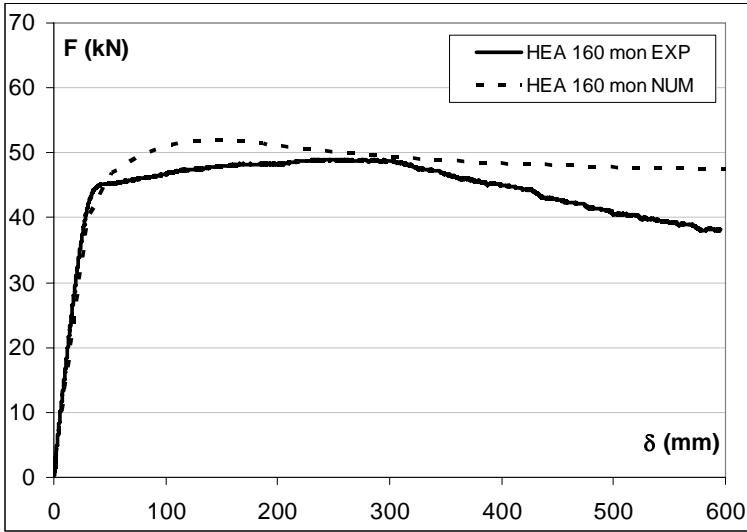


Figure 5.14 Experimental vs numerical monotonic curve HEA 160.

HEA 160 cyclic

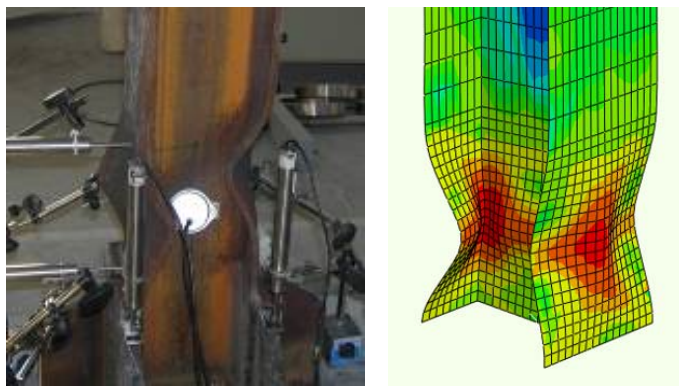


Figure 5.15 Failure mechanism for cyclic loading HEA 160.

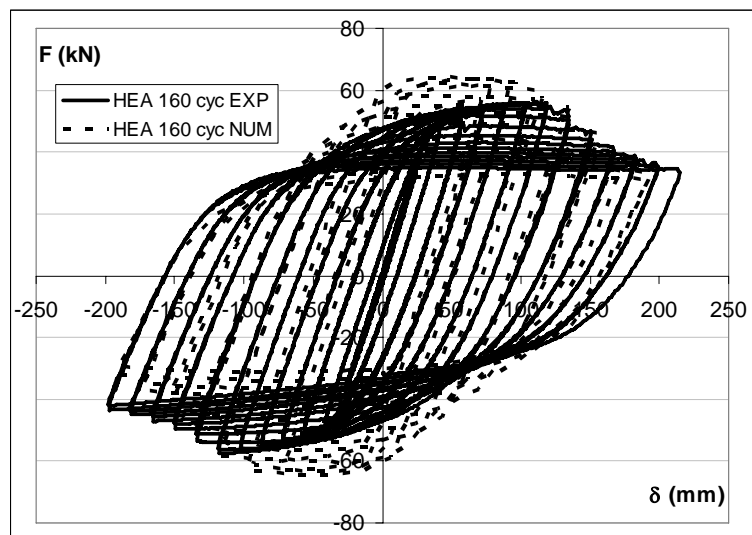


Figure 5.16 Experimental vs numerical cyclic curve HEA 160.

HEB 240 monotonic

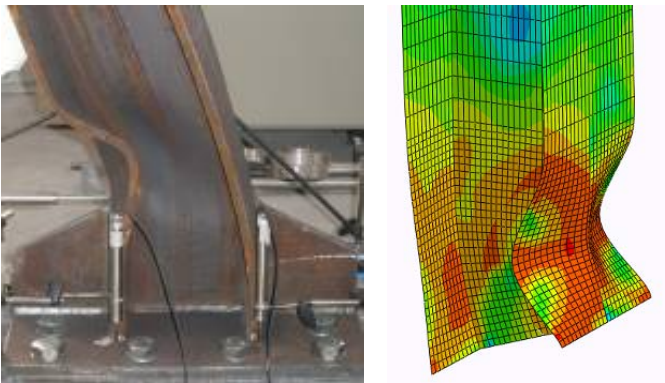


Figure 5.17 Failure mechanism for monotonic loading HEB 240.

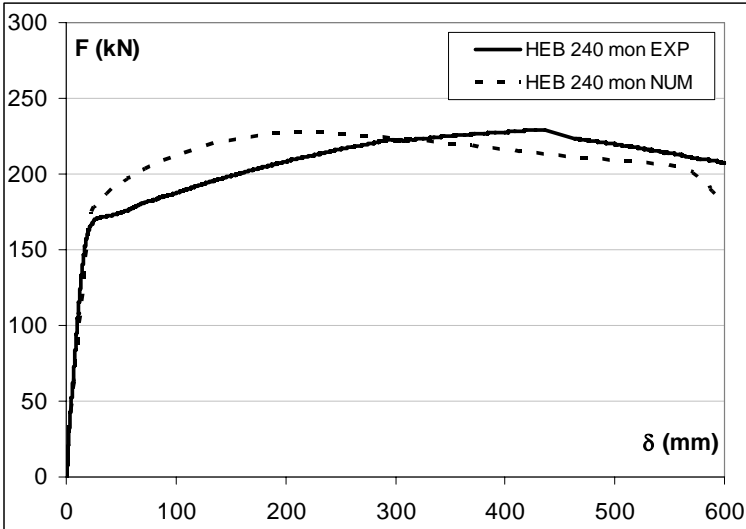


Figure 5.18 Experimental vs numerical monotonic curve HEB 240.

HEB 240 cyclic

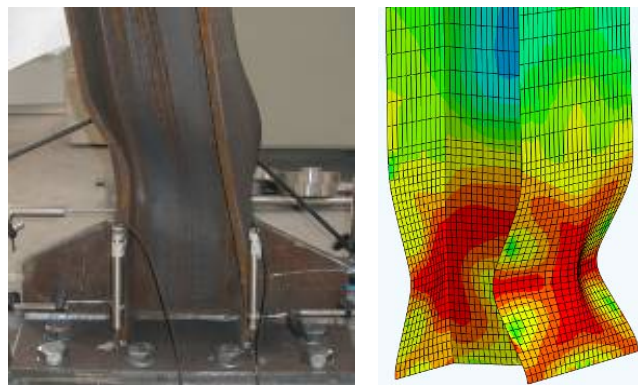


Figure 5.19 Failure mechanism for cyclic loading HEB 240.

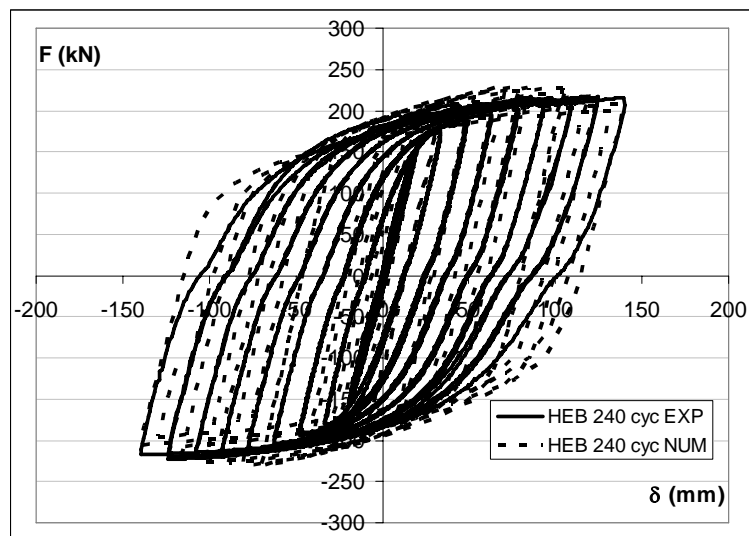


Figure 5.20 Experimental vs numerical cyclic curve HEB 240.

IPE 300 monotonic

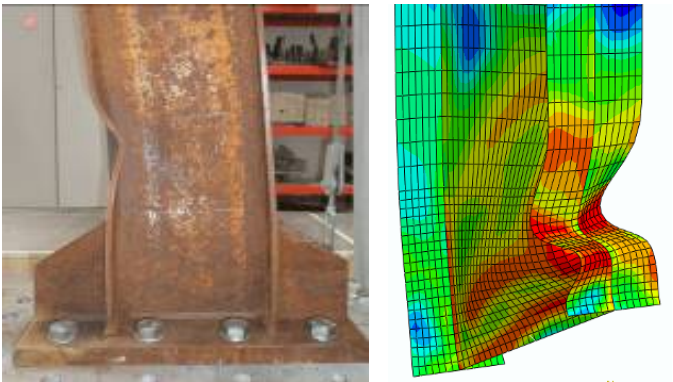


Figure 5.21 Failure mechanism for monotonic loading IPE 300.

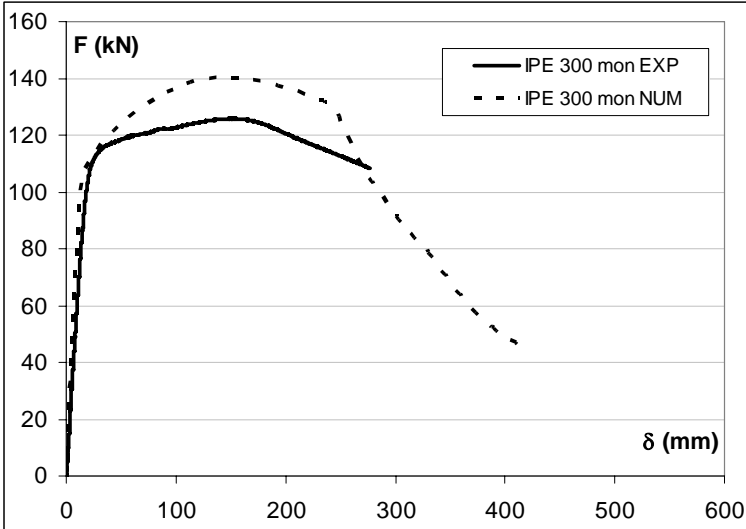


Figure 5.22 Experimental vs numerical monotonic curve IPE 300.

IPE 300 cyclic

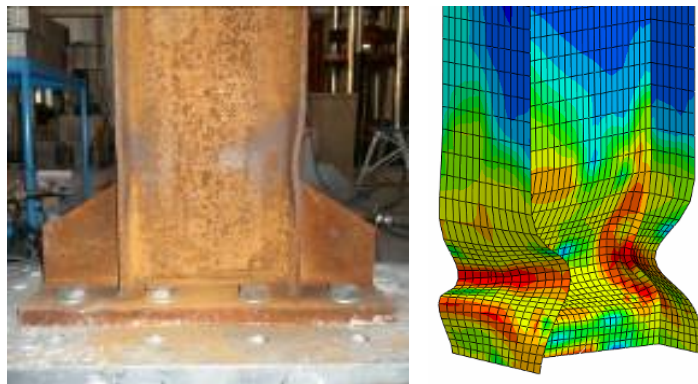


Figure 5.23 Failure mechanism for cyclic loading IPE 300.

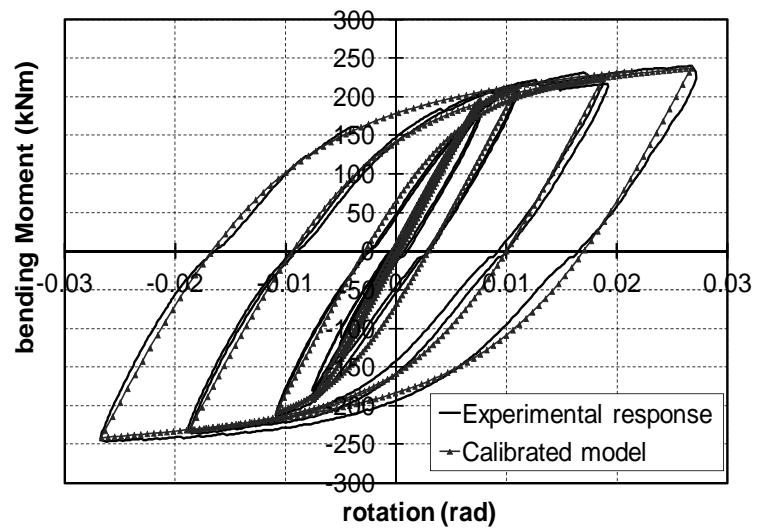


Figure 5.24 Experimental vs numerical cyclic curve IPE 300.

Rectangular Hollow Section profiles:

RHS 150x100x5 monotonic

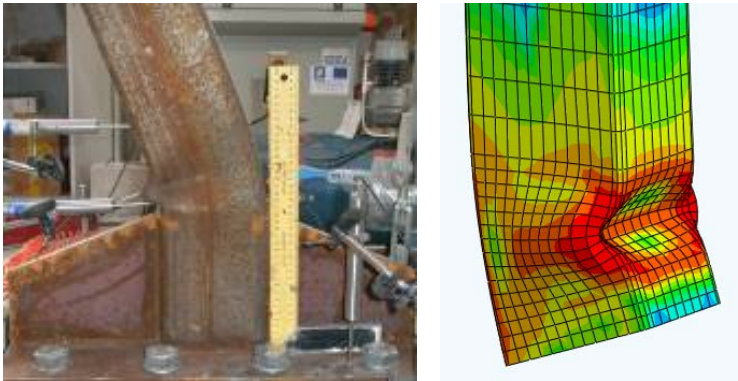


Figure 5.25 Failure mechanism for monotonic loading 150x100x5.

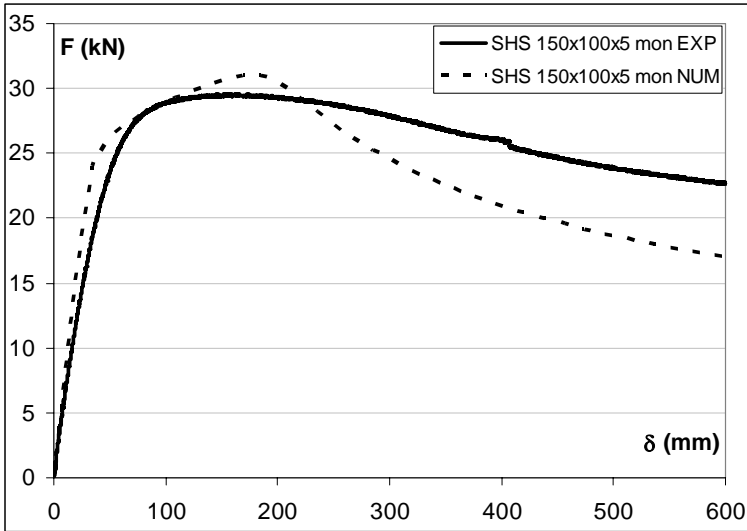


Figure 5.26 Experimental vs numerical monotonic curve 150x100x5.

RHS 150x100x5 cyclic

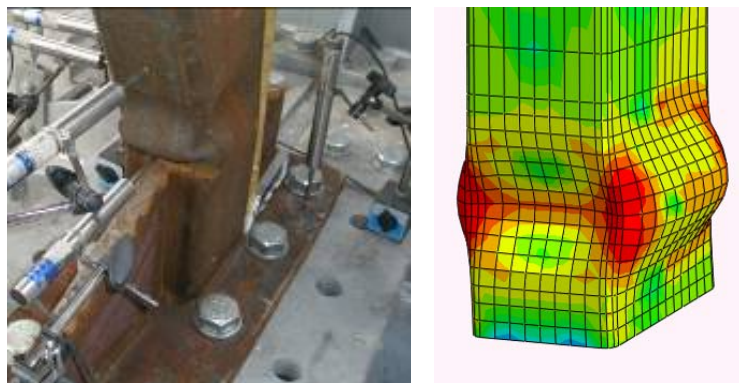


Figure 5.27 Failure mechanism for cyclic loading 150x100x5.

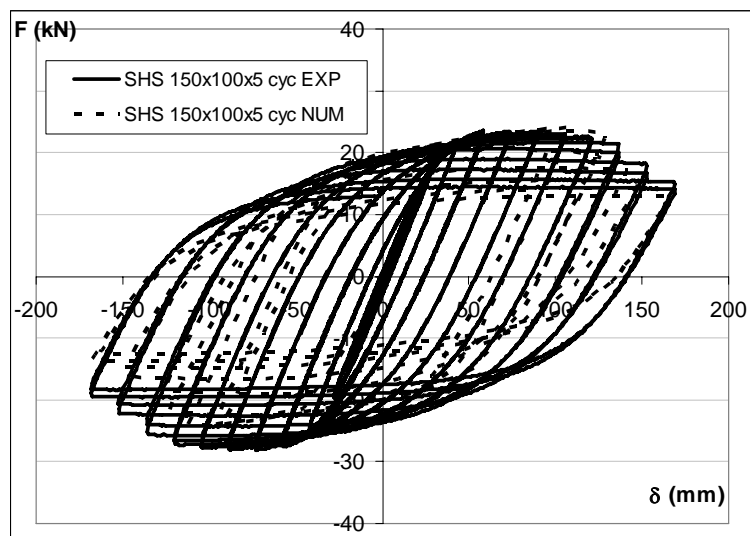


Figure 5.28 Experimental vs numerical cyclic curve 150x100x5.

RHS 160x80x4 monotonic

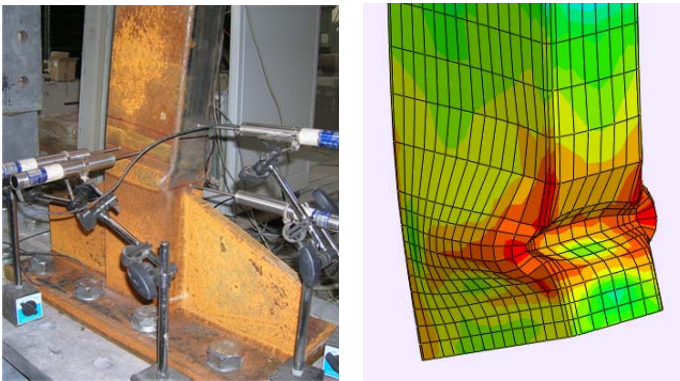


Figure 5.29 Failure mechanism for monotonic loading 160x80x4.

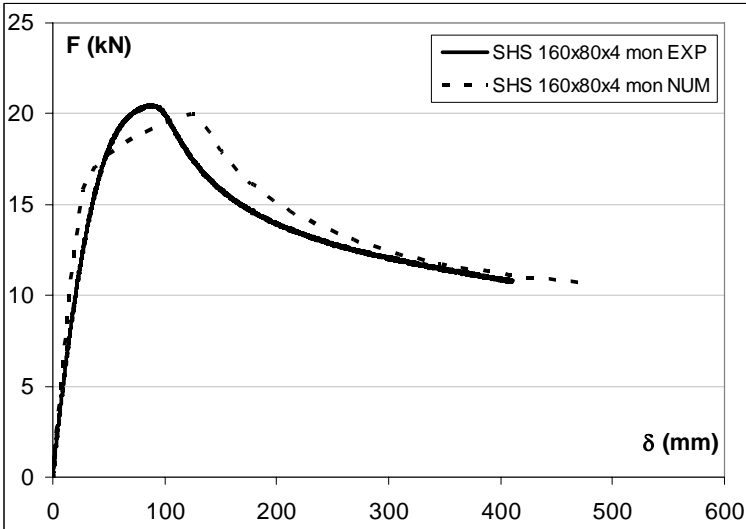


Figure 5.30 Experimental vs numerical monotonic curve 160x80x4.

RHS 160x80x4 cyclic

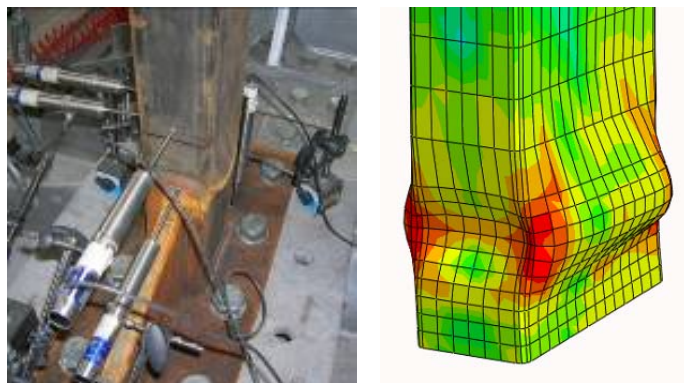


Figure 5.31 Failure mechanism for cyclic loading 160x80x4.

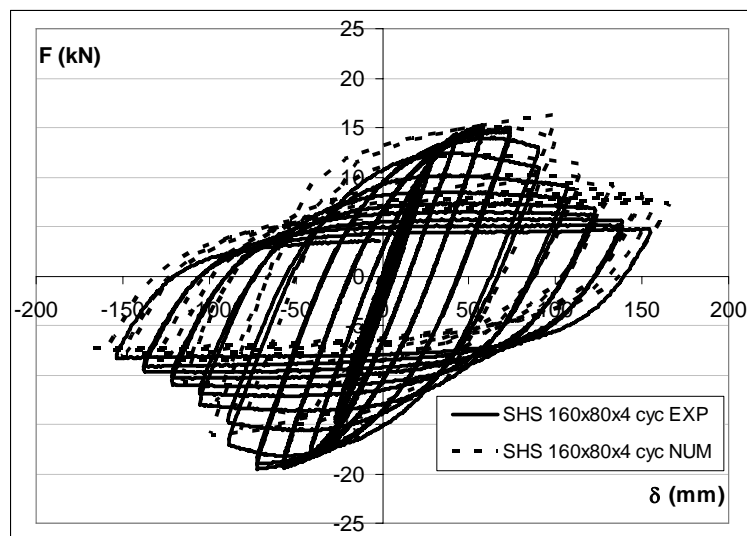


Figure 5.32 Experimental vs numerical cyclic curve 160x80x4.

RHS 250x100x10 monotonic

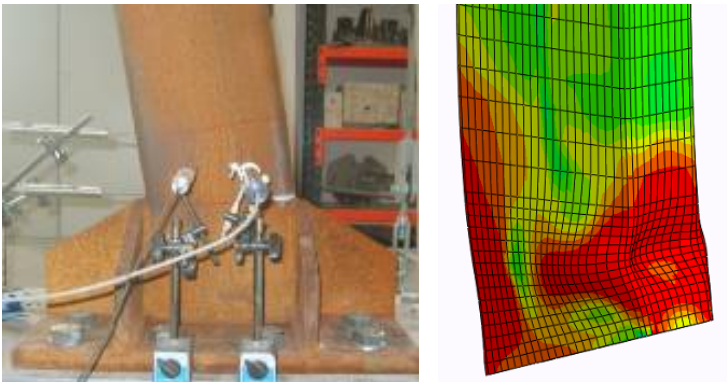


Figure 5.33 Failure mechanism for monotonic loading 250x100x10.

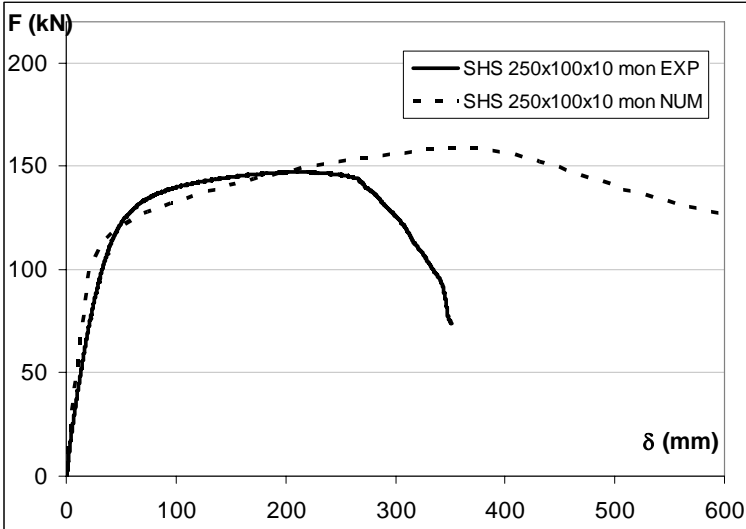


Figure 5.34 Experimental vs numerical monotonic curve 250x100x10.

RHS 250x100x10 cyclic



Figure 5.35 Failure mechanism for cyclic loading 250x100x10.

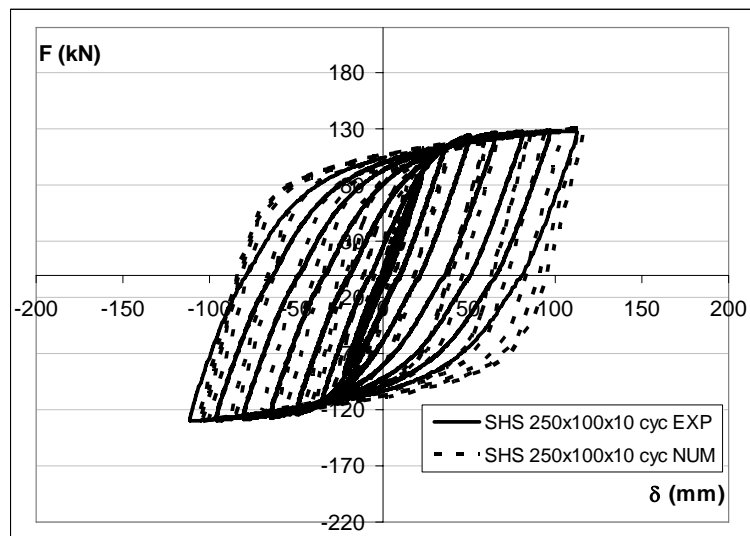


Figure 5.36 Experimental vs numerical cyclic curve 250x100x10.

Square Hollow Section profiles:

SHS 160x160x6.3 monotonic

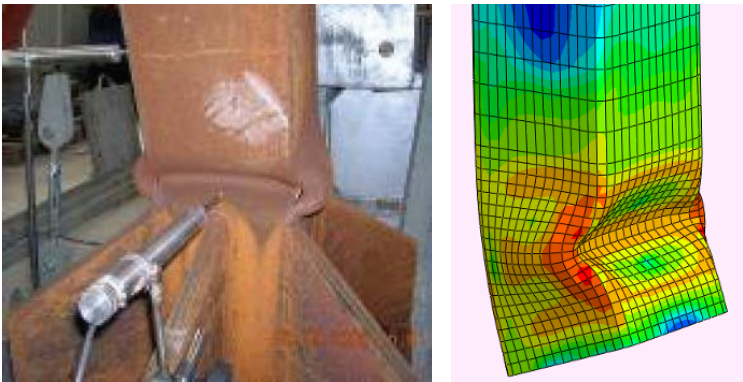


Figure 5.37 Failure mechanism for monotonic loading 160x160x6.3.

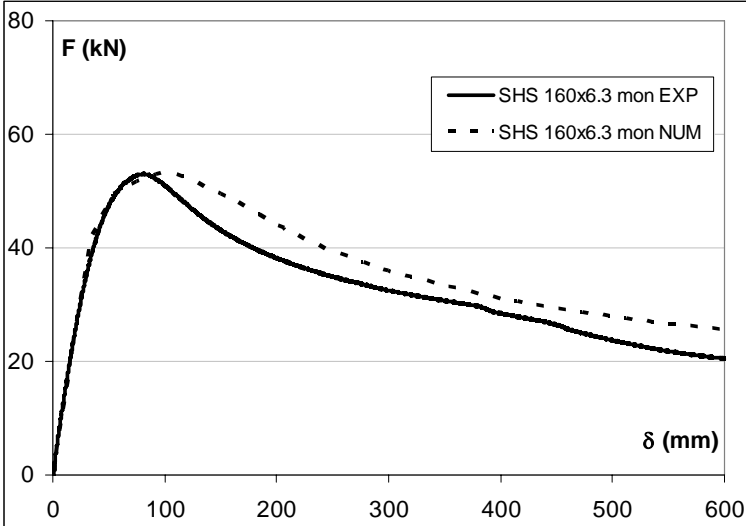


Figure 5.38 Experimental vs numerical monotonic curve 160x160x6.3.

SHS 160x160x6.3 cyclic

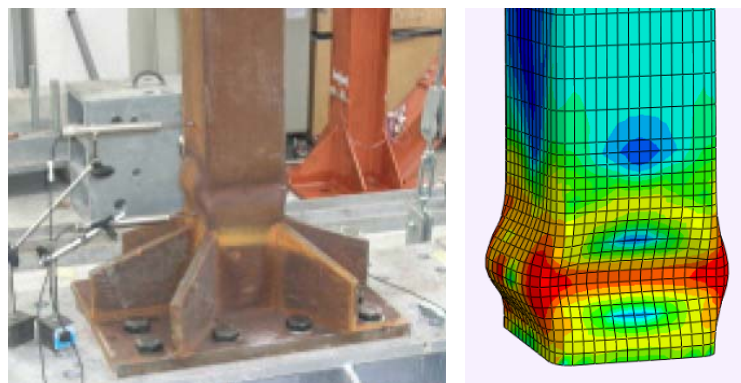


Figure 5.39 Failure mechanism for cyclic loading 160x160x6.3.

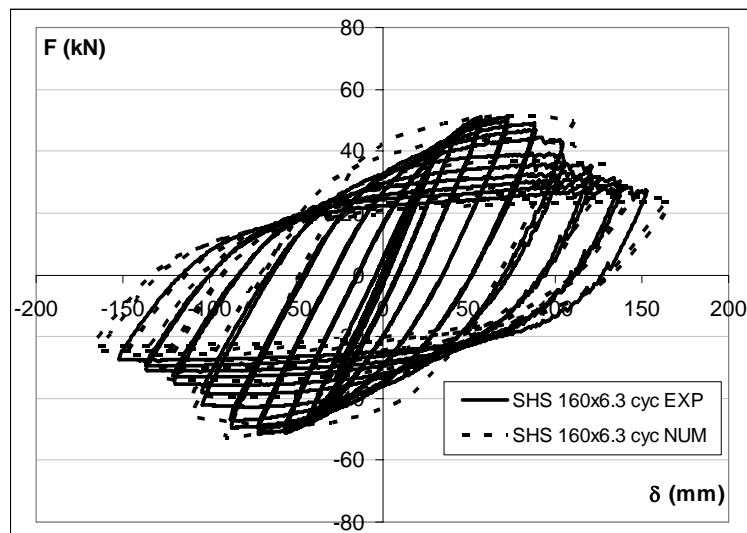


Figure 5.40 Experimental vs numerical cyclic curve 160x160x6.3.

SHS 200x200x10 monotonic

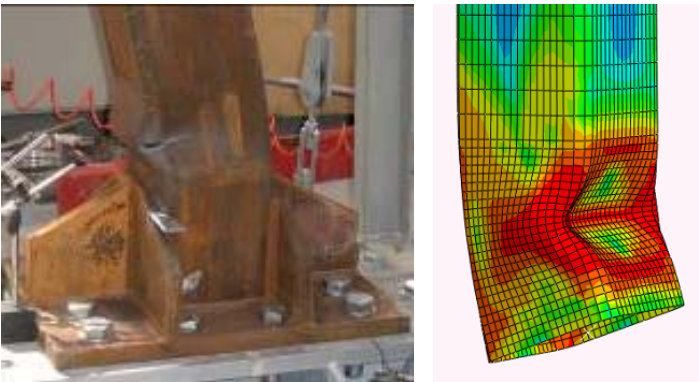


Figure 5.41 Failure mechanism for monotonic loading 200x200x10.

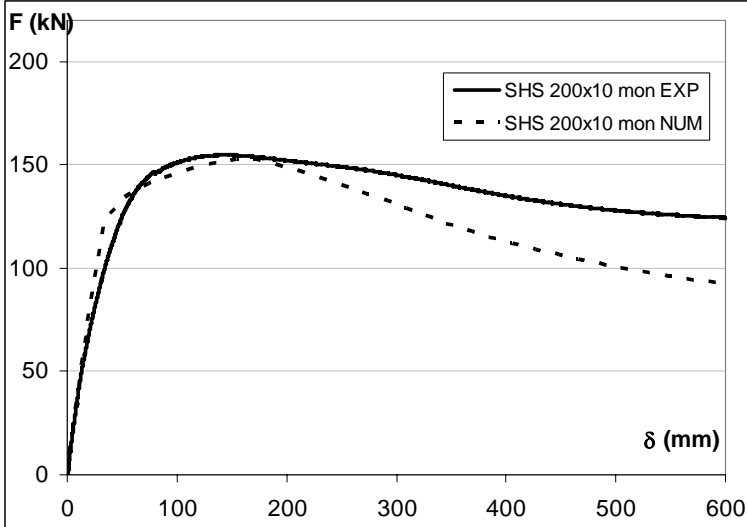


Figure 5.42 Experimental vs numerical monotonic curve 200x200x10.

SHS 200x200x10 cyclic

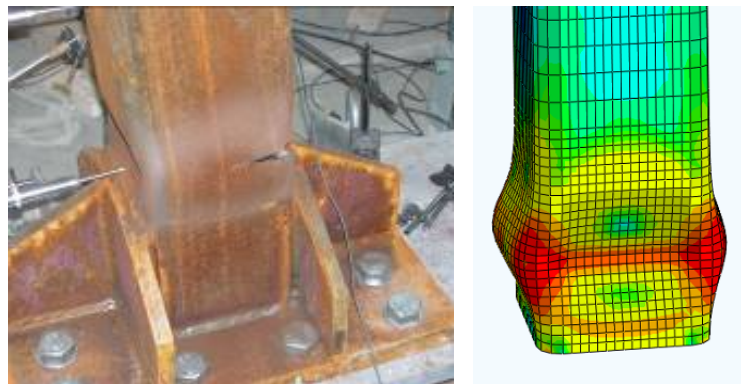


Figure 5.43 Failure mechanism for cyclic loading 200x200x10.

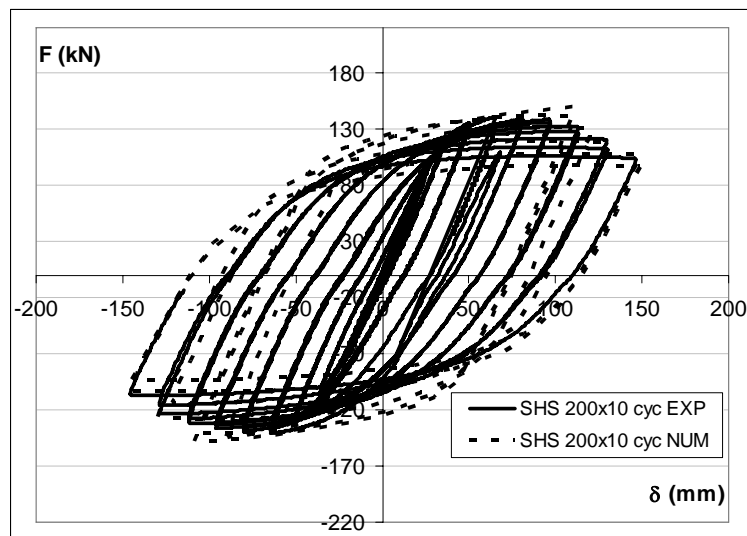


Figure 5.44 Experimental vs numerical cyclic curve 200x200x10.

SHS 250x250x8 monotonic

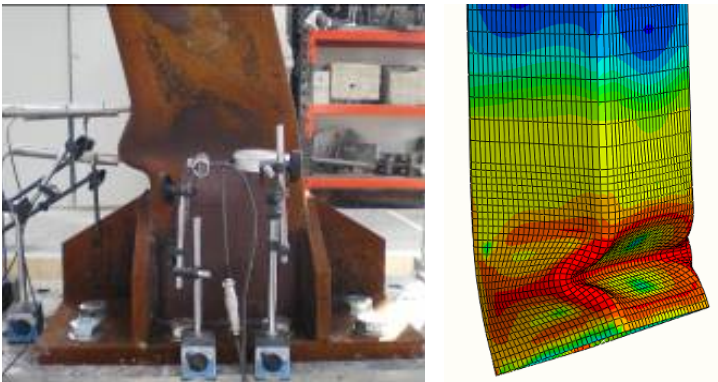


Figure 5.45 Failure mechanism for monotonic loading 250x250x8.

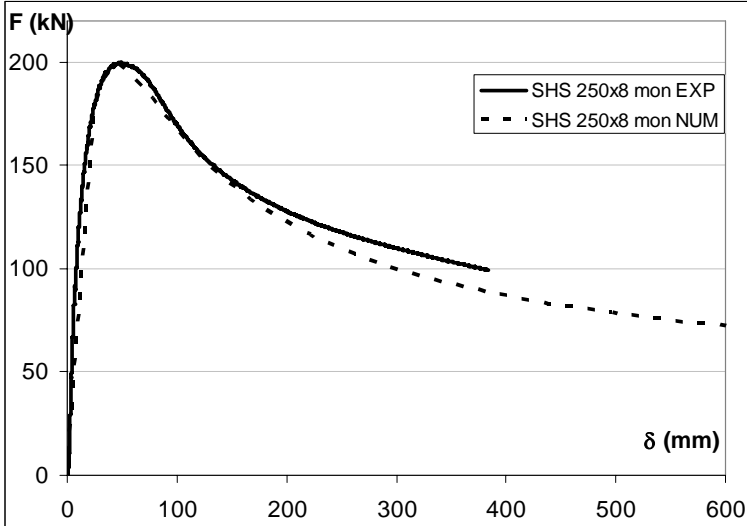


Figure 5.46 Experimental vs numerical monotonic curve 250x250x8.

SHS 250x250x8 cyclic

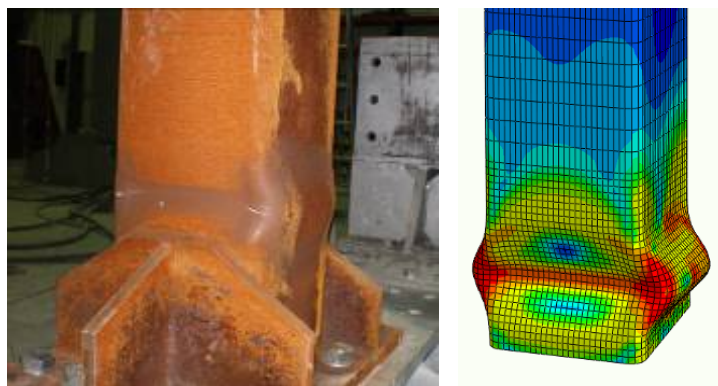


Figure 5.47 Failure mechanism for cyclic loading 250x250x8.

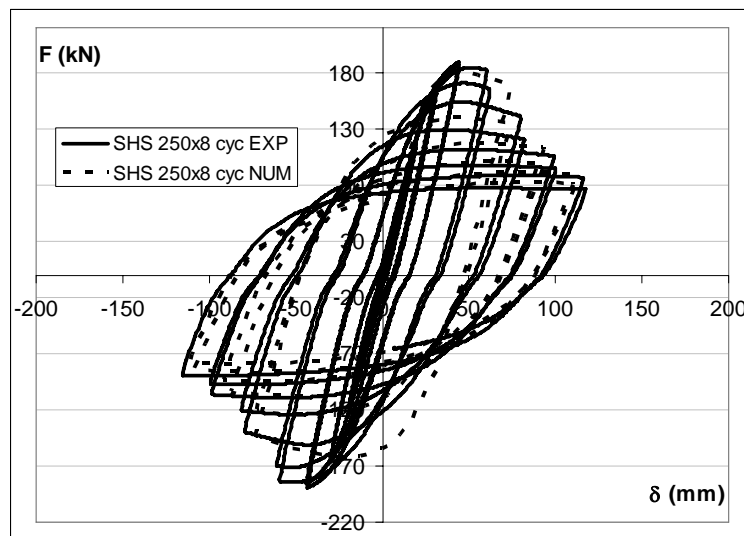


Figure 5.48 Experimental vs numerical cyclic curve 250x250x8.

5.4 CONCLUDING REMARKS

From the comparison between the experimental results and the results of numerical simulations, as visible in the figures of the previous paragraph, it can be recognized the reliability of the adopted numerical model.

It can be noticed that in the results there is a good agreement in terms of: general phenomenology, stiffness, strength and ductility.

Some differences can be noticed in the failure mechanisms, because in the experimental tests torsion effects occurred, caused by imperfect lateral-torsional restrains.

A brief recapitulation on the failure mechanisms occurred during the tests:

- Double T sections showed a coupled failure mechanism made of a combination of in-plane and out-of plane buckling. Indeed, the flange buckling occurred first and then the asymmetric-torsional buckling was triggered involving the web panel. It is very interesting to notice that the height of the web plastic mechanism increased increasing flange width, and this increase is associated with a reduction of rotation capacity.

- In hollow sections the local buckling was dominant and the hardening effects had not significant influence. These profiles experienced web local buckling which produced a rapid decreasing of the load, with increased deflection. The buckling of the web and the compatibility of rotations at the corner, caused deformations of the flange. In all cases, the buckling has been formed adjacent to one of the loading plates. This phenomenon was more significant for specimens having the higher local slenderness. In any case no specimen behaved as a slender section. The failure mechanisms were characterized by the so-called elephant foot shape that is the bulging of the compressed plates at the base of the specimen. This particular failure shape was due to the concentration of deformation in the compressed plates. In monotonic tests a transverse crack was observed in the tensile part at the base of the specimens. In cyclic tests it was recognized the beginnings of cracks, caused by the reversal deformation in the tensile zone, early bulged in compression. Cracks developed at the web-to-flange corners.

6 MONOTONIC BEHAVIOUR OF STEEL BEAMS

This chapter is devoted to present the results of a wide parametrical analysis, carried out by means of finite element simulations, on the basis of the previous calibration of the numerical models (Chapter 5), avoiding additional expensive experimental campaigns.

The varied parameters are those investigated by technical literature yet, so the obtained results goes to enlarge the existing database of results, to be able, in the end, to propose a new empirical formulation for the parameters “R” and “s” in case of monotonic loads.

6.1 PARAMETRICAL ANALYSIS: PLANNING

With the aim to integrate the database of results, obtained collecting data from technical literature and from experimental tests, it has been planned a wide parametrical analysis. It has been carried out by means of finite element models, to avoid additional expensive experimental campaigns.

The final scope is to obtain a large database, to be able to develop a new empirical formulation of the expressions for the prediction of the flexural capacity of steel beams, namely the parameters “R” and “s”.

To be sure to integrate the available data, the main geometrical ratios that are commonly used for the classification of steel members have been calculated for the all the double T and hollow profiles commercially available. In particular the web and flange slenderness has been taken into account as parameters to make a choice among all the available commercial profiles.

For double T sections, the technical literature and the experimental tests already reach a great amount of results, so the chosen profiles are those available in the commercial profile lists, only avoiding the ones that are not commonly used for beams in MRF structures. The analyzed sections

Chapter 6

are so the 19% of the total database results used to develop the multiple linear regression for the formulation, and not always have slenderness ratios not investigated, because the data were already complete enough.

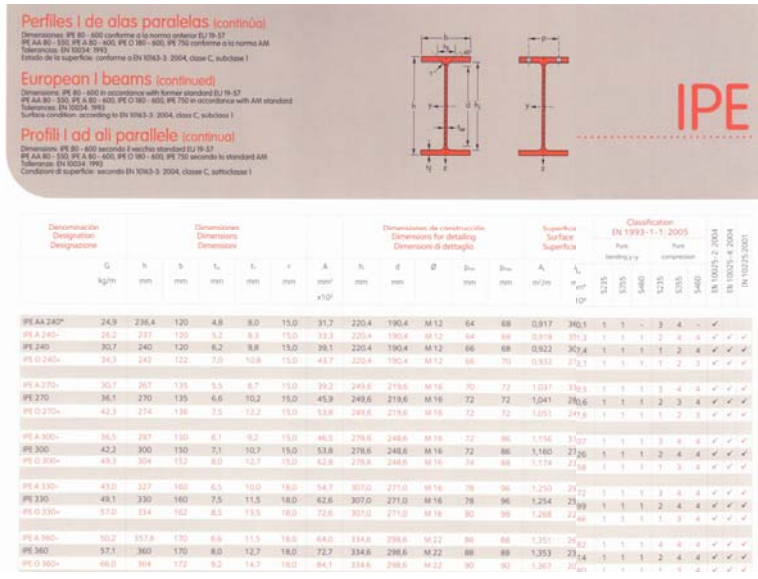


Figure 6.1 Commercial profile list for IPE sections.

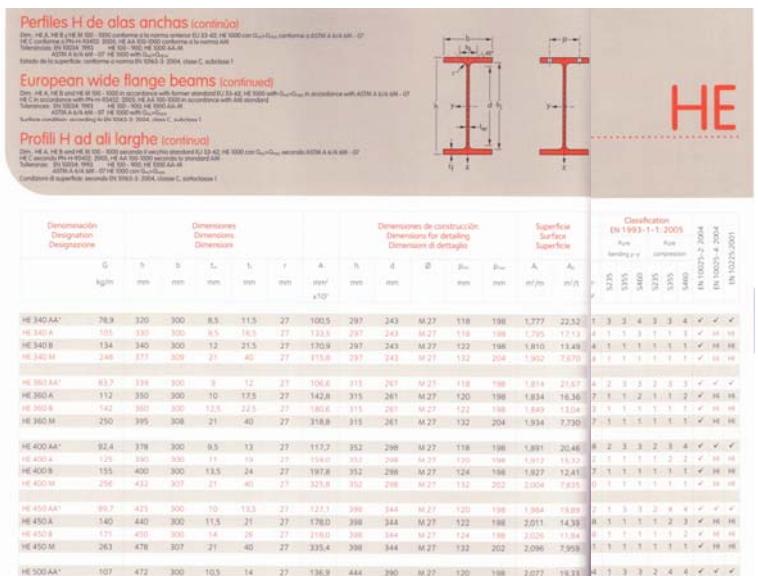


Figure 6.2 Commercial profile list for HE sections.

For hollow sections, the data available in technical literature are less than for double T, and the profiles available in the commercial profile lists are much more than double T, so the choice of sections to be analysed were made differently. It has been chosen only the profiles which have the slenderness ratios really different from the ones by technical literature. In the end the analyzed sections are the 42% of the total database results used for the new formulation.

Tubi rettangolari strutturali
 Rectangular structural hollow sections
 Rechteckige Stahlbauhohlprofile
 Tubes structuraux rectangulaires
 Tubos rectangulares estructurales

Gamma produttiva Product range



TUBI RETTANGOLARI STRUTTURALI ELETTRISALDATI Rectangular structural welded tubes

External dimensions	Thickness					
	4	5	6	8	9	10
A x B mm						
200 x 100	█	█	█	█	█	█
200 x 120	█	█	█	█	█	█
200 x 150	█	█	█	█	█	█
250 x 100	█	█	█	█	█	█
250 x 150	█	█	█	█	█	█
300 x 100	█	█	█	█	█	█
300 x 150	█	█	█	█	█	█
300 x 200	█	█	█	█	█	█
350 x 150	█	█	█	█	█	█
350 x 250	█	█	█	█	█	█
400 x 200	█	█	█	█	█	█
400 x 250	█	█	█	█	█	█

Figure 6.3 Commercial profile list for RHS sections.

Tubi quadri strutturali
 Square structural hollow sections
 Quadratische Stahlbauhohlprofile
 Tubes structuraux carrés
 Tubos cuadrados estructurales

Gamma produttiva Product range



TUBI QUADRI STRUTTURALI ELETTRISALDATI Square structural welded tubes

External dimensions	Thickness					
	4	5	6	8	9	10
A x A mm						
150 x 150	█	█	█	█	█	█
160 x 160	█	█	█	█	█	█
175 x 175	█	█	█	█	█	█
180 x 180	█	█	█	█	█	█
200 x 200	█	█	█	█	█	█
220 x 220	█	█	█	█	█	█
250 x 250	█	█	█	█	█	█
260 x 260	█	█	█	█	█	█
300 x 300	█	█	█	█	█	█
325 x 325	█	█	█	█	█	█

Figure 6.4 Commercial profile list for SHS sections.

In the following, there are some histograms showing the distribution along the variability range of the section slenderness, chosen to perform the analyses for the integration of the existing database. And subsequently the final list of analyzed sections is showed in the table.

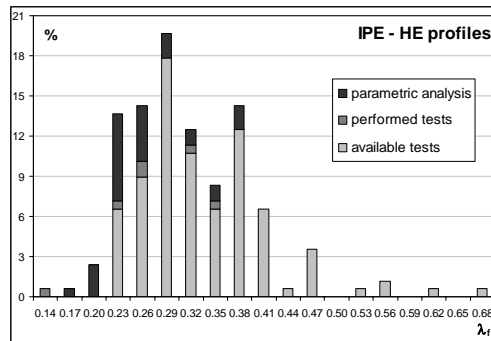


Figure 6.5 Integration of the existing database for IPE-HE profiles.

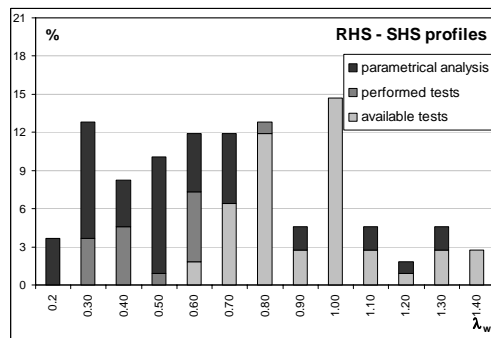


Figure 6.6 Integration of the existing database for IPE-HE profiles.

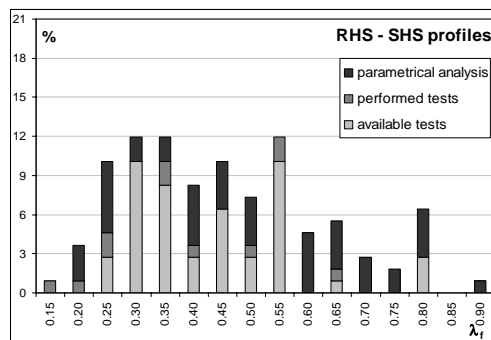


Figure 6.7 Integration of the existing database for RHS-SHS profiles.

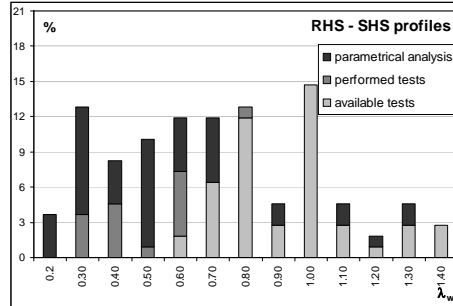


Figure 6.8 Integration of the existing database for RHS-SHS profiles.

Table 6.1 Database of sections for the parametric analysis.

IPE	HEA	HEB	RHS	SHS
IPE 270	HEA 240	HEB 240	RHS 200X100X5	SHS 150X150X6
IPE 300	HEA 260	HEB 260	RHS 200X100X8	SHS 150X150X10
IPE 330	HEA 280	HEB 280	RHS 200X100X10	SHS 160X160X5
IPE 360	HEA 300	HEB 300	RHS 200X120X8	SHS 160X160X6
IPE 400	HEA 320	HEB 320	RHS 200X120X10	SHS 160X160X10
IPE 450	HEA 340	HEB 340	RHS 200X150X8	SHS 175X175X5
IPE 500	HEA 360	HEB 360	RHS 200X150X10	SHS 175X175X8
IPE 550	HEA 400	HEB 400	RHS 250X100X8	SHS 175X175X10
IPE 600	HEA 450	HEB 450	RHS 250X150X10	SHS 180X180X8
	HEA 500	HEB 500	RHS 300X100X8	SHS 180X180X10
	HEA 550	HEB 550	RHS 300X100X10	SHS 200X200X6
	HEA 600	HEB 600	RHS 300X150X8	SHS 200X200X8
			RHS 300X150X9	SHS 220X220X6
			RHS 300X200X9	SHS 220X220X8
			RHS 350X150X6	SHS 220X220X10
			RHS 350X250X6	SHS 250X250X8
			RHS 400X200X6	SHS 250X250X9
			RHS 400X200X8	SHS 260X260X8
			RHS 400X200X9	SHS 300X300X8
			RHS 400X250X8	SHS 300X300X9
			RHS 400X250X9	SHS 325X325X9

6.2 NUMERICAL MODELING

The features of the adopted numerical models used for the parametrical analysis are the same of the ones described in the previous chapter, and they are briefly listed below:

- The 4-nodes shell element (S4) with 4 nodes per element, 6 degrees of freedom per node and a linear interpolation function was adopted for the modeling of all the beams.
- Two different levels of mesh refinements has been adopted: one for the plastic hinge zone (highly refined) and another for the remaining part of the beam (roughly refined), as shown in the following figure. The width of plastic hinge region, that is the one in which the main plastic deformations are expected, has been fixed case by case, calculating the length of the plastic hinge (L_m) by the equations available in scientific literature (Haaijer 1957 and Lay 1965).

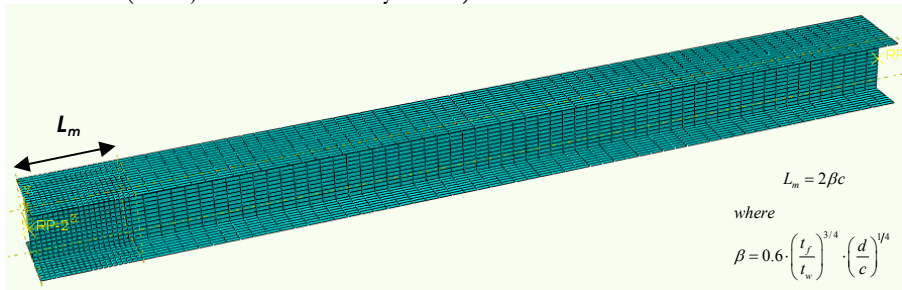


Figure 6.9 Different levels of mesh refinements (double T profile).

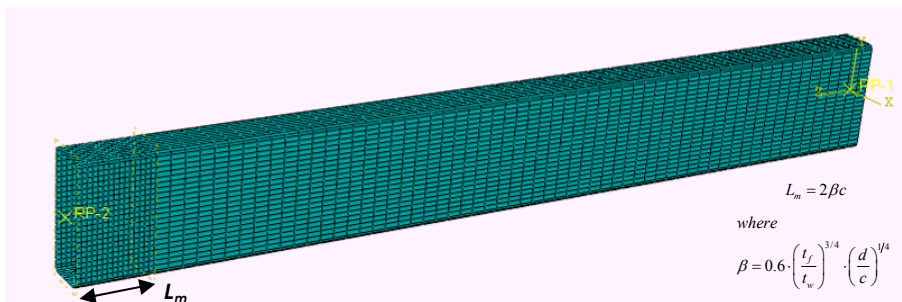


Figure 6.10 Different levels of mesh refinements (hollow profile).

- The geometry of the section of each shell model corresponds to the centerline dimensions of the beams, and the length of the whole model corresponds to the same of the experimental tests, to have the possibility to compare the final results.

- The boundary conditions are imposed as described: nodes belonging to the cross-sections at the ends of the beam were constrained to two reference points (RP-1 and RP-2).

RP-2 is the master node at the left end of the beam and was restrained against displacements and rotations in all directions.

RP-1 is the master node at the right end of the beam and was restrained against displacements in two directions and rotations in two directions, providing a restraint for the torsional degree of freedom and out-of plane displacements, and the beam deformation was imposed by applying displacements in the 2-direction (vertical).

The combination of these boundary conditions imposed a constant shear force in the element and a linear bending moment distribution (namely cantilever scheme).

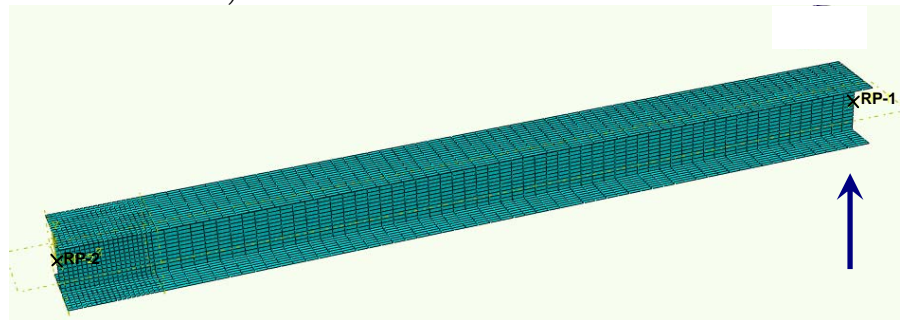


Figure 6.11 Displacement and boundary conditions (double T profile).

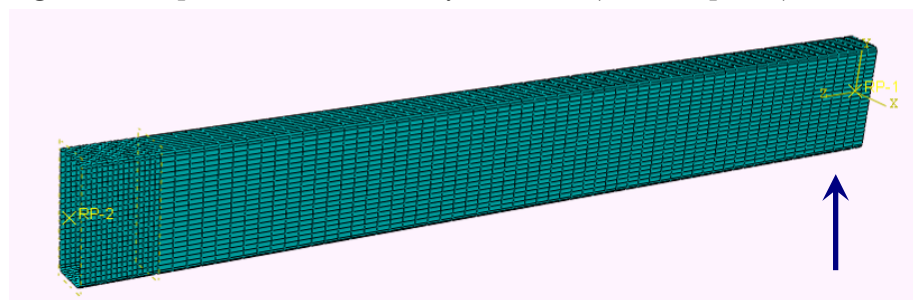


Figure 6.12 Displacement and boundary conditions (hollow profile).

- The numerical analyses are devoted to investigate the monotonic behaviour of steel beams, so in each model it has been created a static step, corresponding to the monotonic loading pattern, up to collapse. The loading was simulated by imposing the displacement in the vertical direction in the RP-1 node.

- For the material properties, this time was not possible to use the “true stress” - “true strain” format of the experimental test results, so the average stress-strain relationship of the European S275 steel grade has been used. Yielding has been modeled by means of the von Mises yield criteria. Plastic hardening was represented using a nonlinear kinematic hardening law calibrated on the basis of the cyclic material properties derived from cyclic coupon tests performed by Kaufmann et al. (2001). The same cyclic material properties were used for the flanges and web of the I beams and for the section of hollow beams. Modelling of strength deterioration due to buckling has been taken into account by using the large displacement option.

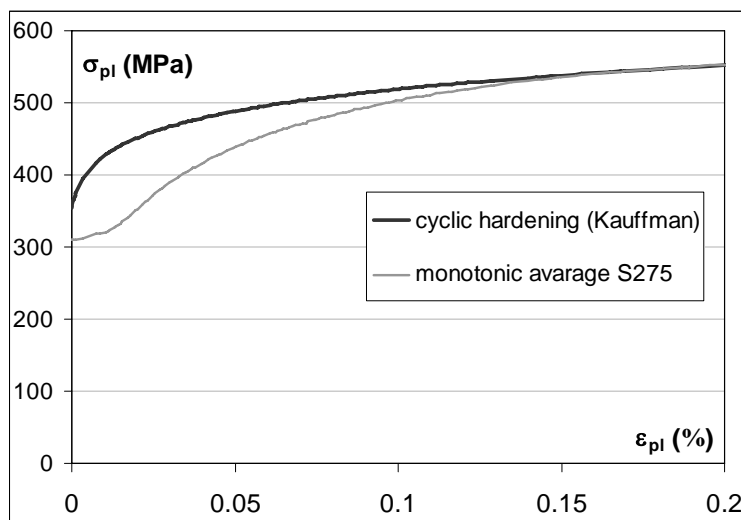


Figure 6.13 Stress-strain diagram resulting from experimental tests.

6.3 PARAMETRIC ANALYSIS: RESULTS

6.3.1 Double T profiles

IPE

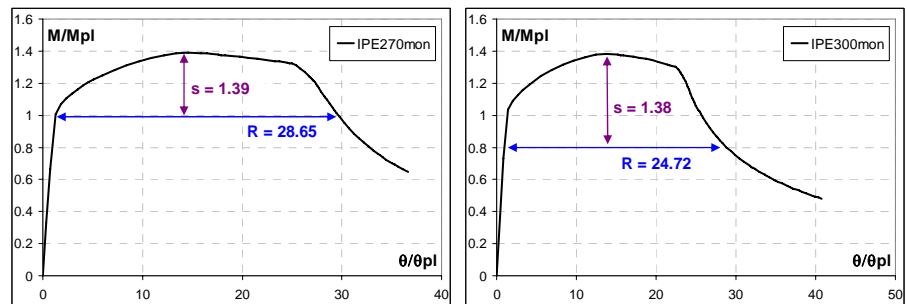


Figure 6.14 Monotonic response of IPE 270 and IPE 300.

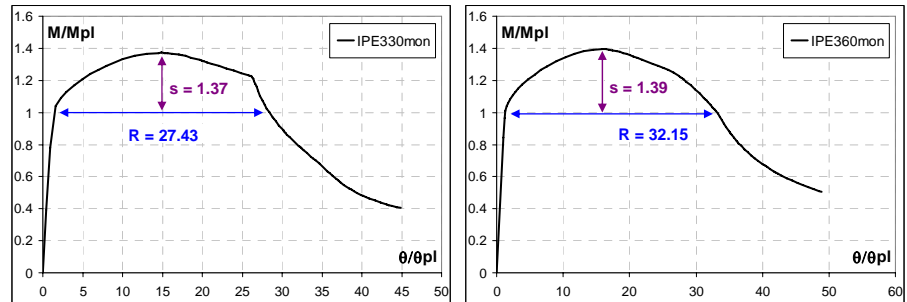


Figure 6.15 Monotonic response of IPE 330 and IPE 360.

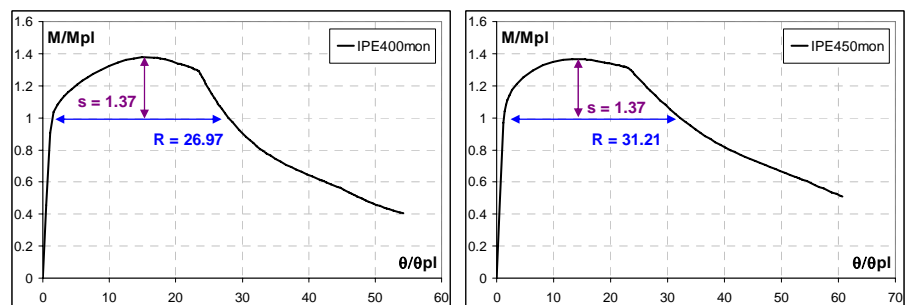


Figure 6.16 Monotonic response of IPE 400 and IPE 450.

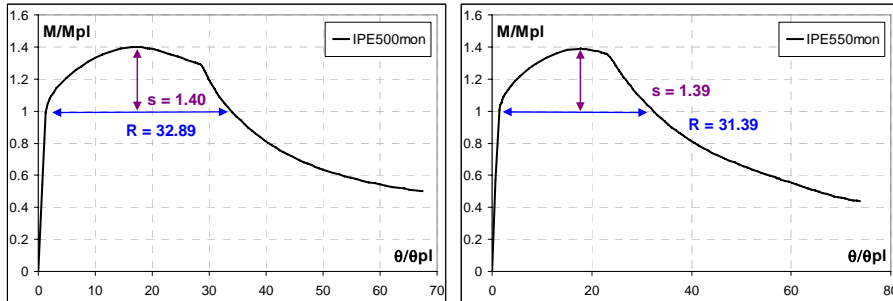


Figure 6.17 Monotonic response of IPE 500 and IPE 550.

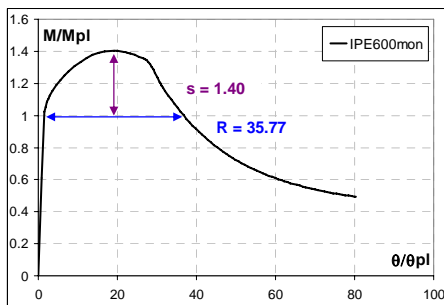


Figure 6.18 Monotonic response of IPE 600.

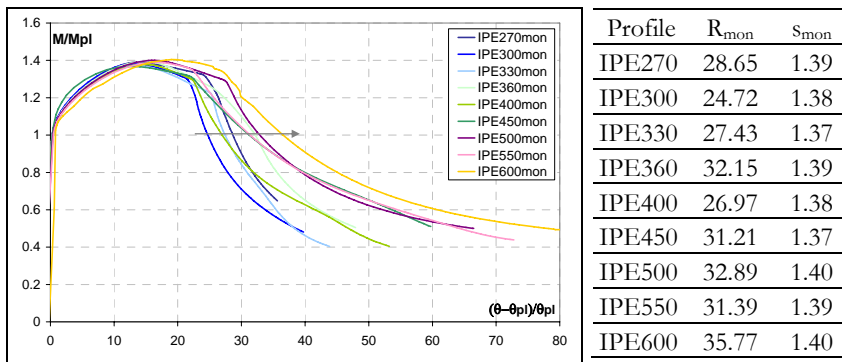


Figure 6.19 Comparison of monotonic response of all IPE profiles.

HEA

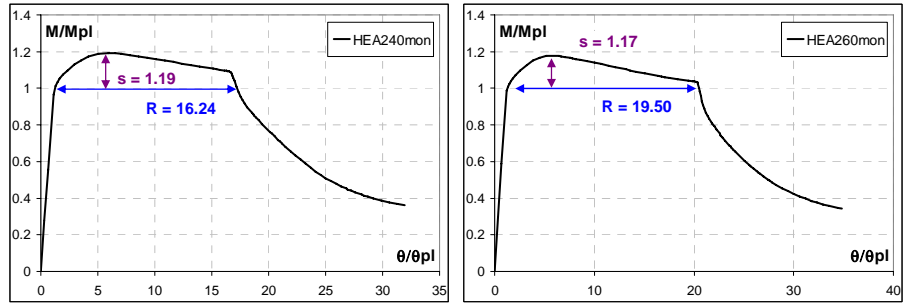


Figure 6.20 Monotonic response of HEA 240 and HEA 260.

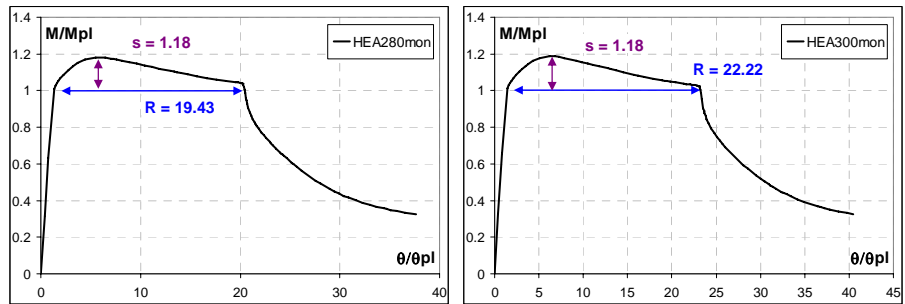


Figure 6.21 Monotonic response of HEA 280 and HEA 300.

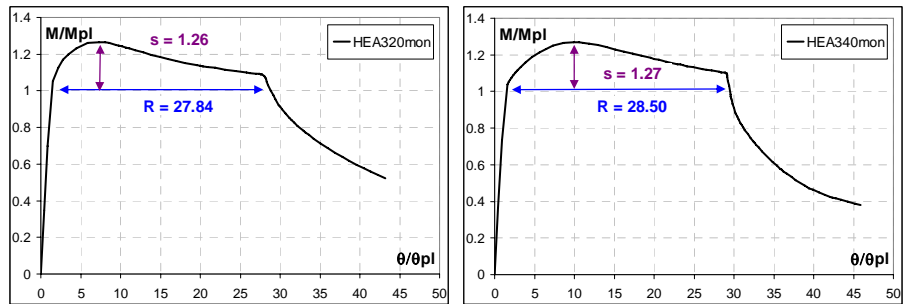


Figure 6.22 Monotonic response of HEA 320 and HEA 340.

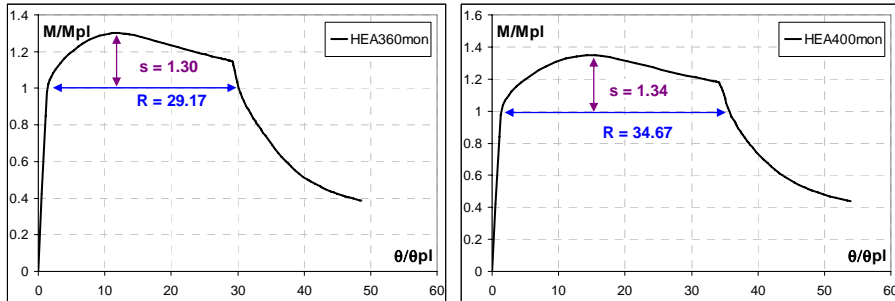


Figure 6.23 Monotonic response of HEA 360 and HEA 400.

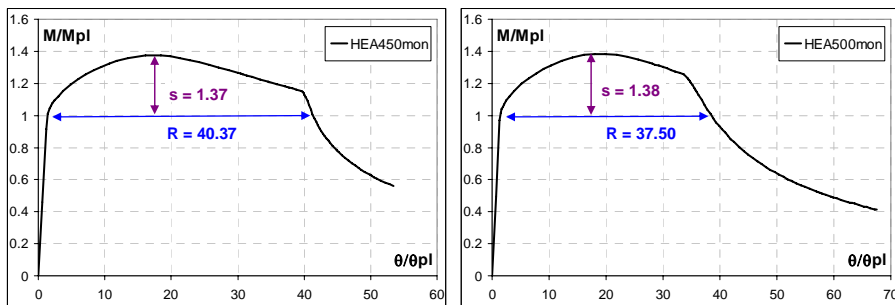


Figure 6.24 Monotonic response of HEA 450 and HEA 500.

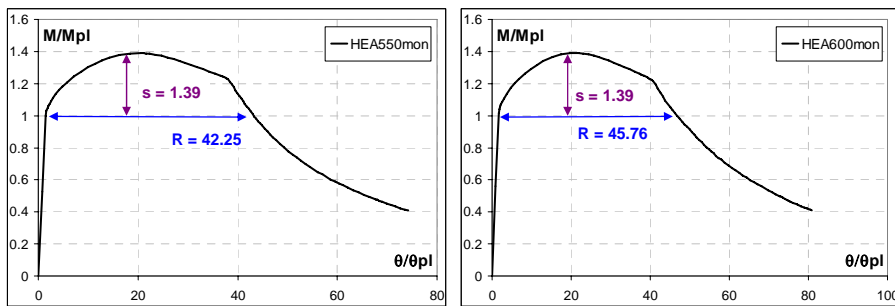


Figure 6.25 Monotonic response of HEA 550 and HEA 600.

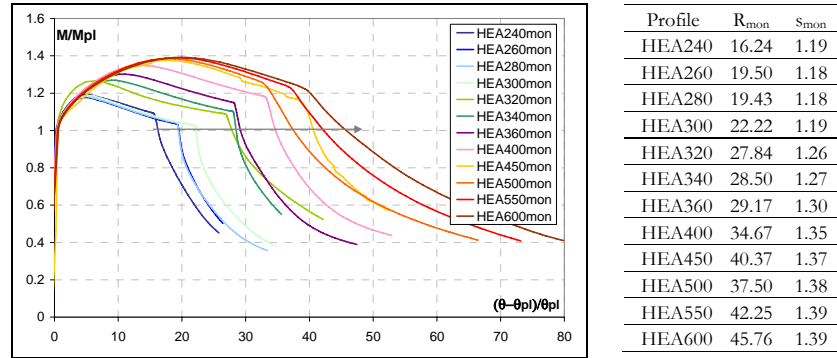


Figure 6.26 Comparison of monotonic response of all HEA profiles.

HEB

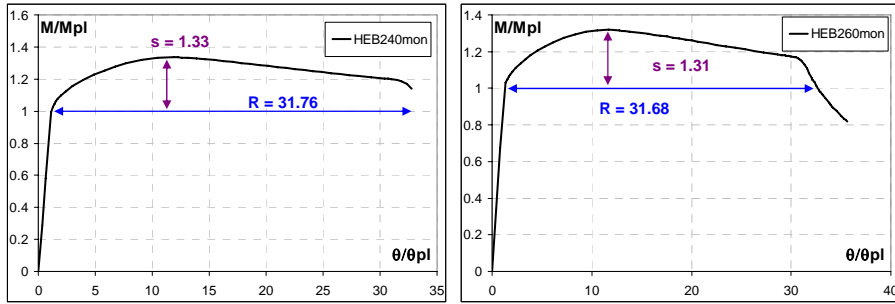


Figure 6.27 Monotonic response of HEB 240 and HEB 260.

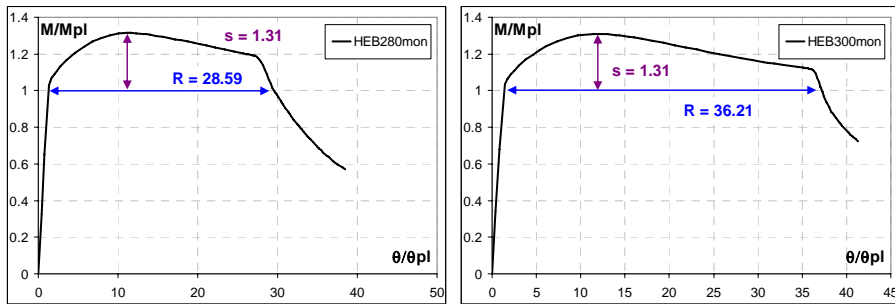


Figure 6.28 Monotonic response of HEB 280 and HEB 300.

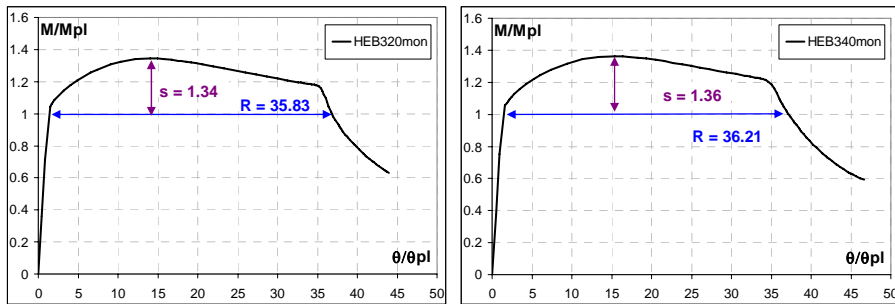


Figure 6.29 Monotonic response of HEB 320 and HEB 340.

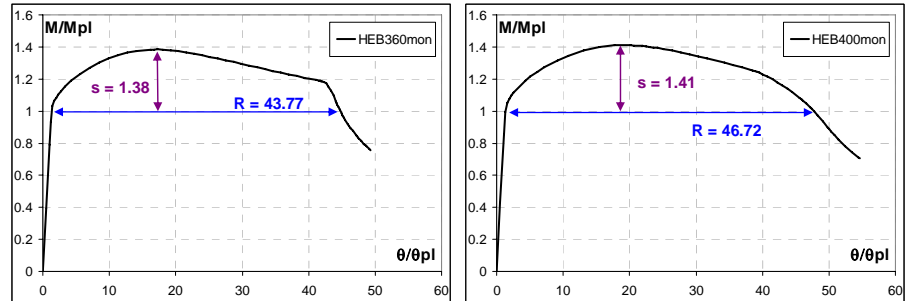


Figure 6.30 Monotonic response of HEB 360 and HEB 400.

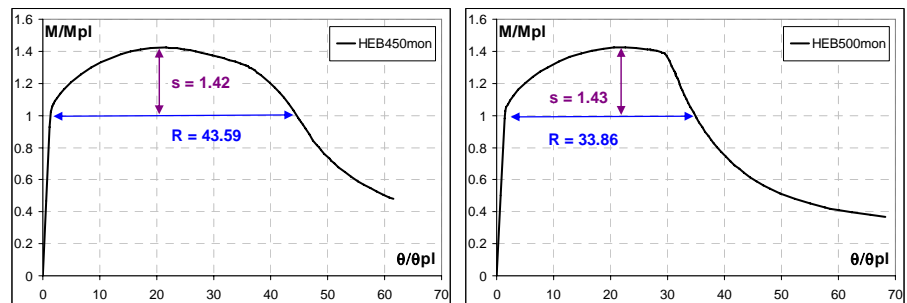


Figure 6.31 Monotonic response of HEB 450 and HEB 500.

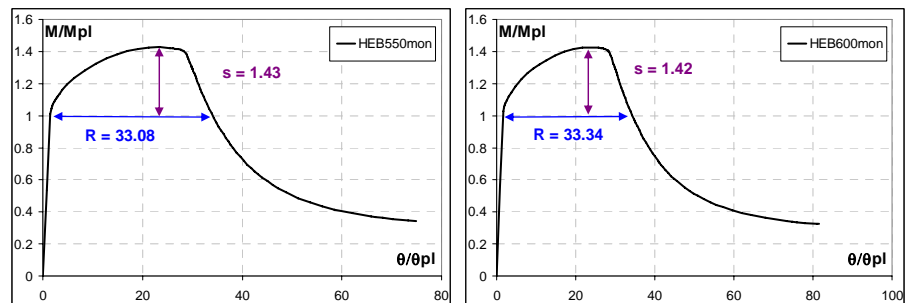
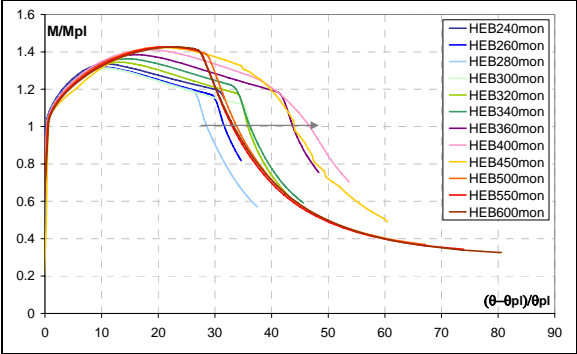


Figure 6.32 Monotonic response of HEB 550 and HEB 600.



Profile	R_{mon}	S_{mon}
HEB240	31.76	1.33
HEB260	31.68	1.32
HEB280	28.59	1.31
HEB300	36.21	1.31
HEB320	35.83	1.34
HEB340	36.21	1.36
HEB360	43.77	1.38
HEB400	46.72	1.41
HEB450	43.59	1.42
HEB500	33.86	1.43
HEB550	33.08	1.43
HEB600	33.34	1.43

Figure 6.33 Comparison of monotonic response of all HEB profiles.

6.3.2 Hollow profiles

RHS

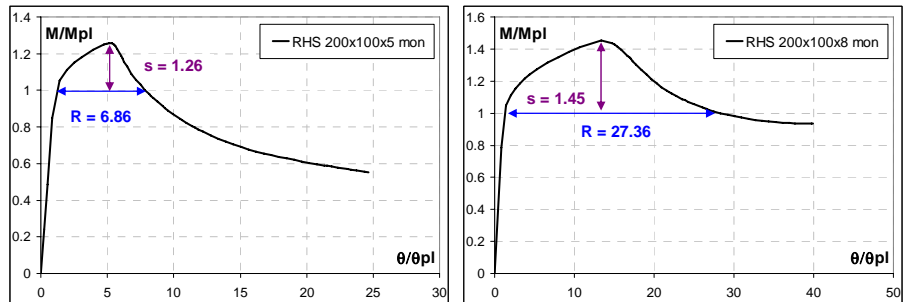


Figure 6.34 Monotonic response of 200x100x5 and 200X100X8.

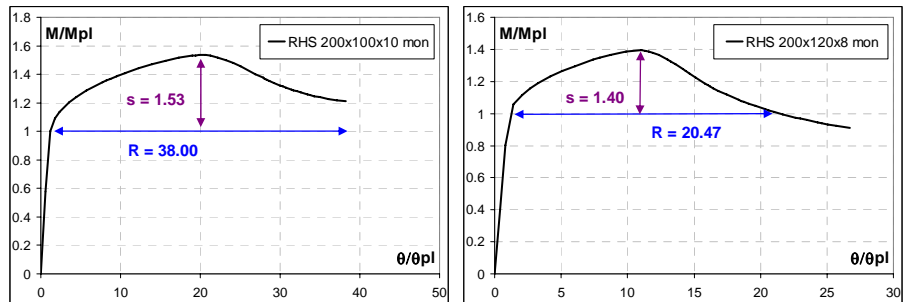


Figure 6.35 Monotonic response of 200x100x10 and 200x120x8.

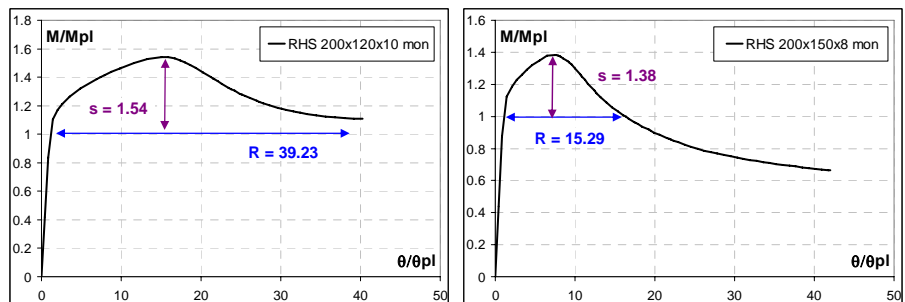


Figure 6.36 Monotonic response of 200x120x10 and 200x150x8.

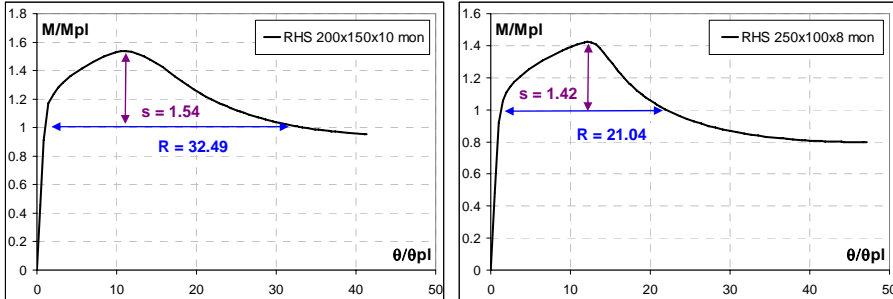


Figure 6.37 Monotonic response of 200x150x10 and 250x100x8.

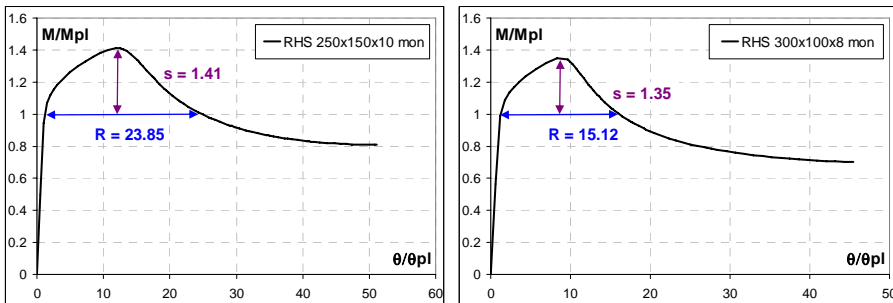


Figure 6.38 Monotonic response of 250x150x10 and 300x100x8.

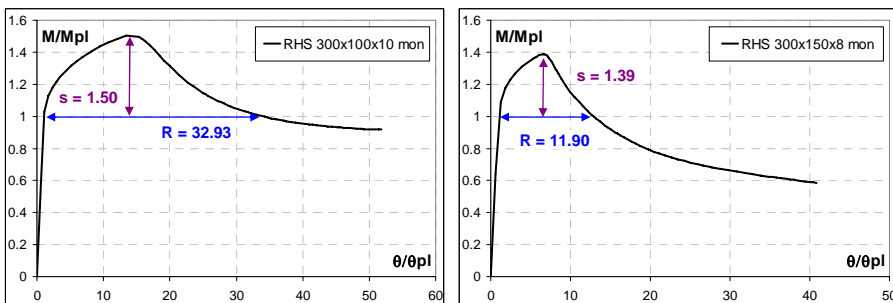


Figure 6.39 Monotonic response of 300x100x10 and 300x150x8.

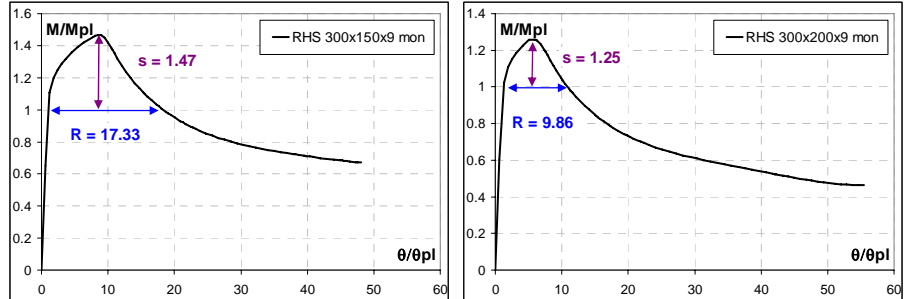


Figure 6.40 Monotonic response of 300x150x9 and 300x200x9.

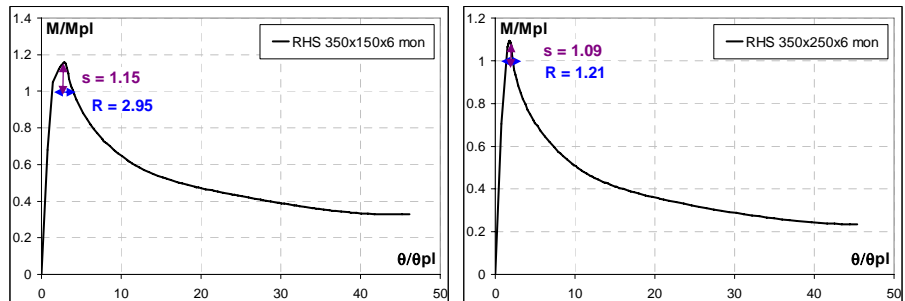


Figure 6.41 Monotonic response of 350x150x6 and 350x250x6.

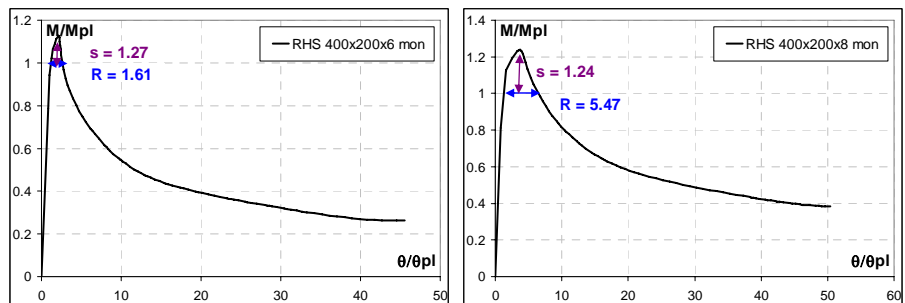


Figure 6.42 Monotonic response of 400x200x6 and 400x200x8.

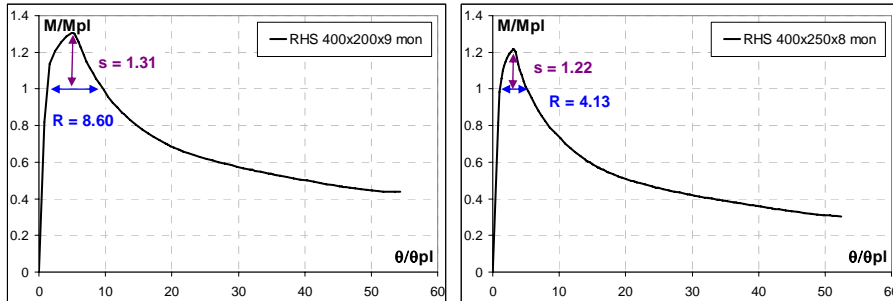


Figure 6.43 Monotonic response of 400x200x9 and 400x250x8.

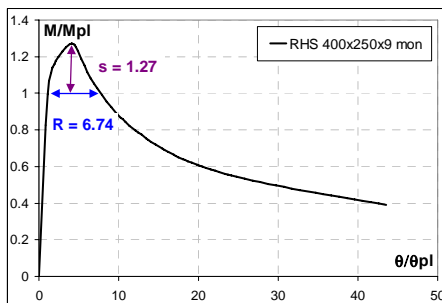


Figure 6.44 Monotonic response of 400x250x9 .

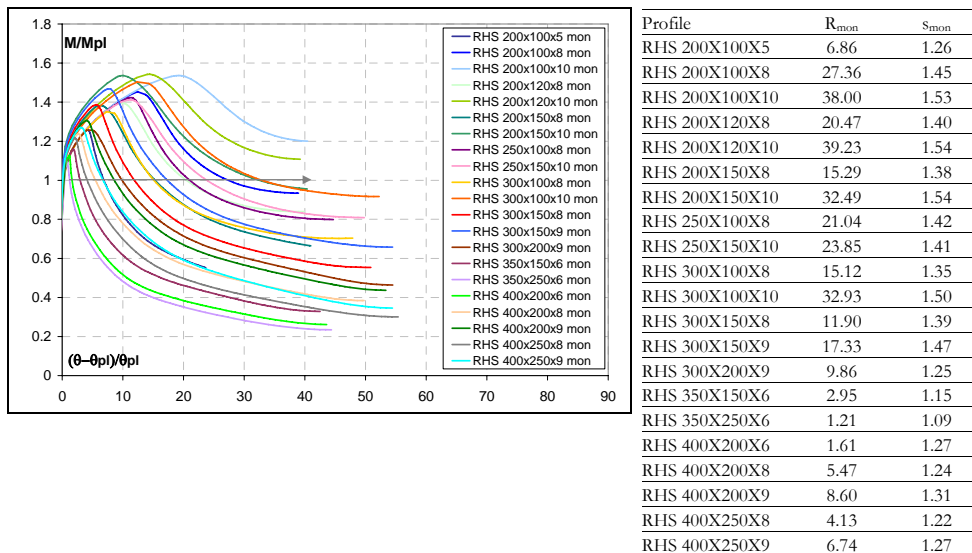


Figure 6.45 Comparison of monotonic response of all RHS profiles.

SHS

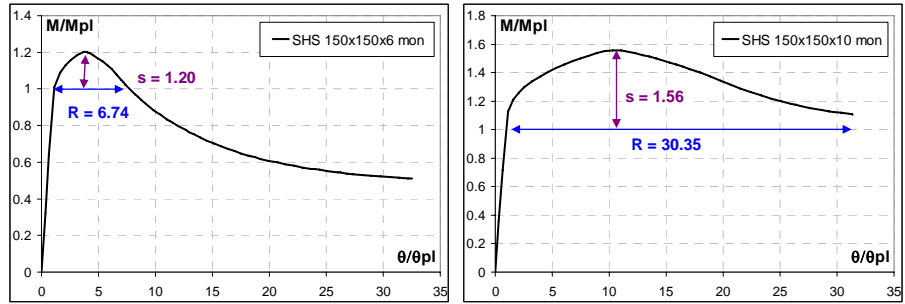


Figure 6.46 Monotonic response of 150x150x6 and 150x150x10.

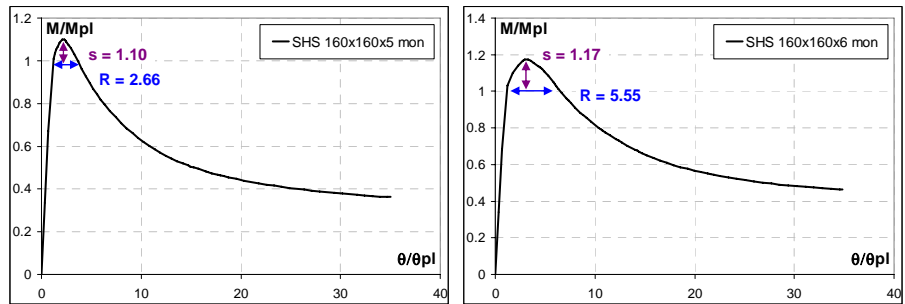


Figure 6.47 Monotonic response of 160x160x5 and 160x160x6.

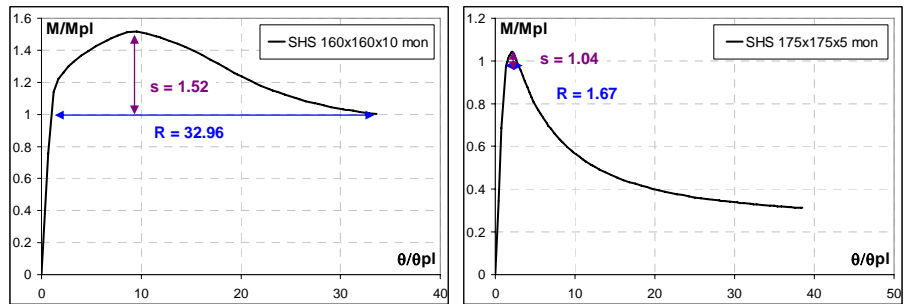


Figure 6.48 Monotonic response of 160x160x10 and 175x175x5.

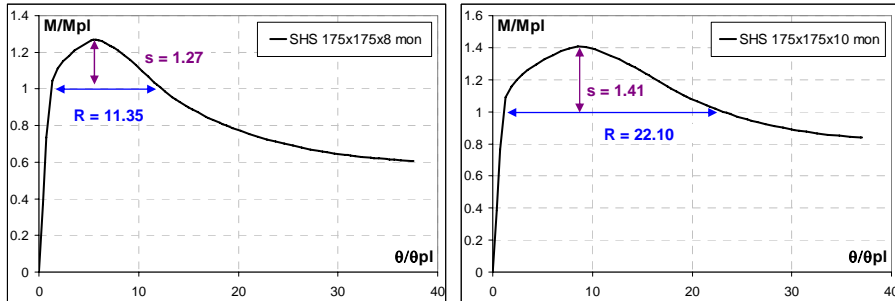


Figure 6.49 Monotonic response of 175x175x8 and 175x175x10.

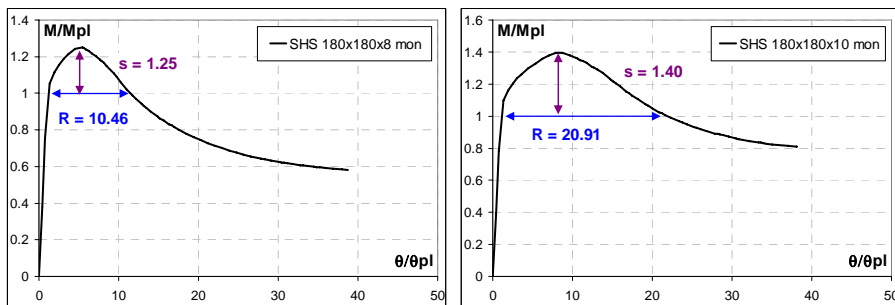


Figure 6.50 Monotonic response of 180x180x8 and 180x180x10.

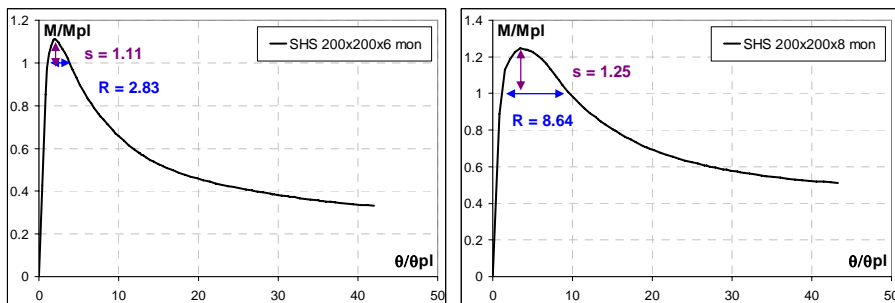


Figure 6.51 Monotonic response of 200x200x6 and 200x200x8.

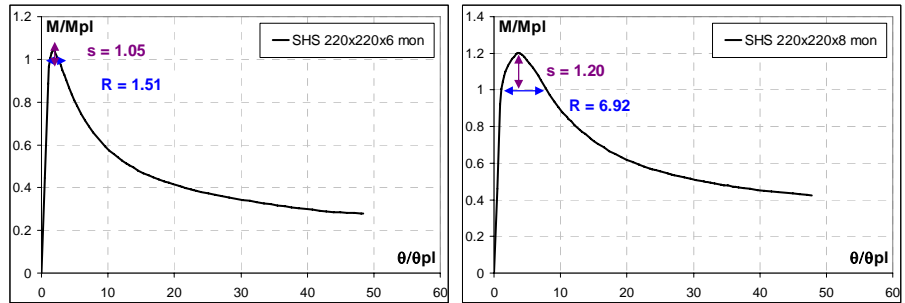


Figure 6.52 Monotonic response of 220x220x6 and 220x220x8.

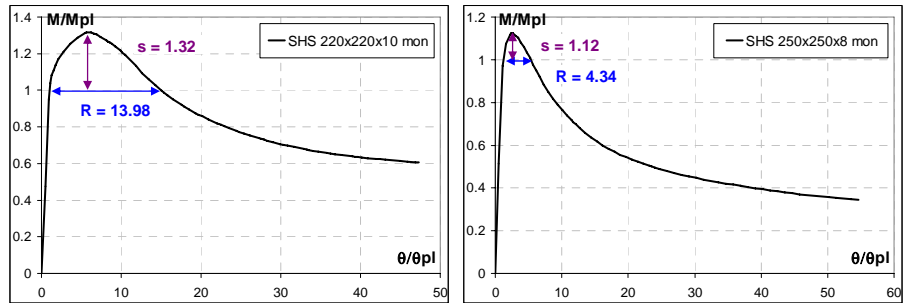


Figure 6.53 Monotonic response of 220x220x10 and 250x250x8.

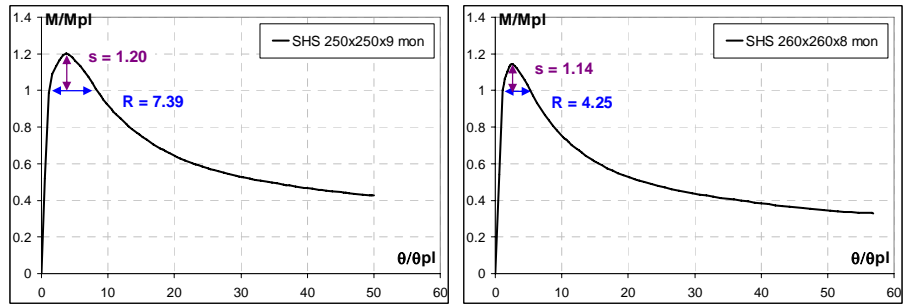


Figure 6.54 Monotonic response of 250x250x9 and 260x260x8.

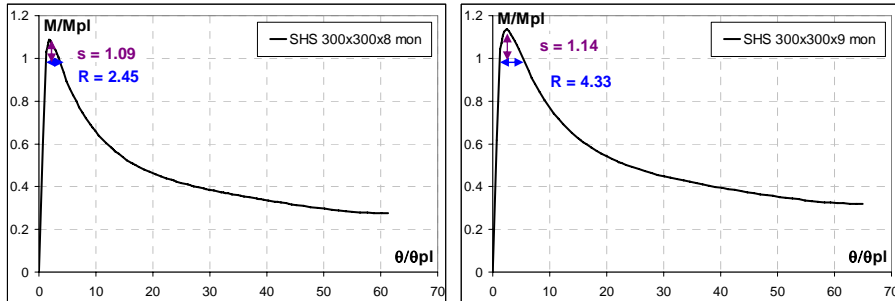


Figure 6.55 Monotonic response of 300x300x8 and 300x300x9.

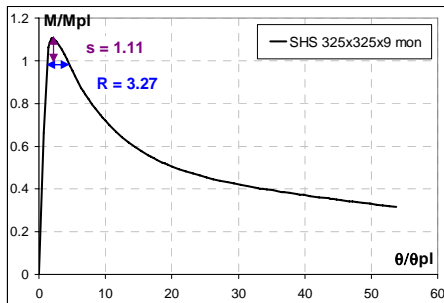


Figure 6.56 Monotonic response of 325x325x9.

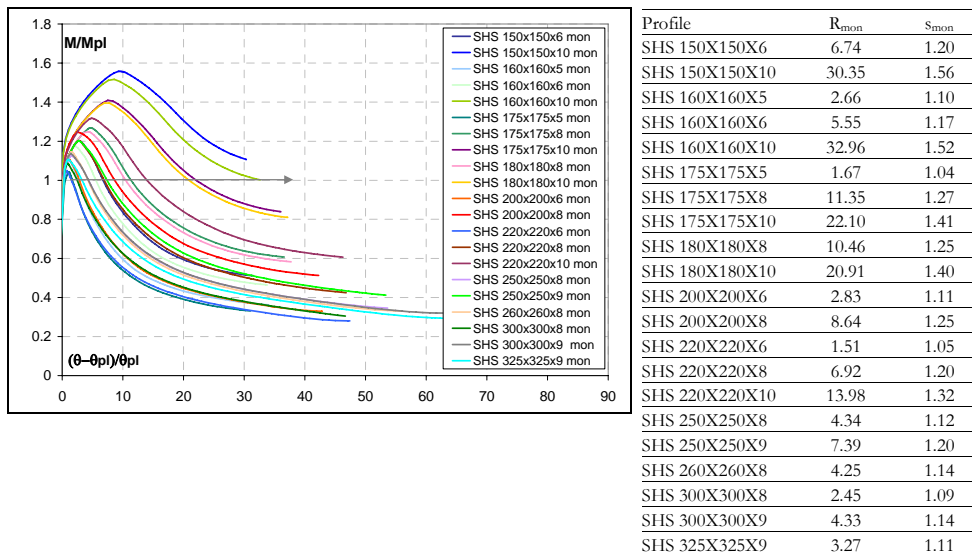


Figure 6.57 Comparison of monotonic response of all SHS profiles.

6.4 NEW EMPIRICAL FORMULATION FOR “R” AND “S”

In the end, taking data from technical literature, performed experimental tests and numerical simulations, new expressions of monotonic “R” and “s” parameters are proposed on the basis of empirical models, and in particular obtained by multiple linear regressions of the collected data.

The rotation capacity “R” and the flexural overstrength “s” are affected by the same mechanical and geometrical parameters, so two generalized formulations have been proposed, as explained below.

For the “s” parameter, the same expression proposed by Mazzolani & Piluso (Mazzolani, Piluso, 1993) was used, but integrating the training data set of the formulation with the new available data carried out for this thesis work, to be more accurate in the definition of the C_i factors. The generalized expression of s is the following:

$$\frac{1}{s} = C_1 + C_2 \lambda_f^2 + C_3 \lambda_w^2 + C_4 \frac{b_f}{L} + C_5 \frac{E}{E_h} + C_6 \frac{\varepsilon_h}{\varepsilon_y} \quad (6.1)$$

In the equation (6.1) the mechanical properties of the material, the geometrical features of the section and of the beam are taken into account as well as the influence of moment gradient, being λ_f the flange slenderness, λ_w the web slenderness, b_f/L the ratio between the flange width and the shear length of the beam, $\varepsilon_h/\varepsilon_y$ and E/E_h are ratios depending on the mechanical properties of the material, and their average values with reference to the common European steel grades are exposed in the table below.

Table 6.2 Stress-strain characteristics of common European steel .

Steel	f_y	f_u	E	E_h	E/E_h	ε_h	ε_y	$\varepsilon_h/\varepsilon_y$
	N/mm ²	N/mm ²	N/mm ²	N/mm ²	-	%	%	-
S 235	235	360	210000	5600	37.5	1.41	0.115	12.3
S 275	275	430	210000	4906	42.8	1.47	0.134	11.0
S 355	355	510	210000	4357	48.2	1.70	0.173	9.8

The C_i coefficients have been determined by the multiple regression of collected data and are exposed in the table below for double T and hollow profiles.

Table 6.3 C_i coefficients in the new expression of “s” factor.

	C_1	C_2	C_3	C_4	C_5	C_6
IPE - HE	1.378769	0.510995	0.018995	-0.104819	-0.003777	-0.042869
RHS - SHS	0.958392	0.524065	-0.011891	-0.818582	0.013801	-0.074537

For the “R” parameter, it was noticed that the expressions early present in technical literature, based on empirical considerations, keep directly into account the effects of mechanical properties, but they consider the influence of the geometrical properties only through the overstrength factor “s”. One of the scopes of this work is to obtain, instead, an empirical relationship of the rotation capacity, directly based on the geometrical and mechanical parameters that concur to influence it.

Therefore, the new proposed expression of the assumes the following generalized form:

$$R = C_1 + C_2 \frac{1}{\lambda_f^2} + C_3 \frac{1}{\lambda_w^2} + C_4 \frac{b_f h}{L^2} + C_5 \frac{b_f t_f}{hL} + C_6 \frac{A_f}{A_{TOT}} + C_7 \frac{L_m}{L} + C_8 s \quad (6.2)$$

This equation is very similar to the expression early present in literature for the overstrength parameter s, thanks to the consideration that both parameters are affected by the same geometrical and mechanical parameters. The difference is that in this case the geometrical parameters are arranged in such a way to be able to provide a considerable reduction of the scatters between predicted and experimental values as well as sufficiently conservative results. To this end a lot of different parameters ratios has been investigated, quantifying also their influence on the final result trough the calculation of $p_i = R/C_i x_i$, in which x_i is the generic factor multiplying C_i .

Looking at the (6.2) equation, it can be noticed that the rotation capacity has been assumed inversely proportional to the web and flange slenderness (λ_f and λ_w), and proportional to the factors: $b_f h/L^2$ that represents the ratio between the cross section and the total length of the beam; $b_f t_f/hL$ that represents the ratio between the flange and the web; A_f/A_{TOT} that is the ratio between the area of the flange over the total area of the cross section; L_m/L that is the ratio between the length of the plastic hinge and the total length of the beam. For this last factor it has been considered the early studies of Haaijer (1957) and Lay (1965) on the

definition of the half-wave length of the flange plastically buckled, whose equation is showed in the following, being c the half-width of the flange:

$$L_m = 2\beta c \quad \text{dove} \quad \beta = 0.6 \cdot \left(\frac{t_f}{t_w}\right)^{3/4} \cdot \left(\frac{d}{c}\right)^{1/4} \quad (6.3)$$

In the equation (6.2) the C_i coefficients have been obtained by the multiple linear regression of collected data and are exposed in the table below for double T and hollow profiles.

Table 6.4 C_i coefficients in the new expression of “R” factor.

	C_1	C_2	C_3	C_4	C_5	C_6	C_7	C_8
IPE - HE	-69.960	0.142	3.098	-59.047	-1300	56.952	286.215	-27.654
RHS - SHS	0.967	83.940	31.232	-1114.476	-181.939	1.063	0.646	-39.018

In the following figures the dispersion between R (collected data) and R (proposed formulation) and the dispersion between M_{\max} (collected data) and sM_{pl} (proposed formulation) are plotted, evidencing also the R^2 factor, called coefficient of determination, a statistical parameter for the error estimation .

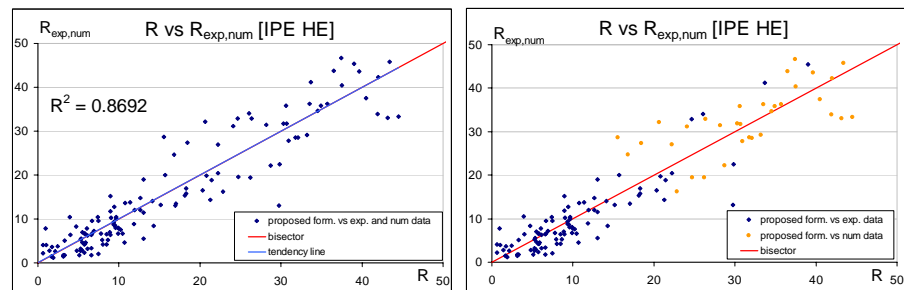


Figure 6.58 Experimental - numerical data vs theoretical R (double T profiles).

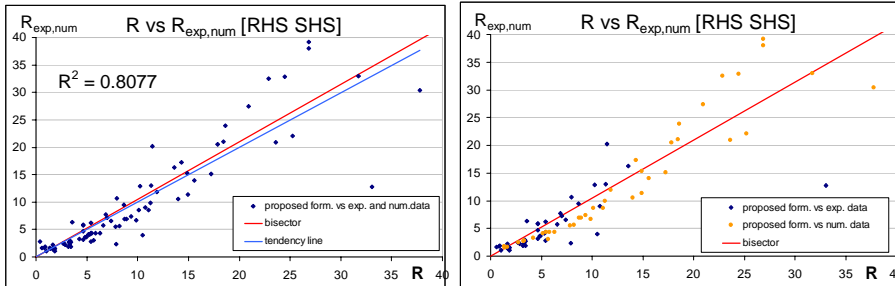


Figure 6.59 Experimental - numerical data vs theoretical R (hollow profiles).

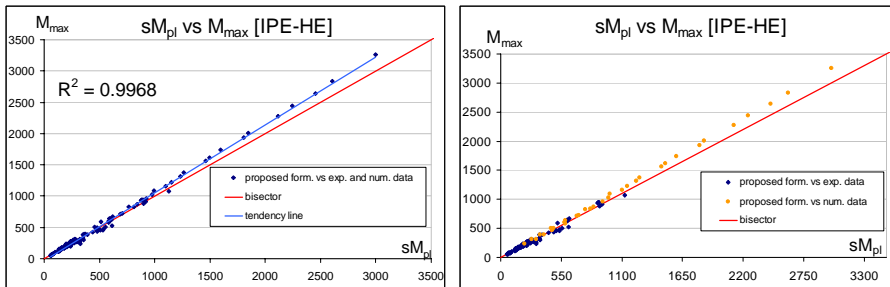


Figure 6.60 Experimental - numerical data vs theoretical s (double T profiles).

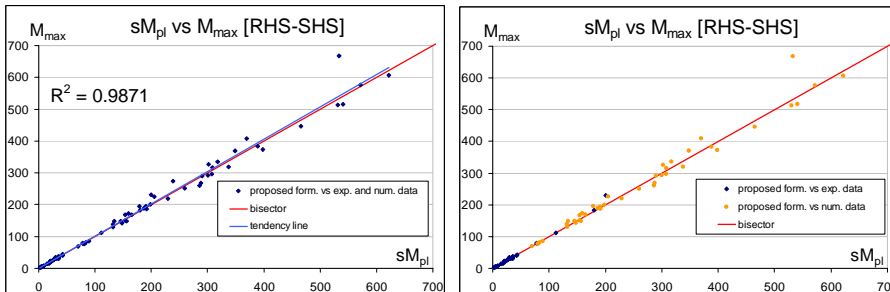


Figure 6.61 Experimental - numerical data vs theoretical s (hollow profiles).

6.5 CONCLUDING REMARKS

The proposed equations are obtained from a multiple linear regression of data sampled from experimental tests and numerical analysis under monotonic conditions. It was observed that interaction between web and compression flange slenderness could limit the rotation capacity of flexural members. This interaction can reduced the inelastic deformation capacity, measured as rotation capacity, when either the web or the compression flange slenderness is too large.

The experimental and numerical results indicated that the loading condition has a significant influence on rotation capacity. In particular, it decreased when the loading is cyclic, as compared to monotonic loading, but this topic is discussed in the next chapter.

Some final considerations can be made, in the light of all the previous work:

- steel beam classification can be considered outdated, due to the fact that the rotation capacity “R” and the flexural overstrength “s” can be properly calculated by means of the tools provided by this work;
- the correct value of the flexural overstrength “s”, as calculated with the new proposed formulation, can be properly used for the application of the capacity design criteria;
- for seismic application, it is auspicious the use of rotation capacity “R”, as calculated by means of the new formulation, but it should be referred to the cyclic properties of the beams (next chapter);
- and finally, for seismic design it will be necessary to correlate cyclic “R” and behaviour factor “q” of steel structures.

7 CYCLIC BEHAVIOUR OF STEEL BEAMS

The present chapter has quite the same structure of the previous chapter, but in this case it focuses on the behaviour of steel beams under cyclic actions. An analogous parametric analysis has been performed, but this time it was not extracted another analytical formulation. Instead, critical considerations on the differences between the monotonic and the cyclic behaviours were made, and in future they can be used to go beyond the final scope of this thesis. In particular it can be used to start a study to establish a connection between seismic demand and seismic capacity of steel beams, and so steel framed structures in general.

7.1 PARAMETRICAL ANALYSIS: PLANNING

The data available in technical literature are all referred to monotonic loading patterns, as it can be noticed in tables 4.1 and 4.2 (Chapter 4), so it has been decided to plan also cyclic experimental tests, as well as numerical parametrical analysis. The most of it has been carried out by means of finite element models, to avoid additional expensive experimental campaigns.

The sections analyzed are the same of the monotonic parametrical analysis, to be able to compare the obtained results, so the criteria used to choose the profiles are the same: to select sections with geometrical ratios in order to integrate the available data, in particular section slenderness ratios are selected. The final scope is to obtain a large database to make a significant comparison. But, by now, only the simulations of double T sections has been carried out, for time reasons, because the cyclic simulations are more expensive in terms of computational cost (monotonic simulations can be measured in minutes, cyclic simulations must be measured in hours).

In the following, there is a summarizing table in which the analyzed sections are reported.

Table 7.1 Database of sections for the parametric analysis.

IPE	HEA	HEB
IPE 270	HEA 240	HEB 240
IPE 300	HEA 260	HEB 260
IPE 330	HEA 280	HEB 280
IPE 360	HEA 300	HEB 300
IPE 400	HEA 320	HEB 320
IPE 450	HEA 340	HEB 340
IPE 500	HEA 360	HEB 360
IPE 550	HEA 400	HEB 400
IPE 600	HEA 450	HEB 450
	HEA 500	HEB 500
	HEA 550	HEB 550
	HEA 600	HEB 600

7.2 NUMERICAL MODELING

The features of the adopted numerical models used for the parametrical analysis are the same of the ones described in the previous chapter, and they are briefly listed below:

- The 4-nodes shell element (S4) with 4 nodes per element, 6 degrees of freedom per node and a linear interpolation function was adopted for the modeling of all the beams.
- Two different levels of mesh refinements has been adopted: one for the plastic hinge zone (highly refined) and another for the remaining part of the beam (roughly refined), as shown in the following figure. The width of plastic hinge region, that is the one in which the main plastic deformations are expected, has been fixed case by case, calculating the length of the plastic hinge (L_m) by the equations available in scientific literature (Haaijer 1957 and Lay 1965).

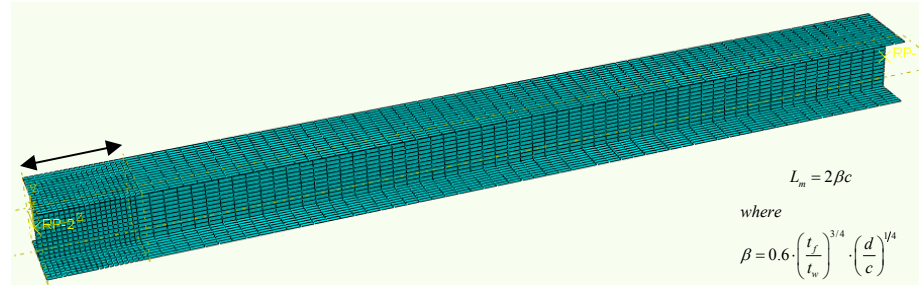


Figure 7.1 Different levels of mesh refinements (double T profile).

- The geometry of the section of each shell model corresponds to the centerline dimensions of the beams, and the length of the whole model corresponds to the same of the experimental tests, to have the possibility to compare the final results.

- The boundary conditions are imposed as described: nodes belonging to the cross-sections at the ends of the beam were constrained to two reference points (RP-1 and RP-2).

RP-2 is the master node at the left end of the beam and was restrained against displacements and rotations in all directions.

RP-1 is the master node at the right end of the beam and was restrained against displacements in two directions and rotations in two directions, providing a restraint for the torsional degree of freedom and out-of plane displacements, and the beam deformation was imposed by applying displacements in the 2-direction (vertical).

The combination of these boundary conditions imposed a constant shear force in the element and a linear bending moment distribution (namely cantilever scheme).

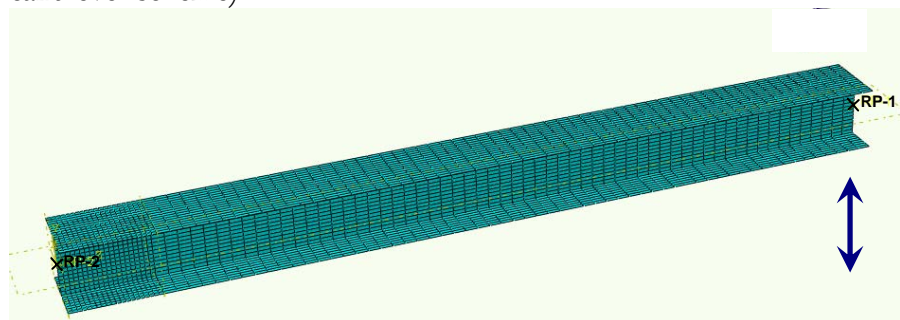


Figure 7.2 Displacement and boundary conditions (double T profile).

- The numerical analyses are devoted to investigate the cyclic behaviour of steel beams, so in each model it has been created a static step, corresponding to the cyclic loading pattern, up to collapse. The loading was simulated by imposing the displacement history in the vertical direction in the RP-1 node.

The AISC2005 loading protocol was used. The sequence suggested by the code is reported below in terms of chord rotation (θ), then displacements were obtained by rotations ($\delta = \theta L$):

- 6 cycles with $\theta = 0.00375$ rad
- 6 cycles with $\theta = 0.005$ rad
- 6 cycles with $\theta = 0.0075$ rad
- 4 cycles with $\theta = 0.01$ rad
- 2 cycles with $\theta = 0.015$ rad
- 2 cycles with $\theta = 0.02$ rad
- 2 cycles with $\theta = 0.03$ rad
- 2 cycles with $\theta = 0.04$ rad

If failure does not occur, the test continues increasing the rotation amplitude of 0.01rad for 2 successive cycles up to collapse.

The following figure shows the applied displacement history.

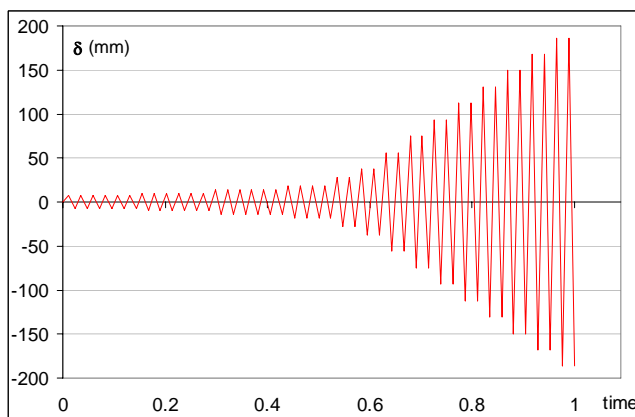


Figure 7.3 Displacement history for cyclic simulations.

- For the material properties, this time was not possible to use the "true stress" - "true strain" format of the experimental test results, so the average stress-strain relationship of the European S275 steel grade has been used. Yielding has been modeled by means of the von Mises yield

criteria. Plastic hardening was represented using a nonlinear kinematic hardening law calibrated on the basis of the cyclic material properties derived from cyclic coupon tests performed by Kaufmann et al. (2001). The same cyclic material properties were used for the flanges and web of the I beams and for the section of hollow beams.

Modelling of strength deterioration due to buckling has been taken into account by using the large displacement option.

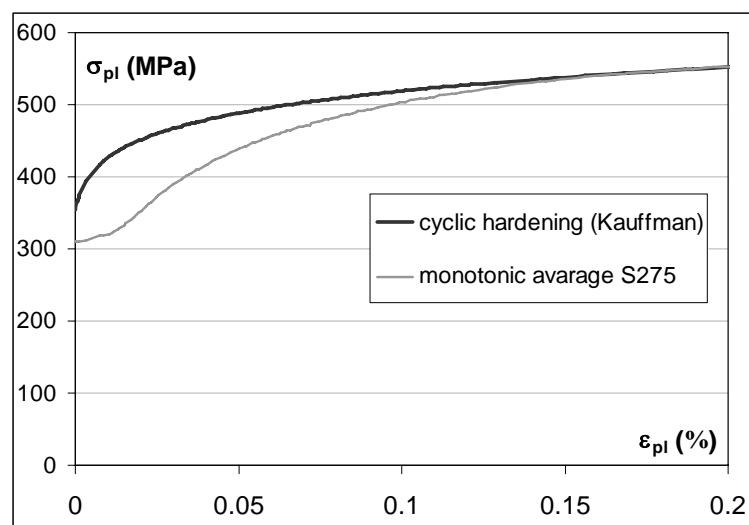


Figure 7.4 Stress-strain diagram resulting from experimental tests.

7.3 PARAMETRIC ANALYSIS: RESULTS

7.3.1 IPE profiles

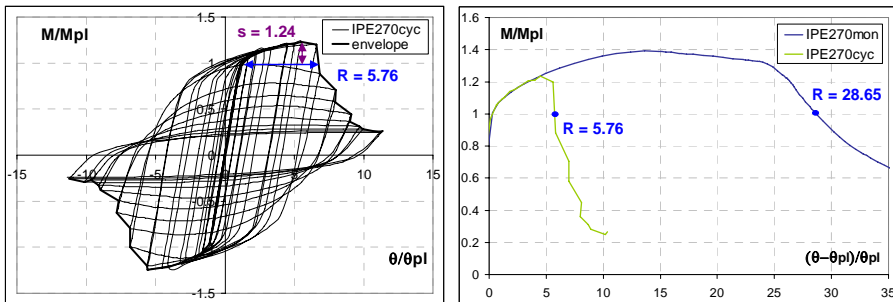


Figure 7.5 Cyclic response of IPE 270 and monotonic comparison.

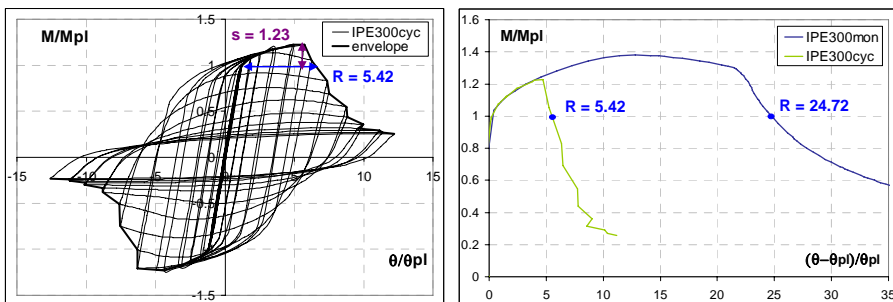


Figure 7.6 Cyclic response of IPE 300 and monotonic comparison.

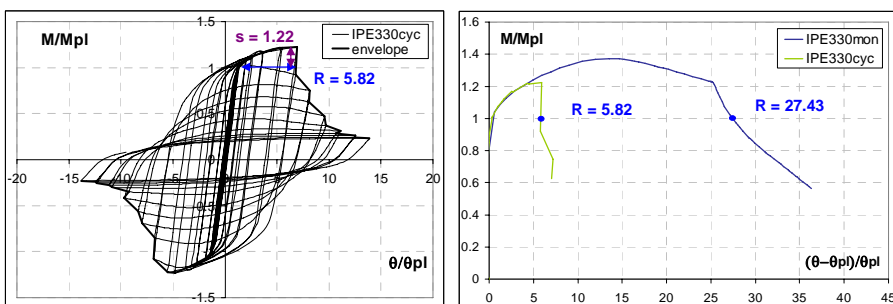


Figure 7.7 Cyclic response of IPE 330 and monotonic comparison.

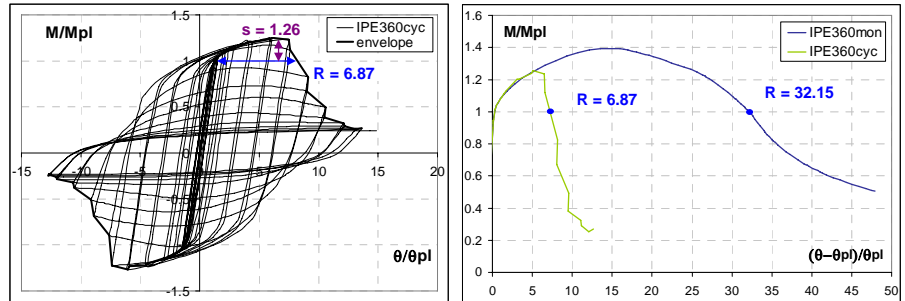


Figure 7.8 Cyclic response of IPE 360 and monotonic comparison.

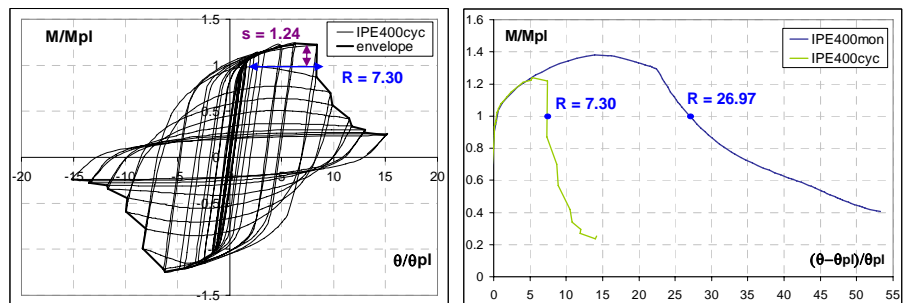


Figure 7.9 Cyclic response of IPE 400 and monotonic comparison.

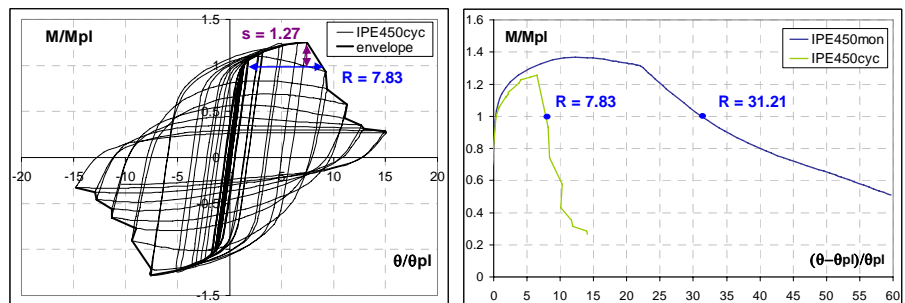


Figure 7.10 Cyclic response of IPE 450 and monotonic comparison.

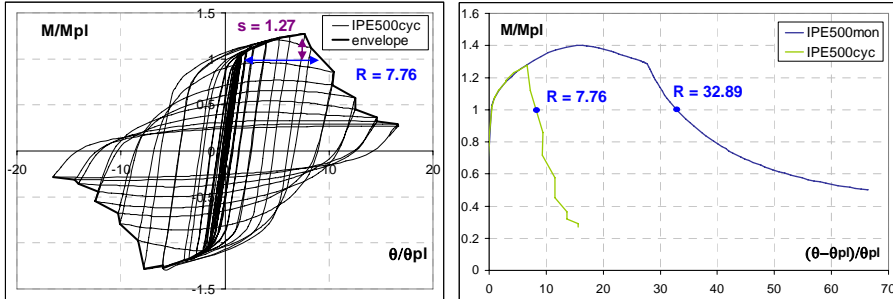


Figure 7.11 Cyclic response of IPE 500 and monotonic comparison.

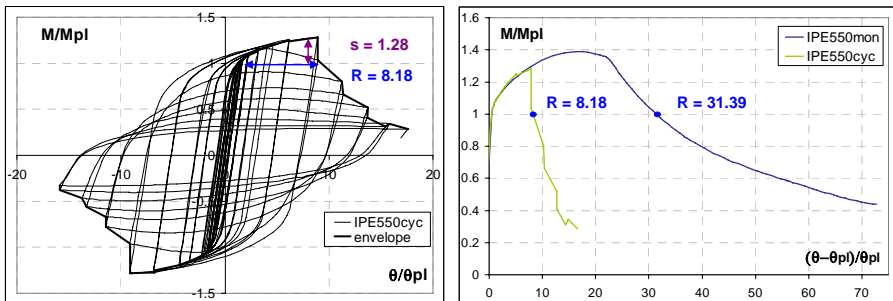


Figure 7.12 Cyclic response of IPE 550 and monotonic comparison.

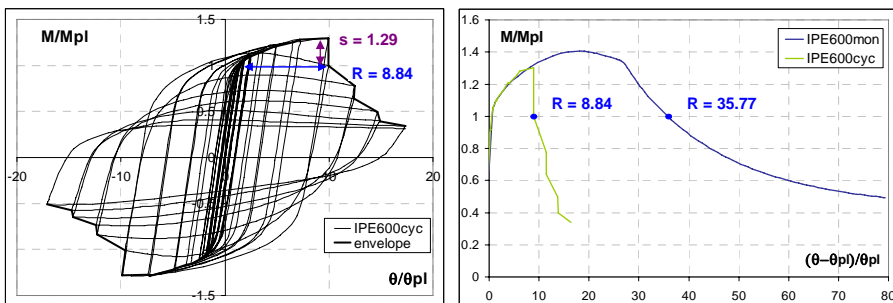


Figure 7.13 Cyclic response of IPE 600 and monotonic comparison.

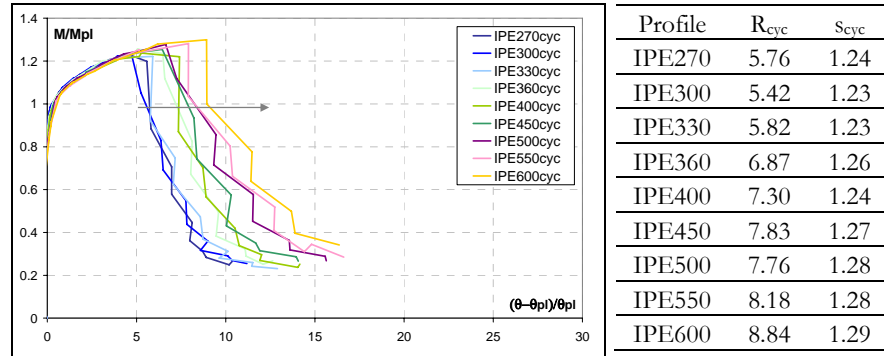


Figure 7.14 Comparison of cyclic envelope response of all IPE profiles.

7.3.2 HEA profiles

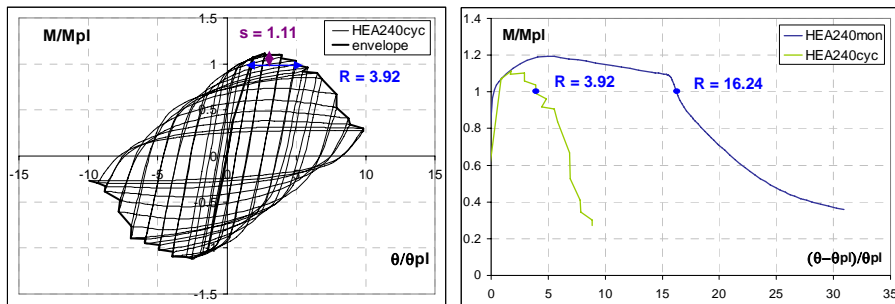


Figure 7.15 Cyclic response of HEA240 and monotonic comparison.

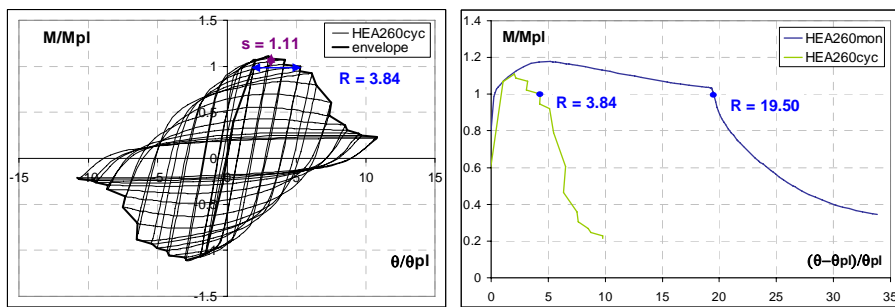


Figure 7.16 Cyclic response of HEA260 and monotonic comparison.

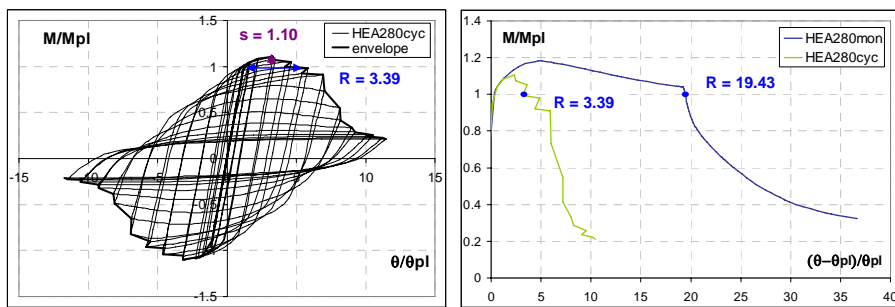


Figure 7.17 Cyclic response of HEA280 and monotonic comparison.

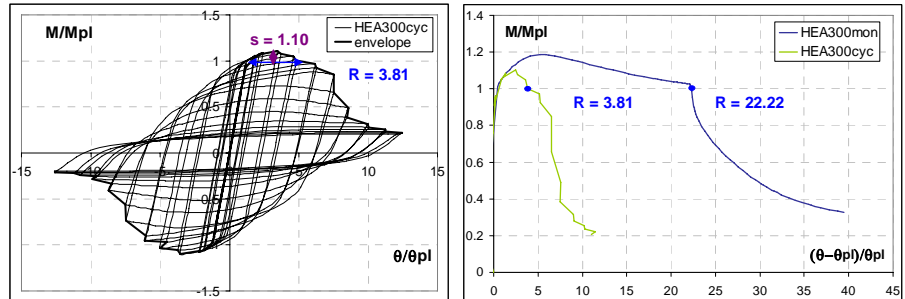


Figure 7.18 Cyclic response of HEA300 and monotonic comparison.

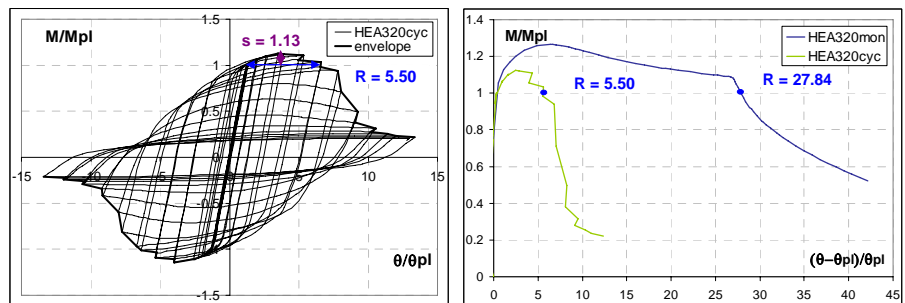


Figure 7.19 Cyclic response of HEA320 and monotonic comparison.

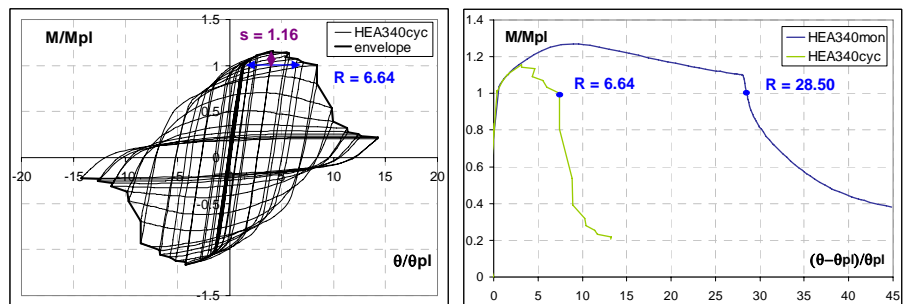


Figure 7.20 Cyclic response of HEA340 and monotonic comparison.

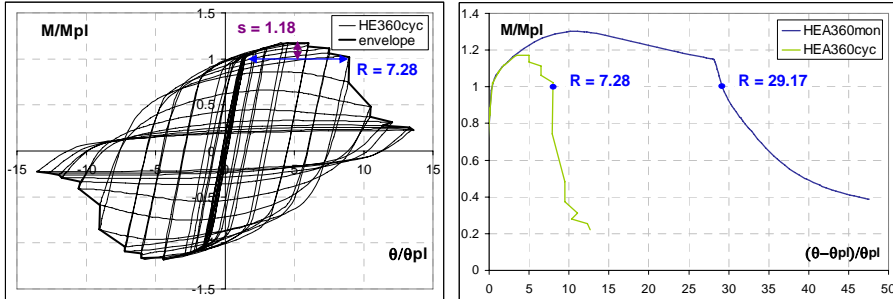


Figure 7.21 Cyclic response of HEA360 and monotonic comparison.

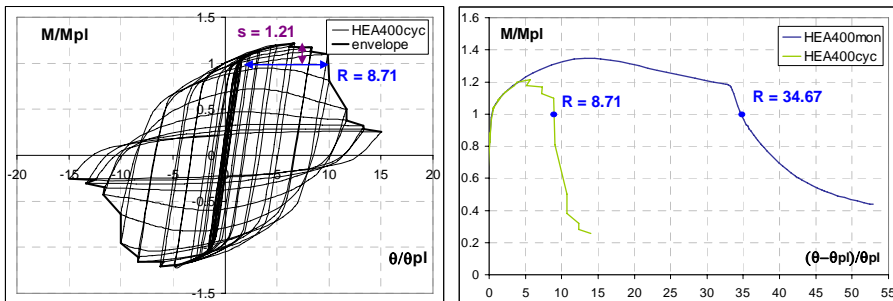


Figure 7.22 Cyclic response of HEA400 and monotonic comparison.

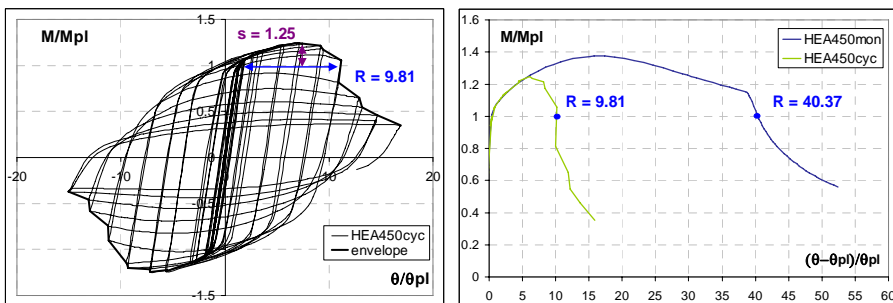


Figure 7.23 Cyclic response of HEA450 and monotonic comparison.

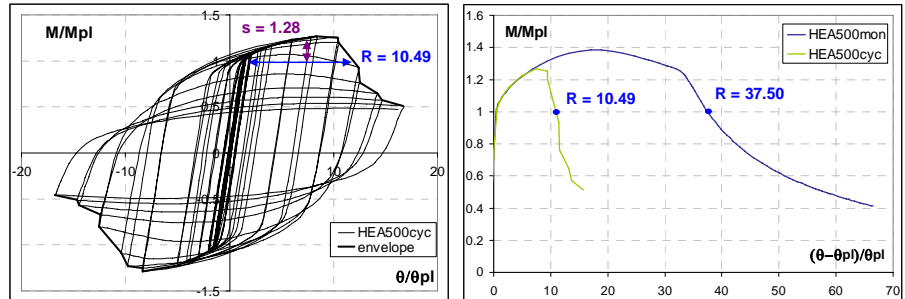


Figure 7.24 Cyclic response of HEA500 and monotonic comparison.

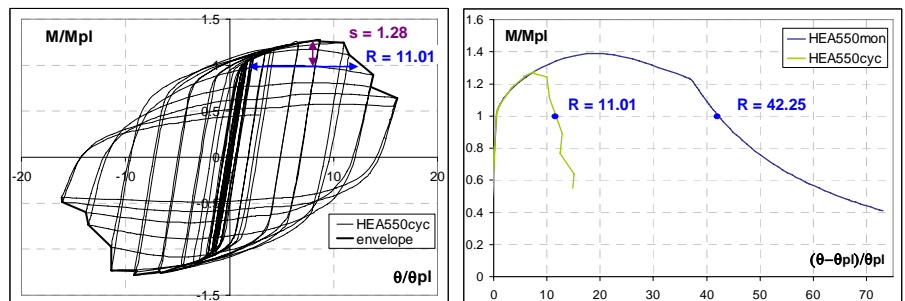


Figure 7.25 Cyclic response of HEA550 and monotonic comparison.

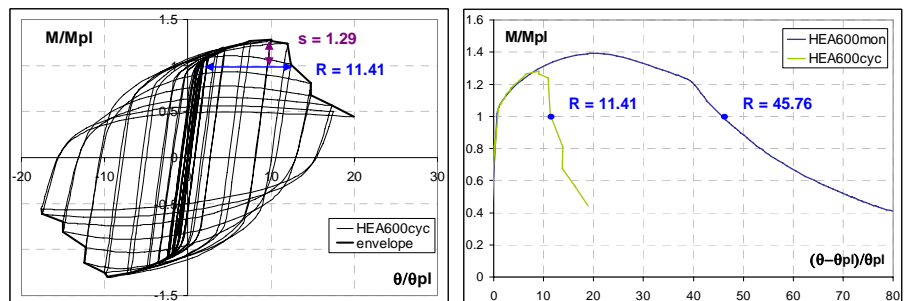
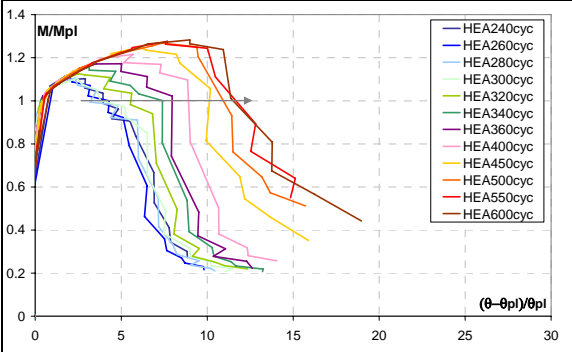


Figure 7.26 Cyclic response of HEA600 and monotonic comparison.



Profile	R_{cyc}	S_{cyc}
HEA240	3.92	1.11
HEA260	3.84	1.11
HEA280	3.39	1.10
HEA300	3.81	1.10
HEA320	5.50	1.13
HEA340	6.64	1.16
HEA360	7.28	1.18
HEA400	8.71	1.21
HEA450	9.81	1.25
HEA500	10.49	1.28
HEA550	11.01	1.28
HEA600	11.41	1.29

Figure 7.27 Comparison of cyclic envelope response of all HEA profiles.

7.3.3 HEB profiles

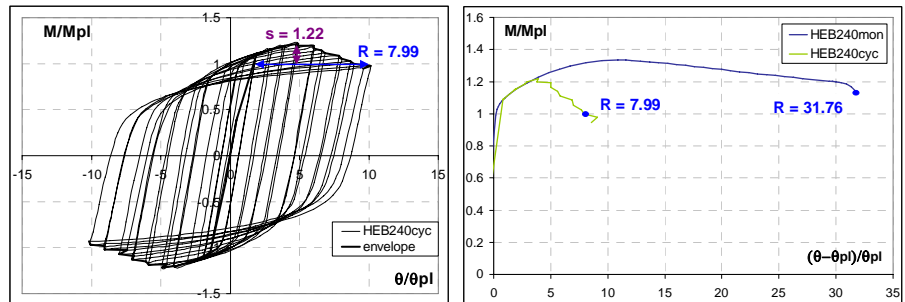


Figure 7.28 Cyclic response of HEB240 and monotonic comparison.

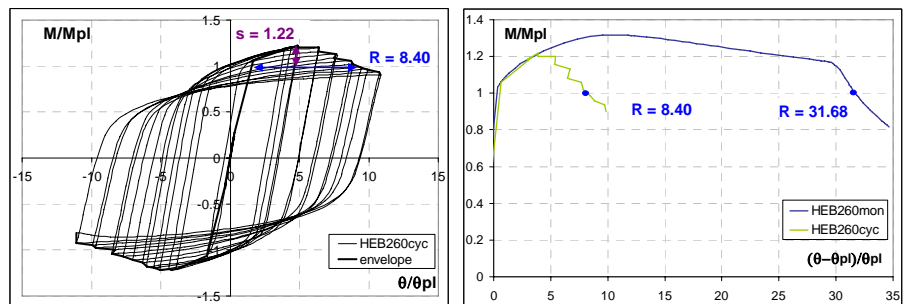


Figure 7.29 Cyclic response of HEB260 and monotonic comparison.

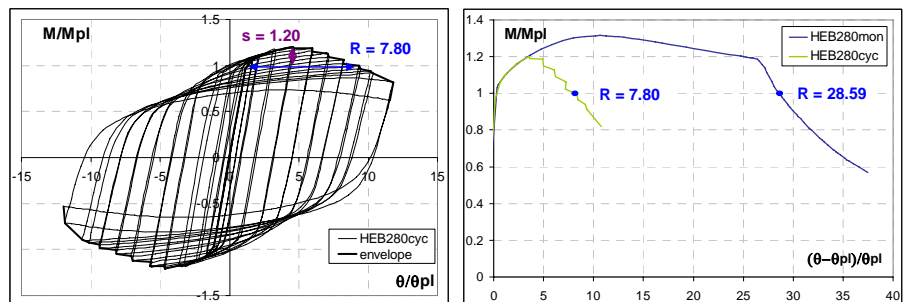


Figure 7.30 Cyclic response of HEB280 and monotonic comparison.

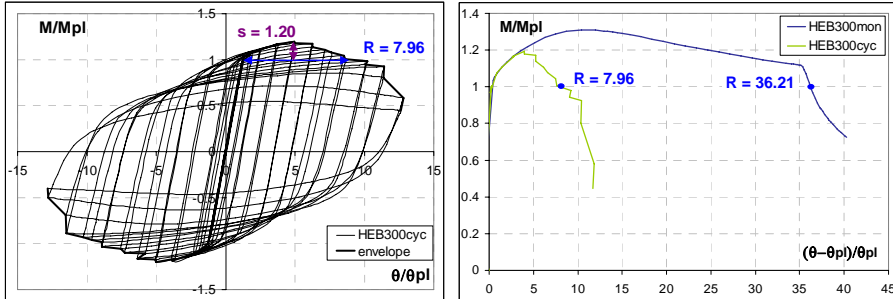


Figure 7.31 Cyclic response of HEB300 and monotonic comparison.

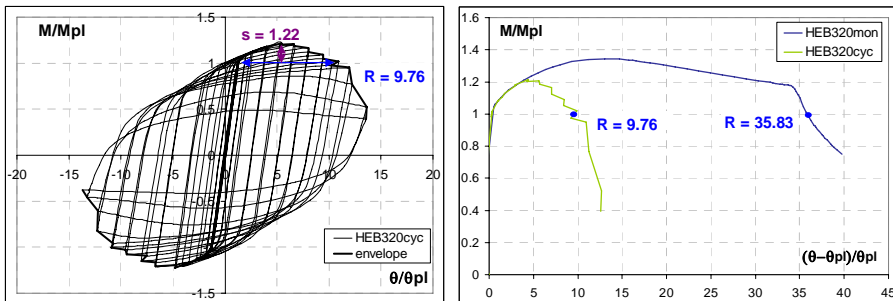


Figure 7.32 Cyclic response of HEB320 and monotonic comparison.

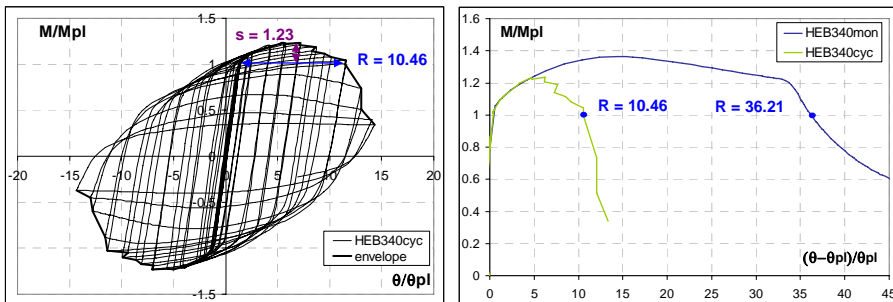


Figure 7.33 Cyclic response of HEB340 and monotonic comparison.

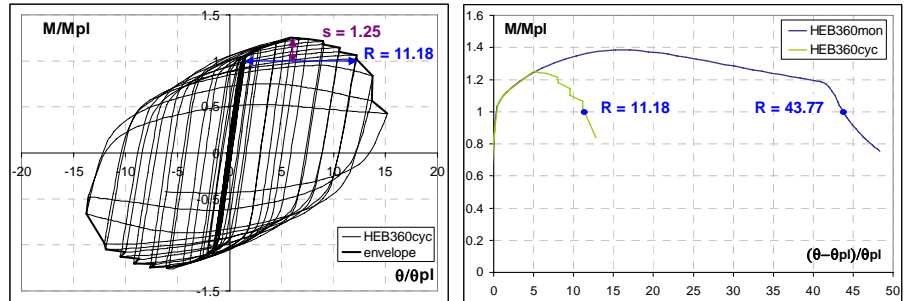


Figure 7.34 Cyclic response of HEB360 and monotonic comparison.

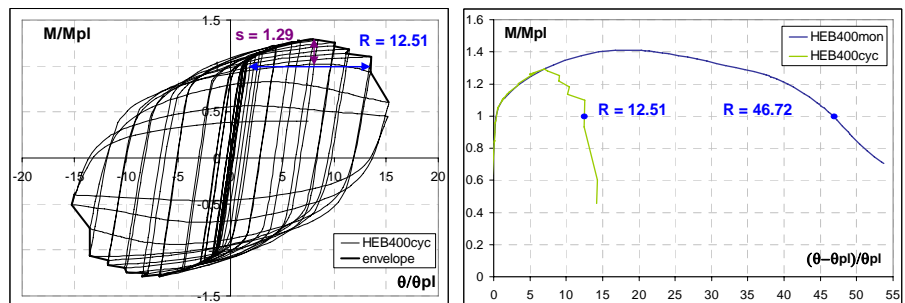


Figure 7.35 Cyclic response of HEB400 and monotonic comparison.

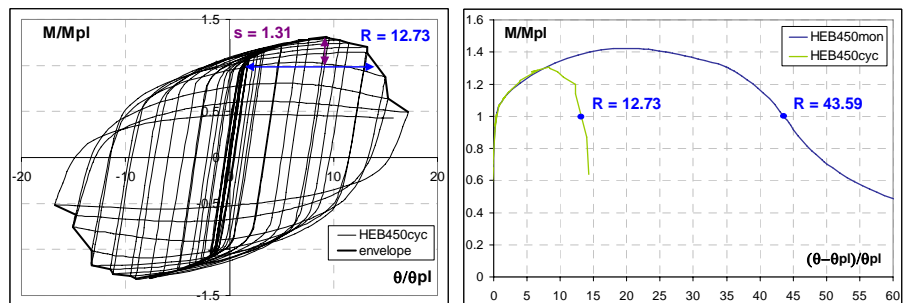


Figure 7.36 Cyclic response of HEB450 and monotonic comparison.

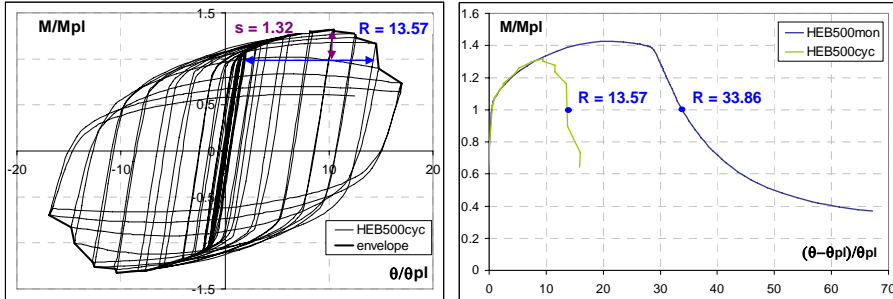


Figure 7.37 Cyclic response of HEB500 and monotonic comparison.

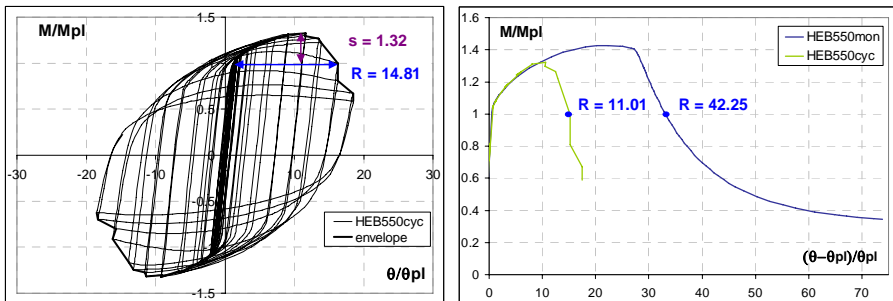


Figure 7.38 Cyclic response of HEB550 and monotonic comparison.

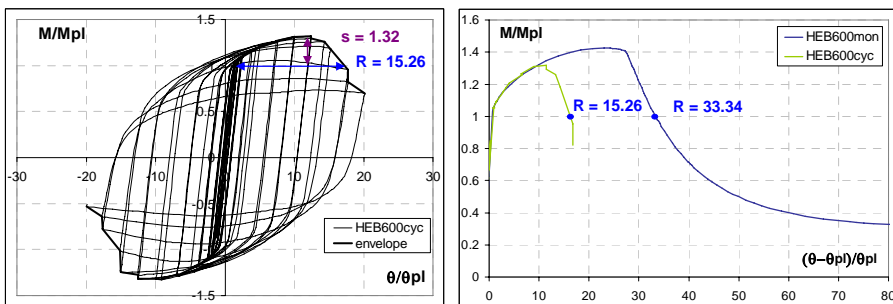


Figure 7.39 Cyclic response of HEB600 and monotonic comparison.

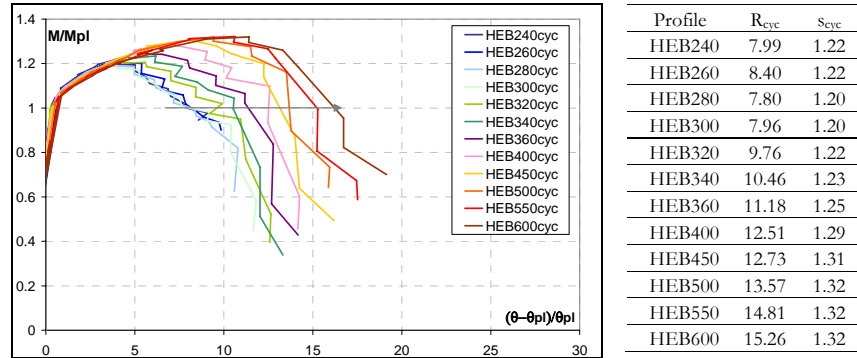


Figure 7.40 Comparison of cyclic envelope response of all HEB profiles.

7.4 CONCLUDING REMARKS

At the light of the results of the cyclic parametrical analysis, it can be noticed that the loading condition has a significant influence on the results in terms of rotation capacity.

In particular, it decreased when the loading pattern is cyclic, as compared to monotonic one, resulting that R_{cyc} is about from 20% to 40% of R_{mon} . On the other hand, the cyclic flexural overstrength s could be larger than the one observed for monotonic loading patterns, thanks to the steel isotropic hardening.

In the following tables there are the results in terms of R and s , for monotonic and cyclic loading patterns and the comparison between them in terms of average values of cyc/mon.

Table 7.2 Comparison between monotonic and cyclic results (HEA).

Profile	R_{cyc}	R_{mon}	R_{cyc}/R_{mon}	s_{cyc}	s_{mon}	s_{cyc}/s_{mon}
HEA240	3.92	16.24	0.24	1.11	1.19	0.93
HEA260	3.84	19.50	0.20	1.11	1.18	0.94
HEA280	3.39	19.43	0.17	1.10	1.18	0.93
HEA300	3.81	22.22	0.17	1.10	1.19	0.92
HEA320	5.50	27.84	0.20	1.13	1.26	0.90
HEA340	6.64	28.50	0.23	1.16	1.27	0.91
HEA360	7.28	29.17	0.25	1.18	1.30	0.91
HEA400	8.71	34.67	0.25	1.21	1.35	0.90
HEA450	9.81	40.37	0.24	1.25	1.37	0.91
HEA500	10.49	37.50	0.28	1.28	1.38	0.93
HEA550	11.01	42.25	0.26	1.28	1.39	0.92
HEA600	11.41	45.76	0.25	1.29	1.39	0.93
	average value (%)		23%	average value (%)		91%

Table 7.3 Comparison between monotonic and cyclic results (HEB).

Profile	R_{cyc}	R_{mon}	R_{cyc}/R_{mon}	s_{cyc}	s_{mon}	s_{cyc}/s_{mon}
HEB240	7.99	31.76	0.25	1.22	1.33	0.92
HEB260	8.40	31.68	0.27	1.22	1.32	0.92
HEB280	7.80	28.59	0.27	1.20	1.31	0.92
HEB300	7.96	36.21	0.22	1.20	1.31	0.92
HEB320	9.76	35.83	0.27	1.22	1.34	0.91
HEB340	10.46	36.21	0.29	1.23	1.36	0.90
HEB360	11.18	43.77	0.26	1.25	1.38	0.91
HEB400	12.51	46.72	0.27	1.29	1.41	0.91
HEB450	12.73	43.59	0.29	1.31	1.42	0.92
HEB500	13.57	33.86	0.40	1.32	1.43	0.92
HEB550	14.81	33.08	0.45	1.32	1.43	0.92
average value (%)			23%	average value (%)		91%

Table 7.4 Comparison between monotonic and cyclic results (IPE).

Profile	R_{cyc}	R_{mon}	R_{cyc}/R_{mon}	s_{cyc}	s_{mon}	s_{cyc}/s_{mon}
IPE270	5.76	28.65	0.20	1.24	1.39	0.89
IPE300	5.42	24.72	0.22	1.23	1.38	0.89
IPE330	5.82	27.43	0.21	1.23	1.37	0.90
IPE360	6.87	32.15	0.21	1.26	1.39	0.91
IPE400	7.30	26.97	0.27	1.24	1.38	0.90
IPE450	7.83	31.21	0.25	1.27	1.37	0.93
IPE500	7.76	32.89	0.24	1.28	1.40	0.91
IPE550	8.18	31.39	0.26	1.28	1.39	0.92
IPE600	8.84	35.77	0.25	1.29	1.40	0.92
average value (%)			23%	average value (%)		91%

Further developments of this branch of the research are needed to better investigate the influence of cyclic actions on the behaviour of steel beams. In particular, it should be investigated other cyclic loading protocols. In this case was used the AISC 2005, but it can be applied also ECCS, ATC 24, SAC and SAC near fault.

Moreover, the same kind of cyclic parametrical analysis should be developed also for RHS and SHS profiles.

Further research is also needed to establish criteria for web and compression flange slenderness, as well as the unbraced length, in order that beams can be properly proportioned to ensure adequate rotation capacity under cyclic loading.

Also in this case some final considerations can be made, in the light of all the previous work:

- for seismic application, it is auspicious the use of the cyclic rotation capacity “R”, and not the monotonic one, calculated by means of the new proposed formulation,
- cyclic rotation capacity “R” can be estimated as about 30% of monotonic “R”,
- and finally, for seismic design it will be necessary to correlate cyclic “R” and behaviour factor “q” of steel structures.

8 CONCLUSIONS

In the end, this chapter is a brief recapitulation of the achieved results and considerations on the innovative contents of the thesis.

In this thesis the results of different kinds of investigation about both monotonic and cyclic behaviour of steel beams are presented.

First of all are presented details on the experimental activity performed in the Civil Engineering Laboratory at the University of Salerno in the framework of ReLUIIS project.

In particular, the planning of the experimental campaign, the test set-up scheme, the tested profiles, the loading history patterns and the main results of the experimental tests are given.

At the light of these experimental results, and with the aim to continue the study on the behaviour of steel beams avoiding additional expensive experimental campaigns, finite element models has been used to perform numerical simulations (in Abaqus 6.10) of the experimental tests actually carried out. The numerical results have been compared with the experimental ones to demonstrate the validity of the assumptions made in the modelling phase, with positive response.

Then, a wide parametrical analysis, carried out by means of finite element simulations, has been performed, on the basis of the previous calibration of the numerical models.

In this way the obtained results goes to enlarge the existing database of results, to be able, in the end, to propose a new empirical formulation for the parameters “R” and “s” in case of monotonic loads.

The proposed equations are obtained from a multiple linear regression of experimental and numerical data on monotonic tests, from literature and from the work carried out for this thesis. It was observed that interaction between web and compression flange slenderness could limit the rotation capacity of flexural members. This interaction can reduce the rotation capacity, when either the web or the compression flange slenderness is too large.

So, steel beam classification can be considered outdated, due to the fact that the rotation capacity “R” and the flexural overstrength “s” can be properly calculated by means of the tools provided by this work.

The correct value of the flexural overstrength “s”, as calculated with the new proposed formulation, can be properly used for the application of the capacity design criteria.

An analogous parametric analysis has been performed for cyclic loading pattern, demonstrating that the experimental and numerical results indicated that the loading condition has a significant influence on rotation capacity. In particular, it decreased when the loading is cyclic, and cyclic rotation capacity “R” can be estimated as about 30% of monotonic “R”. So, for seismic application, it is auspicious the use of the cyclic rotation capacity “R”, and not the monotonic one.

These critical considerations on the differences between the monotonic and the cyclic behaviours that were made, in future can be used to go beyond the final scope of this thesis. In particular it can be used to start a study to establish a connection between seismic demand and seismic capacity of steel beams, and so steel framed structures in general. In particular, for seismic design it will be necessary to correlate cyclic “R” and behaviour factor “q” of steel structures.

REFERENCES

CHAPTER 1

- COST ACTION C26 (2006). *Urban Habitat Constructions under Catastrophic Events: Memorandum of Understanding*.
- ReLUIIS-DPC (2011). *The development of innovative approaches for the design of steel and composite steel-concrete structural systems, The line 5 of the ReLUIIS-DPC 2005-2008 Project*. Mazzolani Zandonini editors.
- Landolfo R., Piluso V., Brescia M., D'Aniello M., Mammana O., Tortorelli S., (2008). Rotation capacity vs demand of steel beams under catastrophic events. *WG2 Datasheet of COST Action C26 conference*, Malta, pp. 146-151.

CHAPTER 2

- ATC 40. (1996). *Seismic evaluation and retrofit of existing concrete buildings*. Redwood City (CA). Applied Technology Council.
- Chopra R., (2004). Estimating seismic demands for performance-based engineering of buildings. *Proceedings of 13th WCEE*, CD-ROM: Paper No. 5007.
- ECCS. (1994). *ECCS Manual on Design of Steel Structures in Seismic Zones*.
- EN 1993:1-1. (2005). *Design of Steel Structures*. UNI.
- EN 1998:1-1. (2005). *Design of Structures for Earthquake Resistance*. UNI.
- FEMA 273. (1997). *NEHRP guidelines for the seismic rehabilitation of buildings*; Washington (DC). Federal Emergency Management Agency.
- FEMA 274. (1996). *Commentary*. Washington (DC): Federal Emergency Management Agency.
- Ganzerli G., Pantelides CP., Reaveley L.D., (2000). Performance-based design using structural optimization. *Earthquake Engineering and Structural Dynamics*, Vol. 29 No. 11: 1677-1690.
- Georgescu D., (1996). Earthquake-Recent developments in theoretical and experimental results on steel structures: seismic resistant braced frames. *Costruzioni metalliche* n.1: 39-52.
- Ghobarah A., (2001). Performance-based design in earthquake engineering: state of development. *Engineering Structures*, 23.

- Hamburger R.O., (1997). A framework for performance-based earthquake resistive design. *UBC/EERC-97/05, The EERC-CURE Symposium in honor of Vitelmo V. Bertero*: 101-108.
- Krawinkler H., (1995). New Trends in seismic design methodology. *Proceedings of 10th European Conference on Earth-quake Engineering*, Vol. 2: 821-830.
- Mahoney M., Hanson R.D., (1998). An action plan for performance-based design. *Proceedings of the 6th US National Conference on Earthquake Engineering*, EERI.
- Mazzolani F.M., Piluso V., (1993). Member behavioural classes of steel beam and beam-columns. *Proceedings of XIV CTA, Ricerca Teorica e sperimentale*: 405-416.
- Ricles J. M., Popov E. P., (1994). Inelastic Link Element for EBF Seismic Analysis. *Journal of Structural Engineering*, vol.120, No. 2: 441-463.
- SEAOC - Vision 2000. (1995). *Performance based seismic engineering of buildings, vols. I and II: Conceptual framework*. Sacramento (CA): Structural Engineers Association of California.
- Tortorelli S., (2009). Tipologie Sismoresistenti Innovative per la Progettazione di Edifici in Acciaio. in *Costruzioni Metalliche n°6-2009*, pp. 72-73
- Tortorelli S., D’Aniello M., Landolfo R., (2010). Lateral capacity of steel structures designed according to EC8 under catastrophic seismic events. *Proceedings of COST C26 Final Conference “Urban Habitat Constructions under Catastrophic Events”*, Naples, pp. 409-414.
- Tremblay R., (2002). Inelastic seismic response of steel bracing members. *Journal of constructional steel research* n.58: 665-701.

CHAPTER 3

- D.M. (2008), *Nuove Norme Tecniche per le Costruzioni*. Official Gazette of the Italian Republic, Rome.
- Driscoll G. C., (1957). *Rotation capacity of a 3-span continuous beam*. Fritz Engineering Laboratory Report N0.268.2, Lehigh University
- Driscoll G. C., (1958). *Rotation capacity requirements for single-span frames*. Fritz Engineering Laboratory Report N0.268.5, Lehigh University.
- Driscoll G. C., (1958). *Rotation capacity requirements for beams and portal frames*. Ph.D. thesis. Lehigh University.
- Gioncu V., (1999). Framed structures: Ductility and seismic response: General report. In *6th international conference on stability and ductility of steel*

- structures, SDSS 99, Timisoara. *Journal of constructional steel research*, vol55, no.13, pp.125-154.
- Gioncu V., Mazzolani F.M., (1995). Alternative methods for assessing local ductility. *Proceedings of Behaviour of steel structures in seismic areas, STESSA'94*. Mazzolani & Gioncu editors, London: E&FN Spon, pp. 182–90.
- Gioncu V., Mazzolani F. M., (2002). *Ductility of seismic resistant steel structures*, Spoon Press
- Haaijer G., (1957). Plate buckling in the strain-hardening range. *Journal of the Engineering Mechanics Division*, ASCE Publications, 83(EM2), pp. 1-47.
- Hasan S. W., Hancock G. J., (1989). Plastic bending tests of cold-formed rectangular hollow sections. *Steel Construction, Journal of Australian Institute of Steel Construction*, 23(4):2–19.
- Kato B., Akiyama H., (1973). Theoretical prediction of the load-deflection relationship of steel members and frames. *Proceedings of LABSE symposium*, Lisbon.
- Kato B., Akiyama H., (1981). Ductility of Members and Frames subject to Buckling, Proceedings of ASCE convention, May 11-15.
- Kato B., (1988). Rotation capacity of steel members subject to local buckling, *9th World Conference on Earthquake Engineering*, Vol. 4, paper 6-2-3, Tokyo Kyoto.
- Kato B., (1989). Rotation Capacity of H section members as determined by local buckling, *Journal of Constructional Steel Research*, vol. 13, pp. 95-109.
- Kato B., (1990). Deformation capacity of steel structures, *Journal of Construction Steel Research*, Vol.17, 33-94
- Kemp A. R., (1985). *Commentary on SABS 0162-1984: Code of Practice for the use of structural steel: Chapter 12: Plastic design*, South African Institute of Steel Construction.
- Kemp A. R., (1985). Interaction of Plastic Local and Lateral Buckling, *Journal of Structural Engineering*, ASCE, vol.111. n.10 pp. 2181-2196
- Kemp A. R., (1986). Factors affecting the rotation capacity of plastically designed members, *The Structural Engineer*, vol. 64B, No. 2, pp: 28-35
- Korol R. M., Hudoba J., (1972). Plastic behaviour of hollow structural sections. *Journal of the Structural Division*, ASCE, 98(5):1007-23.
- Lay M. G., (1965). Flange Local Buckling in Wide Flange Shape. *Journal of Structural Division*, ASCE Publications, Vol. 91(ST6), 95-116.

- Lay M.G., Galambos T. V., (1965). Inelastic Beams Under Uniform Moment. *Journal of Structural Division*, ASCE Publications, vol.91.
- Mazzolani F. M., Piluso, V., (1993). Member behavioural classes of steel beam and beam-columns. Proceedings of XIV CTA, Ricerca Teorica e sperimentale: 405-416.
- OPCM 3274, (2003). *First elements in the matter of general criteria for seismic classification of the national territory and of technical codes for structures in seismic zones*. Official Gazette of the Italian Republic, Rome.
- Plumier A., (2000). General report on local ductility, *Journal of Constructional Steel Research*, vol. 55, pp: 91-107.
- Sedlacek G., Feldmann M., (1995). *Background document 5.09 for chapter 5 of Eurocode 3 Part 1.1 - The b/t ratios controlling the applicability of analysis models in Eurocode 3 Part 1.1*. Aachen.
- Zhao X. L., Hancock G. J., (1991). Tests to determine plate slenderness limits for cold-formed rectangular hollow sections of grade C450. *Steel Construction, Journal of Australian Institute of Steel Construction*, 25(4):2-16.

CHAPTER 4

- AISC 2005. *Seismic Provisions for Structural Steel Buildings*. American Institute of Steel Constructions.
- Boerave P., Lognard B., (1997). Elasto-plastic behaviour of steel frame works. *Journal of constructional steel research*, vol. 27, pp: 3-21.
- Brescia M., (2008). *Rotation capacity and overstrength of steel members for seismic design*. PhD thesis.
- Dean M., Wilkinson T., Hancock G. J. (2001). Bending and compression tests on cold formed rectangular hollow sections. *Proceedings of 9th International Symposium on Tubular Structures*, Dusseldorf, Germany, pp: 349-358.
- Gioncu V., Pecteu D., (1997). Available rotation capacity of wide flange beams and beam-columns Part 1. Theoretical approaches. *Journal of constructional steel research*, vol. 43, Nos.1-3, pp: 161-217.
- Gioncu V., Pecteu D., (1997). Available rotation capacity of wide flange beams and beam-columns Part 2. Experimental and numerical tests. *Journal of constructional steel research*, vol. 43, Nos.1-3, pp: 219-244.
- Guzelbey I. H., Cevik A., Gogus M. T., (2006). Prediction of rotation capacity of wide flange beams using neural networks. *Journal of constructional steel research*, vol. 62, pp: 950-961.
- Kemp A. R., (1985). Interaction of plastic local and lateral buckling. *Journal of structural engineering*, ASCE, vol. 111, No. 10, pp: 2181-2196.

- Kemp A. R., (1996). Inelastic local and lateral buckling in design codes. *Journal of structural engineering*, vol.122, No.4, pp: 374-382.
- Kuhlman U., (1989). Definition of flange slenderness limits on the basis of rotation capacity values. *Journal of Construction Steel Research*, vol. 14, pp: 21-40.
- Ito M., Karatani E., Komuro Y., (2002). Moment-Inelastic rotation behaviour of longitudinally stiffened beams. *Journal of Bridge Engineering*, vol.7, No. 4, pp: 223-228.
- Ito M., Nozaka K., Shirosaki T., Yamasaki K., (2005). Experimental study on moment–plastic rotation capacity of hybrid beams. *Journal of Bridge Engineering*, vol.10, No.4, pp: 490-496.
- Landolfo R., D’Aniello M., Brescia M., Tortorelli S., (2011). Rotation Capacity and Classification Criteria of Steel beams. In *The development of innovative approaches for the design of steel and composite steel-concrete structural systems, The line 5 of the ReLUIS-DPC 2005-2008 Project*. Mazzolani Zandonini editors, pp. 37-88.
- Luckey A. F., Adams P. R., (1969). Rotation capacity of wide flanged beams under moment gradient. *Journal of Structural Division*, ASCE, vol. 95, pp: 1173-1188.
- Nakashima M., Nakamura T., Wakabayashi M., (1983). Post buckling instability of steel beam-columns. *Journal of structural engineering*, vol. 109, No. 6, pp: 1414-1430.
- Suzuki T., Ogawa T., Ikarashi K., (1994). A study on local buckling behaviour of hybrid beams. *Thin Walled Structures*, vol. 19, pp: 337-351.
- Spangemacher R., (1992). *Zum rotationsnachweis von stablkonstruktionen, die nach dem traglastverfahren berechnet werde*. PhD thesis.
- Wilkinson T., (1999). *The plastic behaviour of cold-formed rectangular hollow sections*. PhD thesis.
- Wilkinson T., Hancock G. J., (1997). *Tests for the compact web slenderness of cold-formed rectangular hollow sections*. Research report R744.
- Wilkinson T., Hancock G. J., (1998). Tests to examine the compact web slenderness of cold-formed rhs. *Journal of structural engineering*, vol. 124, No. 10, pp: 1166-1174.

CHAPTER 5

- ABAQUS, Inc. (2005). *User’s Manual*, ABAQUS Standard V6.5.
- Esposito M., (2008). *PTED beam-to-column connections for steel moment resisting frames: structural identification based on numerical analyses*. PhD thesis.

Zienkiewicz O.C., Taylor R.L., Zhu J.Z., (2004). *The Finite Element Method: its basis and fundamentals* (sixth edition).

CHAPTER 6

ABAQUS, Inc. (2005). *User's Manual*, ABAQUS Standard V6.5

Haaiker G., (1957). Plate buckling in the strain-hardening range. *Journal of the Engineering Mechanics Division*, ASCE Publications, 83(EM2), pp. 1-47.

Kaufmann E. J., Metrovich B. R., Pense A. W., (2001). *Characterization of cyclic inelastic strain behavior on properties of A572 Gr. 50 and A913 Gr. 50 rolled sections*. ATLSS Rep. No. 01-13, Lehigh Univ., Bethlehem, Pa.

Lay M.G., (1965). Flange Local Buckling in Wide Flange Shape. *Journal of Structural Division*, ASCE Publications, Vol. 91(ST6), 95-116.

Lay M.G., Galambos T.V., (1965). Inelastic Beams under Uniform Moment. *Journal of Structural Division*, ASCE Publications, vol.91.

Mazzolani F.M., Piluso V., (1993). Member behavioural classes of steel beam and beam-columns. *Proceedings of XIV CTA, Ricerca Teorica e sperimentale*: 405-416.

Tortorelli S., D'Aniello M., Landolfo R., (2011). Prediction of the flexural capacity of steel beams – Empirical formulation. *Proceedings of EUROSTEEL 2011 - 6th European Conference on Steel and Composite Structures*, Budapest, Hungary, pp. 963-968.

Tortorelli S., D'Aniello M., Landolfo R., (2011). Formulazione empirica per il calcolo della capacità flessionale di travi di acciaio. *Proceedings of XIII Congresso C.T.A. Le Giornate Italiane della Costruzione in Acciaio*, Ischia, Italy, pp. 725-732.

CHAPTER 7

ABAQUS, Inc. (2005). *User's Manual*, ABAQUS Standard V6.5

D'Aniello M., Tortorelli S., Landolfo R., (2012). The influence of cyclic loading on flexural response of steel beams. *Proceedings of STESSA 2012*, Santiago del Chile, Chile, (in publication).